Title
Elucidation of the Developmental Role of Janus Kinase and Microtubule-Interacting Protein 1, JAKMIP1, an Autism Candidate Gene

Author
Berg, Jamee Mae

Publication Date
2013

Peer reviewed|Thesis/dissertation

UNIVERISITY OF CALIFORNIA

Los Angeles

Elucidation of the Developmental Role of Janus Kinase and Microtubule-Interacting Protein 1, *JAKMIP1*, an Autism Candidate Gene

A dissertation submitted in partial satisfaction of the requirements for the degree of

Doctor of Philosophy in Neuroscience

By

Jamee Mae Berg

2013

ABSTRACT OF THE DISSERTATION

Elucidation of the Developmental Role of Janus Kinase and Microtubule-Interacting Protein 1, *JAKMIP1*, an Autism Candidate Gene

Jamee Mae Berg

Doctor of Philosophy in Neuroscience

University of California, Los Angeles 2013

Professor Daniel Geschwind, Chair

Autism Spectrum Disorders (ASD) are heritable neurodevelopmental disorders, affecting one in 88 children and involving hundreds of genes. The study of convergent biological pathways and simpler, monogenic forms of ASD are useful tools in understanding ASD. Fragile X syndrome (FXS) meets both criteria, as FMRP, the protein disrupted in FXS, regulates neuronal translation, a biological convergence point in autism, and is caused by a single gene mutation. Our group recently identified JAKMIP1 as downstream of both FMRP and CYFIP1, a regulator of FMRP-dependent translation at the synapse, in patient, *in vitro* and *in vivo* studies. However, little is known about JAKMIP1's developmental function in the CNS, and more specifically its relationship with FMRP.

To ascertain JAKMIP1's function, we determined when and where JAKMIP1 was expressed during brain development and used a gel free mass spectrometry, Multidimensional Protein Identification Technology (MudPIT), to uncover JAKMIP1's developmental protein interactome. We conducted gene ontology analysis of high confidence interactors to determine

JAKMIP1 function via guilt-by association and validated top targets by co-immunoprecipitation. These studies predicted a role for JAKMIP1 in FMRP translational control during postnatal brain development. We confirmed this by showing that JAKMIP1 binds to FMRP protein and associates with and regulates well-established FMRP mRNA targets, including *PSD95*, which showed decreased expression at synaptosomal membranes and unloading from translational complexes in *Jakmip1* KO mice. Gene expression profiling of postnatal *Jakmip1* KO mouse brains implicates JAKMIP1 in regulating FMRP mRNA targets, as *Jakmip1* KO brain expression profiles show statistical overlap with high confidence FMRP RNA binding partners.

We validated JAKMIP1's role in translation and membership in translational complexes through *in vivo* polyribosome fractionation in mice administered puromycin or with *Jakmip1* knockout, JAKMIP1 co-immunoprecipitation with eGFP-tagged polyribosomes, and colocalization of JAKMIP1 with translational complexes in neurons. We found that JAKMIP1 is expressed in polyribosomes *in vivo* and *in vitro*, contributes to the protein makeup of translational complexes *in vivo*, and regulates neuronal translation. To test if disruptions in JAKMIP1 function translate into FXS and ASD related behaviors, we generated a *Jakmip1* knockout mouse. We found that loss of *Jakmip1* leads to behavioral abnormalities overlapping those of *Fmr1* knockout mice and mouse models of ASD, including restrictive and repetitive behaviors, impaired social behavior and altered anxiety profiles.

Taken together, these studies demonstrate a major role for JAKMIP1 in neurological development involving FMRP-related translational control critical for establishing and/or maintaining normal social, repetitive, and anxiety-associated behavior.

The Dissertation of Jamee Mae Berg is approved.

David Krantz

James Wohlschlegel

Thomas O'Dell

William Yang

Daniel Geschwind, Committee Chair

University of California, Los Angeles

2013

I dedicate this work to all of the communities inextricably woven into these discoveries:

My scientific, musical, and running communities

My friends (who are my family) and my family (who are my friends)

Table of Contents

List of Figures and Tables

Acknowledgements

I am extremely grateful to the community of people that facilitated this work. The most prominent member of this community, Daniel Geschwind, is not only my advisor, but is also my friend. His passionate nature and drive is inspiring. He is an alchemist, being able to combine people and resources in such a way that results in innovate discoveries leading to tangible hopes for once-thought impossible cures. He is a rare type of genius, and I am privileged to be part of his research team. I am additionally thankful for the insightful input and guidance of my thesis committee members: David Kranz, James Wohlschlegel, Thomas O'Dell, and William Yang. I greatly appreciate their time and deep consideration of the work presented here. I owe a great deal of thanks to all those part of 'Team Jakmip1', as we lovingly call it. Leslie Chen, Elyse Kite, Alvin Li, Eric Tam, Chang Hoon Lee, and Mary Starks, I am so grateful for all of you as researchers and as friends. I won the research team lottery. I give special thanks to Leslie Chen, who has been particularly influential in the quality of this work. I would be remiss without giving great thanks to my good friend and lab manager, Lauren Kawaguchi, who has been a constant source of support. I additionally thank Ezra Rosen, Genevieve Konopka, Carrie Heusner and Brett Abrahams for their mentorship and friendship.

Chapter 1 contains information from the *Genome Biology* review article, 'Autism genetics: searching for specificity and convergence' (Berg and Geschwind, 2012). Chapters 2 through 4 include work from a manuscript under review at *Cell,* titled, 'JAKMIP1 is a novel component of an FMRP-associated RNP complex and regulates neuronal translation.' I give great thanks to the following coauthors of this publication: Changhoon Lee, Leslie Chen, Asami Oguro-Ando, Jason Stein, Jeremy A. Miller, Ajay A. Vashisht, Elyse P. Kite, Alvin Li, Olga Peñagarikano, James A. Wohlschlegel, and Daniel Geschwind. I also thank Dr. Sandra

Pellegrini for the $J1_{269-286}$ rabbit polyclonal antibody, rabbit preimmune serum, and the human *JAKMIP1* expression plasmid. I thank Dr. Joseph Dougherty for N2A BacTrap cell lines, Dr. Claudia Bagni for protocols related to IP/RT-PCR experiments, Dr. Larry Simpson for use of an Isco Fractionator, Hongmei Dong for technical assistance with C57BL/6 mice for developmental profiling, Eric Tam for help with image curation, Michelle Bailhe for technical assistance with subcellular fractionation and RNA extraction, and Dr. Lars Ittner for pLVU/RED plasmid ID 24178. Olga Peñagarikano, Alvin Li, and Andrew Poulos were additionally instrumental in the mouse work presented in Chapter 5. Giovanni Coppola and Fuying Gao made large contributions to the gene ontology and differential gene expression analysis presented in Chapter 6. I am lastly so very thankful for the generous grants from the NIMH (F31MH088083), the NIH (T32MH073526), the UCLA Chancellor's Award, and the Achievement Rewards for College Scientists.

This work would not have occurred without the support of my friends and family, two indistinguishable groups. They honor and hold the space for my big dreams and curiosities. They look at me and really see me. They weave nets of support for me when rugs get pulled. They remind me to breath, to laugh, to sing, to run, and to gain perspective under Michigan stars or on top of California mountains. Names must be mentioned. Jeremy Berg, for the fantastical nature of you. For your unconditional love. For making Science seem cool in the eyes of a ten year-old girl. Nancy Anne Berg, who always, always, always believes in me. For your creative genius. For believing in women in science. For teaching me Algebra before the first grade, because 'of course I could do it.' Chelsea O'Brien and Deva Berg. You are powerhouse women who are brilliant and beautiful. I want to be like both of you when I grow up. Aaron Berg, for really understanding the fabric of me, for being like me, and for being authentically interested in

my research. Walter Amorim and Kevin O'Brien, for being such incredible brother in laws. You are all so much more than family to me. You are my chosen friends and confidantes. Lastly, I am forever grateful for my tribe of women: Libby Andersen, Carolyn Arcella, Melissa Matich, Rachel Dooley, Sarah Schofield, Linda Suh, Shannon Brady, Moumita Basak, April Ho, Julie Perederiy, Jessica Rich, Ivy Joeva, Lisa Amorim, Kaycee Hitsman, Marie Spinali, Katherine Castro, Jessica Boswell and Nataly Hakakian. You are my strength and my mirrors.

VITA

2002	B.S. Biology, University of Michigan, Ann Arbor, Summa cum laude
2002-2005	University of Michigan, Ann Arbor, Staff Research Associate
2005-2007	University of California, Los Angeles, Staff Research Associate
2007	UCLA Chancellor's Award Recipient
2007-2011	Achievement Rewards for College Scientists (ARCS) Recipient
2008	UCLA Quality of Graduate Education Award Recipient
	FSL/Freesurfer Course Brisbane, Australia
2009-2011	UCLA Neurobehavioral Genetics Training Program Fellowship
2009-2012	Ruth L. Kirchstein National Research Service Award Recipient
	"Elucidation of the Developmental Role of JAKMIP1"
2009	Teaching Assistant Neuroanatomy
2013	Invited Instructor, OIST Molecular Neuroanatomy Course, Okinawa, Japan

PUBLICATIONS

Bomar JM, Benke PJ, Slattery EL, Puttagunta R, Taylor LP, Seong E, Nystuen A, Chen W, Albin RL, Patel PD,Kittles RA, Sheffield VC, Burmeister M. 2003. *Mutations in a novel gene encoding a CRAL-TRIO domain cause human Cayman ataxia and ataxia/dystonia in the jittery mouse*. **Nature Genetics**. 35(3):264-9. PMID:14556008

Gilbert N, **Bomar JM**, Burmeister M, Moran JV. 2004. *Characterization of a mutagenic B1 retrotransposon insertion in the jittery mouse*. **Human Mutations**. 24(1):9-13. PMID: 15221784

Elizabeth Spiteri, Genevieve Konopka, Giovanni Coppola, **Jamee Bomar**, Michael Oldham, Jing Ou, Sonja C. Vernes, Simon E. Fisher, Bing Ren, Daniel H. Geschwind. 2007. *Identification of the transcriptional targets of FOXP2, a gene linked to speech and language, in developing human brain***. The American Journal of Human Genetics.** 81(6):1144-57. PMCID: PMC2276350

Alarcón M, Abrahams BS, Stone JL, Duvall JA, Perederiy JV, **Bomar JM**, Sebat J, Wigler M, Martin CL, Ledbetter DH, Nelson SF, Cantor RM, Geschwind DH. 2008. *Linkage, association, and gene-expression analyses identify CNTNAP2 as an autism-susceptibility gene*. **The American Journal of Human Genetics**. 82(1):150-9. PMCID: PMC2253955

Leanne M Dibbens, Patrick S Tarpey, Kim Hynes, Marta A Bayly, Ingrid E Scheffer, Raffaella Smith, **Jamee Bomar** *and fifty additional authors*. 2008. *X-linked protocadherin 19 mutations cause female-limited epilepsy and cognitive impairment*. **Nature Genetics.** 40(6):776-81. PMID: 18469813

Konopka G, **Bomar JM**, Winden K, Coppola G, Jonsson ZO, Gao F, Peng S, Preuss TM, Wohlschlegel JA, Geschwind DH. 2009. *Human-specific transcriptional regulation of CNS development genes by FOXP2*. **Nature**. Nov 12;462(7270):213-7. PMID:19907493

Chowdhury TG, Jimenez JC, **Bomar JM**, Cruz-Martin A, Cantle JP, Portera-Cailliau C. 2010. *Fate of cajal-retzius neurons in the postnatal mouse neocortex*. **Front Neuroanat**. Mar 3;4:10.PMID: 20339484

Berg JM and Geschwind DH. 2012. *Autism genetics: Searching for specificity and convergence*. **Genome Biology.** Jul 31;13(7):247. PMID: 22849751.

Berg JM, Changhoon Lee, Leslie Chen, Asami Oguro-Ando, Jason Stein, Jeremy A. Miller, Ajay A. Vashisht, Elyse P. Kite, Alvin Li, Olga Peñagarikano, James A. Wohlschlegel, and Daniel Geschwind. *JAKMIP1 is a novel component of an FMRP-associated RNP complex and regulates neuronal translation*. **Cell**. *In submission*.

Chapter 1: Introduction

1.1 ASD Background and Features

Autism Spectrum Disorders (ASD) are a group of neuropsychiatric disorders that include autism, pervasive developmental disorder not otherwise specified (PDD-NOS), and Asperger's syndrome (Bill and Geschwind, 2009). First described in 1943, its diagnostic features continue to evolve based on an expanding clinical and biological understanding (Kanner, 1943). A child is diagnosed with ASD if he or she exhibits early childhood deficits in social communication and interaction, involving social reciprocity, non verbal communication, and maintenance of relationships, language development (such as delay of language onset and maintenance of conversation), as well as restrictive and repetitive behaviors, including speech, motor movements, routines, and interests (DSM-IV, American Psychiatric Association). Classic autism, formally known as autistic disorder is the most severe of the ASDs, with patients showing impairments in social, communication, and restrictive and repetitive domains before the age of three. Additional features often comorbid with ASD include sensory and motor abnormalities, ADHD, epilepsy, and developmental regression (Bill and Geschwind, 2009; Tuchman and Rapin, 2002). Those with ASD can range from being mentally disabled to having above average intelligence (Chakrabarti and Fombonne, 2005). ASDs are extremely prevalent in our society, with males being affected more than females, especially in high-functioning cases, including what is currently known as Asperger's syndrome. Currently, it is estimated that 1 out of 88 children has ASD, representing a 78% increase over the last 6 years (CDC, ADDM network, 2012). This drastic increase is most likely due to sociocultural factors rather than biological factors, including age at diagnosis, changing diagnostic criteria and broader inclusion rates, although genetic as well as environmental factors cannot be ruled out (Cantor et al., 2007; Hertz-Picciotto and Delwiche, 2009; King and Bearman, 2009; Volk et al., 2011).

ASD has a large genetic component. Concordance rates among monozygotic twins, dizygotic twins, and siblings range between 50-90%, 0-30%, and 3-26%, respectively, supporting a major genetic contribution (Hallmayer et al., 2011; Ozonoff et al., 2011; Rosenberg et al., 2009). Interestingly, the risk is 3-fold in second born male siblings versus females, supporting models of reduced penetrance in females (Ozonoff et al., 2011; Zhao et al., 2007). Moreover, a recent study found a roughly two fold increase in ASD concordance among full versus half siblings, additionally supporting a genetic contribution and heritability of greater than 50% (Constantino et al., 2012). Multiple converging research strategies to account for ASD genetic liability have identified a variety of genetic causes that account for roughly 20% of ASD cases. These include genetic copy number variation (CNV; duplicated or deleted regions of the genome greater than 1 kb (Abrahams and Geschwind, 2008)), syndromic forms of autism (ASD which occurs within a defined syndrome, such as Fragile X syndrome), and single gene and metabolic disorders (Bourgeron, 2007; Schaaf et al., 2011). Recent studies based on CNV and single nucleotide variant (SNV) data put the number of ASD-implicated genes between 200 and 1000 (Iossifov et al., 2012; Levy et al., 2011; Neale et al., 2012; O'Roak et al., 2012; Sanders et al., 2011; Sanders et al., 2012) and multiple modes of inheritance have been proposed (Girirajan et al., 2011; Leblond et al., 2012; State and Levitt, 2011). Additionally, many ASD-implicated genes are also associated with other neuropsychiatric disorders including schizophrenia, attention-deficit disorder, epilepsy, and intellectual disability (Alarcon et al., 2008; Arguello and Gogos, 2012; Arking et al., 2008; Bakkaloglu et al., 2008; Elia et al., 2010; Friedman et al., 2008; Geschwind, 2011; Girirajan et al., 2011; Guilmatre et al., 2009; Malhotra and Sebat, 2012; Niklasson et al., 2009; O'Roak et al., 2012; Zahir et al., 2008) and none are specific for autism,

suggesting that additional modifying factors dictate the clinical outcome of having disruptions in a specific gene.

The genetic complexity of ASD mirrors its phenotypic complexity. The core domains within ASD phenotypes- social, language and restrictive and repetitive- also exist as a spectrum, with a distribution intersecting normally defined behavior at their most extreme end (Geschwind, 2008). These subclasses of impairments, or endophenotypes, are also observed at some degree in unaffected family members, but are below threshold for clinical diagnosis (Gottesman and Gould, 2003).

1.2 ASD genetics

ASD-associated variants have been identified over the past 3 decades using various techniques; currently, next-generation sequencing on large cohorts has ushered in a wave of gene discovery that has greatly enhanced our understanding of the inheritance of ASD. Prior work involved the cataloging of ASD-associated major gene disorders, such as Fragile X syndrome and Tuberous Sclerosis (Hatton et al., 2006; Hunt and Shepherd, 1993), cytogenetic analysis, which identified large structural genomic rearrangements, and genetic linkage studies (Abrahams and Geschwind, 2010). Over the last several years, genome wide association studies (GWAS) have revealed a handful of common alleles of modest effect size likely to contribute ASD (Anney et al., 2010; Wang et al., 2009; Weiss et al., 2009). Analysis of copy number variation (CNV) has additionally implicated rare genomic structural changes, both de novo and inherited, of large effect size (Levy et al., 2011; Marshall et al., 2008; Pinto et al., 2010; Sanders et al., 2011; Sebat et al., 2007; Szatmari et al., 2007). Most recently, exome sequencing has lent insight into the contribution of de novo single nucleotide variants (Iossifov et al., 2012; Neale et al., 2012; O'Roak et al., 2012; Sanders et al., 2012). This section will review the major studies

that have identified both common and rare variants associated with ASD and will discuss models for how these variants may contribute to ASD pathology.

The contribution of common alleles vs. rare alleles

The contribution of both common and rare alleles to ASD has been assessed using GWAS and CNV/exome sequencing studies. Given that ASD is highly prevalent, it was initially thought (consistent with the prevailing common variant-common disease model (CVCD)(Risch and Merikangas, 1996)) that common genetic SNP variants, (those occurring in at least 5% (Voineagu, 2012) of the population) would lead to this common disorder.

An alternative model is that rare variants (RVs) with moderate to large effect size lead to ASD (the rare variant common disease model (RVCD) (Bodmer and Bonilla, 2008)). This is supported by mathematical modeling based on recurrence in multiplex families, which posits a relatively large contribution from spontaneous, de novo mutations with lower penetrance in females (Zhao et al., 2007). The contribution of RVs has been tested by measuring the frequency of rare copy number variation and single nucleotide variants (SNV) in cases and controls and is emerging as an exciting area in ASD genetics. Both types of studies have been aided by the availability of large cohorts of ASD and control subjects, specifically the Autism Genetic Resource Exchange (AGRE), Simons Simplex Collection (SSC), Autism Center of Excellence (ACE), and the Autism Genome Project Consortium (AGPC). Findings from these studies are discussed below.

Three large-scale GWAS studies have been conducted to date (Anney et al., 2010; Wang et al., 2009; Weiss et al., 2009) that are adequately powered to detect CVs of modest effect size. Only two variants reached genome wide significance: an intergenic variant, rs4307059, between cadherin 9 (*CDH9*) and cadherin 10 (*CDH10*) (Wang et al., 2009) and rs4141463 in an intronic

region of MACRO domain containing 2 (*MACROD2*) (Anney et al., 2010). An additional intergenic variant, rs10513025, between *SEMA5A* and *TAS2R1* was suggestive of genome-wide significance (p=2.1 E-7) (Weiss et al., 2009).

What conclusions can be made from these GWAS studies? First, the effect size for any single common variant (CV) is quite small, as studies have had the power to detect odds ratios (OR) of greater than 1.5, but have not found such variants. This suggests either widespread epistasis or multiple common variants of small effect size are needed for disease or, alternatively, that the role for CVs in limited. Second, using unaffected relatives as controls, who under some models may harbor a sub-threshold genetic load of associated variants, would decrease the association signal. Studies of endophenotypes or intermediate phenotypes are one strategy that may help in this regard (Geschwind, 2011). Third, the epistatic interaction of combinations of CVs, rather than single variants, may confer disease risk, prompting the need for bioinformatic tools capable of testing combinatorial models. In sum, GWAS studies have not provided evidence that single CVs ranging from modest to large effect contribute significantly to ASD risk. However, at the same time, the cohorts tested have been relatively small compared with the tens of thousands of patients tested in other common diseases (Harold et al., 2009; Ripke et al., 2011)

This has led many to a model whereby RVs (either CNVs or rare SNVs) of moderate to large effect explain a large proportion of ASD heritability (Zhao et al., 2007). Over the past 5 years, six major studies have conducted refined screens of the genome to identify rare copy number variations, both inherited and de novo, in ASD subjects and matched controls. These studies have shed light on the contribution of rare CNVs to ASD pathophysiology, with several themes emerging. First, in all five studies that examined inherited CNVs, inherited CNVs were

equally prevalent in ASD cases versus controls (Levy et al., 2011; Marshall et al., 2008; Sanders et al., 2011; Szatmari et al., 2007). Although one study reports a 1.19 fold increase of CNVs (de novo and inherited) in cases versus controls, this signal is driven by the contribution of rare de novo CNVs, as removing these CNVs from the analysis results in an equal distribution of CNVs between cases and controls (Pinto et al., 2010). Second, the emerging consensus from multiple studies is that larger CNVs, containing more genes, are observed in probands versus controls (Levy et al., 2011; Marshall et al., 2008; Pinto et al., 2010; Sanders et al., 2011). Third, these studies do not consistently find simplex families to harbor many more de novo mutations relative to multiplex families. For example, while two studies report an increased number of de novo events in simplex versus multiplex families (10% simplex versus 3%multiplex (Sebat et al., 2007) and 7% simplex versus 2% multiplex (Marshall et al., 2008)), another reports an even distribution of de novo events across the two types of families (5.6% simplex/5.5% multiplex (Pinto et al., 2010)). Lastly, many CNVs are multigenic, especially in ASD cases, making it difficult to determine the putative causative gene. Determination of pathogenicity of specific genes or pathways may be aided by modeling in animals (Golzio et al., 2012), intersection with other functional data such as gene expression (Luo et al., 2012), and systems biology approaches, as will be discussed below. In any case, these large scale CNV studies have generated the following list of intriguing ASD candidate genes disrupted by rare de novo CNVs in ASD subjects: *A2BP1*, *ANKRD11*, *C16orf72*, *CDH13*, *CDH18*, *DDX53*, *DLGAP2* (Marshall et al., 2008; Pinto et al., 2010), *DPP6*, *DPYD*, *FHIT*, *FLJ16237*, *NLGN4*, *NRXN1*, *SHANK2*, *SHANK3*, *SLC4A10*, *SYNGAP1*, *USP7* (Levy et al., 2011; Sanders et al., 2011).

Advances in next-generation sequencing now permit the most powerful approach to finding de novo RVs. Four independent groups have recently conducted whole exome

sequencing projects using non-overlapping samples (Iossifov et al., 2012; Neale et al., 2012; O'Roak et al., 2012; Sanderson, 2012). Strikingly, across all four studies, the frequency of de novo mutation was equal between ASD and control subjects. Another commonality across studies was the correlation between older fathers and increased number of de novo point mutations, which could help explain the paternal-age dependent risk for ASD (Gabis et al., 2010; Lauritsen et al., 2005; Lundstrom et al., 2010; Reichenberg et al., 2006). Additionally, two studies report an increase in gene-disrupting SNVs in cases versus unaffected siblings, although the overall SNV mutation rate is equal between probands and siblings (Iossifov et al., 2012; Sanders et al., 2012). In one study, there is a significant increase in the number of non-synonymous and nonsense de novo SNVs in cases compared to unaffected sibs when looking across all genes [OR of 1.93 (all non-synonymous to silent SNVs); OR of 4.03 (nonsense/splice site to silent SNVs)] and brain-expressed genes only [OR of 2.22 (all non-synonymous to silent SNVs); OR of 5.65 (nonsense/splice site mutations to silent SNVs)], with silent SNVs showing an equal mutation rate between cases and controls (Sanders et al., 2012). The other study reports a two-fold increase in frame shift, splice site, and nonsense de novo mutations in cases versus controls, although there is an equal distribution of de novo missense mutations in this study (Iossifov et al., 2012). By combining genes that harbor frame shift, splice site or nonsense de novo variants in cases across all four studies, five high-priority genes were identified that were disrupted in two independent probands: *DYRK1A, POGZ*, *SCN2A, KATNAL2* and *CHD8*. There are several interesting lessons from these studies, including the utility of having data from other family members, which can help prioritize variants. One example is that the Wnt/b-catenin signaling pathway was implicated in one study (O'Roak et al., 2012), but another that included a larger cohort of unaffected siblings (Sanders et al., 2012) found that this pathway was over-

represented in the unaffected siblings. These data suggest that more detailed pathway analysis is needed to understand the precise balance of signaling in this complex pathway (Wexler et al., 2011) and its relationship to disease.

The study of rare variants as ASD risk factors poses some challenges. Rareness does not indicate pathogenicity; rare events are seen in controls in addition to ASD subjects, and inherited CNVs, by nature, will be present in the transmitting unaffected parent. Additionally, a variant may be rare to the point of uniqueness for the sample sizes currently being studied, making causation difficult to establish and increasing the number of false negatives. Given these challenges, it is hard to determine which rare variants are risk factors, which modulate risk, and which are unrelated to phenotype. The rarity of these events may preclude using traditional statistical techniques given that these techniques require a much larger sample to prove statistical association with disease (Freimer and Sabatti, 2004). Some reasonable statistical solutions are being developed (Sanders et al., 2012).

One approach to elucidate the intersection of large candidate gene lists is to use system biology techniques to leverage our knowledge of protein interactomes. Toward this end, one group conducted network based analysis of genetic associations (NETBAG) from a list of genes found to harbor de novo CNVs in ASD cases (Levy et al., 2011) and found a preponderance of network genes involved in neuronal motility, targeting of axons, and synapse development (Gilman et al., 2011). Additionally, exome sequencing studies have found that proteins encoded by genes harboring de novo missense or nonsense mutations have a significantly enriched number of protein interactions (Neale et al., 2012) and form protein networks enriched for ASD candidate genes that have specific molecular functions (O'Roak et al., 2012). Another approach is to integrate genetic data with gene expression to identify CNVs that perturb gene expression,

thus validating a functional effect. Such a study recently demonstrated the power of this method and identified several new potential ASD risk CNV (Luo et al., 2012). Moving forward, to fully understand the wealth of genomics data currently being generated, we will need both appropriate statistical techniques and bioinformatics approaches to identify significant points of convergence among candidate genes.

Integrating genetic findings into a notion of ASD genetic architecture

How do these findings inform our genetic models of disease? Several models have been put forth to explain the inheritance of ASD. We discuss here the 'major effect model' and several polygenic models: A combination of CVs (1), a major effect RV in a background of CVs (2), a combination of rare and common variants (3), and an oligogenic 'two hit' model (4). None of these are truly absolute and we expect that a wide range of genetic models will explain ASD in the individual (Geschwind, 2008).

The 'major effect' model proposes that one major insult to the genome is sufficient for the disorder. This scenario is supported by the observation that disruptions of single genes can lead to ASD in an apparently Mendelian fashion with reduced penetrance, as is seen in several syndromic forms of ASD. For example, mutations in *FMR1* (Fragile X syndrome (Hatton et al., 2006)), *MECP2* (Rett Syndrome (Khwaja and Sahin, 2011)), *TSC1* and *TSC2* (Tuberous sclerosis (Khwaja and Sahin, 2011)), *CNTNAP2* (Cortical dysplasia-focal epilepsy syndrome (Strauss et al., 2006)), *DHCR7* (Smith–Lemli–Optiz syndrome (Tierney et al., 2001)), *CACNA1C* (Timothy syndrome (Splawski et al., 2004)) and *PTEN* (Butler et al., 2005) all result in syndromes with phenotypes overlapping those of ASD (Abrahams and Geschwind, 2008). However, each of these syndromes exhibit incomplete penetrance for ASD and variable expressivity. For example, 10% of subjects with *FMR1* mutations do not show any ASD

phenotypes (Iossifov et al., 2012), and those that do express a wide range of phenotypes, with no more than 30% crossing a threshold for clinical diagnosis of ASD (Harris et al., 2008). This incomplete penetrance and variable expressivity suggest that additional factors -genetic, epigenetic, and environmental-modulate the presence of ASD in a subject with a major genetic disruption (Geschwind, 2008). This pattern of highly variable expressivity should not be unexpected even with major effect alleles, as it has been observed frequently in dominantly inherited neurologic diseases, including a wide range of neurodegenerative diseases (Kertesz, 2011). Additional examples of 'major hits' come from early cytogenetic studies. Examples are maternally inherited duplications of 15q11–15q13, deletions of 22q13, deletions of 2q37, and disruptions in 5p15, 17p11 and Xp22 (Vorstman et al., 2006).

An alternative to the 'major effect model' is the polygenic model, in which various combinations of genetic variants in an individual lead to disease. Here, we highlight four, non-exclusive, polygenic models to illustrate the range of likely possibilities. In the first model, ASD results from a combination of CVs that exceed a tolerance threshold. In this model, relatives of ASD subjects carry a subclinical genetic load of ASD associated CVs. Evidence to support this model is that ASD endophenotypes are sometimes observed in relatives, suggesting that subsets of CV combinations are sufficient for endophenotypes (Abrahams and Geschwind, 2008). Additionally, several ASD endophenotypes have a normal distribution in the population, which would be predicted by multiple contributory factors of modest to low effect (Geschwind, 2008). The second and third polygenic models are (1) a RV in a genetic milieu of CVs that results in ASD when the load of CVs is sufficient to exceed an arbitrary threshold and (2) A combination of rare and common variants of various effect sizes that exceed a threshold of tolerance. Shared lines of support for both models are that 1) ASD risk factors, such as 15q11–15q13 (Bucan et al.,

2009) and 16p11.2 (Kumar et al., 2008), that are rare inherited disruptions, are present in both the unaffected parent and the affected offspring. This phenomenon suggests that additional genetic modifiers are needed to confer disease risk 2) De novo CNVs are found in both cases and unaffected controls, again suggesting that additional genetic modifiers are needed for disease state or that some of these variants do not contribute to disease state 3) Neuronal networks identified by bioinformatic analysis of transcriptome data are enriched for ASD associated common and rare variants (Ben-David and Shifman, 2012) 4) ASD-related component phenotypes are present in relatives due to sub-threshold loading of common and rare variants. Additional support for the polygenic models comes from the observation that even rare, de novo nonsense and splice site mutation increase the odds for ASD by an average of only six fold (Iossifov et al., 2012; Sanders et al., 2012). This likely represents a large range of genotype-risk, but suggests that many rare deleterious mutations are not alone sufficient to cause ASD. Another form of the polygenic model involves 'two hits', wherein one RV is tolerated, but two hits leads to a disease state, similar to cancer (Berger et al., 2011). Some examples of this model have been presented (Leblond et al., 2012; O'Roak et al., 2011), and the model is consistent with inherited RVs being present in the transmitting parent (discussed above), de novo CNVs found in unaffected controls, and relatives manifesting subthreshold ASD traits. However, a 'two hit' model is not likely the predominant cause based on recent exome data (Iossifov et al., 2012; Neale et al., 2012; O'Roak et al., 2012; Sanders et al., 2012) and even in cancer, where this model originated, a more continuous model of genetic contribution is now supported (Berger et al., 2011). Taken together, there is the greatest support for a more continuous, and highly heterogeneous, polygenic model in which ASD results from a combination of rare and common variants that build to exceed a clinical threshold in many different combinations

1.3 Emerging biological themes in ASD

ASD genes fall into many potential functional classes; this heterogeneity begs the question, 'How do such diverse mechanisms lead to ASD?' To answer this question, it is critical to identify the points of potential convergence among autism candidate genes in developmental and anatomical terms. Toward this end, expression patterns of ASD genes have been annotated using whole genome transcriptome profiling in blood and brain from ASD versus control subjects (Voineagu, 2012). At the same time, large efforts have been made to build proteomic interactomes of autism candidate genes (Neale et al., 2012; O'Roak et al., 2012; Sakai et al., 2011) to understand how these molecules functionally intersect. These efforts have been concurrent with the development of large protein and RNA expression databases that provide genome-wide spatial and temporal expression information (The Allen Brain Atlas, http://www.brain-map.org/, Gene Paint, http://www.genepaint.org/, The Cerebellar Development Transcriptome Database, http://www.cdtdb.neuroinf.jp/CDT/Top.jsp, Ref-Seq Atlas, http://medicalgenomics.org/rna_seq_atlas, The Human Protein Reference Database (Prasad et al., 2009) http://www.hprd.org/, NIA mouse protein-protein interaction database http://lgsun.grc.nia.nih.gov/mppi/, and the Genes to Cognition database, http://www.g2conline.org).

Effective drug design would be facilitated by convergence at the level of molecular pathways. However, convergence at higher levels is also plausible. In fact, some of the most reproducible clinical signatures have been at the level of brain structure and function. For example, the trajectory of head growth, which corresponds to brain size, seems to be reproducibly abnormal in ASD subjects, who exhibit smaller head circumferences (HC) at birth followed by a burst in HC postnatally, eventually reaching normal size around adolescence

(Courchesne et al., 2003; Redcay and Courchesne, 2005; Sacco et al., 2007). Studies have also repeatedly shown decreases in white matter tracts in autism (Alexander et al., 2007; Barnea-Goraly et al., 2004). Specifically, long-range connections seem to be weakened, while local connections are strengthened (Courchesne and Pierce, 2005; Geschwind and Levitt, 2007). Cortical structure abnormalities, specifically denser and narrower cortical columns, have also been reported (Casanova, 2006), and functional MRI neural signatures in autism are being defined (Kaiser et al., 2010; Pierce, 2011; Scott-Van Zeeland et al., 2010).

Neuronal Cell Adhesion

ASD associated mutations in several proteins involved in cell adhesion include *CNTNAP2*, *CNTN4*, *CNTN6*, *NLGN1-4*, *NRXN1*, *PCDH9*, and *CHL1*. Multiple converging lines of evidence implicate *CNTNAP2* in ASD pathology, including its role in a syndromic form of autism (Strauss et al., 2006), variants found in linkage and association studies (Alarcon et al., 2008; Arking et al., 2008; Bakkaloglu et al., 2008), presence of RVs (O'Roak et al., 2011), its impact in functional MRI readouts in humans (Scott-Van Zeeland et al., 2010), and molecular evidence that its knockout leads to the behavioral manifestation of all three core domains of autism as well as neuronal migration abnormalities (Penagarikano et al., 2011). A member of the neurexin super family, *CNTNAP2* is involved in cell-cell adhesion, clustering of potassium channels at the juxtaparanode (Poliak et al., 1999), neuronal migration and regulation of GABAergic interneuron numbers (Penagarikano et al., 2011). Data supports an additional contactin family member, *CNTN4*, in autism pathophysiology (Fernandez et al., 2008; Glessner et al., 2009; Roohi et al., 2009), although this has been recently challenged (Cottrell et al., 2011). *CNTN6* has also been implicated by CNV studies (Bucan et al., 2009; Glessner et al., 2009; Itsara et al., 2010; Levy et al., 2011; Marshall et al., 2008; Pinto et al., 2010; Sebat et al., 2007;

Szatmari et al., 2007). Both neurexins and neuroligins have been heavily implicated in ASD pathophysiology. Neurexins are located presynaptically and bind to post-synaptically localized neuroligins. These molecules modulate both excitatory and inhibitory synaptic function (Hines et al., 2008). *NRXN1* has been identified as an ASD risk factor by cytogenic analysis (Kim et al., 2008), large scale CNV studies (Glessner et al., 2009; Sanders et al., 2011; Szatmari et al., 2007), and case reports (Zahir et al., 2008). *NLGN*1, 3 and 4 have also been identified in several studies (Glessner et al., 2009; Jamain et al., 2003; Laumonnier et al., 2004; O'Roak et al., 2012; Sanders et al., 2011), and *CNTNAP2* is homologous to drosophila *Neurexin 4* (Zweier et al., 2009). Additional evidence for the role of *NLGNs* and *NRXN1* in ASD involves introduction of ASD-associated variants, knockout, or overexpression of these proteins in mouse models. These studies have recapitulated various aspects of the ASD phenotype (Etherton et al., 2009; Hines et al., 2008; Tabuchi et al., 2007) and have additionally implicated *NLGN2*. *PCDH9* and *CHL1* may also contribute to ASD based on CNV studies (Bucan et al., 2009; Glessner et al., 2009; Itsara et al., 2010; Levy et al., 2011; Marshall et al., 2008; Pinto et al., 2010; Sebat et al., 2007; Szatmari et al., 2007).

Balancing excitation and inhibition

Functional studies in mouse models have suggested that some of the ASD candidates contribute to network dynamics by altering the balance of excitation and inhibition. For example, a slight increase in NLGN2 in mouse reduces the excitation to inhibition ratio by decreasing the ratio of excitatory to inhibitory synapses, increasing inhibitory synaptic contacts, and increasing the frequency of miniature inhibitory PSCs in the frontal cortex (Hines et al., 2008). Additionally, introducing the ASD associated *NLGN3* missense mutation into a mouse increases inhibitory function in cortex (Tabuchi et al., 2007). Similarly, *Nrxn1* alpha knockout

mice exhibit a decrease in hippocampal excitatory function (Etherton et al., 2009). Knocking out *Cntnap2* in a mouse reduces cortical GABAergic interneuron numbers, potentially altering the balance of excitation and inhibition (Penagarikano et al., 2011). Additionally, *Shank3* knockout decreases cortical excitatory transmission (Peca et al., 2011). *Fmr1* knockout mice show several excitatory/inhibitory imbalances, including impaired inhibitory transmission in the amygdala (Olmos-Serrano et al., 2010), decreased excitatory inputs into inhibitory neurons in the cortex (Gibson et al., 2008), and an increased inhibitory transmission in the striatum (Centonze et al., 2008).

There is corroborating data for the role of excitation and inhibition in autism from whole transcriptome studies of human postmortem brain. One recent study used a sophisticated systems biology approach, weighted gene co-expression network analysis (WGCNA), to build transcriptome networks from human postmortem brain samples in ASD and control cases (Voineagu et al., 2011). The top autism associated WGNCA network, enriched for ASD associated GWAS targets, showed high overlap with a previously identified interneuron-related module (Oldham et al., 2008). Understanding how perturbations in this delicate balance of excitation and inhibition lead to disease will be key in understanding ASD pathophysiology. Considerations in this endeavor will include a clear understanding of how deficits affect both microcircuits and more long distance connectivity.

Neuronal Activity and ASD

One potential point of convergence developing from gene finding studies is that autism pathophysiology involves proteins that both modulate neuronal activity and exhibit activity-dependent expression. Of the handful of proteins identified by whole exome sequencing reviewed above, *SCN2A*, *SCN1A*, and *GRIN2B* all code for subunits of synaptic ion channels,

with *SCN2A* and *SCN1A* coding for the alpha subunits of voltage gated sodium channels (O'Roak et al., 2012; Sanders et al., 2012). *GRIN2A*, an NMDA receptor subunit mapping within the 16p11-13 region, was additionally identified in a large scale ASD association study (Barnby et al., 2005). NMDA receptors are ionotropic ion channels that are critical regulators of activity-dependent synaptic plasticity. Other notable ASD candidate genes that code for ion channels are the ionotropic glutatmate receptors, *GRIK2* (Jamain et al., 2002) and *GRIA3* (Jacquemont et al., 2006), and subunits of voltage-dependent calcium channels, *CACNA1C* (Splawski et al., 2004) and *CACNA1H* (Splawski et al., 2006).

ASD candidate genes are also enriched in sets of transcripts regulated by neuronal activity. For example, *UBE3A* (Glessner et al., 2009; Sanders et al., 2011), *DIA1* (Morrow et al., 2008) and *PCDH10* (Morrow et al., 2008), are all regulated by *MEF2A/D*, a transcription factor that plays a major role in activity dependent development of the synapse (Flavell et al., 2008). Moreover, the autism candidate gene *NHE9* is regulated by *NPAS4*, a transcription factor regulated by neuronal activity (Morrow et al., 2008). Lastly, a recent study identified ASD candidate genes *UBE3B*, *CLTCL1*, *NCKAP5L*, and *ZNF18* by whole exome sequencing and found their expression to be regulated by neuronal depolarization (Chahrour et al., 2012). In sum, these results point to a potential contribution of genes regulated by or regulating neuronal activity to autism pathophysiology.

Translation regulation at the postsynaptic density

Another potential point of molecular convergence in autism genetics is activity-dependent protein metabolism at the postsynaptic density, a protein rich specialization at the postsynaptic membrane critical for effective neural transmission. Single gene disorders that intersect with ASD gave us first clues that this process is important in the pathophysiology of

autism. Mutations in *FMR1*, the leading inherited cause of ASD (De Rubeis and Bagni, 2011), results in the absence of FMRP, a key regulator of activity-dependent protein synthesis at the synapse (Bassell and Warren, 2008). FMRP-mediated translation is regulated in an activity dependent manner by the autism candidate gene, *CYFIP1*, located within the 15q11-13 duplication region (Napoli et al., 2008). Recently, whole exome studies have reported an enrichment of FMRP associated genes in the lists of genes disrupted by rare variants in ASD subjects (Iossifov et al., 2012). FMRP is associated with the autism candidate genes *MET* (Campbell et al., 2006), *PTEN*, *TSC1*, *TSC2* and *NF1* (Williams and Hersh, 1998), which are also located within the postsynaptic density (Kelleher and Bear, 2008; Waung and Huber, 2009; Zoghbi and Bear, 2012). These genes are part of the PI3K-AKT-mTOR pathway which is activated by mGluR signaling (Hou and Klann, 2004; Waung and Huber, 2009), is an upstream effector of translation regulation, and is involved in cellular proliferation (Sarbassov et al., 2005). Probands with RVs in several of these genes have been found in the large gene finding studies outlined above (*PTEN* (O'Roak et al., 2012), *TSC* (O'Roak et al., 2012), *MET* (Sanders et al., 2011), *NF1* (Sanders et al., 2011)).

Ubiquitination pathways, which regulate protein metabolism at the postsynaptic density, are also associated with autism. Most notably, *UBE3A*, a gene implicated in the ASD associated disorder, Angelman's syndrome (Abrahams and Geschwind, 2008), is involved in ubiquitination of its target proteins, such as the FMRP translational target *ARC* (Scheiffele and Beg, 2010), which leads to their degradation at excitatory postsynaptic densities. RVs in *UBE3A* and associated proteins have been found in recent large-scale CNV studies (*UBE3A*, *PARK2*, *RFWD2*, *FBXO40* (Glessner et al., 2009); *USP7*, *UBE3A* (Sanders et al., 2011)).

Although not directly involved in protein metabolism, another large group of ASD

proteins converge at excitatory postsynaptic densities. The most notable are the synaptic scaffolding proteins, SHANK2 and 3, identified as ASD risk factors in several studies (Berkel et al., 2010; Durand et al., 2007; Leblond et al., 2012; Pinto et al., 2010). Recently, an autism protein interactome built using a human yeast two hybrid screen and 35 ASD implicated proteins as bait, found that a large group of PSD localized ASD-associated proteins interact. This study additionally confirmed the SHANK3-PSD95 interaction, added nine additional protein binding partners to this interaction, and identified novel PSD interactions such as the SHANK3-TSC1-ACTN1-HOMER3 interaction (Sakai et al., 2011). In sum, these data point to the excitatory post synaptic density as a hot spot for ASD associated molecules, making it a potential target for drug discovery.

1.4 Using mouse models to understand ASD

Definitive demonstration of convergence will require experiments testing causality in model systems. Currently, there are several vertebrate and invertebrate systems including drosphila (Ishizuka et al., 2002; Zhang et al., 2001; Zweier et al., 2009), zebrafish (Golzio et al., 2012), and the mouse which provide a tractable genetic and neurobiological systems for understanding the biological impact of specific susceptibility from the molecular to the complex behavioral level. Most modeling has been done in the mouse, in which many of the complex behaviors involved in autism can be tested, including social responsiveness (Silverman et al., 2010). However, since the common ancestor of mouse and human is separated by 60 million years of evolution, it must be realized that it is not a forgone conclusion that disruption of a gene or genes that cause ASD in humans will lead to similar behaviors in mouse. There is little known about the parallels between neural systems serving social cognition and communication in mouse and human. So, it is reasonable to start without many preconceived assumptions and

view the mouse, similar to the fly or zebrafish, as a genetically sensitized system for exploring the molecular, cellular and circuit level mechanisms of ASD-related genetic variation.

Crawley and colleagues have elegantly outlined three basic levels of model validity: 1) construct validity (contain the same biological perturbation as the human disorder, for instance genetic or anatomical); 2) face validity (display endophenotypes/phenotypes that mirror the human disorder); and 3) predictive validity (similar response to treatments effective in humans) (Silverman et al., 2010). Using this construct, it is remarkable that several ASD associated genetic variants have recapitulated many human ASD endophenotypes when modeled in a mouse including *Cntnap2* knockout (altered vocalization, restrictive/repetitive, social) (Penagarikano et al., 2011), *Nlgn4* knockout (altered vocalization and social) (Jamain et al., 2008), *En2* knockout (restrictive/repetitive, social) (Cheh et al., 2006; Moy et al., 2009), 15q11-13 duplication; chromosome 7 in mouse (altered vocalization, restrictive/repetitive, social) (Nakatani et al., 2009), *Gabrb3* knockout (restrictive/repetitive, social) (DeLorey et al., 2008), *Oxt* knockout (altered vocalization, social) (Crawley et al., 2007; Ferguson et al., 2000; Winslow et al., 2000), *Avpr1b* knockout (altered vocalization, social) (Scattoni et al., 2008; Wersinger et al., 2002) and *Fgf17* knockout (altered vocalization, social) (Scearce-Levie et al., 2008). Inbred strains of mice, such as BTBR, BALB, and C58/J also display ASD endophenotypes (Silverman et al., 2010). However, it is unclear exactly how a behavior in mouse, such as deficits in ultrasonic vocalization, translates into a human phenotype, such as language delay. Indeed, disparity in the molecular, anatomical and neuronal circuitry between mouse and humans is likely and must be interpreted with caution. Keeping these caveats in mind, modeling of ASD variants in mouse is proving to be an exceptionally useful tool in understanding potential ASD mechanisms. It is hoped that combining mouse models and in vitro models will facilitate finding convergence

points, especially at the molecular level, and will provide a tractable avenue for pharmaceutical intervention.

1.5 Fragile X Syndrome and ASD

Fragile X mental retardation syndrome (FXS) is the leading monogenic cause of autism spectrum disorders (Hatton et al., 2006) and mental retardation (Jacquemont et al., 2007). FXS is an X-linked disorder which results from FMR1 gene silencing due to methylation of a trinucleotide CGG repeat expansion in the 5' UTR region of the FMR1 gene. Up to half of those with FXS are diagnosed with ASD, exhibiting repetitive behaviors, impaired communication and social deficits (Moss and Howlin, 2009). The grand majority of FXS subjects that do not meet DSMIV criteria for ASD exhibit ASD-associated behaviors (Bassell and Warren, 2008).

Although discovered over 20 years ago, progress has been slow in developing a clear picture of FMRP biology. Here, we highlight consistent findings regarding FMRP function. FMRP binds 3% of brain mRNAs and is involved in mRNA stability, translation, and transport, shuttling between the nucleus and cytoplasm in RNA granules (Bassell and Warren, 2008; De Rubeis and Bagni, 2011). FMRP protein is present in stress granules and P bodies in addition to transport granules (Anderson and Kedersha, 2006; Kanai et al., 2004; Zalfa et al., 2006). Protein profiling experiments show FMRP expression restricted to messenger ribonuclear protein complexes (mRNPs), polyribsomes, or distributed in both, likely reflecting heterogeneous FMRP function (Brown et al., 2001; Napoli et al., 2008; Stefani et al., 2004; Zalfa et al., 2003). FMRP plays a role in both basal (Gross and Bassell, 2011; Osterweil et al., 2010; Qin et al., 2005) and activity dependent general translation (Greenough et al., 2001; Muddashetty et al., 2007), although the direction of its effect on translation is nuanced, with FMRP knockout causing increases in basal translation, decreases in activity-dependent translation, and increases and

decreases in the translation of specific targets (Brown et al., 2001; Muddashetty et al., 2007) .

FMRP regulates a subset of well-validated mRNA targets (De Rubeis and Bagni, 2011). FMRP both stabilizes (Zalfa et al., 2007) and affects the translation of PSD-95 (Muddashetty et al., 2007; Todd et al., 2003), transports and regulates the translation of both *Map1b* and *Camk2a* (Dictenberg et al., 2008; Hou et al., 2006; Zalfa et al., 2003), transports *Sapap4* (Dictenberg et al., 2008) and *Rgs5* (Miyashiro et al., 2003), and regulates the translation of *Arc* and *App* (Lee et al., 2010; Zalfa et al., 2003). The most consistent histological result of FMRP loss is an increase in the density, length and immature structure of dendritic spines, which is observed in both mouse and human (Cruz-Martin et al., 2010; Galvez and Greenough, 2005; Irwin et al., 2001; McKinney et al., 2005).

FMRP ablation in mouse leads to various behavioral abnormalities, although results are highly dependent on genetic background (Spencer et al., 2011). Behavioral phenotypes include disrupted social behavior (Spencer et al., 2005; Spencer et al., 2008), audiogenic seizures (Musumeci et al., 2000), decreased acoustic startle response at high decibels (Nielsen et al., 2002), increased or decreased prepulse inhibition (Nielsen et al., 2002; Spencer et al., 2006), increased repetitive behavior as measured by increased digging in the marble burying test and repetitive behavior in the open field (Spencer et al., 2011), decreased anxiety (Peier et al., 2000; Yan et al., 2004), and impaired fear memory (Zhao et al., 2005). Interestingly, a Knock-in mouse model of FXS, I304N, which replicates a single FXS patient in which an isoleucine to asparagine substitution is made, disallows association of FMRP with polyribosomes and RNA and recapitulates the grand majority of the behavioral deficits reported in *Fmr1* null mice (Zang et al., 2009).

1.6 JAKMIP1 as an FMRP-related ASD candidate gene

Fragile X mental retardation syndrome (FXS) and maternally inherited dup (15q11-13) are known highly penetrant mutations with clear association with ASD (Cook et al., 1997; Hatton et al., 2006; Rogers et al., 2001; Schroer et al., 1998). The 15q11-13 duplicated region often contains *CYFIP1,* which regulates FMRP-dependent translation at the synapse (Napoli et al., 2008) and is also over-expressed in patients with (dup) 15q11-13 (Nishimura et al., 2007). Integrating expression profiling in lymphoblastoid cell lines from patients with two forms of ASD, FXS and (dup) 15q11-13, with *in vitro* and *in vivo* studies in neural tissue, *JAKMIP1* was found to be dysregulated in both of these monogenic forms of ASD (Nishimura et al., 2007). Moreover, *JAKMIP1* RNA is reduced in the frontal cortex of postmortem brains of patients with autism and 15q duplications that include *CYFIP1* (Oguro-Ando and Geschwind, unpublished), extending these observations to brain. Additional genetic evidence supporting a role for *JAKMIP1* in ASD pathophysiology comes from recent observations that *JAKMIP1* is contained within *de novo* CNVs in two subjects with ASD (Sebat et al., 2007; Szatmari et al., 2007), and a 4 kb deletion removing two exons of JAKMIP1 was recently found in a female autistic individual, although a JAKMIP1 CNV was also found in a control subject (Hedges et al., 2012). JAKMIP1 may also play a more global role in neurodevelopmental and neuropsychiatric disorders, as one study found that *JAKMIP1* was hypermethylated in the frontal cortex of post mortem tissue from bipolar, schizophrenic, and major-psychosis female subjects (Mill et al., 2008). However, JAKMIP1 function in the CNS, and more specifically the molecular relationship between JAKMIP1 and FMRP, remains elusive.

JAKMIP1 is a member of a family of three JAKMIPs that are expressed primarily in neural and lymphoid tissues and are conserved across vertebrates (Steindler et al., 2004). The

JAKMIPs contain coiled coils that facilitate dimerization, but these proteins do not contain other known functional domains (Steindler et al., 2004). In some non-neural systems, JAKMIP1 binds to the FERM domain of janus kinase 1 (JAK1) and tyrosine kinase 2 (TYK2), both janus kinases, at its C-terminal (C-ter) region and interacts with microtubules, most likely through kinesin-1 (Vidal et al., 2007), at its N-terminal (N-ter) region (Steindler et al., 2004). Additionally, JAKMIP1 appears to be bidirectionally mobile in the dendrites of cultured hippocampal neurons (Vidal et al., 2007) and shows high expression in dendritic shafts (Vidal et al., 2009). One study also suggests that JAKMIP1 transports and regulates the expression of $GABA_B$ receptor mRNA and protein (Vidal et al., 2007). Other data support an RNA-binding role for JAKMIP1, as it binds to synthetic RNA polymers (Couve et al., 2004). However, other than GABABR1, GABABR2, and kinesin-1, none of its protein or RNA interactors have been identified in a neural system (Couve et al., 2004; Vidal et al., 2008; Vidal et al., 2007). Although some recent progress has been made to uncover JAKMIP1's neural function (Vidal et al., 2012), its role in central nervous system development and its relationship to FMRP function remains essentially unknown.

1.7 Outline of This Study

Given JAKMIP1's strong relationship to the ASD-associated disorders, FXS and maternally inherited dup (15q11-13), as well as other neuropsychiatric illnesses, establishing its role in CNS development would increase our understanding of ASD pathophysiology and facilitate drug discovery. Here, I took an unbiased, multilevel approach to elucidate the developmental role of JAKMIP1.

I used Multidimensional Protein Identification Technology (MudPIT) to ascertain JAKMIP1's proteomic interactome at a time and place where JAKMIP1 is prominently

expressed during mammalian brain development. Identification and validation of high confidence interactors along with gene ontology analysis directed us toward JAKMIP1's involvement in translation and association with an FMRP RNP complex.

I took a multifaceted approach to test JAKMIP1's relationship to an FMRP RNP complex and its regulation of translation. To test JAKMIP1's role in neuronal translation, we assayed JAKMIP1's contribution to nascent translation in differentiated neurons, determined JAKMIP1's association with polyribosomes *in vivo* and in an engineered cell culture system, tested JAKMIP1's membership in puromycin-disrupted polyribosomes, and conducted immunocytochemistry experiments to determine if JAKMIP1 colocalizes with the translational machinery. To ascertain JAKMIP1's involvement with an FMRP RNP complex, we performed JAKMIP1-FMRP co-immunoprecipitation in postnatal neocortices, tested JAKMIP1's ability to bind and transport FMRP's mRNA translational targets, and determined JAKMIP1's affect on these targets' protein expression in whole cortex and at the synapse. To understand JAKMIP1's role in FMRP and ASD-related behavior, we characterized the behavior of a novel *Jakmip1* knockout mouse. We, additionally, surveyed the cortical, striatum, hippocampal, and cerebellar transcriptome of these mice and compared them to transcriptome signatures of models of Fragile X syndrome.

By testing JAKMIP1 function from multiple angles and levels, a clear picture of JAKMIP1's role in FMRP translational regulation has emerged. This work introduces JAKMIP1 as a novel FMRP interactor and opens the door for JAKMIP1-related targeted therapeutics for FXS, maternally inherited dup (15q11-13), and ASD subjects.

Chapter 2: JAKMIP1 expression: when and where

2.1 Introduction

Although aspects of JAKMIP1 function have been studied, little is known about its developmental expression or regulation. Because autism is a neurodevelopmental disorder, it is critical to understand the developmental context under which an ASD candidate gene is operating, as cellular and anatomical localization as well as expression levels are critical variables in central nervous system function. This first step is descriptive, but foundational in nature.

We determined JAKMIP1's protein expression pattern during development and adulthood in the cortex and cerebellum. We chose cortex, as JAKMIP1 protein is decreased in the neocortex of *Fmr1* KO mice (Nishimura et al., 2007) and cortical dendritic spine abnormalities are one of the most reproducible and robust phenotypes in both *Fmr1* KO mice and FXS patients (Bagni and Greenough, 2005; Cruz-Martin et al., 2010; Galvez and Greenough, 2005; Irwin et al., 2001; McKinney et al., 2005). We examined JAKMIP1's cerebellum expression as FMRP is highly expressed in cerebellar Purkinje cells (Tamanini et al., 1997), both *Fmr1* knockout mice and FXS patients show cerebellum-mediated associative learning impairments (Koekkoek et al., 2005), and loss of FMRP leads to Purkinje cell dendritic spine abnormalities (Koekkoek et al., 2005).

In both the cortex and the cerebellum, we determined JAKMIP1's neuronal sub-type expression and the cortical or cerebellar layer(s) that JAKMIP1 is expressed in. Understanding JAKMIP1's cellular context orients us its function as different neuronal subtypes, such as GABAergic and glutamatergic cells, have specific roles and well-defined connections. We, additionally, determined JAKMIP1's protein and RNA expression during mammalian neural cell

differentiation, as timing of gene expression during cell fate informs function, and genes involved in differentiation have recently been implicated in ASD (Konopka et al., 2012).

We conducted the majority of our studies using mouse brain tissue, with notable exceptions including differentiation and protein expression studies in which human brain was also used. We chose to use mouse because it is a tractable model system and many pathways involved in brain development (Monuki and Walsh, 2001) and JAKMIP1 itself are conserved between mouse and human (Costa et al., 2007). Additionally, mouse models are frequently used to study autism etiology, both from a behavioral and biological standpoint (Chapter 1: 1.4).

To study JAKMIP1, we obtained two published antibodies, anti-JAKMIP1, $J1_{269\text{-}286}$ and anti-JAKMIP1, $J1_{609\text{-}626}$ (Steindler et al., 2004), henceforth referred to as JAKMIP1 #1 and #3, respectively. Both are specific to JAKMIP1 and do not recognize JAKMIP1 family members, JAKMIP2 and JAKMIP3. JAKMIP1 #1 successfully recognizes JAKMIP1 in multiple cell types including Jurkat cells, T cell blasts, B lymphoblasts, a natural killer cell line, rat pheochromocytoma P12 cells, and adult mouse brain extract (Steindler et al. 2004). Moreover, we have found that JAKMIP1 #1 immunoprecipitates JAKMIP1 more robustly than any other protein by mass spectrometry and recognizes human JAKMIP1 overexpressed in a cell system. For protein expression profiling, we have additionally used a commercial antibody (Rabbit anti JAKMIP1, Proteintech group, Chicago, IL), henceforth referred to as JAKMIP1 #2. We found that JAKMIP1 #2 successfully recognizes JAKMIP1 protein immunoprecipitated by JAKMIP1#1 and shows an absence of JAKMIP1 protein signal in *Jakmip1* knockout mice brains compared with wild-type littermate controls.

We focused our protein expression studies on canonical JAKMIP1 isoform A. This isoform is highly conserved between mouse and human, having the same length (626 amino

acids), 95% protein sequence homology, an 83% homologous mRNA transcript, and containing the same protein and RNA binding domains (Costa et al., 2007; Steindler et al., 2004). All antibodies successfully recognize this isoform.

In this Chapter, we demonstrate the following points. JAKMIP1 protein shows a decrease of expression from development to adulthood in mouse and human cortex and cerebellum, with a postnatal burst of expression in the mouse neocortex concomitant with neurite outgrowth and synapse development. During this postnatal burst of expression, JAKMIP1 is expressed in the nuclei and large debris, synapses, and light membranes. JAKMIP1 is expressed across neocortical layers, where it is predominantly present in glutamatergic projection neurons, rarely colocalizing with GABAergic interneurons both during development and adulthood. In the cerebellum, JAKMIP1 is expressed in the Purkinje cell layer, and broadly in Purkinje cell soma and dendrites. Lastly, JAKMIP1 shows a large increase in expression during cell differentiation. These findings provide a neurological context for JAKMIP1, critical for understanding its function.

2.2 JAKMIP1's mammalian cortical expression

Jakmip1 is expressed in neural tissue and is enriched in neurons (Cahoy et al., 2008). *Jakmip1* mRNA transcript is present and shows neural-specificity at embryonic day 14.5 in mouse (http://www.genepaint.org) and is expressed pan neuronally in the adult mouse brain (http://www.brain-map.org). Moreover, northern blot analysis shows that *Jakmip1's* mRNA transcript is expressed much more highly in human and mouse brain tissue than in peripheral tissues (Steindler et al., 2004). We extended these findings by conducting an in depth characterization of the time and place of JAKMIP1 expression in the mammalian neocortex. We determined when JAKMIP1 protein is expressed most highly in human and mouse neocortex

during development. During its time of greatest expression, we ascertained JAKMIP1's subcellular expression pattern using fractionation. Finally, we conducted an immunohistochemical analysis of JAKMIP1's cortical expression during its developmental expression peak and in adulthood.

To characterize the developmental expression pattern of JAKMIP1, we harvested neocortices from wild-type mice in triplicate throughout postnatal development into late adulthood. We started from postnatal day one (p1), which, based on our preliminary data, is early enough to capture JAKMIP1's expression peak, which we estimated to be near the end of the first postnatal week. We sampled more densely from p8 to p14 to capture transient bursts of JAKMIP1 during this critical developmental window when processes such as neurite outgrowth and synapse development are occurring (Judson et al., 2009). Protein fraction S2 was interrogated by western blotting (Methods), as JAKMIP1 is enriched in this fraction (Vidal et al., 2007). We additionally tested JAKMIP1 expression in neocortical tissue from human fetal and adult subjects using two independent antibodies against JAKMIP1. Paucity of human tissue precluded conducting a time series analysis as was done in the mouse. We found that JAKMIP1 bursts in expression from p8 to p14, after which its abundance diminishes (Figure 2-1, A). We observed scarce levels of JAKMIP1 into late adulthood (p60-p120, data not shown). JAKMIP1 demonstrated a similar attenuation from development to adulthood in human neocortical tissue (Figure 2-1, B).

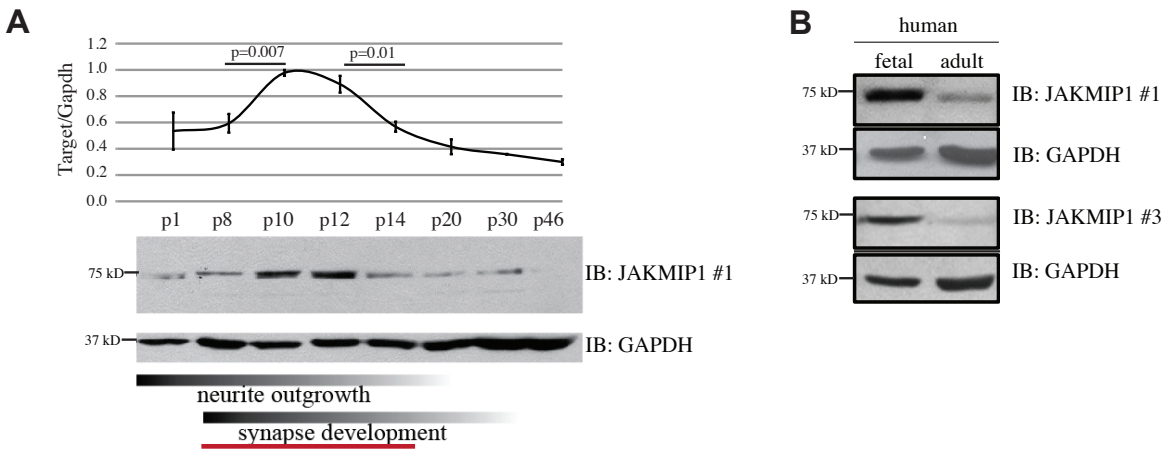

Figure 2-1. JAKMIP1 expression during neocortical development. (A) JAKMIP1 bursts in expression during the second postnatal week in mouse neocortex. Upper graph displays relative JAKMIP1 protein levels between p1 and p46. The Y axis represents normalized values from Image J densitometry analysis of JAKMIP1 protein levels. Signal is normalized to corresponding GADPH signal and the highest value of the series is set to 1. A representative western blot is shown below. There is a significant increase in JAKMIP1 expression between p8 and p10 (65% increase, two sample, two-tailed t test) followed by a significant decrease in expression from p12 to p14 (36% decrease, two sample, two tailed t test). Error bars are +/- SEM. (B) JAKMIP1 decreases in expression during neocortical development in human. Protein from human fetal cortex (20 gestational weeks) or adult cortex (47 years) was immunoblotted for JAKMIP1 or GAPDH (loading control).

JAKMIP1's subcellular location during its time of peak expression provides a cellular context for JAKMIP1 function. To ascertain this, we conducted subcellular fractionation in mouse neocortices during JAKMIP1's postnatal burst of expression (Figure 2-1, A) using established protocols (Hallett et al., 2008). We immunoblotted fractions for JAKMIP1 and DDX5, a novel interactor which we identified by mass spectrometry (Table 3-1). We additionally probed for PSD95, a marker of synaptosomal membranes and an experimental positive control, as well as βtubulin and GAPDH, which serve as loading controls. We found that JAKMIP1 is expressed in the nuclei (P1), synapses (P2, LP1, LS1), and light membranes (P3) as well as intermediate fractions S1 and S2 (Figure 2-2). JAKMIP1's subcellular expression profile is nearly identical to that of its protein binding partner, DDX5 (Figure 2-2).

PSD95 was expressed most highly in synaptosomal membrane fractions, P2 and LP1, confirming the efficacy of the fractionation.

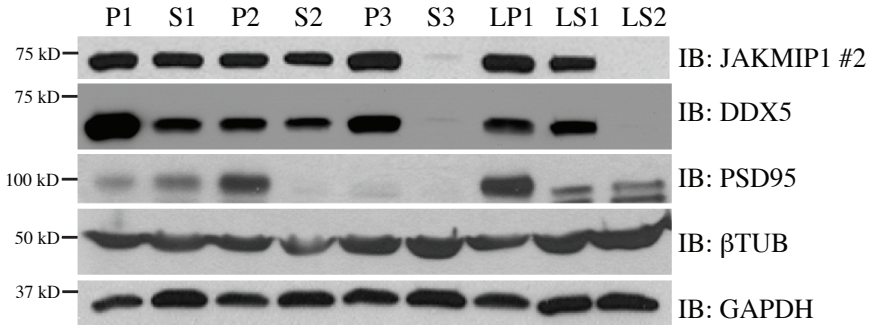

Figure 2-2. JAKMIP1 is expressed across subcellular fractions in mouse postnatal neocortex. Subcellular fractionation was conducted using C57BL/6 mouse postnatal neocortices. Subcellular fractions were immmunoblotted (IB) for JAKMIP1, DDX5 (a JAKMIP1 protein interactor), PSD95 (positive control) and βTUB and GAPDH (loading controls). Fractions are: P1 (nuclei and large debris), P2 (crude synaptosomal membranes), P3 (light membranes), S3 (cytosol), LP1 (synaptosomal membranes), LS1 (synapses minus membranes), LS2 (cytosol of synapes). All other fractions are obtained from intermediate fractionation steps.

Inspection of microarray data from sorted neurons indicates that *Jakmip1* mRNA is enriched in neurons postnatally (Cahoy et al., 2008), but the particular subset of neurons and cortical layers in which JAKMIP1 is expressed is not well known. To determine JAKMIP1's cortical layer expression, we conducted double label immunohistochemistry during JAKMIP1's postnatal burst of expression and in adult brains. Two cortical layer markers, cut-like homeobox 1 (CUX1) and forkhead box P2 (FOXP2), were used to determine if JAKMIP1 shows layer-specific expression or is distributed across layers. FOXP2 expression is restricted to layer VI, while CUX1 is expressed in layers II through IV in mouse neocortex (Molyneaux et al., 2007).

We found that JAKMIP1 is expressed across cortical layers in both postnatal (Figure 2-3, A) and adult (Figure 2-3, B) animals.

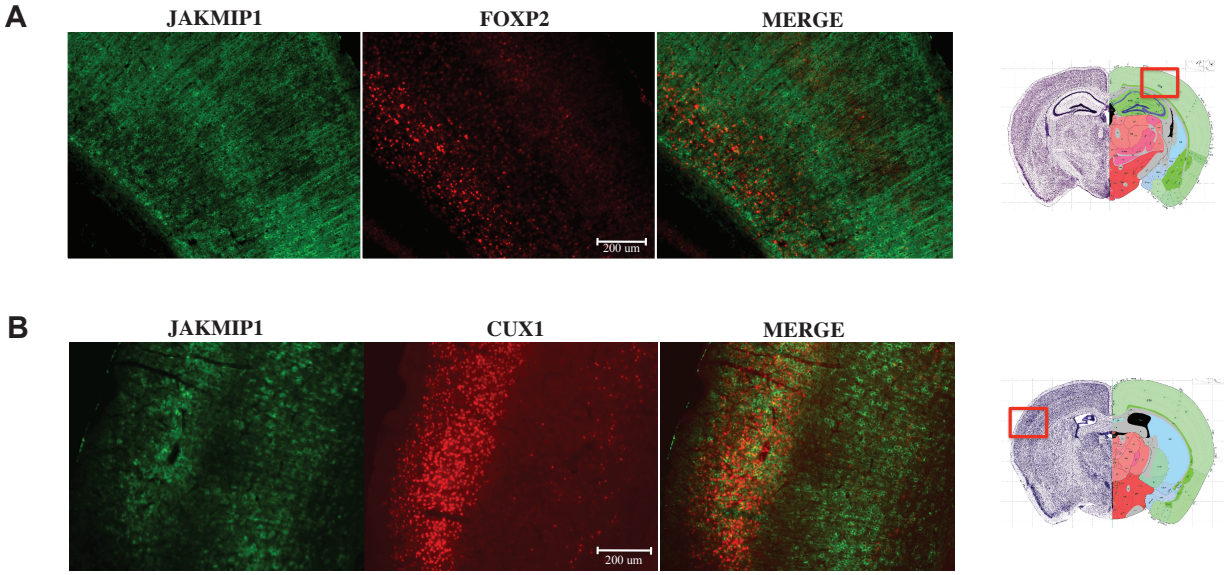

Figure 2-3. JAKMIP1 is expressed broadly throughout the cortex. (A) JAKMIP1 and FOXP2, a cortical layer VI marker, colocalize in postnatal C57BL/6 mouse neocortex. (B) JAKMIP1 and CUX1, a cortical layer II-IV marker, colocalize in adult mouse neocortex. Immunohistochemistry was performed using JAKMIP1#1 on coronal brain sections. Representative stainings are shown. Right-most images depict level of brain section, with region displayed outlined in red. Coronal mouse atlas images are from Allen Mouse Brain Atlas [Internet]. Seattle (WA): Allen Institute for Brain Science. ©2009. Available from: http://mouse.brain-map.org.

To test JAKMIP1's presence in glutamatergic projection neurons of the cortex we conducted double label immunohistochemistry using the markers forkhead box P1 (FOXP1) and neurofilament H non-phosphorylated protein (SMI-32) both in postnatal and adult tissue. FOXP1 is a transcription factor that is expressed postnatally in corticocortical projection neurons of layers layers III-V that are SATB2-positive/CTIP2-negative and in layerVIa corticothalamic projection neurons that are TBR1-positive (Hisaoka et al., 2010). SMI-32 is a neurofilament protein that labels the dendrites and cell body of cortical pyramidal neurons in layers III, V, and VI (van der Gucht et al., 2001). We additionally conducted double label immunohistochemistry with a marker of GABAergic interneurons, calretinin, in adult tissue, as sub-type specific

expression of GABAergic interneuron markers occurs after several weeks of postnatal development (Wonders and Anderson, 2006). We found that JAKMIP1 is largely localized to glutamatergic projection neurons in postnatal (Figure 2-4, A) and adult (Figure 2-4, B) mouse neocortex, and rarely localizes with GABAergic interneurons (Figure 2-4, C).

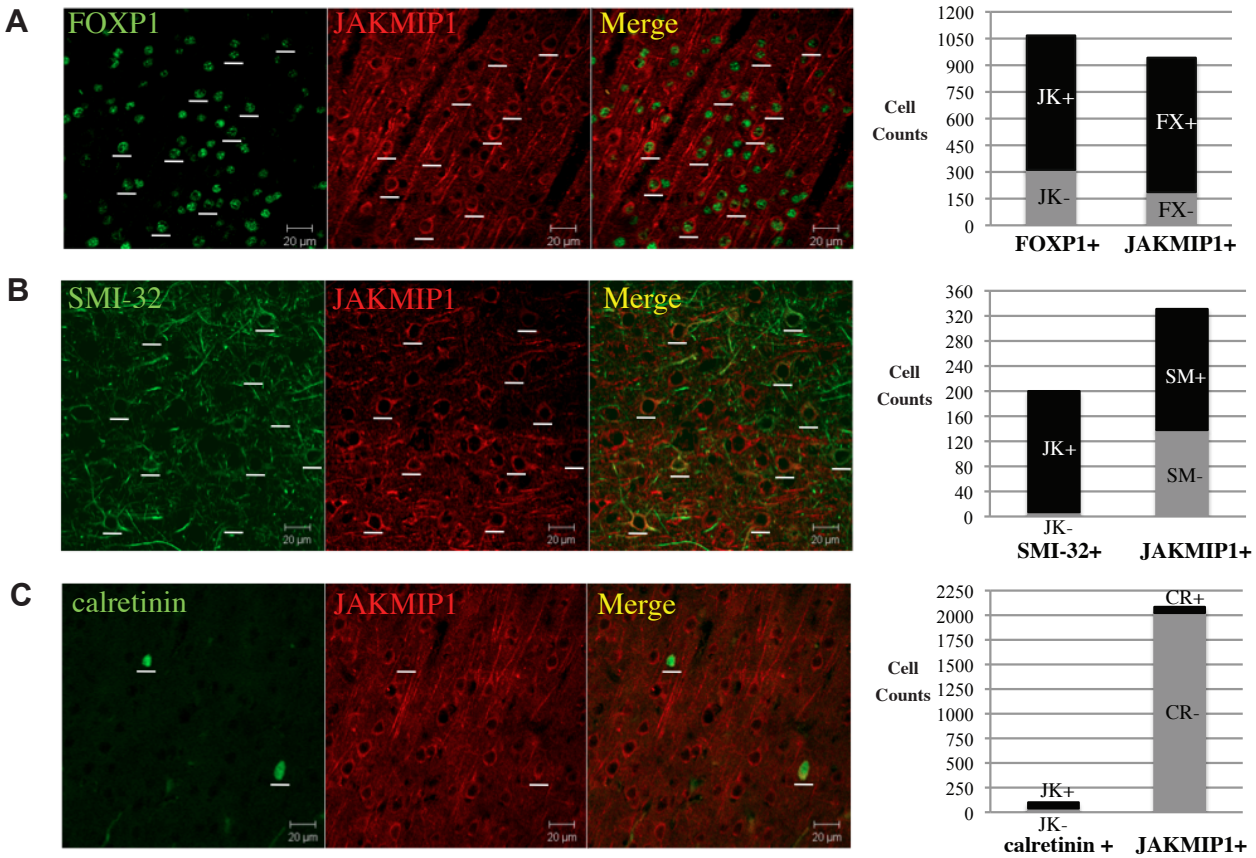

Figure 2-4. JAKMIP1 is expressed predominantly in glutamatergic projection neurons of mouse cortex. (A) JAKMIP1 and FOXP1, a glutamatergic projection neuron marker, colocalize in postnatal C57BL/6 mouse neocortex. (B) JAKMIP1 and SMI-32, a glutamatergic projection neuron marker, colocalize in adult C57BL/6 mouse neocortex. (C) JAKMIP1 rarely colocalizes with calretinin, a GABAergic interneuron marker, in adult C57BL/6 mouse neocortex. Immunohistochemistry was performed using JAKMIP1#1 . Representative stainings are shown. Right-most graphs depict the amount of cells double (black bars) or singly labeled (gray bars). JK is JAKMIP1, FX is FOXP1, SM is SMI-32, and CR is calretinin.

2.3 JAKMIP1's mammalian cerebellar expression

FMRP has high expression in the cerebellum. As such, we tested JAKMIP1's protein expression during human and mouse cerebellum development and its cerebellar layer and neuronal subtype expression in the developing and adult mouse.

To characterize the developmental expression pattern of JAKMIP1, we harvested cerebellar tissue from wild-type mice collected in triplicate throughout postnatal development. Protein fraction S2 was interrogated by western blotting, as above (Section 2.2). We additionally tested JAKMIP1's expression in cerebellar tissue from human fetal and adult subjects using two independent antibodies against JAKMIP1. We found that JAKMIP1 shows a gradual and significant decrease in expression over the course of mouse cerebellar development (Figure 2-5, A). JAKMIP1 continues to decrease in expression into late adulthood (p60-p120, data not shown). Similarly, human cerebellar tissue exhibits decreases in JAKMIP1 expression from development to adulthood (Figure 2-5, B).

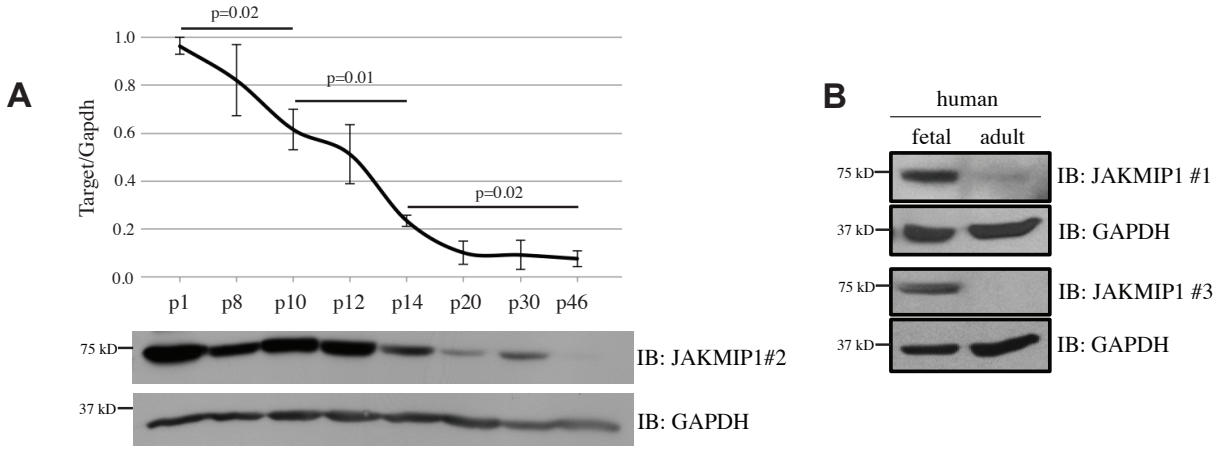

Figure 2-5. JAKMIP1 expression during cerebellar development. (A) JAKMIP1 decreases in expression during cerebellar development. Upper graph displays relative JAKMIP1 protein levels between p1 and p46. The Y axis represents normalized values from Image J densitometry analysis of JAKMIP1 protein levels. Signal is normalized to corresponding GADPH signal and the highest value of the series is set to 1. A representative western blot is shown below. Significant decreases between consecutive timepoints are shown (two sample, two tailed t test). Error bars are +/- SEM. (B) JAKMIP1 decreases in expression during cerebellar development in human. Protein from human fetal cerebellum (19 gestational weeks) or adult cerebellum was immunoblotted for JAKMIP1 or GAPDH (loading control).

The cerebellar cortex is composed of three layers, the granular layer, the Purkinje cell layer and the molecular layer, containing distinct neuronal subtypes, most prominently Purkinje and granule cells (Llinas RR, 2004). We determined in which cerebellar layer (s) JAKMIP1 is expressed during postnatal development, a time concurrent with high JAKMIP1 expression in this brain structure (Figure 2-5, A). To do this, we conducted double label immunohistochemistry for JAKMIP1 and vesicular glutamate transporter 1 (VGLUT1). VGLUT1 associates predominantly with synaptic vesicle membranes and aids in the transport of glutamate (Aihara et al., 2000). In the cerebellum, VGLUT1 is expressed in glutamatergic granule cells, whose cell bodies are located in the granular cell layer and whose axons are the parallel fibers of the molecular layer (Llinas RR, 2004). We found that JAKMIP1 is expressed

largely in the Purkinje cell layer as well as the molecular layer, where the dendrites of Purkinje cells project and receive inputs from the parallel fibers (Figure 2-6).

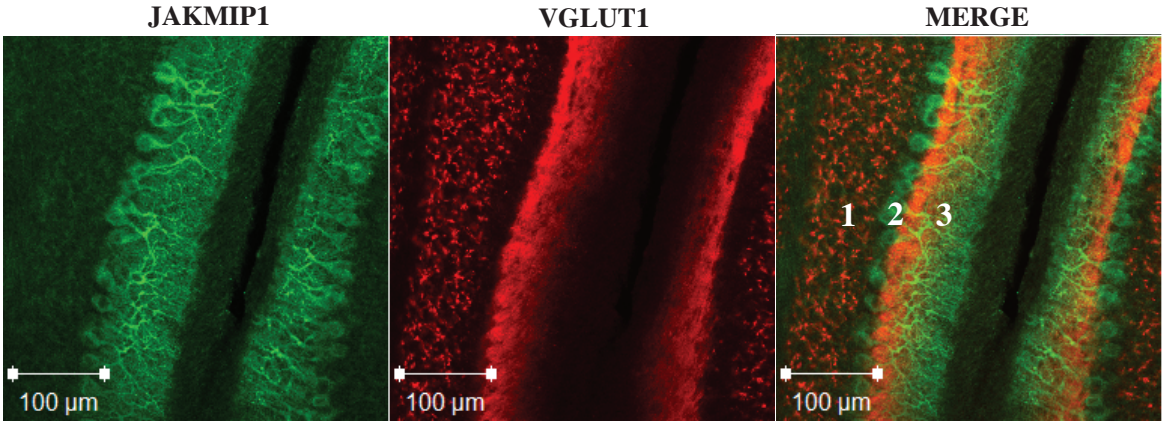

Figure 2-6. JAKMIP1 is expressed in the Purkinje and molecular cell layer of the cerebellar cortex. Postnatal C57BL/6 mouse cerebellar tissue was immunostained with JAKMIP1 (left) and VGLUT1 (middle). Immunohistochemistry was performed using JAKMIP1 #1 on coronal brain sections. Representative stainings are shown. Cerebellar cell layers are denoted on the merged image (right) as follows: 1 is the granular layer, 2 is the Purkinje cell layer, 3 is the molecular layer.

We further explored JAKMIP1's expression in Purkinje cells by conducting double label immunohistochemistry in both postnatal and adult mouse tissue for JAKMIP1 and Calbindin-D28k. Calbindin is a calcium binding protein that is reliably expressed in Purkinje cells (Whitney et al., 2008). We found that JAKMIP1 colocalizes with Calbindin, and therefore Purkinje cells, during both postnatal development (Figure 2-7, A) and adulthood (Figure 2-7, B).

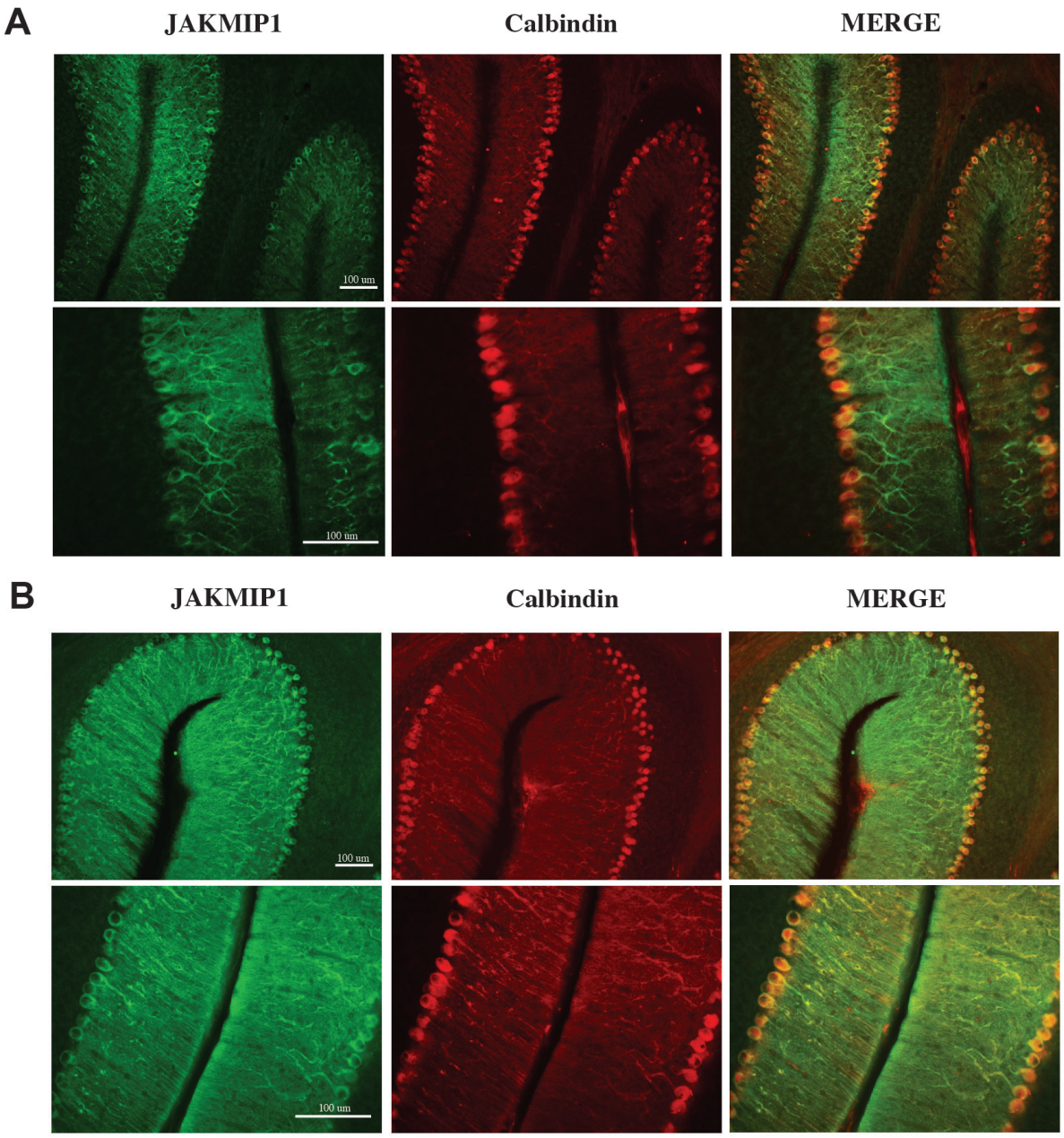

Figure 2-7. JAKMIP1 is expressed in Purkinje cells of the cerebellum. (A) Postnatal C57BL/6 mouse cerebellar tissue was immunostained with JAKMIP1 (left) and Calbindin (middle). (B) Adult mouse cerebellar tissue was immunostained with JAKMIP1 (left) and Calbindin (middle). Immunohistochemistry was performed using JAKMIP1#1 on coronal brain sections. Representative stainings are shown.

2.4 JAKMIP1's expression during differentiation

We ascertained JAKMIP1's expression profile during neural cell differentiation using differentiated mouse and human neural progenitor cells as well as transcriptional profiles from midgestation human brain. We determined JAKMIP1 protein expression throughout the first week and after three weeks of wild-type mouse neural cell differentiation by western blotting. We found that JAKMIP1 protein is not expressed in undifferentiated cells, but begins to show expression at the end of the first week of differentiation. JAKMIP1 demonstrates its highest expression after three weeks of differentiation (Figure 2-8, A). In a separate experiment, we determined *Jakmip1* RNA levels in undifferentiated (week 0) and differentiated (week 3-4) mouse neural progenitor cells infected with non-*Jakmip1* targeting shRNAmir hairpins using quantitative RTPCR. *Jakmip1* RNA is expressed in differentiated, but not undifferentiated cells (Figure 2-8, B).

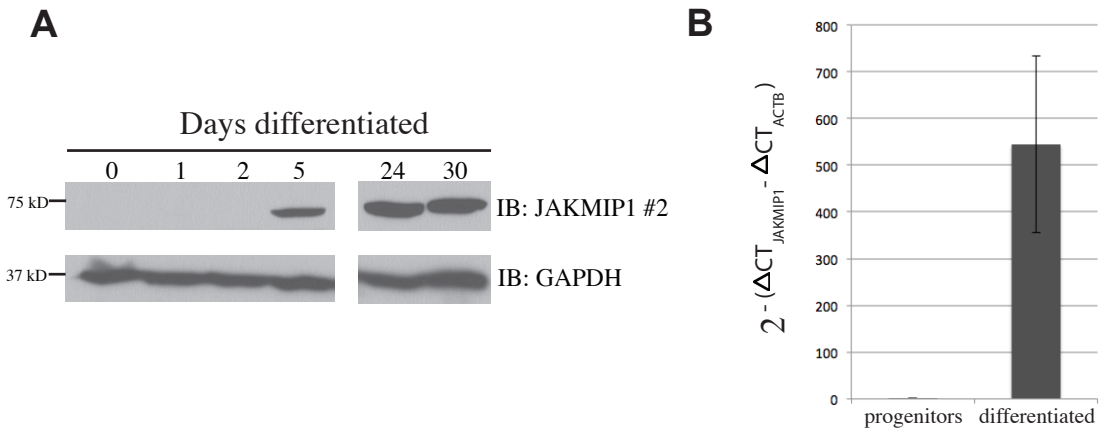

Figure 2-8. JAKMIP1 increases in expression during mouse neural cell differentiation. (A) JAKMIP1 protein increases in expression during differentiation of mouse neural progenitor cells, with highest expression after 3 weeks differentiation. (B) *Jakmip1* RNA is expressed at 3 and 4 weeks of mouse neural cell differentiation, but not in undifferentiated cells (week 0, N=3; week 3/4, N=4). RNA signal is measured by quantitative RTPCR. Values are mean +/- SEM. RNA expression is displayed as fold change from undifferentiated cells, with undetected RNA levels set at a CT value of 40.

To determine if JAKMIP1 is also increased over the course of human neural cell differentiation, we collected JAKMIP1 RNA from normal human neural progenitor cells (NHNP) differentiated for two weeks, four weeks, eight weeks or undifferentiated, and analyzed JAKMIP1 RNA levels by quantitative RTPCR. JAKMIP1 shows a statistically significant increase in expression from two to four weeks of differentiation and from four to eight weeks of differentiation (Figure 2-9).

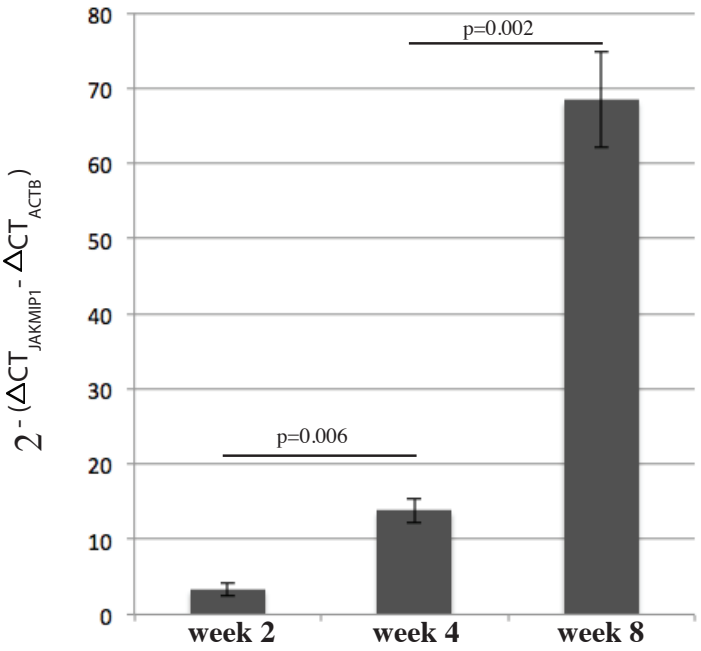

Figure 2-9. JAKMIP1 increases in expression during human neural cell differentiation. RNA levels of human JAKMIP1 isoform A in 2, 4, or 8 week differentiated NHNP cells (week 0, N=2; week 2, N=3; week 4, N=3; week 8, N=2, Samples with high technical replicate variation were removed). RNA signal is measured by quantitative RTPCR. Values are mean +/- SEM. RNA expression is displayed as a fold change from undifferentiated cells. P-values are calculated from a two sample, two tailed t-test of delta CT values (JAKMIP1-βactin).

As JAKMIP1 is expressed in differentiated rather than undifferentiated cells, I hypothesized that JAKMIP1 would be more highly expressed in structures comprised of differentiated cells than in regions composed of progenitor cells. Neural progenitor cells reside in the subventricular zone (SZ), which contains intermediate progenitor cells, and the ventricular zone (VZ), which contains radial glial cells, while differentiated neurons reside in the cerebral cortical plate (CP) (Noctor et al., 2007). I hypothesized that JAKMIP1 is strongly expressed in the cortical plate, consistent with its expression in glutamatergic projection neurons, and weakly expressed in the subventricular and ventricular zones. To test this, we used public data from the Allen Brain Atlas BRAINSPAN Prenatal LMD microarray project. We found *JAKMIP1* to be highly expressed in the CP and weakly expressed in the SZ, VZ and ganglionic eminence (GE). JAKMIP1 shows a 13.3 fold increase in expression in the CP versus the SZ, and a 23.3 fold increase in expression in the CP versus the SZ and the VZ combined (Figure 2-10), confirming our hypothesis.

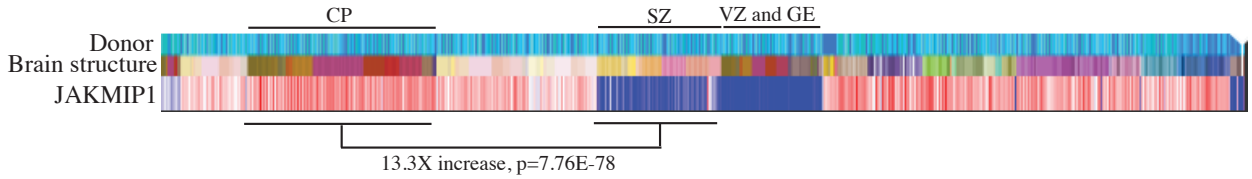

Figure 2-10. JAKMIP1 is differentially expressed in differentiated versus undifferentiated cells in the developing human brain. BRAINSPAN Prenatal LMD Microarray transcriptional profiling of JAKMIP1 RNA from midgestational prenatal human brain (N=4) shows high expression of JAKMIP1 RNA in cortical plate (CP) and low expression in subventricular zone (SZ), ventricular zone (VZ), and ganglionic eminence (GE). Differential search with CP as target structure and SZ as contrast structure shows a 13.3 fold increase of JAKMIP1 expression in CP over SZ. Figure was created using an image from the BrainSpan Atlas of the Developing Human Brain [Internet]. Seattle (WA): Allen Institute for Brain Science. http://brainspan.org/

2.5 Discussion

Elucidating gene function involves gaining a comprehensive understanding of the biological context under which that gene operates. To do this, we took a multifaceted approach, conducting developmental protein expression profiling and immunohistochemical analysis during peak JAKMIP1 expression in two brain structures implicated in FMRP biology. We, additionally, determined the timing of JAKMIP1 expression during neural cell differentiation *in vivo* and *in vitro* in mouse and human.

We found that JAKMIP1 shows peak expression in the postnatal neocortex during synaptogenesis and neurite outgrowth. A recent study confirmed JAKMIP1's high postnatal expression in mouse cerebral cortex, but, due to sparse time sampling, missed JAKMIP1's tight burst of expression from p8 to p14 (Vidal et al., 2012). During this window of peak expression, we found that JAKMIP1 protein is expressed throughout the cortex, consistent with its RNA expression in adult mouse (http://mouse.brain-map.org/) and predominantly in glutamatergic projection neurons. JAKMIP1's expression in glutamatergic neurons is congruous with its potential role in regulating the migration of pyramidal neurons in the neocortex (Vidal et al., 2012). Our finding that JAKMIP1 has sporadic expression in GABAergic neurons of the neocortex agrees with one study that reported partial colocalization of JAKMIP1 with a marker of GABAergic interneurons, glutamic acid decarboxylase (GAD), in a field of primary rat hippocampal cells (Vidal et al., 2009). We, additionally, discovered that JAKMIP1 is located across subcellular fractions, with notable exclusion from the cytosolic fractions, in the postnatal mouse cortex. JAKMIP1's cortical subcellular localization mirrors that of its localization in adult rat CA1 hippocampus to the Golgi apparatus, endoplasmic reticulum, dendritic spines, and partially to the nucleus (Vidal et al., 2009).

In the cerebellum, we found that JAKMIP1 protein decreases in expression throughout development. This finding is consistent with mouse cerebellar transcriptome profiles from The Cerebellar Development Transcriptome Database, which show a decrease in *Jakmip1* RNA over cerebellar development (embryonic day 18 to p56, http://www.cdtdb.neuroinf.jp/CDT/Top.jsp). During postnatal development and adulthood, we found JAKMIP1 to be expressed in the Purkinje cells of the cerebellum by double label immunohistochemistry. This agrees with reports of JAKMIP1 colocalizing with Purkinje cells in adult mouse brain, by morphological assessment of cells stained with a single antibody against JAKMIP1 (Vidal et al 2009). JAKMIP1's role in Purkinje cell function during development may be an interesting area of further study as Purkinje cell involvement in autism is gaining appreciation (Tsai et al., 2012).

Lastly, we demonstrate that JAKMIP1 is expressed in differentiated neurons. We found JAKMIP1 protein and RNA to be expressed in differentiated, but not in undifferentiated, mouse neural progenitor cells. Similarly, JAKMIP1 RNA increases in expression during human neural cell differentiation. Moreover, JAKMIP1 is enriched in human mid-gestation brain structures that contain differentiated cells over brain regions that contain progenitor cells. A recent study using weighted gene coexpression analysis reports that a significant number of ASD candidate genes show coordinated regulation during human neural cell differentiation (Konopka et al., 2012), making JAKMIP1's potential involvement in neural cell differentiation intriguing in the context of ASD pathophysiology. These characterization studies provide a critical biological framework in which to carry out further developmental studies of JAKMIP1 function.

2.6 Methods

Western Blotting

Protein was prepared as previously described from tissue lysed in a Tris-based hypotonic solution (10 mM Tris-CL, 10mM KCl, 0.1mM EDTA) with protease inhibitor (Vidal et al., 2007). A Bradford assay (Bio-Rad, Hercules, CA) was used to determine protein concentration. Equal ug of protein were mixed with an SDS based loading buffer containing a final concentration of dithiothreitol at 10mM. Samples were boiled at 94 °C for 4 minutes and then run out on a SDS-polyacrylamide gel to undergo separation by gel electrophoresis. Proteins were transferred in a 20% methanol-containing transfer buffer onto a PVDF membrane, which was then blocked in a milk block solution containing TBST and 5% milk. After blocking, membranes were incubated in primary antibody diluted in milk block overnight at 4 °C. Blots were then incubated in a secondary antibody diluted in milk block for 1 to 2 hours followed by detection with Supersignal West Pico chemiluminescent substrate (Pierce, Rockford, IL). For protein quantification, experimental bands were normalized to their corresponding GAPDH bands using the web-based Image J program (http://rsbweb.nih.gov/ij/). For developmental characterization experiments, each blot's GAPDH-normalized protein signals were normalized to 1 for between blot comparisons. Three values from each time point were used to calculate a mean and standard error of the mean. Two-tailed t-tests were conducted to test for significant increases or decreases in JAKMIP1 expression between time points.

Subcellular fractionation

Subcellular fractionation was conducted as previously described (Hallett et al., 2008). 50 ug of protein was compared between conditions. Fractions were immunoblotted for βtubulin and GAPDH to control for loading and PSD95 to determine efficacy of fractionation.

Immunohistochemistry

Postnatal and adult mice were anesthetized with isoflurane and perfused transcardially with ice-cold 4% paraformaldehyde (PFA) in 100 mM phosphate buffered saline (PBS). Brains were extracted and incubated in this same fixative for 24 hours at 4°C. Brains were then cryoprotected in 30% sucrose dissolved in 4% PFA/100mM PBS for an additional 48 hours at 4°C followed by cryosectioning in Tissue Tek embedding medium (Sakura, Torrance, CA). Immunohistochemistry was conducted using free-floating 20 micron coronal brain sections. Brain sections were blocked for 1 hour at room temperature in 1% bovine serum albumin, 0.2% fish skin gelatin, and 0.1% Triton X-100 in 100mM Tris Buffered Saline. Primary and secondary antibodies were diluted in blocking buffer. Primary antibody incubations took place overnight at 4°C or for 2 hours at room temperature, while secondary antibody incubations were 2 hours at room temperature. Fluoromount G (SouthernBiotech, Birmingham, AL) was used to mount coverslips to glass slides. For double label experiments with SMI-32, FOXP1, and calretinin, 40X confocal images were taken using an LSM5 Pascal Confocal Laser scanning microscope (Zeiss, Thornwood, NY). Random cortical fields were imaged until 100 calretinin-positive cells or at least 200 FOXP1 or SMI-32-positive cells were obtained, as many more glutamatergic-positive cells in the cortex are present than GABAergic interneurons. Colocalization was determined using LSM5 software and Adobe Photoshop. For each field, the following cells were counted: JAKMIP1+/marker+, JAKMIP1+/marker-, and JAKMIP1-/marker+. To determine JAKMIP1's expression in cortical layers, we tested both rabbit and mouse antibodies against cut-like homeobox 1 (CUX1) and forkhead box P2 (FOXP2). For each, only the antibodies raised in rabbit give appropriate signal. As our JAKMIP1 antibodies

are also raised in rabbit, merged JAKMIP1/CUX1 and JAKMIP1/FOXP2 images between consecutive coronal brain sections were used to determine layer expression.

Antibodies used for Western Blotting and Immunohisochemistry

Name	Antigen/Peptide wording from company website when appropriate	Species/Clonality	Source/Catalogue number
JAKMIP1 #1 $J1_{269\text{-}286}$	JAKMIP1, amino acids 269-286 of human isoform A	Rabbit polyclonal	Sandra Pellegrini, Ph.D. (Steindler et al., 2004)
JAKMIP1 #2	JAKMIP1, amino acids 277-626 of human isoform A	Rabbit polyclonal	Proteintech group 13846-1-AP
JAKMIP1 #3 $J1_{609\text{-}626}$	JAKMIP1, amino acids 609-626 of human isoform A	Rabbit polyclonal	Sandra Pellegrini, Ph.D. (Steindler et al., 2004)
GAPDH	Glyceraldehyde-3-phosphate dehydrogenase from rabbit muscle.	Mouse monoclonal	Millipore MAB374
DDX5	amino acids 471-614 at the C terminus region of human DDX5	Mouse monoclonal	Santa Cruz sc-166167
PSD95	recombinant full length protein (rat)	Mouse monoclonal	Abcam ab13552
BTUB	Synthetic peptide conjugated to KLH derived from within residues 1 - 100 of Human beta Tubulin.	Rabbit polyclonal	Abcam ab6046
FOXP2	Synthetic peptide conjugated to KLH derived from within residues 700 to the C-terminus of Human FOXP2	Rabbit polyclonal	Abcam ab16046
CUX1	amino acids 1111-1332 of CDP (Cutl1, mouse; CUX1, human) of mouse.	Rabbit	Santa Cruz sc-13024
FOXP1	Full length native protein (purified) of Mouse FOXP1	Mouse monoclonal	Abcam ab32010
SMI-32	recognizes an epitope in neurofilament H (nonphosphorylated)	Mouse monoclonal	Covance SMI32R
Calretinin	recombinant, full length mouse protein	Mouse monoclonal	Thermo ScientificMA1-26601

VGLUT1	rat VGLUT1 Synthetic peptide does not have sequence overlap with VGLUT2	Guinea Pig polyclonal	Millipore AB5905
Calbindin	bovine kidney calbindin-D	Mouse monoclonal	Sigma C9848

Quantitative RTPCR

For human neural cell differentiation experiments, lonza normal human neural progenitor cells (NHNP) from a 17 gestation week female brain were differentiated. Three plates of cells for each of the following differentiation time points were collected: 0, 2, 4, and 8 weeks. RNA was extracted using Qiagen's RNeasy kit (Germantown, MD) and quantitative RTPCR was conducted using Oligo(dt)-18 primers (Invitrogen, Carlsbad, CA), Superscript III (Invitrogen, Carlsbad, CA), Applied Biosystems 7900HT instrument, iTaq SyBR green supermix with ROX (Bio-Rad, Hercules, CA) and specific primer sets for *JAKMIP1A*, and human βactin to control for loading. Transcript levels were calculated using the SDS2.1 software (Applied Biosystems, Carlsbad, California). For mouse neural cell differentiation experiments, cells were differentiated for 3 or 4 weeks or kept undifferentiated. Cells previously underwent lentiviral infection with shRNAmir hairpins not targeting *Jakmip1* (Human GIPZ lentiviral shRNAmirs, clone IDs V3LHS-642754, V3LHS-642756, or a GIPZ shRNAmir against GFP, Thermoscientific, Waltham, MA) and were puromycin-selected for infected cells. RNA was extracted from the cells using Qiagen's miRNeasy kit (Germantown, MD). Quantitative RTPCR was conducted using random hexamers (Invitrogen, Carlsbad, CA), Superscript III (Invitrogen, Carlsbad, CA), Light Cycler 480 II (Roche Applied Science, Indianapolis, IN), SensiFAST SYBR No-Rox mix (Bioline, Taunton, MA) and a specific primer sets for *Jakmip1*

(*Jakmip1_exons 3-4)* and βactin to control for loading. Transcript levels were calculated using the LightCycler 480 SW 1.5 software (Roche Applied Science, Indianapolis, IN).

Primers used:

Primers	**Forward 5'-3'**	**Reverse 5'-3'**
Mouse βactin	AGAGGGAAATCGTGCGTGAC	CAATAGTGATGACCTGGCCGT
Human βactin	AGCACAGAGCCTCGCCTTT	CACGATGGAGGGGAAGAC
Mouse Jakmip1_exons 3-4	GCGGAAGAGGCACTCAGTAA	GTTTGCACACCAAGCTCCTT
Human JAKMIP1_A	GCAGCTGCTCATCAGAACAA	TCCCCTTTACACATGCTTGA

Harvesting mouse neural progenitor cells and differentiation

Whole brains from postnatal day 0-2 mice were dissected in DMEM-F12 (Invitrogen, Carlsbad, CA) with removal of the cerebellum and brainstem. Tissue was mechanically dissociated and digested in Papain (Worthington, Lakewood, NJ) or Trypsin (Invitrogen, Carlsbad, CA) for 30 minutes at 37 C with 5% CO_2. Bovine serum albumin (Invitrogen, Carlsbad, CA) in DMEM was added to stop digestion. Brains were triturated in media and centrifuged at 1,500 rpm. The pellet was reconstituted in DMEM-F12 with 1XB27 without retinoic acid (Invitrogen, Carlsbad, CA). A mixture of epidermal growth factor and fibroblast growth factor was added at 1:5000 (PeproTech, Rocky Hill, NJ) and cells were propagated on polyornithine/fibronectin. Cells were differentiated on polyornithine/laminin in media containing brain derived neurotrophic factor (10ng/ml, PeproTech, Rocky Hill, NJ), NT3 (10ng/ml, PeproTech, Rocky Hill, NJ), retinoic acid (500ng/ml, Sigma, St. Louis, MO), Forskalin (10uM, Sigma, St. Louis, MO) and 10mM KCL.

Chapter 3: JAKMIP1 is a novel component of an FMRP-associated RNP complex

3.1 Introduction

Here, we take a first step to determine JAKMIP1's developmental role by ascertaining JAKMIP1's *in vivo* proteomic interactome during its postnatal burst of expression in mouse neocortex. We use the gene ontology of this interactome as a biological compass to orient us to JAKMIP1's own function via guilt by association (Oldham et al., 2008). These data generate specific hypotheses regarding JAKMIP1 function, which we test in subsequent chapters.

To date, very little is known about JAKMIP1's neural protein binding partners. In non-neural systems, JAKMIP1 has been shown to associate with the FERM domain of janus kinase 1 (JAK1) and tyrosine kinase 2 (TYK2). In rodent brain, JAKMIP1 has been reported to bind GABABR1 [adult rat brain, (Vidal et al., 2008)] and kinesin 1 [adult mouse brain (Vidal et al., 2007)]. No additional JAKMIP1 protein interactors have been identified in a neural system.

We use Multidimensional Protein Identification Technology (MudPIT) to perform functional annotation via an unbiased assessment of the JAKMIP1 protein interactome. We find that JAKMIP1 binds FMRP and many of FMRP's known interactors, as well as validated FMRP mRNA translational targets *in vivo* during postnatal cortical development. Bioinformatic analysis of the JAKMIP1 interactome shows a significant enrichment for proteins involved in translation, which we experimentally confirm. These data provide the first functional link between JAKMIP1 and FMRP, implicating JAKMIP1 in translational regulation during development, an emerging theme in the pathophysiology of ASD and related neurodevelopmental disorders (Kelleher and Bear, 2008; Morrow et al., 2008; Santini et al., 2013).

3.2 Defining JAKMIP1's protein interactome during neocortical development *in vivo*

To identify JAKMIP1's *in vivo* interactome at the peak of JAKMIP1 protein expression, we performed a shotgun proteomic analysis using Multidimensional Protein Identification technology (MudPIT) of immunoprecipitated JAKMIP1 complexes isolated from postnatal mouse neocortex using JAKMIP1 #1 and rabbit pre immune serum as a control. JAKMIP1 was immunoprecipitated from cellular fraction S2, in which it is enriched (Vidal et al., 2007). We next conducted a replication experiment using additional postnatal mouse neocortices (Figure 3-1). Analysis by mass spectrometry was carried out as previously described (Wohlschlegel, 2009).

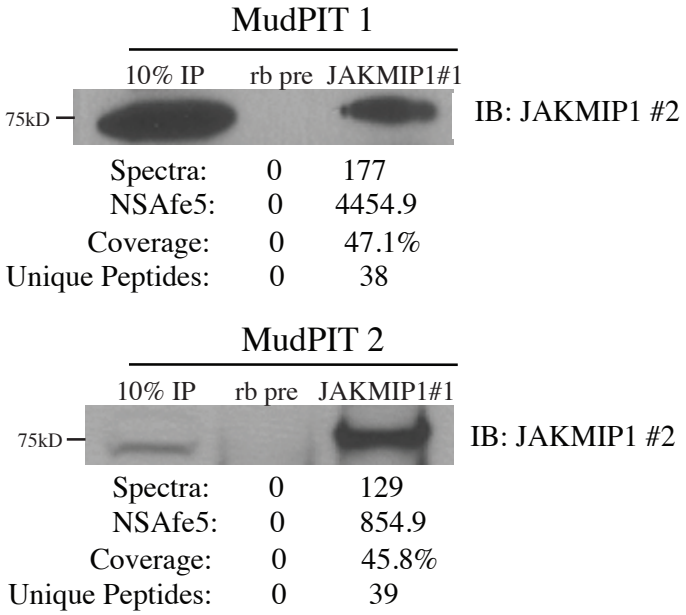

Figure 3-1. JAKMIP1 was successfully immunoprecipitated from mouse postnatal cortex. JAKMIP1 was immunoprecipitated from two pools of postnatal wild-type mouse neocortices. Protein was imunoprecipitated with rabbit pre immune serum (rb pre) as a negative control. MudPIT 1 (top panel) denotes the first experimental round, while MudPIT 2 (bottom panel) denotes the replication round. Effectiveness of JAKMIP1 pull down was tested by immunoblotting (IB) with JAKMIP1 #2. 10% of the protein used for immunoprecipitation was run in the far left lane. MudPIT readouts are listed below. NSAfe5 is normalized spectra abundance factor.

We defined a JAKMIP1 interactor as: a) being identified in both the initial and the replication MudPIT runs b) having both its normalized spectra abundance factor (NSAfe5), which controls for the size and abundance of the protein (Florens et al., 2006), and its spectral counts above preset conservative threshold values in the JAKMIP1 IP versus control IP for one of the runs and c) both its NSAfe5 and spectral counts enriched in the JAKMIP1 IP over the control IP in the remaining run. PatternLab ACFold analysis (Carvalho et al., 2008) was additionally conducted to identify statistically significantly enriched proteins in the JAKMIP1 immunoprecipitated versus control conditions at a false discovery rate of 15%. Using these criteria, we identified a core set of 33 JAKMIP1 interactors (Table 3-1). Additional proteins, MYO5A, PABPC1, and PURA, met two of the three screening criteria and were also considered potential binding partners to take forward for further validation. The identification of JAKMIP1, which achieved the lowest p-value of all proteins, and YWHAG as a JAKMIP1-interactor both serve as positive controls, as YWHAG was previously identified as a JAKMIP1 human protein interactor in embryonic kidney cells (Jin et al., 2004).

Entrez Gene Name	**Symbol**	**Pattern Lab ACFold p-value**
janus kinase and microtubule interacting protein 1	JAKMIP1	4.42 E-26
actin, alpha, cardiac muscle 1	ACTC1	
calcium/calmodulin-dependent protein kinase II alpha	CAMK2A	
calcium/calmodulin-dependent protein kinase II gamma	CAMK2G	0.028
cytoplasmic linker associated protein 1	CLASP1	2.65 E-09
cytoplasmic linker associated protein 2	CLASP2	2.028 E-06
CAP-GLY domain containing linker protein family, member 4	CLIP4	2.56 E-06
doublecortin-like kinase 1	DCLK1	

DEAD (Asp-Glu-Ala-Asp) box polypeptide 5	DDX5	0.023
eukaryotic translation elongation factor 1 alpha 1	EEF1A1	
eukaryotic translation elongation factor 2	EEF2	
glutamate dehydrogenase 1	GLUD1	
guanine nucleotide binding protein (G protein), beta polypeptide 2-like 1	GNB2L1	
glycogen synthase 1 (muscle)	GYS1	0.012
heterogeneous nuclear ribonucleoprotein K	HNRNPK	
heterogeneous nuclear ribonucleoprotein M	HNRNPM	
myosin VA (heavy chain 12, myoxin)	MYO5A	
poly(A) binding protein, cytoplasmic 1	PABPC1	
plectin	PLEC	3.99 E-04
purine-rich element binding protein A	PURA	
purine-rich element binding protein B	PURB	
ribosomal protein L14	RPL14	
ribosomal protein L5	RPL5	0.023
ribosomal protein L6	RPL6	
ribosomal protein L7a	RPL7A	
ribosomal protein, large, P0	RPLP0	0.020
ribosomal protein S17	RPS17	0.046
ribosomal protein S3	RPS3	
ribosomal protein S8	RPS8	
ribosomal protein SA	RPSA	
RUN and FYVE domain containing 3	RUFY3	
synaptotagmin binding, cytoplasmic RNA interacting protein	SYNCRIP	
tubulin, alpha 4a	TUBA4A	
tyrosine 3-monooxygenase/tryptophan 5-monooxygenase activation protein, gamma polypeptide	YWHAG	
tyrosine 3-monooxygenase/tryptophan 5-	YWHAH	

monooxygenase activation protein, eta polypeptide		
	1810049H19Rik	2.56 E-06
	Igkv1-117	

Table 3-1. Members of JAKMIP1's postnatal *in vivo* proteomic interactome. GOLGA1 (P=0.046) and NME2 (P=0.012) were also identified by Pattern Lab AC Fold analysis, but were only present in one MudPIT run and, therefore, did not meet the inclusion criteria.

The binding of several of these identified protein interactors to JAKMIP1 is consistent with what previous studies suggest about JAKMIP1's function. For example, three of JAKMIP1's identified interactors, CLASP2, CLASP1, and CLIP4, are microtubule plus-end-tracking proteins (+TIPs) (Akhmanova and Hoogenraad, 2005) which gather at the distal end of growing microtubules to increase microtubule stability. JAKMIP1's binding to these TIPS and motor proteins, such as MYO5A, is consistent with JAKMIP1's previously identified microtubule interactions and possible transport function (Steindler et al., 2004; Vidal et al., 2007). These data provide a set of targets that likely mediate some of these functions.

3.3 Experimental validation of JAKMIP1's protein binding partners

To provide more direct experimental validation of specific JAKMIP1 protein interactions, we confirmed several MudPIT-identified JAKMIP1 interactions by co-immunoprecipitation from mouse postnatal neocortices followed by western blotting. We tested the following proteins from network 1 (Figure 3-5, A) that were significantly enriched in JAKMIP1 immunoprecipitates based on PatternLab AC fold analysis of the proteomic data (denoted here by '1') (Table 3-1) and/or had an antibody available that was potentially suitable for immunoprecipitation (denoted here by '2'): DDX5 (1, 2), CLASP2 (1, 2), CAMK2G (1, 2), RPLPO (1, 2), PABPC1 (2), CAMK2A (2), and EEF2 (2). To increase the independence of these experiments, we used a different antibody to JAKMIP1 (JAKMIP1 #2) than the antibody

used for MudPIT (JAKMIP1 #1). DDX5, CLASP2, CAMK2G and PABPC1 were all validated by this method (Figure 3-2, A-D). Three of the four (DDX5, CLASP2, and PABPC1) confirmed in both immunoprecipitation directions, while CAMK2G was confirmed in one direction. Three of the proteins, RPLP0, CAMK2A, and EEF2, were interpretable in only one direction, but we were unable to confirm their binding to JAKMIP1 by this assay, suggesting potentially indirect interactions via other protein intermediates. The JAKMIP1-PABPC1 interaction was additionally confirmed in differentiated mouse neural progenitor cells (Figure 3-2, E).

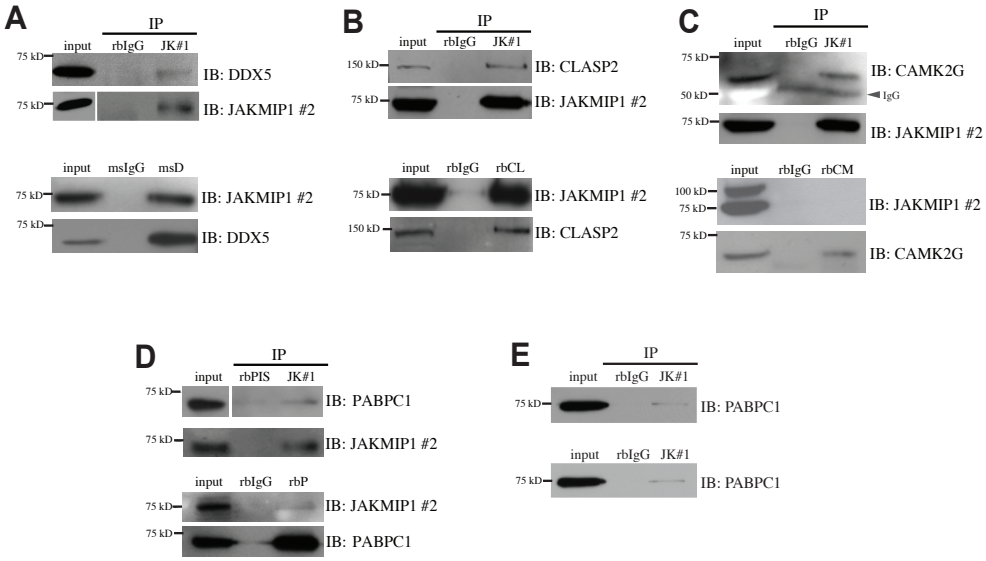

Figure 3-2. Confirmation of JAKMIP1 binding partners by co-immunoprecipitation. (A) JAKMIP1 (top two panels) or DDX5 (bottom two panels) was immunoprecipitated from mouse postnatal neocortices followed by immunoblotting with DDX5 and JAKMIP1. (B) JAKMIP1 (top two panels) or CLASP2 (bottom two panels) was immunoprecipitated from mouse postnatal neocortices followed by immunoblotting with CLASP2 and JAKMIP1. (C) JAKMIP1 (top two panels) or CAMK2G (bottom two panels) was immunoprecipitated from mouse postnatal neocortices followed by immunoblotting with CAMK2G and JAKMIP1. (D) JAKMIP1 (top two panels) or PABPC1 (bottom two panels) was immunoprecipitated from mouse postnatal neocortices followed by immunoblotting with PABPC1 and JAKMIP1. (E) JAKMIP1 was immunoprecipitated from two week differentiated C57Bl/6J mouse neural progenitor cells followed by immunoblotting with PABPC1. Each panel represents a biological replicate. Abbreviations are: JK#1, JAKMIP1 #1; msD, mouse anti DDX5; rbCL, rabbit anti CLASP2 ; rbCM, rabbit anti CAMK2G ; rbP, rabbit anti PABPC1; rbIgG, rabbit IgG; msIgG, mouse IgG ; rbPIS, rabbit pre-immune serum.

3.4 JAKMIP1 associates with an FMRP-containing translational complex

Notably, within the group of 36 proteins identified by the initial analyses, we noticed that ten were known to exist in FMRP containing protein complexes: HNRNPK (Angenstein et al., 2002), PABPC1 (Napoli et al., 2008; Villace et al., 2004), MYO5A (Ohashi et al., 2002; Villace et al., 2004), PURA (Kanai et al., 2004; Ohashi et al., 2002), PURAB (Kanai et al., 2004), EEF1A (Kanai et al., 2004), SYNCRIP (Kanai et al., 2004), DDX5 (Kanai et al., 2004), RPLPO (Villace et al., 2004), and RPL6 (Villace et al., 2004). Moreover, thirteen of FMRP's thirty-three known protein interactors (39%) listed in the Human Protein Reference Database (HPRD) (Prasad et al., 2009) were identified as JAKMIP1 interactors in one (denoted by '1') or both (denoted by '2') MudPIT runs: CYFIP2 (1), FXR1 (1), HNRNPD (1), HNRNPK (2), HNRNPR (1), HNRNPU (2), HNRNPF (1), MYO5A (2), SYNCRIP (2), Nucleolin (1), PABPC1 (2), PURA (2), and YBX1 (1). JAKMIP1's proteomic interactome identified here also shows a significant overlap with other FMRP-associated RNP complexes (Table 3-2) identified by kinesin-1 immunoprecipitation from adult mouse brain (Kanai et al., 2004; hypergeometric probability, P=9.68 E-08) and hStaufen immunoprecipitation from embryonic human kidney cells (Villace et al. 2004; P=1.33 E-11).

A

Functional Category	Protein name	JAKMIP1 binder	MudPIT
RNA transport	FMR1	co-IP evidence	
RNA transport	FXR1	X	1
RNA transport	FXR2	-	
RNA transport	PURA*	X	2
RNA transport	PURB*	X	2
RNA transport	Staufen	-	
Protein Synthesis	EF-1a	X	2
Protein Synthesis	eIF2a	-	

Protein Synthesis	eIF2b	-	
Protein Synthesis	eIF2y	-	
Protein Synthesis	Hsp70	-	
Protein Synthesis	RPL3	X	1
RNA helicase	DDX1*	X	1
RNA helicase	DDX3*	X	1
RNA helicase	DDX5	X	2
hnRNP	hnRNPA/B	-	
hnRNP	hnRNPA0	-	
hnRNP	hnRNPA1	-	
hnRNP	hnRNPD	X	1
hnRNP	hnRNPU*	X	2
Other RNA associated	ARF-GEP100/BRAG2	-	
Other RNA associated	ALY*	-	
Other RNA associated	CIRBP	-	
Other RNA associated	EWS	-	
Other RNA associated	NONO*	X	1
Other RNA associated	Nucleolin	X	1
Other RNA associated	PSPC1	-	
Other RNA associated	PSF*	-	
Other RNA associated	RTCD1	-	
Other RNA associated	RNA binding motif protein 3	-	
Other RNA associated	SYNCRIP*	X	2
Other RNA associated	TLS*	-	
Other known protein	Ser/Thr kinase receptor associated protein	-	
Other known protein	TRIM2	-	
Other known protein	TRIM3	X	1

***** Most conservative granule members (Kanai et al., 2004)
Hypothetical proteins from Kanai 2004 complex excluded from table

B

Functional Category	Protein name	JAKMIP1 binder	MudPIT
cytoskeleton	b-5 Tubulin	-	
cytoskeleton	a-Tubulin	X	2
cytoskeleton	Tau	-	
RNA transport	hStaufen isoform 2	-	
cytoskeleton	ACTB	-	
motor protein	Myosin heavy chain	X	2

RNA helicase	RNA-dependent RNA helicase A	-	
Other RNA associated	Nucleolin	X	1
hnRNP	hnRNPU	X	2
Protein Synthesis	PABP1	X	2
cytoskeleton	a-Internexin	X	1
motor protein	Dynein intermediate chain	X	1
motor protein	Kinesin	X	1
protein kinase	p-Associated protein kinase II	-	
GTPase-activating	Ras GAP	-	
cytoskeleton control	Rac1	-	
cytoskeleton control	Cdc42	-	
cytoskeleton control	IQGAP1	-	
Protein Synthesis	FMRP	co-IP evidence	
Protein Synthesis	RPLP0	X	2
Protein Synthesis	RPS4	X	2
Protein Synthesis	RPS6	X	1
Protein Synthesis	RPL6	X	2
Protein Synthesis	RPL28	-	

Table 3-2. MudPIT-identified JAKMIP1 protein interactors show a statistically-significant overlap with previously identified FMRP-associated translational RNP complexes. (A) Modified from Kanai et al. 2004. (B) List of RNP components from Villace et al. 2004. Proteins listed under 'Protein name' are part of the RNP complex. X denotes a MudPIT-identified JAKMIP1 interactor. Numbers listed under 'MudPIT' denote the number of MudPIT runs that identified the protein of interest. 'Identification' denotes positive values for both spectral and NSAfe5 counts in the JAKMIP1 immunoprecipitated versus control condition.

Although FMRP itself was not identified under conditions used for MudPIT experiments (200mM NaCl, 0.1% NP40), under less stringent conditions (50mM NaCl, 0.1% NP40) which are more permissive for indirect protein interactions, FMRP co-immunoprecipitated with JAKMIP1 bi-directionally in mouse postnatal neocortex (Figure 3-3, A). We found that this interaction is not dependent on the presence of single or double stranded RNA (Figure 3-3, B).

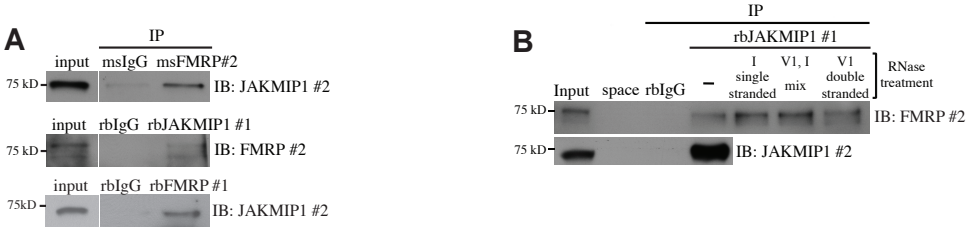

Figure 3-3. JAKMIP1 and FMRP associate in mouse postnatal neocortices. (A) FMRP and JAKMIP1 were immunoprecipitated from mouse postnatal neocortices and immunoblotted for JAKMIP1 and FMRP, respectively. (B) JAKMIP1's association with FMRP does not depend on RNA. JAKMIP1 immunoprecipitation reactions were conducted in the presence of RNases and immunoblotted for FMRP (top panel) and JAKMIP1 (bottom panel). Lanes labeled 'single stranded', 'mix', and 'double stranded' are immunoprecipitations conducted in the presence of RNase I, RNase I and V1, and RNaseV1, respectively. Lanes denoted by (-) represent immunoprecipitations conducted without RNases. rbIgG is rabbit IgG, and msIgG is mouse IgG. Antibody designations are the following: FMRP#1 is rabbit anti FMRP (H-120), and FMRP#2 is mouse anti FMRP (MAB2160).

Previously, the drosophila homologue of DDX5, dmp68, was reported to bind FMRP in a RISC complex (Ishizuka et al., 2002) and was found to associate with an FMRP-associated RNP complex in adult mouse brain (Kanai et al., 2004) (Table 3-2, A). Consistent with this, we found that DDX5 co-immunoprecipitates with FMRP in mouse postnatal neocortex, mouse N2A cells, and in human SY5Y cells (Figure 3-4, A-B), demonstrating this DDX5–FMRP relationship is conserved in mammalian neural systems. DDX5 also interacts with JAKMIP1 in these systems as well as in differentiated mouse neural progenitor cells (Figure 3-4, A-C). DDX5 interacts with JAKMIP1 and FMRP, and PABCP1 interacts with JAKMIP1 (Table 3-1) and FMRP (Napoli et al., 2008; Villace et al., 2004). Thus, we asked if DDX5 and PABPC1 interact. Indeed, we found that DDX5 and PABPC1 co-immunoprecipitate *in vitro* and *in vivo* in mouse cortex (Figure 3-4, D).

Since several members of the JAKMIP1 interactome, including PABPC1, bind single stranded RNA as part of their role in translational control in the RNP complex, we tested whether DDX5's relationship with JAKMIP1 and FMRP is dependent on single stranded RNA.

DDX5 failed to co-immunoprecipitate with FMRP and JAKMIP1 when single, but not double, stranded RNA was digested (Figure 3-4, A and C), indicating that these protein interactions are single stranded RNA dependent. In sum, these data provide multiple lines of evidence that JAKMIP1 is part of a translational RNP complex containing DDX5, PABPC1, and FMRP.

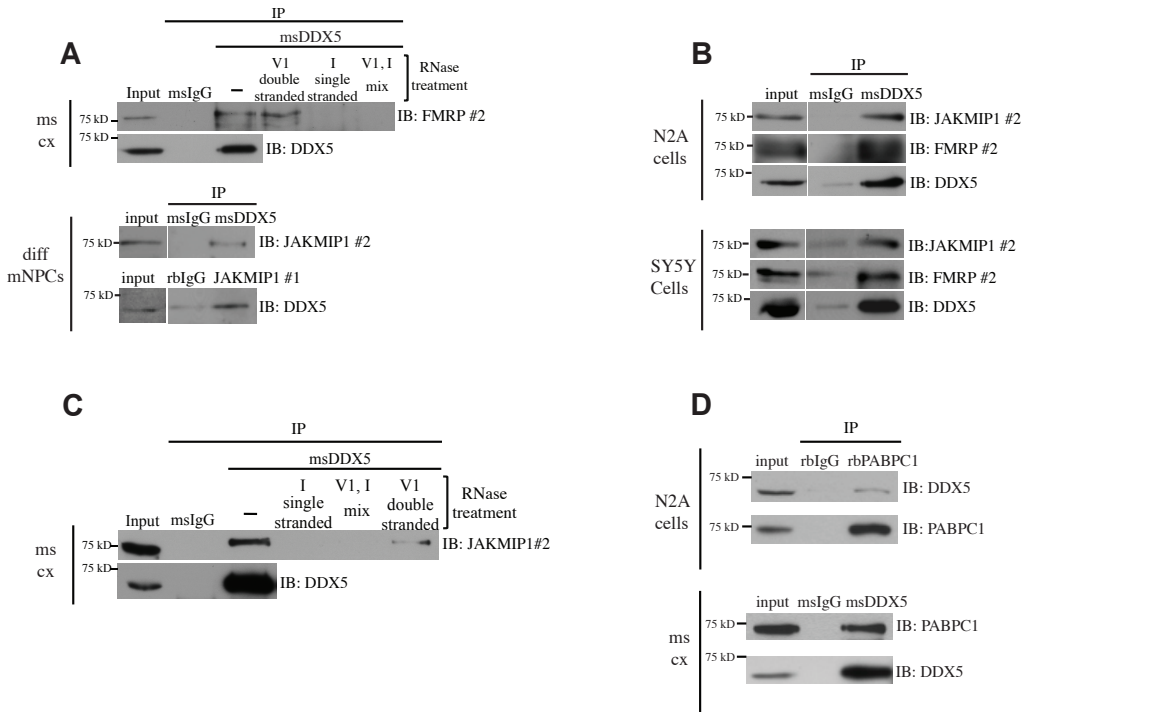

Figure 3-4. JAKMIP1, FMRP, DDX5, and PABPC1 co-immunoprecipitate *in vitro* and *in vivo*. (A) DDX5's association with FMRP is dependent on single-stranded, but not double-stranded, RNA. DDX5 immunoprecipitation reactions were conducted in the presence of RNases as described in Figure 3-3, B and immunoblotted for FMRP (top panel) and DDX5 (bottom panel) to confirm the immunoprecipitation reaction. Bottom panels: DDX5 and JAKMIP1 associate in differentiated mouse neural progenitor cells. DDX5 or JAKMIP1 was immunoprecipitated from two week differentiated mNPCs and immunoblotted with JAKMIP1 and DDX5, respectively. (B) DDX5, JAKMIP1, and FMRP co-immunoprecipitate in N2A and SY5Y cells. DDX5 was immunoprecipitated from mouse N2A cells (top panels) or human SY5Y cells (bottom panels) and immunoblotted for JAKMIP1, FMRP, and DDX5. (C) DDX5's association with JAKMIP1 is dependent on single-stranded, but not double-stranded, RNA. DDX5 immunoprecipitation reactions were conducted in the presence of RNases as described in Figure 3-3, B and immunoblotted for JAKMIP1 (top panel) and DDX5 (bottom panel). (D) DDX5 interacts with PABPC1 by immunoprecipitation in mouse N2A cells and postnatal neocortices. Top panels for each experiment demonstrate the PABPC1-DDX5 interaction, while the bottom panels shows specific PABPC1 or DDX5 pull down.

3.5 Pathway analysis suggests JAKMIP1 is involved in protein translation

We next conducted pathway analysis of JAKMIP1's top binding partners (Table 3-1) using Ingenuity Network Analysis software. JAKMIP1 was not included in the analysis, to

provide an unbiased view of the protein network interactions irrespective of JAKMIP1. The JAKMIP1 protein interactions identified by MudPIT exist in two Ingenuity networks: Network 1 (Figure 3-5, A), 'cell to cell signaling and interaction, nervous system development and function, protein synthesis,' which contains a remarkable 20 of the JAKMIP1 protein binders identified here out of its 34 network members, and network 2 (Figure 3-5, B), 'protein synthesis, RNA post-transcriptional modification, cell death,' which contains the remaining 11 JAKMIP1 interactors. 'Protein synthesis' was the common denominator between both of these networks and the most significant molecular and cellular function (p=3.73 E-16 – 2.8 E-3) (Figure 3-5, C). These bioinformatic results suggest that JAKMIP1 is involved in translational control because a significant preponderance of its close network neighbors are involved in that specific biological function (Oldham et al., 2008). Table 3-3 below denotes the network membership and MudPIT parameter readouts for each JAKMIP1 protein interactor.

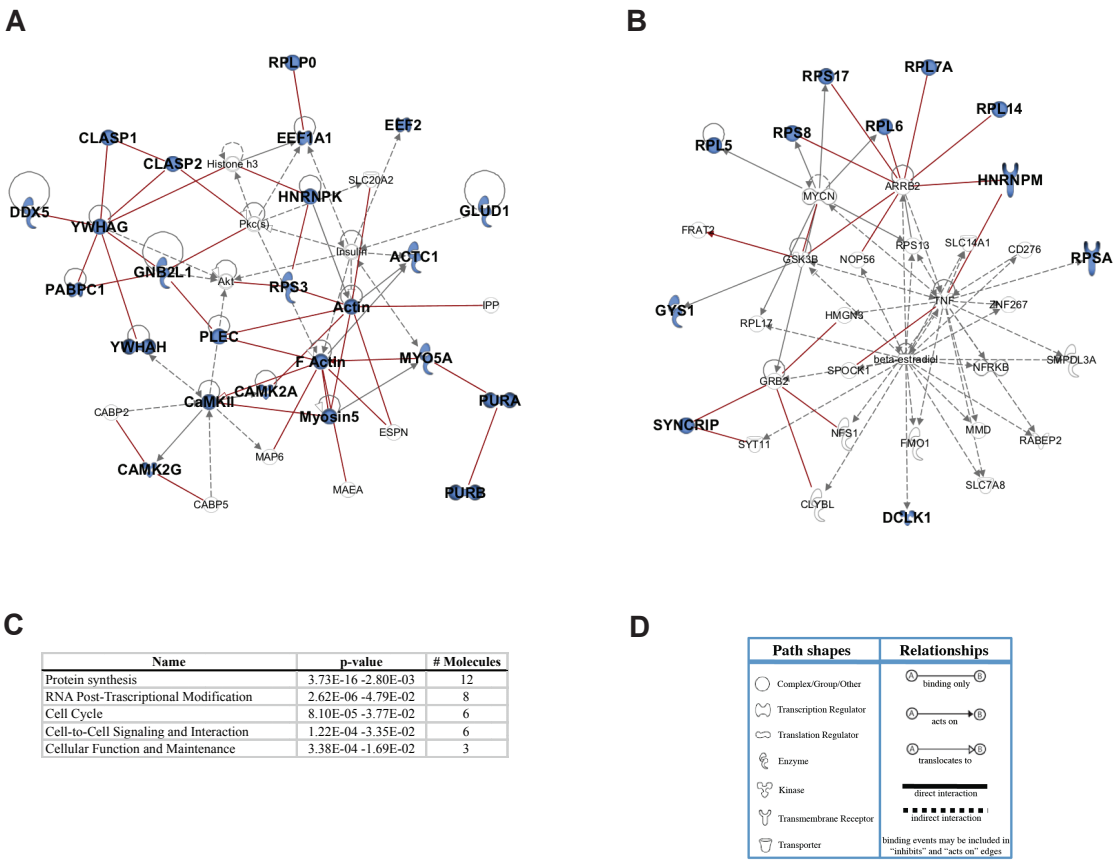

Name	p-value	# Molecules
Protein synthesis	3.73E-16 -2.80E-03	12
RNA Post-Trascriptional Modification	2.62E-06 -4.79E-02	8
Cell Cycle	8.10E-05 -3.77E-02	6
Cell-to-Cell Signaling and Interaction	1.22E-04 -3.35E-02	6
Cellular Function and Maintenance	3.38E-04 -1.69E-02	3

Figure 3-5. Ingenuity Network Analysis of JAKMIP1's top interactors highlights protein translational regulation. (A) Top scoring Ingenuity network 1, 'cell to cell signaling and interaction, nervous system development and function, protein synthesis,' from Ingenuity Pathway analysis of MudPIT-identified JAKMIP1 protein associates. (B) Second ranked gene ontology network, 'protein synthesis, RNA post- transcriptional modification, cell death.' (C) Most significant molecular and cellular functions of JAKMIP1 interactors. (D) Ingenuity Pathway Analysis Network Legend. Proteins highlighted in blue are JAKMIP1 protein interactors. Red lines indicate known protein-protein interactions.

Entrez Gene Name	Symbol	MudPIT run #1 NSAFe5*	MudPIT run #2 NSAFe5 *	MudPIT run #1 Spectral counts*	MudPIT run #2 Spectral counts*	Networks	Location
janus kinase and microtubule interacting protein 1	JAKMIP1	4455/0	855/0	177/0	129/0		Cytoplasm
actin, alpha, cardiac muscle 1	ACTC1	585/0	1255/0	14/0	114/0	1	Cytoplasm
calcium/calmodulin-dependent protein kinase II alpha	CAMK2A	264/0	260/0	8/0	30/0	1	Cytoplasm
calcium/calmodulin-dependent protein kinase II gamma	CAMK2G	208/0	118/0	7/0	15/0	1	Cytoplasm
cytoplasmic linker associated protein 1	CLASP1	554/0	149/0	54/0	55/0	1	Cytoplasm
cytoplasmic linker associated protein 2	CLASP2	881/127	132/0	72/6	41/0	1	Cytoplasm
CAP-GLY domain containing linker protein family, member 4	CLIP4	895/0	194/0	40/0	33/0		unknown
doublecortin-like kinase 1	DCLK1	229/0	181/0	11/0	33/0	2	Cytoplasm
DEAD (Asp-Glu-Ala-Asp) box polypeptide 5	DDX5 ✦	436/0	41/0	17/0	6/0	1	Nucleus
eukaryotic translation elongation factor 1 alpha 1	EEF1A1 ✦	102/0	871/0	3/0	97/0	1	Cytoplasm
eukaryotic translation elongation factor 2	EEF2	202/0	174/0	11/0	36/0	1	Cytoplasm
glutamate dehydrogenase 1	GLUD1	819/195	37/0	29/4	5/0	1	Cytoplasm
guanine nucleotide binding protein (G protein), beta polypeptide 2-like 1	GNB2L1	696/257	275/0	14/3	21/0	1	Cytoplasm
glycogen synthase 1 (muscle)	GYS1	534/0	11/0	25/0	2/0	2	Cytoplasm
heterogeneous nuclear ribonucleoprotein K	HNRNPK ✦	306/235	116/0	9/4	13/0	1	Nucleus
heterogeneous nuclear ribonucleoprotein M	HNRNPM	108/0	61/0	5/0	10/0	2	Plasma Membrane
myosin VA (heavy chain 12, myoxin)	MYO5A** ✦	51/0	16/0	6/0	7/0	1	Cytoplasm
poly(A) binding protein, cytoplasmic 1	PABPC1** ✦	124/0	46/0	5/0	7/0	1	Cytoplasm
plectin	PLEC	118/0	10/0	35/0	11/0	1	Cytoplasm
purine-rich element binding protein A	PURA** ✦	147/0	65/0	3/0	5/0	1	Nucleus
purine-rich element binding protein B	PURB ✦	584/0	51/0	12/0	4/0	1	Nucleus
ribosomal protein L14	RPL14	871/0	76/0	12/0	4/0	2	Cytoplasm
ribosomal protein L5	RPL5	955/0	70/0	18/0	5/0	2	Cytoplasm
ribosomal protein L6	RPL6 ✦	586/0	70/0	11/0	5/0	2	Cytoplasm
ribosomal protein L7a	RPL7A	829/0	31/0	14/0	2/0	2	Cytoplasm
ribosomal protein, large, P0	RPLP0 ✦	845/0	92/0	17/0	7/0	1	Cytoplasm
ribosomal protein S17	RPS17	1634/0	154/0	14/0	5/0	2	Cytoplasm
ribosomal protein S3	RPS3	1167/0	102/0	18/0	6/0	1	Cytoplasm
ribosomal protein S8	RPS8	1212/522	100/0	16/4	5/0	2	Cytoplasm
ribosomal protein SA	RPSA	694/0	56/0	13/0	4/0	2	Plasma Membrane
RUN and FYVE domain containing 3	RUFY3	235/174	88/0	7/3	10/0		unknown
synaptotagmin binding, cytoplasmic RNA interacting protein	SYNCRIP ✦	253/0	27/0	10/0	4/0	2	Nucleus
tubulin, alpha 4a	TUBA4A	1512/0	2695/0	43/0	291/0		Cytoplasm
tyrosine 3-monooxygenase/tryptophan 5-monooxygenase activation protein, gamma polypeptide	YWHAG	191/0	739/0	3/0	44/0	1	Cytoplasm
tyrosine 3-monooxygenase/tryptophan 5-monooxygenase activation protein, eta polypeptide	YWHAH	128/0	641/0	2/0	38/0	1	Cytoplasm
	1810049H19Rik	1112/0	895/0	18/0	55/0		
	Igkv1-117	1787/0	122/0	27/0	7/0		

*(JAKMIP1 IP values/Control IP values)

**Did not meet spectral criteria, but did meet 2 of 3 screening criteria

✦FMRP interactors

Table 3-3. Network membership and MudPIT readout of JAKMIP1 protein interactors in postnatal mouse neocortex.

It is notable that Ingenuity network 1 is built on protein-protein interactions, rather than on other relationships used to assemble Ingenuity networks, consistent with this network representing a true proteomic interactome. To further explore known protein-protein interactions, we used the Human Protein Reference Database (Prasad et al., 2009) and identified a statistically significant enrichment of known protein-protein interactions (PPIs), direct or complex, in network 1. This analysis identifies protein interactions conserved between mouse and human, as the MudPIT experiments were conducted in mouse, while the protein reference database is based on human protein-protein interactions. Filtering out self-interactions, we identified seventeen protein associations within the list of HPRD protein interactions: CAMK2G/CAMK2A, HNRNPK/DDX5, HNRNPK/GNB2L1, PABPC1/GNB2L1, PABPC1/HNRNPK, PURA/MYO5A, PLEC1/ACTC1, PLEC1/GNB2L1, PURB/PURA, RPS3/DDX5, RPLP0/DDX5, RPLP0/EEF2, RPLP0/RPS3, YWHAG/CLASP1, YWHAG/EEF1A1, YWHAG/PABPC1, YWHAH/YWHAG. Of note, 8 of the 17 protein-protein interactions (47%) identified by HPRD analysis were not reported by Ingenuity (HNRNPK/DDX5, HNRNPK/GNB2L1, PABPC1/HNRNPK, RPS3/DDX5, RPLP0/DDX5, RPLP0/EEF2, RPLP0/RPS3, YWHAG/EEF1A1), suggesting that network 1 is even more tightly connected than reflected by Ingenuity. A permutation analysis to test the statistical significance of seventeen interactions occurring within a list of 20 proteins versus random chance yielded a p value of p=3.36 E-12, confirming the pathway-based enrichment analysis.

3.6 JAKMIP1 binds FMRP mRNA targets independently of FMRP

Given that JAKMIP1 associates with FMRP and the translational machinery, we next asked whether JAKMIP1 binds to mRNAs whose translation is regulated by FMRP. To test this, we conducted RNA immunoprecipitation (RIP) reactions. We immunoprecipitated JAKMIP1

from developing mouse cortex under RNase-free conditions at a stringency where FMRP is not bound to JAKMIP1 based on our MudPIT analysis and tested for associated RNA using RTPCR for nine known FMRP mRNA targets (Dictenberg et al., 2008; Napoli et al., 2008; Santoro et al.; Zalfa et al., 2007): *Sapap4*, *Dag1*, *Map1b, αCaMKII, App*, *PSD95*, *Ef1a*, *BC1*, *Fmr1*. As a positive control, we immunoprecipitated FMRP from the same protein lysate and tested for the association of the same mRNA targets. Of the nine mRNAs tested, we found that *Sapap4*, *Dag1*, *App*, *PSD95*, *Ef1a*, *BC1*, and *Fmr1* all demonstrated enrichment in the JAKMIP1 IP condition over the rabbit IgG control condition (Figure 3-6, A). *Map1b* and *αCaMKII* were also enriched in the JAKMIP1 IP over the control IP, but to a lesser degree than what was observed in the FMRP positive control (Figure 3-6, A). To test if JAKMIP1 is able to bind FMRP mRNA targets in the absence of FMRP, we repeated this experiment in *Fmr1* KO postnatal mouse neocortex. JAKMIP1 retained association with FMRP's mRNA targets independent of FMRP (Figure 3-6, B). We conducted JAKMIP1 immunoblotting of JAKMIP1 immunoprecipitation reactions as well as FMRP immunoblotting of *Fmr1* wild-type (WT) and KO mouse cortical tissue to validate immunoprecipitation and knockout, respectively (Figure 3-6, A and B bottom panels).

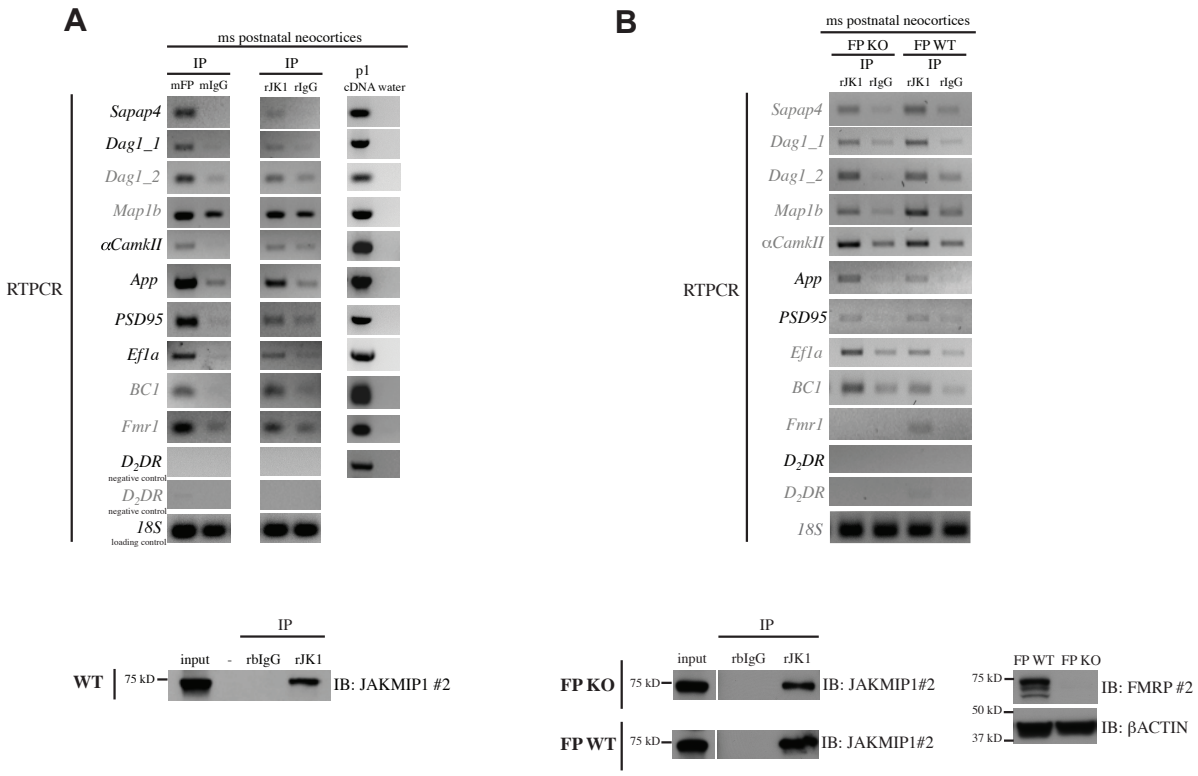

Figure 3-6. JAKMIP1 immunoprecipitates with validated FMRP mRNA targets.
(A) JAKMIP1 immunoprecipitates with FMRP mRNA targets in mouse postnatal neocortices. Left column: RNA immunoprecipitating with FMRP (positive control) or mouse IgG (negative control). Middle column, RNA immunoprecipitating with JAKMIP1 or rabbit IgG (control). Right column, all tested mRNA targets are present in p1 cortex. D2DR, not regulated by FMRP, serves as a negative control while 18S, a highly abundant RNA species, serves as a loading control. Bottom panel shows corresponding JAKMIP1 IP reaction. (B) JAKMIP1 immunoprecipitates with FMRP mRNA targets in the absence of FMRP. From left to right: RNA immunoprecipitating with JAKMIP1 (lane 1) or rabbit IgG (lane 2) in FMRP KO mouse neocortex, and JAKMIP1 (lane 3) or rabbit IgG (lane 4) in WT mouse neocortex. Bottom leftmost panel show corresponding JAKMIP1 IP reactions. Bottom rightmost panel shows loss of FMRP protein in the *Fmr1* KO mouse brain used for RIP experiments. RTPCR targets analyzed at 30 cycles are in black and at 35 cycles in grey. Abbreviations are: rJK1, JAKMIP1 #1; mFP, FMRP #2; rIgG, rabbit IgG; mIgG, mouse IgG; FP, FMRP.

To further validate the binding of FMRP's mRNA targets with JAKMIP1, we conducted quantitative RTPCR from RNA immunoprecipitating with JAKMIP1 or rabbit IgG in independent mouse postnatal neocortices from both WT and *Jakmip1* KO mice (negative control), which we generated in collaboration with the UC Davis KOMP Repository Knockout Mouse Project (Figure 5-1). As a positive control, we repeated these experiments by

immunoprecipitating FMRP or IgG from an additional set of postnatal neocortices from WT mice and analyzed bound RNA by quantitative RTPCR. *Sapap4*, *App*, *Dag1*, *PSD95* and *Camk2a* all showed statistically significant enrichment in JAKMIP1 immunoprecipitation conditions in WT versus *Jakmip1* KO postnatal mouse brains (Figure 3-7, A). *Map1b* and *Jakmip1*, itself, showed a trend toward enrichment as well. *D2DR*, not regulated by FMRP, served as a negative control in these experiments and did not demonstrate binding in any of the conditions tested (Figure 3-7, B). Interestingly, FMRP showed statistically significant binding to *Jakmip1* RNA (Figure 3-7, A). This is consistent with the fact that both human and mouse *JAKMIP1* RNA contain two G-quadruplex motifs (Nishimura et al., 2007), which FMRP is known to associate with. We validated JAKMIP1 immunoprecipitations and confirmed knockout of JAKMIP1 in the *Jakmip1* KO mouse used (Figure 3-7, B).

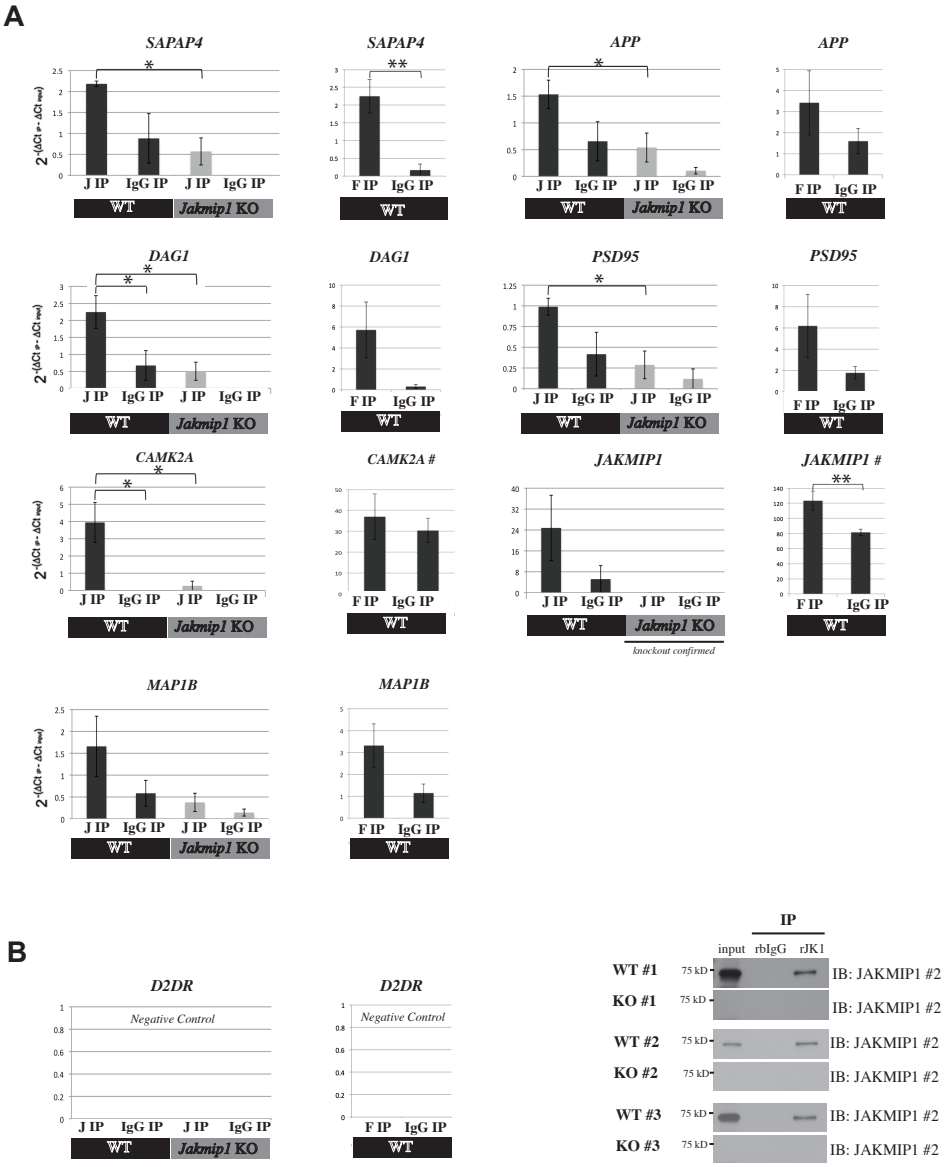

Figure 3-7. JAKMIP1 immunoprecipitates with validated FMRP mRNA targets by quantitative RTPCR. (A) Quantitative RTPCR of FMRP mRNA targets extracted from JAKMIP1 (J IP) or rabbit IgG (IgG IP) immunoprecipitations from wild-type (WT, N=3) and *Jakmip1* knockout (KO, N=3) postnatal brains. FMRP IP (F IP) and control IPs (IgG IP) were conducted as a positive control and shown to the right of each graph (WT, N=4). Number sign denotes data from an additional experiment using modified immunoprecipitation conditions (WT, N=5). (B) D2DR, not regulated by FMRP, serves as a negative control and shows no signal by qRTPCR. Western blots to the right show JAKMIP1 (rJK1, JAKMIP1 #1) and rb IgG IP reactions in (A). Fold change values were transformed linearly. Statistical significance determined using a two sampled, one tailed t test with unequal variance. *$p < 0.05$, ** $p<0.01$.

3.7 Discussion

In this chapter, we identified translational control as JAKMIP1's overarching biological function through gene ontology analysis of its developmental protein interactome by mass spectrometry. We further found JAKMIP1 to be a novel member of an FMRP translational RNP complex by demonstrating that FMRP and JAKMIP1 share protein and RNA high confidence interactors and by showing significant overlap of JAKMIP1's proteomic interactome with known FMRP RNP complexes. Additionally, we identified single-stranded RNA dependent interactions within the JAKMIP1 protein complex, consistent with this complex being involved in translational regulation.

The relationships within the JAKMIP1-FMRP RNP complex are not only consistent with other proteomic interactomes (Prasad et al., 2009; Sakai et al., 2011), but also show a statistically significant overlap with known FMRP-associated translational mRNP complexes (Kanai et al., 2004; Villace et al., 2004). However, it is striking that JAKMIP1 was not previously identified in these complexes. One possibility is that these complexes were in adult mouse brain (Kanai et al., 2004) and human embryonic kidney cells (Villace et al., 2004). As we show here, JAKMIP1 levels peak during the second postnatal week in mouse brain, coincident with the height of synaptogenesis, while its levels are low in adult brain. Therefore, it is plausible that low JAKMIP1 levels in the adult previously challenged its detection in these complexes, or that its binding to FMRP-associated RNP complexes is a more transient developmental phenomenon. Its absence in kidney cell RNA complexes is most certainly due to its undetectable expression in this tissue (Steindler et al., 2004).

We show here that the JAKMIP1-FMRP relationship does not depend on RNA. Given this and the lack of JAKMIP1-FMRP binding at the high salt conditions used for MudPIT, this

association is likely mediated by a protein intermediate. One candidate, FXR1, one of three 'FMRPs' (Kanai et al., 2004), sits at a point of convergence between our study and a recently reported human yeast two hybrid screen (Sakai et al., 2011). FXR1 was identified as a JAKMIP1 interactor in one of our MudPIT trials and was found to directly bind human JAKMIP1 *in vitro* (Sakai et al., 2011). Notably, CAMK2A, CAMK2G, and HNRNPM, JAKMIP1 MudPIT interactors, were also found to be FXR1 binders in this study, bolstering the validity of the protein complex identified here. Testing the dependency of the JAKMIP1-FMRP relationship on FXR1 will be an interesting area of future study.

Taken together, these data implicate JAKMIP1 as a novel component of an FMRP translational complex. The subsequent chapter will present functional analyses that test JAKMIP1's role in FMRP-related translational control.

3.8 Methods

Mass Spectrometry

JAKMIP1 was immunoprecipitated from the S2 fraction (Vidal et al., 2007) from duplicate pools of independent C57BL/6 mouse neocortices (N=8) during the height of JAKMIP1 protein expression, p8-p12, using protein A Dynabeads (Invitrogen) and JAKMIP1 #1 (Steindler et al., 2004) (JAKMIP1 IP) or rabbit preimmune serum (control IP). Analysis by mass spectrometry was conducted as previously described (Wohlschlegel, 2009).

Gene ontology analysis.

GO analysis was conducted using Ingenuity Pathway Analysis software (http://www.ingenuity.com). MudPIT-identified JAKMIP1 protein interactors listed in Table 3-1 were analyzed after removing JAKMIP1 and two proteins not recognized by Ingenuity, 1810049H19Rik and Igkv1-117.

Permutation analysis

The R programming language was used to identify JAKMIP1 protein interactors from gene ontology network 1 that are listed in HPRD (http://www.hprd.org/query; release 9) with at least one protein-protein interaction (PPI). All 20 Network 1 JAKMIP1 interactors met this criteria (ACTC1, CAMK2A, CAMK2G, CLASP1, CLASP2, DDX5, EEF2, EEF1A1, GNB2L1, HNRNPK, MYO5A, PABPC1, PURA, PLEC, PURB, RPS3, GLUD1, RPLP0, YWHAG, YWHAH). A permutation analysis was conducted by sampling 20 proteins 10,000 times from the pool of proteins in HPRD with at least one interaction (N=9819), where interactions include protein pairs with known direct interactions as well as protein pairs that are part of known protein complexes. Since we never saw more than six PPIs in any permutation, significance was estimated by first fitting the PPI counts with a logarithmic distribution, and then estimating the expected number of permutations required to obtain the 17 PPIs observed in network 1 by chance.

Hypergeometric Probability Calculations

JAKMIP1 interactors were defined being present in both MudPIT runs, having NSAfe5 and spectral counts positive for JAKMIP1 IP versus rabbit preimmune serum IP in both runs and NSAfe5 differentials greater than 50 in at least one run (N=72). There were 4 and 7 JAKMIP1 interactors, respectively, also belonging to previously defined FMRP-RNP complexes each containing 10 (Kanai et al., 2004) or 24 (Villace et al., 2004) members, respectively (Table 3-2). Hypergeometric probability was calculated using R code 1-phyper (k-1, j, m-j, n) with the following definitions: ‘m’ is the universe of proteins defined as all brain expressed genes (15,132) (Kang et al., 2011), k is number of overlapping proteins, j is the number of FMRP complex members, and ‘n’ is the number of JAKMIP1 interactors.

Immunoprecipitation

Immunoprecipitations were conducted using Dynabead protein A (for rabbit antibodies) or protein G (for mouse antibodies) according to manufacturer's instructions (Invitrogen) in a ratio of 60:4:1 [lysate (ug): Dynabeads (ul): antibody (ug)]. For RIP experiments, JAKMIP1 IPs and FMRP IPs were conducted at a ratio of 60:4:0.2 [lysate (ug): Dynabeads (ul): antibody (ug)]. FMRP IPs denoted by # were conducted at a ratio of 60:4:2 (Figure 3-7, A). Proteins were precipitated with an equal or greater ug amount of rabbit or mouse IgG (Millipore) in control conditions.

Antibodies

Additional antibodies used in this chapter are the following:

Name	Antigen/Peptide wording from company website when appropriate	Species/Clonality	Source/Catalogue number
PABPC1	synthetic peptide conjugated to KLH derived from within residues 600 to the C terminus of hu PABP	Rabbit polyclonal	Abcam ab21060
CAMK2G	Cter of Camk2g immunogen ID ag3348	Rabbit polyclonal	Proteintech Group 12666-2-AP
CLASP2	Amino acids 21-60 mapping near the Nter of human Clasp2	Rabbit polyclonal	Santa Cruz sc-98440
BACTIN	slightly modified β-cytoplasmic actin N-terminal peptide, Ac-Asp-Asp-Asp-Ile-Ala-Ala-Leu-Val-Ile-Asp-Asn-Gly-Ser-Gly-Lys, conjugated to KLH.	Mouse monoclonal	Sigma A1978
FMRP #1	Amino acids 513-632 at the C terminus of human FMRP	Rabbit polyclonal	Santa Cruz sc-28739
FMRP #2	the N-terminal half of human	Mouse monoclonal	Millipore

	FMRP		MAB2160

IP followed by RT-PCR and RT-Quantitative PCR analysis

Immunoprecipitation followed by RTPCR and quantitative RTPCR reactions were conducted as previously described (Napoli et al., 2008) with the following modifications. For immunoprecipitation reactions, Protein A Dynabeads (Invitrogen, Carlsbad, CA) were used with JAKMIP1 #1, and rabbit IgG control, while Protein G Dynabeads (Invitrogen, Carlsbad, CA) were used with mouse anti FMRP (Millipore) and mouse IgG control. RNA was extracted using a miRNeasy kit (Qiagen, Germantown, MD) and reverse transcriptase reactions were carried out using Superscript III and random hexamers (Invitrogen, Carlsbad, CA) according to manufacture's instructions. The following primer sets were used for Reverse Transcriptase PCR reactions: *Sapap4_set2*, *a-CaMKII, PSD95_3', Map1b, Fmr1, Ef1a1, Dag1_set1, Dag1_set2, D_2DR, BC1, App, and 18S*. PCR Thermocycler conditions were the following: 94°C for 2 minutes, 30 or 35 cycles of 94°C for 30 seconds, 60°C for 30 seconds, and 72°C for 1 minute, then 72°C for 2 minutes and hold at 4°C. Quantitative RTPCR was carried out using Light Cycler 480 II (Roche Applied Science, Indianapolis, IN) and SensiFAST SYBR No-Rox mix (Bioline, Taunton, MA). Transcript levels were calculated using the LightCycler 480 SW 1.5 software (Roche Applied Science, Indianapolis, IN).

Primer Sets Used

Primers	Forward 5'-3'	Reverse 5'-3'	reference
α-CaMKII	AGCCATCCTCACCACTATGCTGG	ACCCTGGCCTGGTCCTTCAATG	Napoli et al. 2008
Sapap4_set2	CATCGGGATTCAGGTAGAGG	ATAGGAGAGGTTGCGCTTGA	
PSD-95_3'	GGCTTCATTCCCAGCAAACG	CATCAAGGATGCAGTGCTTC	Zalfa et al. 2007
Map1b	GGCAAGATGGGGTATAGAGA	CCCACCTGCTTTGGTATTTG	Napoli et al. 2008

Jakmip1_exons 3-4	GCGGAAGAGGCACTCAGTAA	GTTTGCACACCAAGCTCCTT	
Fmr1	GTGGTTAGCTAAAGTGAGGATGAT	CAGGTTTGTTGGGATTAACAGATC	Napoli et al. 2008
Ef1a1	CCAATGGAAGCAGCTGGCTT	CCGTTCTTCCACCACTGATTA	Zalfa et al. 2007
Dag1_set2	GTGAGCATTCCAACGGATTT	TGGCTCATTGTGGTCTTCAG	
Dag1_set1	CTGGAAGAACCAGCTTGAGG	GGACAGTCACTGGCTCATCA	
D_2DR	GGCCATGCCTATGTTGTATAA	CCCATTCTTTTCTGGTTTGG	Napoli et al. 2008
BC1	GTTGGGGATTTAGCTCAGTGG	AGGTTGTGTGTGCCAGTTACC	Napoli et al. 2008
App	GGTGGCTGAGGAGATTCAAG	TCACGGTTGCTATGACAACGC	Napoli et al. 2008
18S	CATTAAATCAGTTATGGTTCCTTTGG	TCGGCATGTATTAGCTCTAGAATTACC	
bactin	AGAGGGAAATCGTGCGTGAC	CAATAGTGATGACCTGGCCGT	

Chapter 4: JAKMIP1 regulates neuronal translation and FMRP mRNA targets

4.1 Introduction

We previously demonstrated JAKMIP1's membership in an FMRP RNP complex and its involvement in translation by relationship to proteins involved in this process. Here, we conduct several complementary experiments to further test JAKMIP1's membership in the translational machinery and its role in regulating neuronal translation.

Because JAKMIP1 likely influences translation in concert with its binding partner, FMRP, whose predominant function is translational control (De Rubeis and Bagni, 2011; Rousseau et al., 2011; Santoro et al., 2012), we asked if JAKMIP1 affects the translational regulation and synaptic localization of mRNA targets shared with FMRP. I hypothesized that JAKMIP1 would be involved in transporting its RNA to the synapse as it is bidirectionally mobile in the dendrites of cultured hippocampal neurons (Vidal et al., 2007) and shows high expression in dendritic shafts (Vidal et al., 2009). Moreover, one study also suggests that JAKMIP1 transports and regulates the expression of $GABA_B$ receptor mRNA and protein (Vidal et al., 2007). Other data support an RNA-binding role for JAKMIP1, as it binds to synthetic RNA polymers (Couve et al., 2004).

We find that JAKMIP1 shows clear association with the translational machinery *in vitro* and in postnatal mammalian cortex. Furthermore, we demonstrate that loss of JAKMIP1 leads to decreased neuronal translation. Additionally, absence of JAKMIP1 decreases PSD95 protein, but not RNA levels, in postnatal neocortices, suggesting a role for JAKMIP1 in PSD95 translational regulation. We support this result by showing attenuated loading of PSD95 RNA on polyribosomes *in vivo*. Our data also support a role for JAKMIP1 in transport of its targets, as ablation of *Jakmip1* in postnatal mouse neocortices results in a significant reduction of FMRP mRNA targets at the synapse. These results identify JAKMIP1 as a functional component of an

FMRP RNP translational complex.

4.2 JAKMIP1 and its protein interactome associate strongly with the translational machinery

Gene ontology assessment of JAKMIP1's postnatal, neocortical proteomic interactome suggest JAKMIP binding to the translational machinery. To confirm that JAKMIP1 co-fractionates with the translational machinery *in vivo*, we conducted polyribosome fractionation from WT mouse postnatal neocortices in independent mice (N=3). We found that JAKMIP1 shows strong expression in polyribosome fractions (Figure 4-1, A). We tested two additional JAKMIP1 binding partners identified here and known FMRP protein binding partners, DDX5 (Ishizuka et al., 2002; Kanai et al., 2004) and PABPC1 (Napoli et al., 2008), for polyribosome expression. Both were expressed in polyribosomes (Figure 4-1, A, B). PABPC1 serves as a polyribosome-positive control; it is critical for polyribosome formation, as it circularizes the mRNA to be translated (Gebauer and Hentze, 2004; Napoli et al., 2008). Importantly, other top JAKMIP1 interactors identified here (Table 3-3) are known to be enriched in polyribosomes, such as EEF2, EEF1A (Kanai et al., 2004), PURA (Ohashi et al., 2002), MYO5A (Ohashi et al., 2002) and ribosomal subunits proteins.

We next tested JAKMIP1's association with the polyribosome complex by *in vivo* intraperitoneal administration of puromycin, which causes premature release of the growing peptide chain and disrupts the translational machinery (Stefani et al., 2004). Intraperitoneal injection of puromycin in mouse has been shown to effectively reduce cortical translation (Flexner et al., 1962). Puromycin treated postnatal neocortices showed less JAKMIP1 in polyribosome fractions than phosphate buffered saline injected controls, consistent with JAKMIP1 being a member of the translational machinery (Figure 4-1, A). PABPC1 and DDX5,

JAKMIP1 protein interactors identified here, also shifted to lighter fractions upon puromycin treatment (Figure 4-1, A). We found that PABCP1 and DDX5 polyribosome profiles were also disrupted in *Jakmip1* KO mice (N=3), both showing shifts to lighter fractions compared to WT controls resembling the changes seen with *in vivo* puromycin injection (Figure 4-1, A-B).

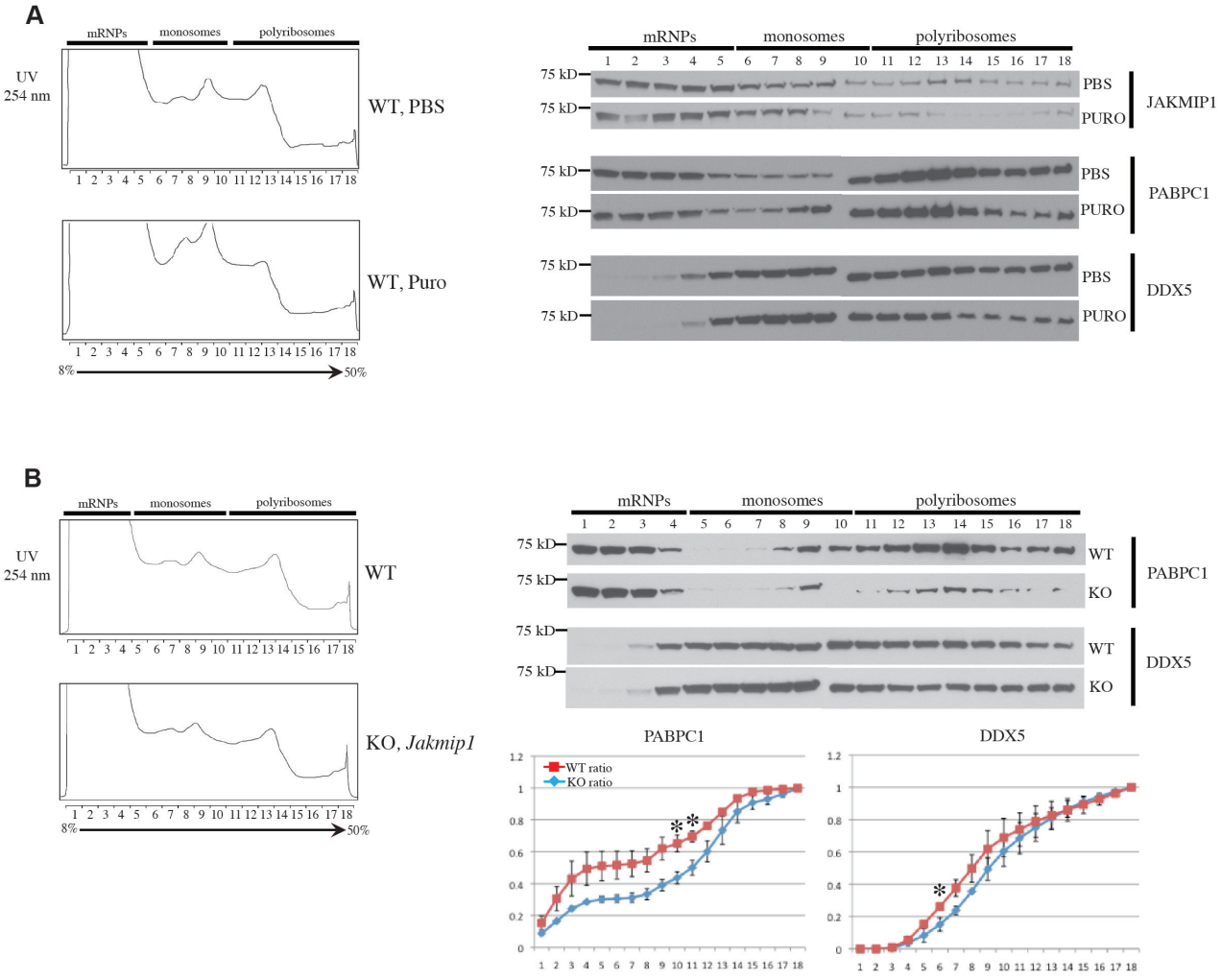

Figure 4-1. JAKMIP1 is an integral component of the translational machinery.
(A) Representative polyribosome fractionation profiles from mouse postnatal neocortices injected intraperitoneally with PBS or 1.26 mg/gram puromycin (left). Neocortices were harvested seven hours post injection. Representative western blots demonstrating protein expression in each polyribosome fraction are shown to the right. (B) Representative polyribosome fractionation profiles from mouse postnatal neocortices of WT or *Jakmip1* KO (left). Representative western blots demonstrating protein expression in each polyribosome fraction are shown to the right. Graphs below are the cumulative ratio of protein signal (Y-axis) per fraction (X-axis). Values are mean +/- SEM.
* $p < 0.05$, two sample, one-tailed t-test.

In a complementary test of JAKMIP1's association with the translational machinery, we determined if JAKMIP1 binds to eGFP fused polyribosomes in mouse N2A cells by co-immunoprecipitation. We took advantage of a BacTRAP cell line in which RPL10A, an integral part of the 60S ribosome subunit, is fused to an enhanced green fluorescent protein tag (Heiman et al., 2008). We used anti eGFP antibodies to isolate the translational machinery by immunoprecipitation and immunoblotted the reaction for PABPC1, DDX5, JAKMIP1, and eGFP (positive control). JAKMIP1, DDX5, and PABPC1 all immunoprecipitated with the translational machinery (Figure 4-2, A). Non specific binding of eGFP to polyribosomes was discounted as a possible interpretation of this result (Figure 4-2, B).

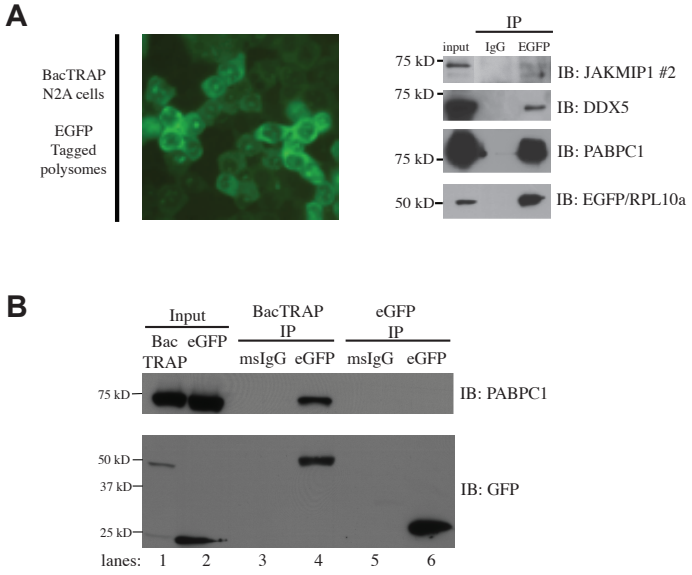

Figure 4-2. JAKMIP1 associates with the translational machinery in vitro.
(A) JAKMIP1, DDX5 and PABCP1 coimmunoprecipitate with EGFP-L10a polyribosomes in BacTRAP N2A cells. Polysomes were immunoprecipitated using anti-eGFP antibody followed by immunoblotting for JAKMIP1, DDX5, PABPC1, and eGFP. (B) The eGFP protein of the BacTRAP fusion protein does not bind non specifically to polyribosomes. PABPC1, a component of the polyribosome and JAKMIP1 interactor, associates with BacTRAP eGFP-RPLP0 fusion proteins (lane 4, top panel) but not eGFP alone (lane 6, top panel). GFP is effectively immunoprecipitated from BacTRAP cell lines (lane 4, bottom panel) and cell lines expressing eGFP alone (lane 6, bottom panel).

Lastly, we tested if JAKMIP1 colabels with PABPC1-containing RNP granules. RNP granules are dynamic structures with heterogeneous members and functions (Kiebler and DesGroseillers, 2000). We reasoned that JAKMIP1 is a likely member of a transport RNP, as these structures are involved in translation (Kiebler and DesGroseillers, 2000) and, like JAKMIP1(Vidal et al., 2007), are motile. Additionally, known transport RNPs contain several JAKMIP1 binding partners identified by MudPIT (Table 3-2), including PABPC1, which is a component of an FMRP containing RNP (Villace et al., 2004). To test if JAKMIP1 co-labels with PABPC1 positive granules, we overexpressed human JAKMIP1 and human PABPC1 in differentiated mouse neural progenitor cells lacking *Jakmip1* and assessed localization by immunocytochemistry. We observed that JAKMIP1 co-localizes with PABPC1-positive RNP granules, providing another independent line of evidence for its membership in these complexes (Figure 4-3).

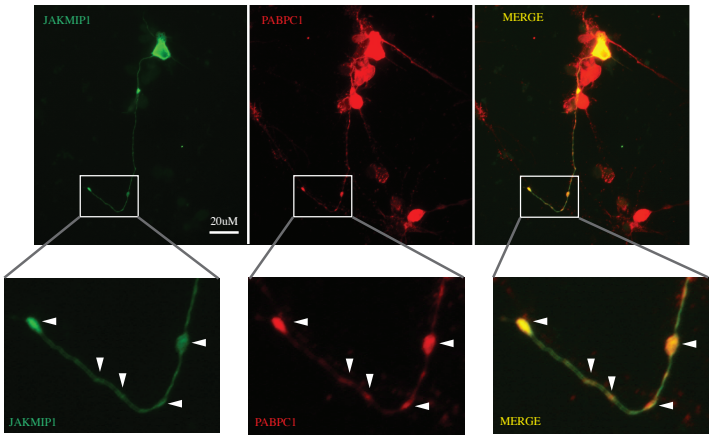

Figure 4-3. JAKMIP1 colocalizes with PABPC1 *in vitro*.
JAKMIP1 is present in PABPC1-positive granules (arrows). A human PABPC1-dsRED fusion protein and human JAKMIP1 N-ter construct were coexpressed in differentiated mouse neurons of *Jakmip1* KO mice and immunolabled using an anti RFP antibody (middle panel) or an anti V5 antibody (left panel). Scale bar is 20 um.

4. 3 JAKMIP1 regulates FMRP shared mRNA targets

Since our data show that JAKMIP1 binds several known FMRP RNA targets, I hypothesized that JAKMIP1 might regulate the expression of these targets, as FMRP is heavily involved in translational control. We tested this by analyzing the protein and RNA expression of the aforementioned targets, *Sapap4*, *App*, *Dag1*, *PSD95*, and *Camk2a,* both in the total postnatal neocortex and in synaptosomal fractions, where FMRP translational control is known to occur. *Map1b* was also included in this study, as it showed a trend toward binding to JAKMIP1 protein in RIP-RTPCR experiments. PSD95 showed a statistically significant decrease in protein expression, both in total cortical protein and in protein from synaptosomal membranes (Figure 4-4, A). PSD95 RNA levels from total cortex, however, did not change (Figure 4-4, C left), suggestive of a role for JAKMIP1 in translation of this target.

To determine if the reduction of PSD95 protein in postnatal neocortex of *Jakmip1* KO mice is due to a disruption of translation, we tested if PSD95 mRNA showed reduced loading in the polyribosome fraction of *Jakmip1* KO mice (N=3) compared to sex-matched littermate controls. We found that *PSD95* mRNA is reduced in the monosome and polyribosome fractions of *Jakmip1* KO mice (Figure 4-4, B). This further implicates JAKMIP1 in PSD95 translational control.

Interestingly, JAKMIP1 mRNA targets, *Sapap4*, *App*, *Dag1*, *PSD95*, and *Camk2a,* combined showed a significant reduction in expression in synaptosomal fractions from *Jakmip1* KO postnatal neocortices versus WT controls (Figure 4-4, C right), potentially implicating JAKMIP1 in the transport of these targets to the synapse.

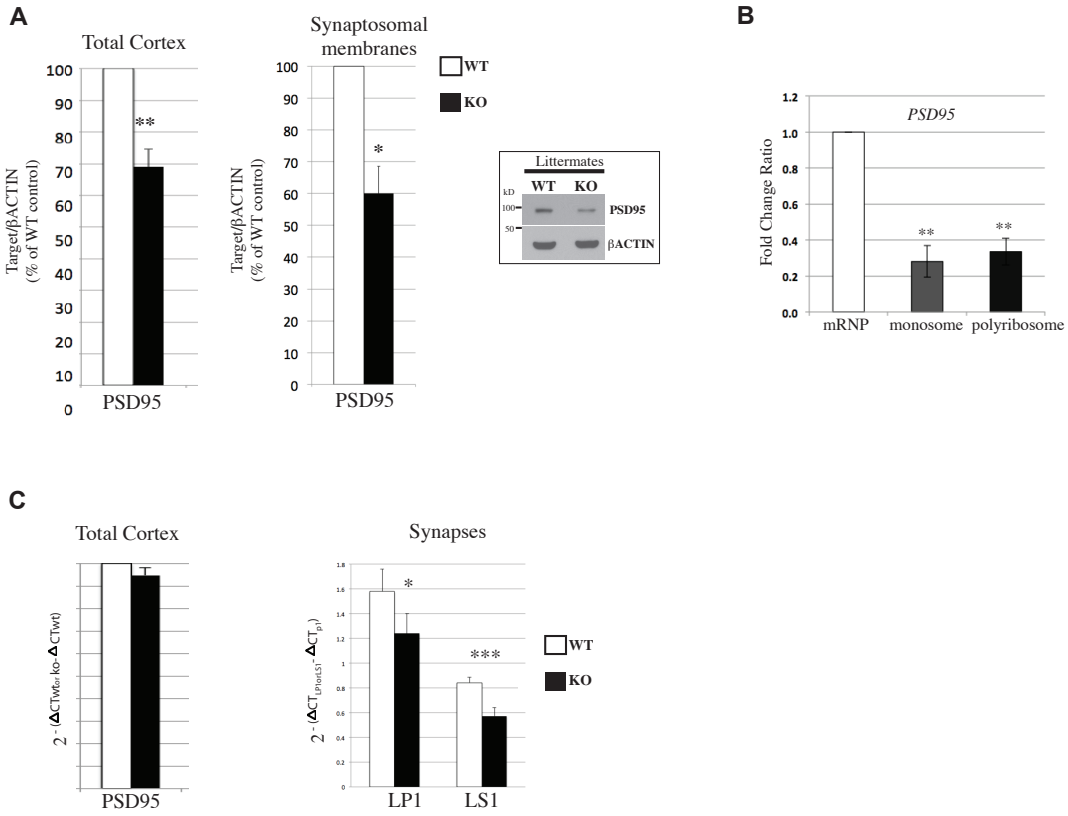

Figure 4-4. Loss of JAKMIP1 in mouse postnatal neocortices decreases PSD95 protein and target RNA expression in synaptosomal fractions.

(A) Reduction of PSD95 protein in total cortex and synaptosomal membranes of *Jakmip1* KO mice shown as a percentage of WT littermate protein levels measured by image densitometry. Values are mean +/- SEM (WT, N=3; KO, N=4, as one litter contains two KOs). Statistical significance for total cortex protein levels is determined using a linear mixed-effects model controlling for random effects of litter (P=0.005). For synaptosomal membranes, the fixed effects of blot and random effects of litter was controlled for (P=0.03). A representative western blot is shown to the right. (B) PSD95 mRNA is reduced in the monosome and polyribosome fractions of *Jakmip1* KO mice (N= 4; Monosomes, p=0.0020; Polyribosome, p=0.0015; one-tailed unpaired Student's t-tests). Values are mean +/- SEM. ** p< 0.01 (C) RNA levels of PSD95 in total cortex (left) or of JAKMIP1/FMRP shared RNA targets in synaptosomal fractions (right). Expression of PSD95 RNA in total cortex is displayed as fold change from WT littermate control and is measured by quantitative RTPCR. Values are mean +/- SEM (WT, N=3; KO, N=4). P-values were calculated from a two sample, two tailed t-test of delta CT values (Target-βactin). Statistical significance for reduction of RNA targets in synaptosomal fractions is determined using a linear mixed-effects model controlling for the random effects of litter and fixed effects of gene (WT, N=6; KO, N=7, litter or cagemates: LPI, P=0.046; LS1, P=0.0006).

* p <= 0.05, ** p<= 0.01, *** p <= 0.001. P1 (nuclei and large debris), LP1 (synaptosomal membranes), and LS1 (synapses minus membranes).

Other shared JAKMIP1/FMRP mRNA targets did not show changes in protein or RNA in total cortex (Figure 4-5, A) or in synaptosomal fractions (Figure 4-5, B). Notable exceptions are that the DAG1 precursor protein showed a statistically significant increase in protein expression in total cortex (Figure 4-5, A) and *Dag1* demonstrated a statistically significant decrease in RNA levels at synapses (Figure 4-5, B). JAKMIP1 protein loss was confirmed in all protein fractions analyzed (Figure 4-5, C).

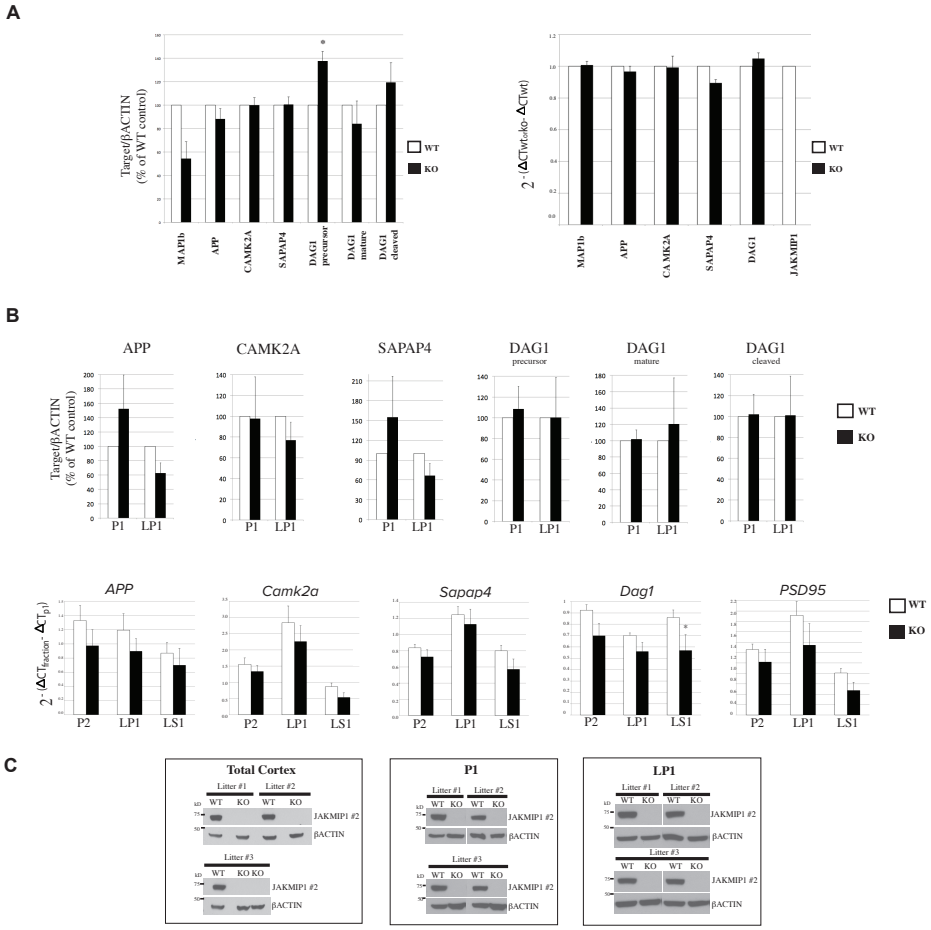

Figure 4-5. Expression of JAKMIP1/FMRP shared mRNA targets in postnatal neocortices of *Jakmip1* KO mice. (A) Protein (left) and RNA (right) levels of mRNA targets in total cortex of *Jakmip1* KO mice. Protein is shown as a percentage of WT levels, measured by image densitometry. Statistical significance for protein level changes is determined using a linear mixed-effects model controlling for random effects of litter. Expression of RNA is displayed as fold change from WT littermate control, measured by qRTPCR. P-values are calculated from a two sample, two tailed t-test of delta CT values (Target-βactin). Values are mean +/- SEM (WT, N=3; KO, N=4). (B) Protein (top) and RNA (bottom) levels of mRNA targets in synaptosomal fractions of *Jakmip1* KO mice and WT controls. Top row: Protein expression of mRNA targets in P1 (nuclei and large debris) and LP1 fractions (WT, N=3; KO, N=4, sex matched littermates). Statistical significance is determined using a linear mixed-effects model controlling for the fixed effects of blot and random effects of litter. Bottom row: Synaptosomal RNA levels in *Jakmip1* KO and WT controls. RNA expression is determined by qRTPCR and normalized to the P1 fraction signal. βactin is used as a control. Values are mean fold change +/- SEM. Statistical significance is determined using a linear mixed-effects model controlling for the random effects of litter. P2 is crude synaptosomal membranes (WT, N=5; KO, N=7), LP1 is synaptosomal membranes (WT, N=6; KO, N=7), and LS1 is synapse minus membranes (WT, N=6; KO, N=7). * p <= 0.05. (C) Loss of JAKMIP1 protein is confirmed in total cortex, P1 and LP1 fractions.

4. 4 JAKMIP1 is involved in neuronal translational control

To determine if JAKMIP1 plays a more general role in translational control, we measured new translation in neurons from *Jakmip1* KO versus WT littermate animals using Fluorescent Non–Canonical Amino Acid Tagging [FUNCAT, commercially ClickIT (Invitrogen, Carlsbad, CA)] (Dieterich et al., 2010). Differentiated mouse neuroprogenitor cells were depleted of methionine followed by incorporation of a nonradioactive reagent, L-homopropargylglycine (HPG), an analog of methionine, into newly synthesized proteins, which is then detected by a fluorescent azide molecule. We quantified the level of nascent protein synthesis by measuring fluorescent signal within neurons identified by TUJ1 immunocytochemical staining (Figure 4-6, boxes 1-3). To do this, we developed a computer program using the R software environment (http://www.r-project.org/) and the packages rimage and pixmap (downloaded via CRAN) (Figure 4-6, box 4). Images were subsequently manually curated to remove overlapping glial signal and to divide the neuron into cell body and neurite compartments (Figure 4-6, boxes 5-7).

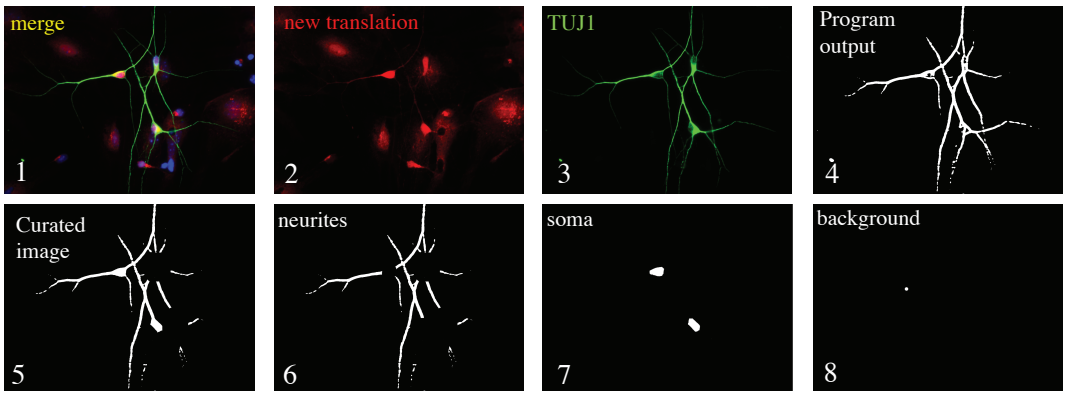

Figure 4-6. Methodology for quantification of nascent translation.
Merged TUJ1/new translation images from Click-IT translational analysis (box 1). New translation is determined by red pixels units (box 2) within the TUJ1-positive space (box 3). Representative mask images from our customized computer analysis (box 4). Images were curated to exclude artifacts and overlapping glia signal (box 5), soma (box 6), or neurites (box 7). Background fluorescence was calculated from a manually placed 19 pixel diameter circle adjacent to the neuronal space and not overlapping glia occupied space (box 8). Brightness and contrast on top row box 2 was slightly adjusted to highlight neuronal and glial translation.

We found a significant reduction in nascent neurite, soma, and whole cell translation in neurons from *Jakmip1* KO mouse brains compared to neurons from matched WT littermates (Figure 4-7). This finding implicates JAKMIP1 in global, basal neuronal translation.

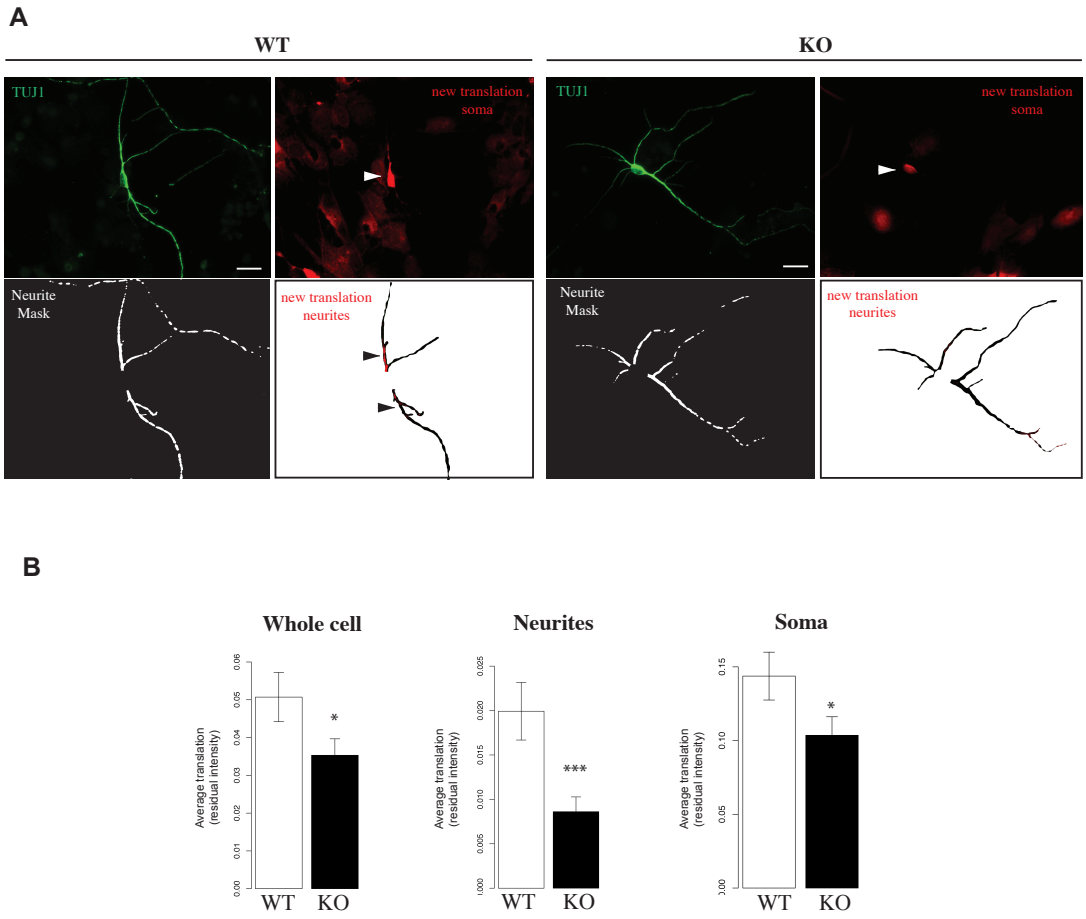

Figure 4-7. *Jakmip1* knockout decreases protein translation in TUJ1-positive neurons.
(A) Representative images used for FUNCAT analysis, where greater pixel intensity (red, Azide 555) demonstrates increased translation. To facilitate visualization of translation, brightness of the red image was increased equally for both genotypes. Two brightness levels are shown to highlight soma (brightness 1) and neurites (brightness 2). Brightness was adjusted slightly for TUJ1 images. Panel descriptions: upper left, TUJ1 (white scale bar is 20uM) ; upper right, Azide 555 (new translation, cell soma); lower left, neurite mask (space analyzed); lower right (new translation, cell neurite, analysis space shown). White arrows indicate cell soma translation, while black arrows indicate neurite translation. (B) Nascent protein synthesis, defined as the mean signal intensity (total pixel intensity/area measured) is decreased in neurites (WT, N=227; KO, N=264 images, P=0.00125) and soma and whole cell (WT, N=199, KO, N= 224 images, P=0.049 and 0.045, respectively) of neurons lacking JAKMIP1. Significance across three trials was estimated using mixed effects regression with a fixed effect covariate for date and a random intercept for litter. Residual intensity after correction for date and littermate set is displayed. * p <= 0.05, ** p<= 0.01, *** p <= 0.001.

4.5 Discussion

In this chapter, we conducted functional testing of JAKMIP1's association with the translational machinery, its regulation of FMRP shared mRNA targets, and its role in global basal translation.

JAKMIP1's membership in the translational machinery was determined using polyribosome profiling *in vivo*, BacTRAP *in vitro* experiments, and double label immunocytochemistry. JAKMIP1's polyribosome profile suggests that it is robustly expressed in polyribosomes, but demonstrates greatest expression in mRNP fractions. mRNPs are involved in the transport of the translational machinery to the synapse (Bassell and Warren, 2008). JAKMIP1 expression in mRNPs is consistent with it binding to an FMRP complex, as FMRP shows high, and sometimes exclusive, expression in mRNPs (Dictenberg et al., 2008; Papoulas et al., 2010; Siomi et al., 1996; Zalfa et al., 2003). JAKMIP1 expression in mRNPs is also consistent with its bidirectional movement along microtubules (Vidal et al., 2007). We further identify JAKMIP1 as an integral component of the translational machinery as its polyribosome profile is disrupted in postnatal neocortices of puromycin-treated mice and *Jakmip1* KO mice show disruptions in the polyribosome profiles of translational machinery components PABPC1 and DDX5 that mirror those of puromycin-injected mice.

JAKMIP1 binds the FMRP mRNA targets, *Sapap4*, *App*, *Dag1*, *PSD95* and *Camk2a*. We show here that JAKMIP1 regulates the expression and subcellular distribution of these targets. JAKMIP1's role in transporting these targets is suggested by their decreased synaptosomal expression in postnatal neocortices from *Jakmip1* KO mice. We further demonstrate that JAKMIP1 exerts translational control over PSD95, which shows protein, but not RNA, reduction in postnatal neocortices of *Jakmip1* KO mice. This is additionally supported

by loss of PSD95 mRNA from the translational machinery in postnatal neocortices of *Jakmip1* KO mice.

PSD95 protein reduction occurs with *Jakmip1* ablation and with *Fmr1* KO (Muddashetty et al., 2007; Zalfa et al., 2007). PSD95 is a major component of the postsynaptic density and a critical mediator of neuronal plasticity (Beique and Andrade, 2003; Steiner et al., 2008; Yao et al., 2004). Therefore, loss of JAKMIP1 leading to decreased PSD95 could have large behavioral ramifications. Importantly, deletion of mouse PSD95, *Dlg4*, leads to autistic like behaviors, such as communication and social abnormalities and repetitive behaviors (Feyder et al., 2010).

We, finally, demonstrate that JAKMIP1 loss reduces basal neuronal translation. This is consistent with *Jakmip1* KO mice showing decreased PSD95 protein and a trend toward reduced APP, CAMK2A, and SAPAP4 at the synapse (Figure 4-5, B). However, global translation reduction with *Jakmip1* loss suggests that JAKMIP1 regulates many additional targets, which could be identified using an 'omics' approach, such as *in vivo* BacTRAP technology (Heiman et al., 2008).

Another area of further research is to determine why absence of *Jakmip1* decreases translation, while loss of FMRP leads to a general increase in translation, seen in *Fmr1* knockout out mice (Osterweil et al., 2010; Qin et al., 2005) and in lymphoblastoid cell lines of FXS patients (Gross and Bassell, 2011). It is important to note here that the direction of FMRP's translational regulation is highly nuanced and dependent on neuronal activity (De Rubeis and Bagni, 2011; Greenough et al., 2001; Muddashetty et al., 2007; Todd et al., 2003). In fact, loss of *Fmr1* ablates activity–dependent increases in translation (Muddashetty et al., 2007).

Data further suggests that JAKMIP1 is downstream of FMRP. Loss of JAKMIP1 does not change FMRP protein or RNA levels (data not shown). However *FMR1* reduction leads to

decreased JAKMIP1 protein and RNA in mouse and human neural systems (Nishimura et al., 2007). Additionally, FMRP binds *Jakmip1* mRNA (Figure 3-7, A), but JAKMIP1 does not bind *Fmr1* mRNA (data not shown). The JAKMIP1-FMRP relationship will be an exciting area for future exploration.

In sum, these data show that JAKMIP1 not only associates with the translational machinery and binds to FMRP translational targets, but also regulates a major component of the synapse, PSD95, and affects translation globally. These data indicate that JAKMIP1 is involved synaptic function. In Chapter 5, we will test if these molecular disruptions result in behavioral abnormalities in a novel *Jakmip1* knockout mouse.

4.6 Methods

Polyribosome fractionation:

Polyribosome fractionation was conducted as described (del Prete et al., 2007) with modifications using postnatal day 8-14 C57BL/6 mouse neocortices. Fractionation experiments were repeated three times from independent mice. Protein fractions were separated through 8-50% sucrose gradient by ultracentrifugation and profiled at 254 nm using a UV Isco Fractionator (Teledyne Isco). Fractions were immunoblotted for PABPC1, DDX5, and JAKMIP1 at equal volumes and were additionally analyzed for presence of RPS6 and EIF4E, polyribosome-positive controls.

To conduct fractionation experiments, mouse neocortices were preincubated at 4 °C for 10 minutes after brief homogenization in 250ul lysis buffer (10mM Tris-HCl at pH 8.5, 150mM NaCl, 50mM $MgCl_2$, 1% Nonidet-P40, 0.1U/ul RNase OUT, 40mM dithiothreitol, 1% Sodium deoxycholate, and 1.73mg/ml cycloheximide). After further homogenization for 50 seconds at 4 °C, we added 720 ul lysis buffer and centrifuged it for 30 minutes at 12,000 g at 4 °C to remove

the nuclei. After taking the supernatant, we repeated centrifugation. The supernatant was, then, supplemented with 500ul of 2X extraction buffer (200mM Tris-HCl at pH 7.5, 300mM NaCl), 1mg/ml heparin, and 10mM phenyl-methyl-sulfonyl fluoride. It was centrifuged at 12,000 g for 5 minutes at 4 °C to remove mitochondria and membranous debris. Its supernatant was centrifuged one more time, and its supernatant was layered onto a linear sucrose gradient (8% – 50% sucrose [w/v], supplemented with 10mM Tris-HCl at pH 7.5, 140mM NaCl, 1.5mM $MgCl_2$, 10mM dithiothreitol, 0.1mg/ml cycloheximide, 0.5mg/ml heparin) and centrifuged in a SW41 rotor for 120 minutes at 38,000 rpm at 4 °C. Fractions were collected in 18 fractions. Equal volume from each faction was analyzed by western blotting.

RNA extraction from polyribosome fractions for quantitative RT-PCR

To extract RNA from polyribosomes fractions, fractions were combined for each mRNP, monosome, and polyribosome fraction based on polyribosome fraction UV profiles. For control RNA, 1ul of pAW109 RNA (Applied Biosystems, Foster City, CA) was added into 100ul of the combined fractions. Fractions were digested in 0.2mg/ml proteinase K in 1% SDS and 10mM EDTA for 60 minutes at 50 °C. Using acid phenol chloroform, RNA was extracted. To remove the high concentration of heparin, 2.5M LiCl was used for precipitation followed by 70% ethanol.

BacTRAP IPs

Immunoprecipitation reactions from BacTRAP N2A cell lines were carried out using the S2 protein fraction and an equal amount of bioreactor supernatants of mouse anti eGFP antibodies clones 19C8 and 19F7 from the Monoclonal Antibody Core Facility at Memorial Sloan-Kettering (New York, NY). Immunoprecipitations for BacTRAP experiments were performed in 0.15M KCl IP wash buffer [20mM HEPES-KOH (pH 7.4), 5mM MgCl2, 150mM KCl,

1%NP40]. Protein was precleared for two hours in mouse IgG bound Protein G Dynabeads (Invitrogen, Carlsbad, CA) prior to 4°C overnight immunoprecipitation reactions. Final washes were conducted in 0.35M KCl IP wash buffer [20mM HEPES-KOH (pH 7.4), 5mM MgCl2, 350mM KCl, 1% NP40], and protein was eluted in eluted in 100mM Tris-HCl, 8M Urea for 30 minutes at room temperature.

Immunocytochemistry

Mouse neural progenitor cells (mNPCs) were grown and differentiated as described in section 2.6. Confluent cells were transfected with 10 μg each of *JAKMIP1* and *PABPC1* containing expression plasmids using Lipofectamine LTX and PLUS Reagents (Invitrogen, Carlsbad, CA) according to manufacturer's instructions. We used a previously published (Steindler et al., 2004) human *JAKMIP1* expression plasmid in which N-ter human *JAKMIP1* (amino acids 1-365) is cloned into pcDNA4/V5-His/zeo (Invitrogen, Carlsbad, CA). We fully sequenced the JAKMIP1 construct and conducted site-directed mutagenesis (QuikChange Multi Site-Directed Mutagenesis Kit, Stratagene, La Jolla, California) to correct erroneous base pair substitutions. PABPC1-dsRED expression constructs were created using Gateway clonase technology (Invitrogen, Carlsbad, CA) with plasmids pENTR PABPC1 (Open BioSystems/Thermo Scientific, Waltham, MA) and pLVU/dsRED destination vector, Addgene 24178 (Krupka et al., 2010). To test these constructs, we conducted immunoblotting for JAKMIP1 and PABPC1 from protein lysates of 293T cells 24 hours post transfection with JAKMIP1 and PABPC1 overexpression constructs. Correct protein expression was observed. We conducted fluorescence immunostaining for PABPC1 and JAKMIP1 24 hours post-transfection of differentiated mNPCS to test for colocalization using anti-RFP and anti-V5 antibodies. Image acquisition was performed using Zeiss AxioCam and all images were taken at 40X/ .75 NA

magnification.

Western Blotting

Conducted as described in section 2.6.

Quantitative RTPCR

Conducted as described in section 3.8

Antibodies

Additional antibodies used in this chapter are the following:

Name	Antigen/Peptide wording from company website when appropriate	Species/Clonality	Source/Catalogue number
TUJ1 (anti Neuronal Class III β-Tubulin)	microtubules derived from rat brain. Does not identify b-tubulin found in glial cells.	Mouse monoclonal	Covance MMS-435P
PSD95	Synthetic peptide corresponding to residues in the N terminal of human PSD95	Rabbit monoclonal	Abcam Ab76115
DAG1	Amino acids 831-895 mapping at the Cter of Dag1 precursor of human origin	Mouse monoclonal	Santa Cruz SC165997
CAMK2A	Synthetic peptide: KWQIVHFHRSGAPSVLPH conjugated to KLH, corresponding to C terminal amino acids 461-478 of Rat CaMKII alpha	Rabbit polyclonal	Abcam ab50202
MAP1B	MAP1B fusion protein ag16255	Rabbit polyclonal	Proteintech Group 216331AP
APP	amino acids of human amyloid A4 protein precursor (APP) corresponding to the amino terminus of the 4K Ab peptide generated by b- and g-secretases .	Rabbit polyclonal	Sigma SAB3500274
SAPAP4	internal region of SAPAP4 human origin	Rabbit polyclonal	Santa Cruz

			sc86852
V5	synthetic peptide based on the V5 epitope	Mouse monoclonal	Invitrogen 37-7500
GFP	highly purified recombinant full length protein made in Ecoli. The antibody is directed against the entire GFP molecule	Rabbit polyclonal	Abcam ab290
RFP	Recombinant RFP expressed in E. coli	Rabbit polyclonal	Abcam ab62341

Subcellular fractionation

Subcellular fractionation was conducted as previously described (Hallett et al., 2008).

Nascent synthesis of proteins

ClickIT (FUNCAT) analysis was performed on TUJ1 immunostained two week differentiated mouse neural progenitor cells using L-homopropargylglycine (HPG) and a 555-fluorophore tagged azide molecule (Invitrogen, Carlsbad, CA). For methods regarding harvesting of mouse progenitor cells and differentiation conditions see section 2.6. Click-iT® L-homopropargylglycine (HPG) was incorporated into newly translated proteins for two hours, as recommended by the manufacturer, followed by conversion to a fluorescently labeled stable triazole conjugate using a 555-fluorophore tagged azide molecule in the presence of copper. The two hour time pulse-chase application of HPG was chosen as this allows translation visualization in distal dendritic segments (Dieterich et al., 2010). To determine background fluorescence, a subset of cells were not given HPG or 555-azide. WT and KO cells were analyzed from same-day images. A baseline exposure time for the red channel (translation) was calculated by sampling random cells. This time interval of exposure was used for all experiments for red

channel images. Background fluorescence for each image was calculated from a manually placed 19 pixel diameter circle adjacent but not overlapping with the neuron and glia occupied space. Translation was assessed across imaging days, which represent independent experiments. Individual coverslips, representing distinct reactions were analyzed and outliers within coverslips were manually checked. A strong relationship between day of imaging and 555 fluorescence was observed, so a covariate was used to control for day of imaging. For FUNCAT analysis, three trials were performed: two trials from one littermate mouse set (trial 1: WT, N=74; KO, N=80: trial 2: WT, N=91; KO, N=92) and one trial from an additional littermate set (trial 3: WT, N=62; KO, N=92). Fluorescent images were acquired using a Zeiss Axio Imager, D1 camera and AxioVison software.

Chapter 5: Determination of JAKMIP1's *in vivo* role: *Jakmip1* KO mouse

5.1 Introduction

I hypothesized that absence of *Jakmip1 in vivo* would result in ASD-associated behaviors for the following reasons. First, JAKMIP1 regulates FMRP function by binding to its translational complex (Figure 3-3, Table 3-2), associates with FMRP mRNA targets (Figure 3-6, Figure 3-7), and regulates the synaptic distribution of these targets (Figure 4-4). As mutations in *FMR1* are the leading inherited cause of ASD (De Rubeis and Bagni, 2011), disrupting FMRP function by loss of a key regulator would likely lead to ASD-related behaviors. Second, loss of JAKMIP1 *in vivo* reduces the expression of PSD95 at the synapse (Figure 4-4). PSD95 is critical for proper synaptic function (Beique and Andrade, 2003; Steiner et al., 2008; Yao et al., 2004), and loss of PSD95 *in vivo* leads to deficits in ASD core behavioral domains (Feyder et al., 2010). Thus, it follows that disrupted PSD95 levels resulting from *Jakmip1* ablation would lead to similar deficits in ASD associated behaviors. Lastly, JAKMIP1 regulates basal translation (Figure 4-7). Perturbations in the translational machinery have recently been found to result in ASD behaviors (Santini et al., 2013). Therefore, I hypothesized that *Jakmip1*-related disruptions in translation would cause impairments in ASD behavioral domains.

To test this hypothesis, we generated a *Jakmip1* KO mouse with the UC Davis KOMP Repository Knockout Mouse Project. This mouse has construct validity [contains the same biological perturbation as the human disorder (Silverman et al., 2010)] for the following reasons. *JAKMIP1* RNA is reduced in postmortem brains of autism patients with 15q duplications that include *CYFIP1* (Oguro-Ando and Geschwind, unpublished), JAKMIP1 is decreased in the cortex of *Fmr1* KO mice and human neural cells with FMRP reduction (Nishimura et al., 2007), and a deletion of JAKMIP1 exons was found in an autistic individual (Hedges et al., 2012).

We conducted an extensive battery of tests to characterize this mouse, including behavioral paradigms centered on ASD related behaviors. We found that *Jakmip1* KO mice weight less and have shorter brains than WT mice. Additionally, *Jakmip1* KO mice have impaired motor coordination, with significant deficits in the rotorod and wire hang test. *Jakmip1* KO also results in an attenuated acoustic startle response not related to hearing loss.

Jakmip1 KO mice show significant deficits in two core domains of ASD, restrictive and repetitive behavior and social abnormalities, confirming our hypothesis. Additionally, *Jakmip1* mice show anxiety and learning deficits, phenotypes associated with both ASD and Fragile X syndrome (De Rubeis and Bagni, 2011). Based on the data reported here, we present the *Jakmip1* KO mouse as a new *in vivo* model of ASD, a valuable resource for gene discovery and drug development.

5.2 Generation of a novel mouse model of ASD

We developed a novel *Jakmip1* KO mouse in collaboration with the trans-NIH Knock-Out Mouse Project (KOMP). We obtained C57BL/6 embryonic stem cells from the KOMP Repository (Jakmip1$^{tm1(KOMP)Vlcg}$; *Jakmip1* coding exons 2-8 replaced with a LacZ-Neo cassette by homologous recombination; Velocigene, Regeneron Pharmaceuticals, Tarrytown, NY) and bred chimeras with C57/BL6 mice (Jackson Laboratories, Bar Harbor, ME) to obtain heterozygote mice, which were then crossed to produce WT, heterozygous (HET), and KO mice. We determined genotypes by performing polymerase chain reaction on the 5 and 3 prime ends of the cassette-gene juncture and sequenced the resulting PCR amplicons for verification of the insertion site (Figure 5-1, A). The observed ratio of genotypes showed a trend toward deviation from expected Mendelian ratios after postnatal day eight, suggesting that loss of *Jakmip1* confers lethality with incomplete penetrance during a time of peak JAKMIP1 expression in WT mice [P

values generated from a Chi-square analysis with 2 degrees of freedom. Category 1; all mice, N=190 (WT=42, HET=110 KO=38), Chi squared = 4.91, P= 0.086: Category 2; mice > p8, N=145 (WT=35 HET=85 KO=25), Chi squared = 5.69, P= 0.058: Category 3; mice < p8, N=45 (WT=7 HET= 25 KO=13), Chi-squared = 2.16, P= 0.34].

We confirmed absence of JAKMIP1 protein in KO mice and a reduction of protein in HET mice in C57BL/6 postnatal mouse neocortices and differentiated mouse neural progenitor cells (Figure 5-1, C and D). Quantitative RTPCR analysis of *Jakmip1* RNA from postnatal brain hemispheres of WT, HET, and KO mice showed a lack of *Jakmip1* RNA in KO brains and a 1.67 +/- 0.054 (SEM) fold increase of *Jakmip1* transcript in WT mice compared to HET mice (P=0.0011, two tailed t test; Figure 5-1, B). β-galactosidase staining was conducted in coronal sections of postnatal *Jakmip1* HET and WT (control) mouse brains to test for proper *Jakmip1* promoter activity. Staining recapitulated known *Jakmip1* RNA expression (Figure 5-1, E).

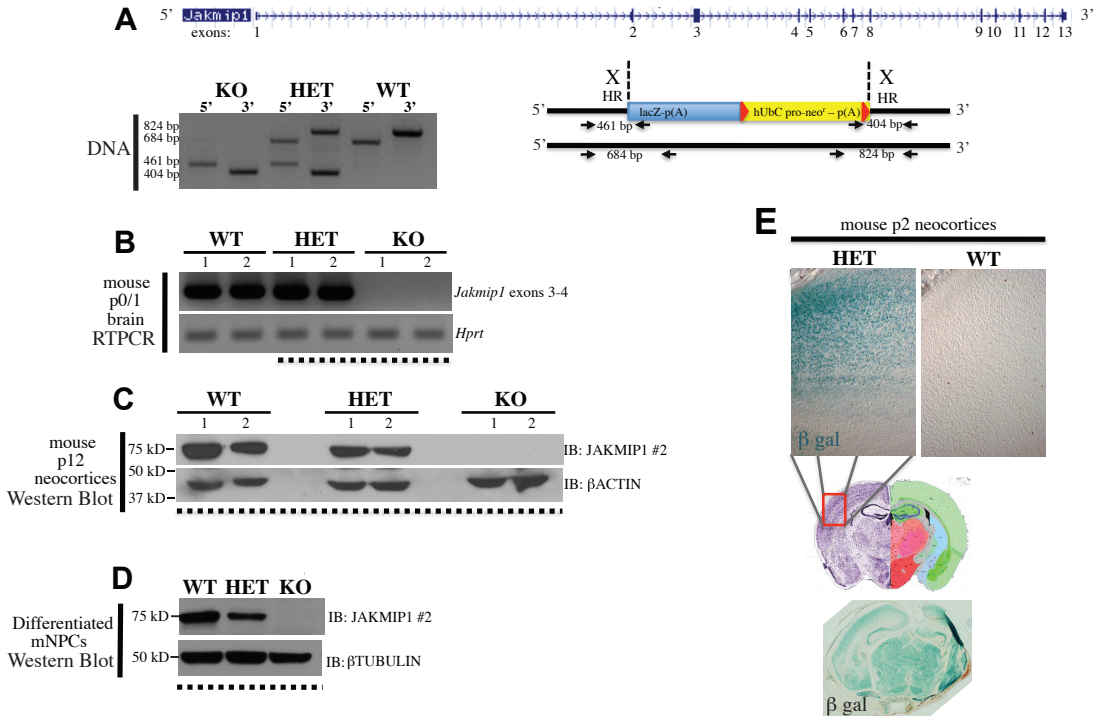

Figure 5-1. Generation of the *Jakmip1* knockout mouse. (A) Schematic representation of gene ablation strategy. *Jakmip1* exons 2 through 8 were replaced with a LacZ/neo cassette. Genotyping strategy is outlined along with representative PCR amplicons from KO, HET, and WT mice. Depiction of *Jakmip1* is from http://www.genome.ucsc.edu. (B) *Jakmip1* RNA is absent from KO, but not HET or WT, mouse postnatal brain by quantitative RTPCR. Signal from the plateau phase (45 PCR cycles) is shown. (C-D) JAKMIP1 protein is absent from KO and is reduced in HET compared to WT mouse in postnatal day 12 neocortex and 3 week differentiated mouse neural progenitor cells by western blotting. (E) LacZ is expressed in *Jakmip1* heterozygote but not wild-type littermate by X-gal staining. (B-D) Dashed line below immunoblots denotes littermates. Coronal image in 'E' is used to show region of imaging and is from Allen Mouse Brain Atlas [Internet]. Seattle (WA): Allen Institute for Brain Science. ©2009. Available from: http://mouse.brain-map.org.

We found that *Jakmip1* KO mice weigh significantly less than WT littermates (Figure 5-2, A). Additionally, *Jakmip1* KO mice have significantly shorter brains and a trending decrease in brain width as compared to WT littermates (Figure 5-2, B). *Jakmip1* HET mice do not show differences in weight or brain width and length (Appendix Figure 1-1). To test for changes in individual brain structures and neuronal numbers, we conducted histology on *Jakmip1* KO, HET and WT brains at p30, time-matched for the observed decrease in brain length. We did not detect any gross morphological abnormalities in the cortex, hippocampus, or cerebellum of *Jakmip1* KO or HET mice compared to WT controls by DAPI and NeuroTrace staining. To test for differences in neuronal number, we conducted NeuN immunohistochemistry in the somatosensory cortex of *Jakmip1* KO and WT controls. We found no change in the number of NeuN positive neurons in *Jakmip1* KO mice compared to WT controls in both total cortex and in individual layers.

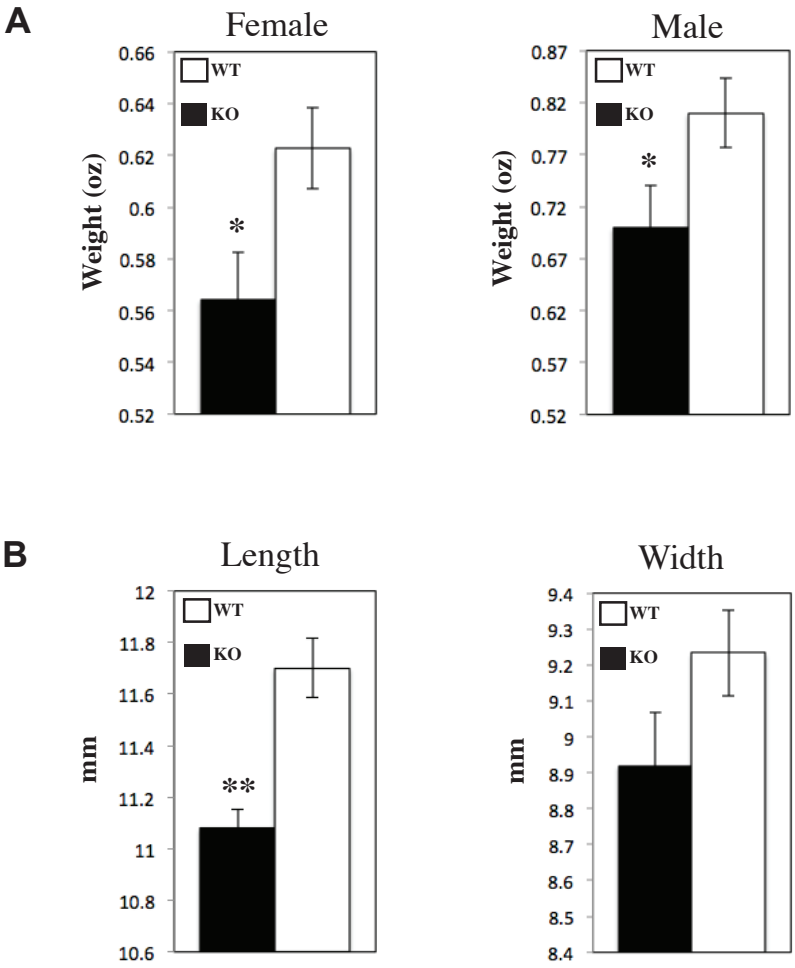

Figure 5-2. Somatic characteristics of the *Jakmip1* KO mouse. (A) *Jakmip1* KO mice weigh signficantly less than WT mice. Mice were weighed between p44 and p47. Female mice: WT, N=11; KO, N=7; P=0.029, two sample, two tailed t-test. Male mice: WT, N=10; KO, N=8; P=0.049, two sample, two tailed t-test. (B) *Jakmip1* KO mice have signficantly shorter brains than WT mice. Brain length and width was measured at p30. Length: WT, N=3; KO, N=5; P=0.003, two sample, two tailed t-test. Width: WT, N=3; KO, N=5. Values are mean +/- SEM. * p <= 0.05, ** p<= 0.01, *** p <= 0.001.

5.3 General Behavioral Characteristics

We examined the general behavioral characteristics of *Jakmip1* KO mice in order to determine if any gross behavioral abnormalities are present that would interfere with additional testing. We conducted a previously published 'Neurological and Neuropsychological Test Battery'(Crawley and Paylor, 1997; Irwin, 1968) and assessed fur, whisker integrity, presence of bald patches, general activity, conducted a cotton tip approach test of the eye, ear and whisker, analyzed postural reflex, and carried out a visual cliff test. *Jakmip1* KO and HET mice did not show signs of abnormality. To conduct a more thorough and quantitative assessment of activity, we performed an open field test and conducted home cage behavior analysis (section 5.4). *Jakmip1* KO and HET mice did not differ from WT controls in either distance traveled or in average velocity in the open field test (Figure 5-3, A). To determine if JAKMIP1 loss affects response to thermal sensory stimuli, we conducted a hot plate startle test in which latency to paw withdrawl from a hot plate is measured. *Jakmip1* KO and HET mice perform normally on this task (Figure 5-3, B). To assess perseverative behavior related to digging, we conducted a marble-burying test and determined the number of marbles buried over a 30 minute period (Thomas et al., 2009). We additionally conducted a nesting test, which pertains to social behaviors in the home cage and involves the dopaminergic system (Szczypka et al., 2001). *Jakmip1* KO and HET mice did not show deficits in nesting or in the marble burying task (Figure 5-3, C and D). However, *Jakmip1* KO mice show a trend toward decreased marble burying ($P=0.098$, two sample, two tailed t test: WT, N=9; KO, N=7), which is consistent with their decreased digging observed in the home cage behavior test (section 5.4, Figure 5-6, A).

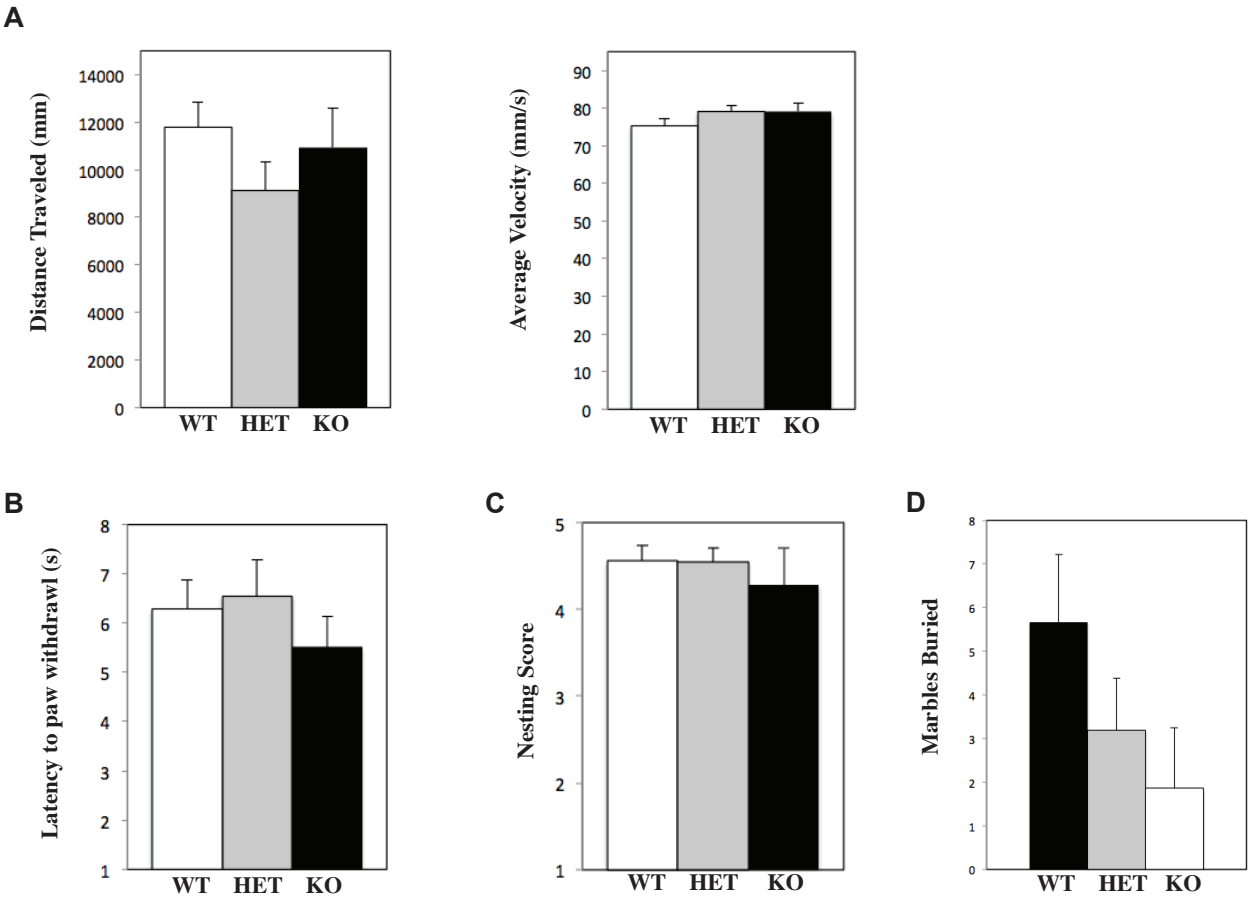

Figure 5-3. *Jakmip1* KO and HET mice do not exhibit behavioral abnormalities on tests of general behavior.

(A) Open field test. Distance traveled and average velocity over a 20 minute recording period (WT, N=15, HET, N=11, KO, N=13).

(B) Hot plate startle. Time before paw is withdrawn from a 55 degrees hot plate (max time is 15 s) (WT, N=8, HET, N=11, KO, N=7).

(C) Nesting behavior. The nesting score represents the nest architecture and amount of material used after an overnight period (1, poor; 5, good). (WT, N=9, HET, N=11, KO, N=7).

(D) Marble Burying Test. The number of marbles buried during a 30 minute trial (12 marbles maximum). (WT, N=9, HET, N=11, KO, N=7).

Values are mean +/- SEM.

To test if JAKMIP1 loss affects motor coordination, we conducted the rotorod test, wire hang test, and hind paw footprint test (Crawley and Paylor, 1997). The rotorod test measures the ability of a mouse to remain on a constantly rotating or accelerating rod. In a complementary test of coordination, we measured the amount of time it took for the mouse to fall from an inverted wire cage top. *Jakmip1* KO mice had significant deficits in both the accelerating rotorod test and the wire hang test, suggestive of a motor coordination abnormality (Figure 5-4, A and B). *Jakmip1* HET mice do not show rotorod deficits, but show reduced latency to fall on the wire hang test (Appendix Figure 1-2, A and B). In the hind paw footprint test, gait architecture is analyzed from colored footprints generated from walking trials of mice with painted front and back paws. We measured stride length, stride difference, stride variation, gait width and linearity, parameters reported to be abnormal in ataxic mice (Barlow et al., 1996). In general, *Jakmip1* KO mice performed normally on this task, with a notable exception of a significantly decreased left mean stride length (Figure 5-4, C). *Jakmip1* HET mice show significant increases in left stride difference and average linearity (Appendix Figure 1-2, C).

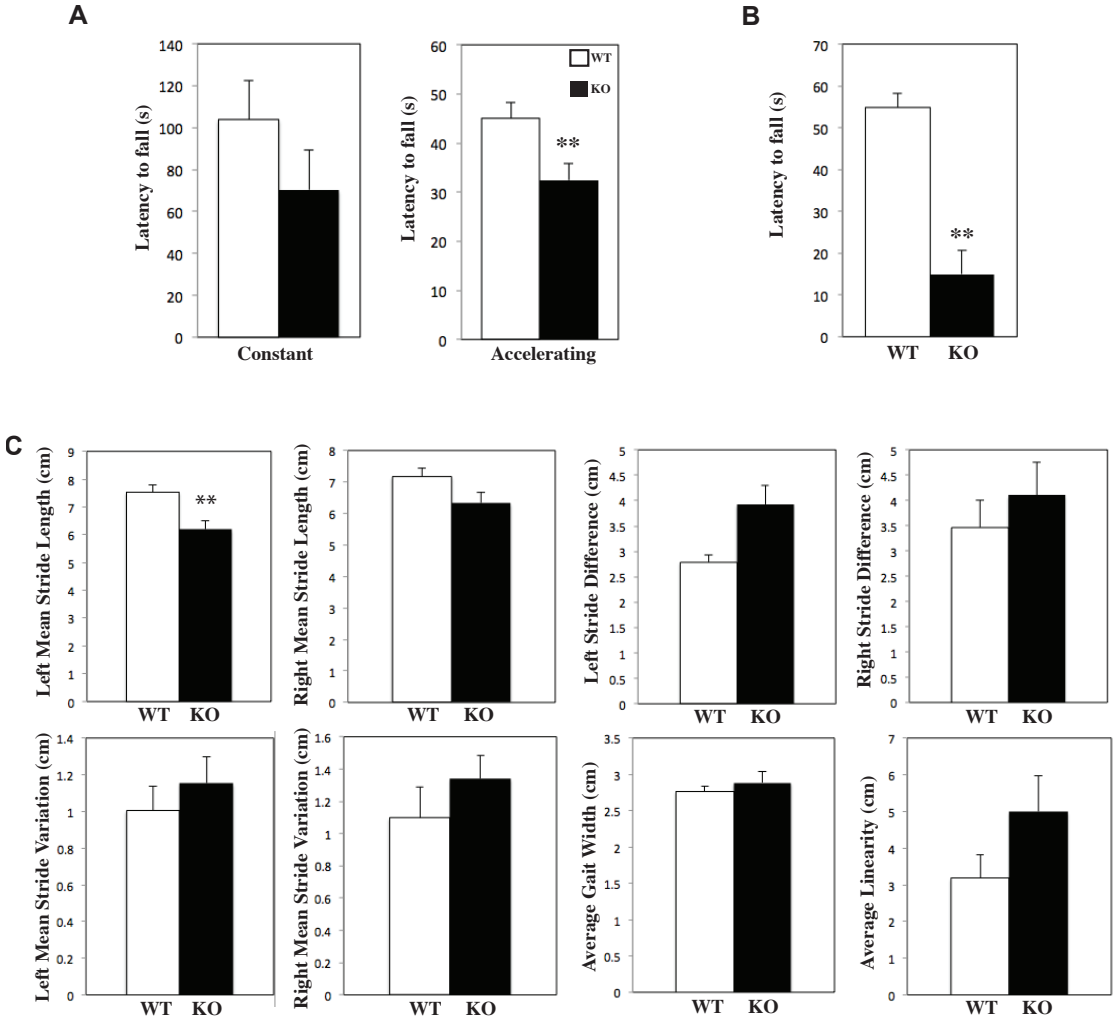

Figure 5-4. *Jakmip1* KO mice show impaired motor coordination.
(A) Rotorod. Constant and accelerating speed tests shown. Y axis is latency to fall from the rotorod. Maximum time of trial is 180 s. P value calculated using the non-parametric Mann-Whitney test (constant test), and a two sample, two tailed t-test (accelerating test, WT, N=15; KO, N=13: P=0.011).
(B) Wire Hang Test. Y axis is latency to fall from an inverted wire cage lid. Maximum time of trial is 60 seconds. P value calculated using the non-parametric Mann-Whitney test (WT, N=9; KO, N=7: P=0.002).
(C) Gait test. Average stride length, stride difference, stride variation, gait width and linearity are shown. P value calculated using a two sample, two tailed t-test (WT, N=9; KO, N=7, mean stride length (left): P=0.0042).
Values are mean +/- SEM. * p <= 0.05, ** p<= 0.01, *** p <= 0.001.

We lastly tested if *Jakmip1* KO mice showed deficits in auditory reflexes by performing an auditory click test and an acoustic startle response test. To assess the hearing of *Jakmip1* KO and HET mice we conducted an auditory click test, in which mice were subjected to an auditory burst from 10 cm away. Orientation to the sound was indicative of an intact auditory reflex. JAKMIP1 reduction did not adversely affect auditory reflexes as measured by this test. We additionally measured auditory startle response by administering an auditory stimulus of 120 decibels (dB) and recording startle. *Jakmip1* KO mice showed a severely attenuated startle response (Figure 5-5, A). In conjunction with the auditory startle response test, we examined sensorimotor gaiting with a prepulse inhibition (PPI) test. In this test, prepulses of 70 dB, 75 dB or 80 dB stimuli precede the startling stimulus of 120 dB, which, in normal mice, decreases the amplitude of startle (Paylor and Crawley, 1997). *Jakmip1* KO mice show a large reduction in PPI compared to WT mice for all prepulses tested (Figure 5-5, B). *Jakmip1* HET mice showed normal acoustic startle response and prepulse inhibition (Appendix Figure 1-3).

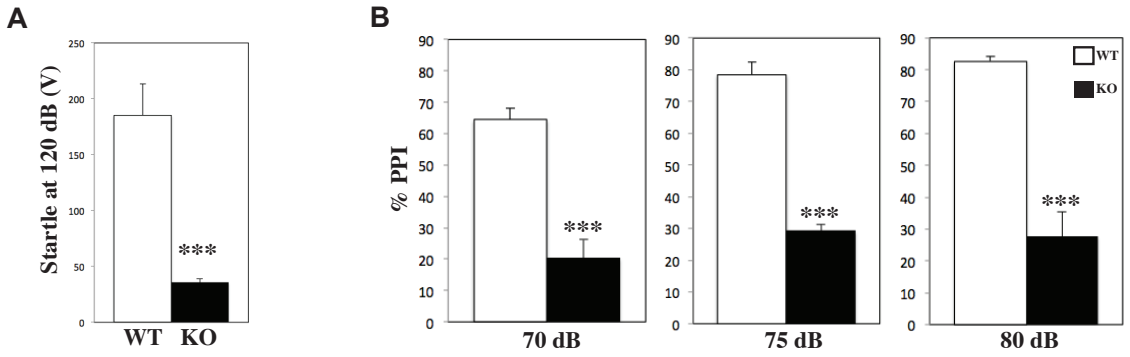

Figure 5-5. *Jakmip1* KO mice show attenuated acoustic startle response.
(A) Startle response. Amplitude of startle following a 120 dB sound. P value calculated using a two sample, two tailed t-test (WT, N=9; KO, N=6: P=0.00097).
(B) Prepulse inhibition. Percentage of inhibition when a 70 dB, 75 dB and 80 dB sound is given prior to a 120 dB tone. P value calculated using a two sample, two tailed t-test (70db, P=1.45 E -05: 75 db, P= 2.14 E-07: 80db, P= 8.35 E-07: WT, N=9; KO, N=6).
Values are mean +/- SEM. * p <= 0.05, ** p<= 0.01, *** p <= 0.001.

5.4 Behavioral characterization with emphasis on ASD

Mice have been effectively used to model the core behavioral domains of ASD [Section 1.4, (DeLorey et al., 2008; Moy et al., 2009; Nakatani et al., 2009; Penagarikano et al., 2011)]. Given JAKMIP1's strong relationship to FMRP and ASD, we performed a battery of tests to determine how loss of *Jakmip1* influences behaviors disrupted in Fragile X syndrome and ASD, including restrictive and repetitive behavior, social behavior, anxiety, and learning (De Rubeis and Bagni, 2011; Silverman et al., 2010).

To assess restrictive and repetitive behaviors, we observed the home cage behavior of *Jakmip1* KO, HET, and WT mice. *Jakmip1* KO mice exhibited two striking motor stereotypies. First, *Jakmip1* KO mice showed a statistically significant increase in grooming and decrease in digging compared to WT mice (Figure 5-6, A). Secondly, all *Jakmip1* KO mice repetitively jumped, which persisted for roughly 30% of the recording period (Figure 5-6, B). *Jakmip1* HET

mice did not show deficits in digging or grooming (Appendix Figure 1-4, A) and only a small subset exhibited repetitive jumping.

A

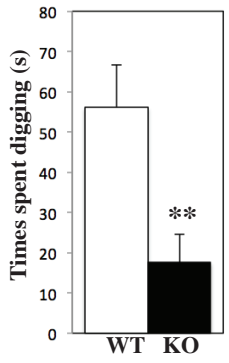

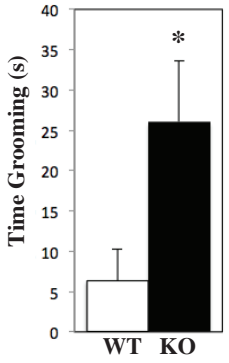

C

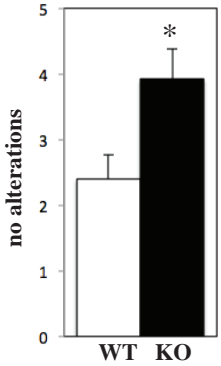

B

	WT	KO
Number of mice with jumping stereotypie	0/15	12/13*
Average jumping episodes over 10 minutes	0	11.38 +/- 2.51
Average jumps per episode over 10 minutes	0	24.72 +/- 5.54
Average time per episode (s)	0	13.85 +/- 2.95
Average percentage of time spent jumping	0	26%

Figure 5-6. *Jakmip1* KO mice show repetitive and perseverative behavior.
(A) Home Cage Behavior. Time spent digging (left) or grooming (right) within a 10 minute period. P value calculated using a two sample, two tailed unpaired t-test (Time spent digging, P=0.0063, Time spent grooming, P=0.025, WT, N=15; KO, N=13).
(B) Home Cage Behavior. Characteristics of repetitive jumping stereotypie in *Jakmip1* KO mice. *Mouse that did not jump showed repetitive jumping in the open field test.
(C) T maze spontaneous alternation test. Number of alterations shown. P value calculated using a two sample, two tailed unpaired t-test (WT, N=15; KO, N=13, P=0.015).
Values are mean +/- SEM. * p <= 0.05, ** p<= 0.01, *** p <= 0.001.

To test for neurological perseveration, we conducted a spontaneous alteration T maze test. In this test, mice are given the choice to explore right or left arms of a T maze over 10 trials. *Jakmip1* KO mice displayed significantly less alterations than WT mice (Figure 5-6, C),

indicating that *Jakmip1* loss affects both motor and neurological stereotypies. *Jakmip1* HET mice showed normal alternations on the T maze test (Appendix Figure 1-4, B).

To test if the *Jakmip1* KO mice exhibit predictive validity [similar response to therapeutics that are effectively used to treat the human disease (Silverman et al., 2010)], we administered Risperidone and tested perseverative behavior in the home cage behavior test. Risperidone is approved by the United Stated Food and Drug Administration to improve ASD symptoms, including repetitive behavior, hyperactivity, self-injury, and aggression (McDougle et al., 2000; McDougle et al., 2008). Risperidone is not sedating to WT mice in the dosage given as tested by the open field test (Penagarikano et al., 2011). *Jakmip1* KO and WT mice were administered Risperidone or phosphate buffered saline (PBS) acutely and home cage behavior was analyzed over a 10 minute period. Mice were then given PBS or Risperidone in a cross over treatment three weeks later and retested. Treatment with Risperidone showed a trend toward decreasing repetitive grooming behavior, decreased the number of KO mice that displayed repetitive jumping, and significantly decreased the number of jumping episodes and percentage of time spent jumping in the *Jakmip1* KO mice (Appendix Figure 1-5, A-C).

Jakmip1 loss also affects social behavior. We performed a three chamber social test to determine the preference of *Jakmip1* KO mice toward interacting with a novel mouse versus an empty cup. We found that *Jakmip1* KO mice spend an equal amount of time interacting with a novel mouse compared to an empty cup, as indicated by sniffing time (Figure 5-7, A) and time in chamber (Figure 5-7, B), while WT mice spend significantly more time exploring the novel mouse (Figure 5-7, A and B). *Jakmip1* HET mice showed social impairments in the time spent in the social chamber, but not in the time spent sniffing the novel mouse (Appendix Figure 1-6).

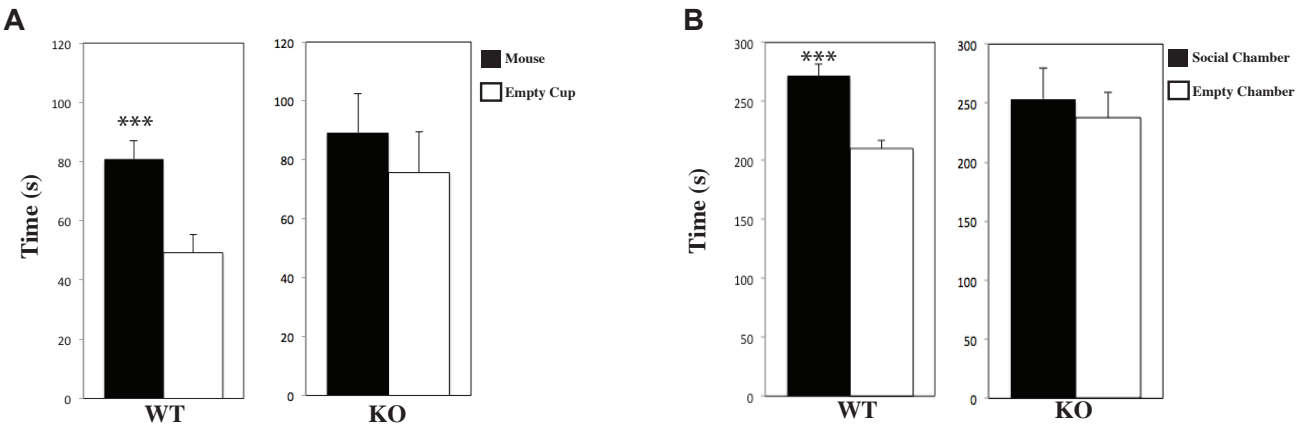

Figure 5-7. *Jakmip1* KO mice show impaired social behavior.
Three-chamber social interaction test.
(A) Time spent sniffing a sex-matched novel mouse or an empty cup over a 10 minute period. P value calculated using a two sample, two tailed, paired t-test [WT, N=15; KO, N=13 : WT, P=0.00051; KO, P=0.51]
(B) Time spent in the social chamber containing a novel mouse or in the chamber containing an empty cup. P value calculated using a two sample, two tailed, paired t-test [WT, N=15; KO, N=13 : WT, P=0.00064; KO, P=0.73]
Values are mean +/- SEM. * p <= 0.05, ** p<= 0.01, *** p <= 0.001.

Both ASD and Fragile X patients often exhibit anxiety, and impairments in anxiety is one of the most consistent phenotypes across various mouse models of Fragile X syndrome. To test if *Jakmip1* KO mice display abnormalities in anxiety, we performed the light dark exploration test. In this test, anxiety is determined by the amount of time a mouse spends in a light versus a dark compartment, the time it takes for the mouse to first enter the light compartment (latency), and the number of border crossings between light and dark compartments. *Jakmip1* KO mice showed a trend toward spending more time in the light compartment compared to the dark compartment than WT mice (Figure 5-8, A), a significant reduction of latency to enter the light compartment (Figure 5-8, B), and a significant increase in border crossings (Figure 5-8, C). This is suggestive of reduced anxiety and possibly increased impulsivity (Zaichenko et al., 2011). *Jakmip1* HET mice make significantly less border crossings, but spend an equal amount of time

in the light compartment and latency to enter the light compartment as WT mice (Appendix Figure 1-7).

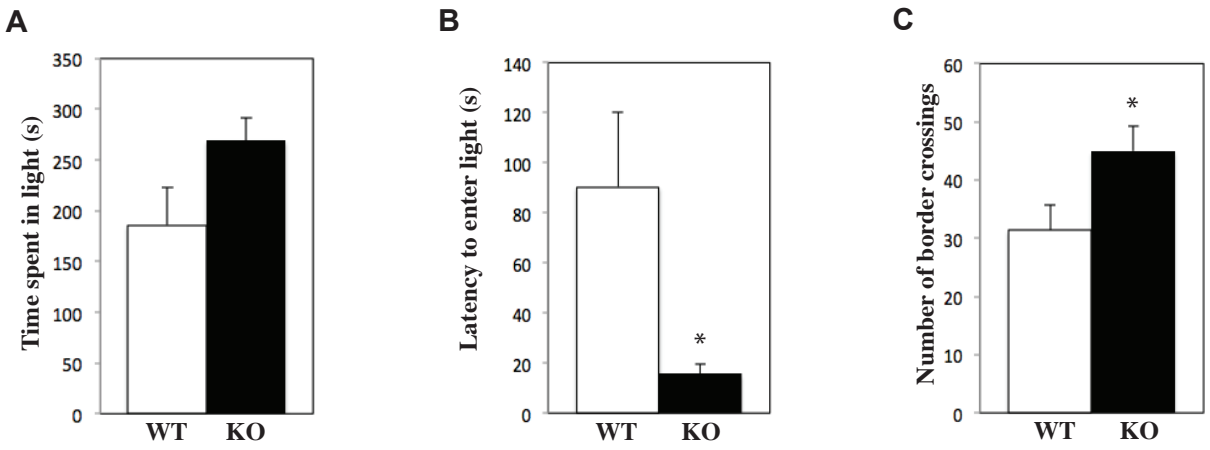

Figure 5-8. *Jakmip1* KO mice show reduced anxiety.
Light-dark box test.
(A) Time spent in the bright compartment over a 10 min period (WT, N=15; KO, N=13 : P=0.075).
(B) Time before the mouse first enters the bright compartment (WT, N=15; KO, N=13 : P=0.029).
(C) Number of times the mouse crosses compartments over a 10 minute period (WT, N=15; KO, N=13: P=0.034).
P values calculated using a two sample, two tailed unpaired t-test.
Values are mean +/- SEM. * p <= 0.05, ** p<= 0.01, *** p <= 0.001.

Mental Retardation is feature of autism and Fragile X syndrome. To test if loss of *Jakmip1* impairs spatial learning and memory, we first performed a Morris Water Maze (MWM) Test. *Jakmip1* KO mice were unable to learn the location of the hidden platform during the training phase of this test and showed impaired swimming. Thus, probe trials were not performed, and we discontinued this test. As an alternative test for learning impairments, we conducted an auditory fear conditioning test, which measures hippocampal and amygdala-dependent learning. *Jakmip1* KO mice were able to learn to freeze to a tone after tone-shock pairings during the acquisition phase of fear conditioning (Figure 5-9, A). Interestingly, *Jakmip1* KO mice showed significant decreases in freezing during the second and third intertone intervals

as compared to WT mice (Figure 5-9, A) not due to impaired sensitivity to shock stimuli (Figure 5-9, B). *Jakmip1* KO mice showed normal context dependent fear conditioning when placed in the same context in which fear conditioning was conducted, indicative of preserved hippocampal dependent learning (Figure 5-9, C). Additionally, they performed normally in a test of generalized fear assessment when placed in a new context (Figure 5-9, C). However, *Jakmip1* KO mice displayed decreased noise cued fear response (Figure 5-9, D). Performance on this test relies on intact amygdala/auditory pathway function. As such, *Jakmip1* KO mice may have amygdala or central nervous system auditory pathway disruptions. Extinction of tone-shock learning was preserved in *Jakmip1* KO mice (Figure 5-9, E).

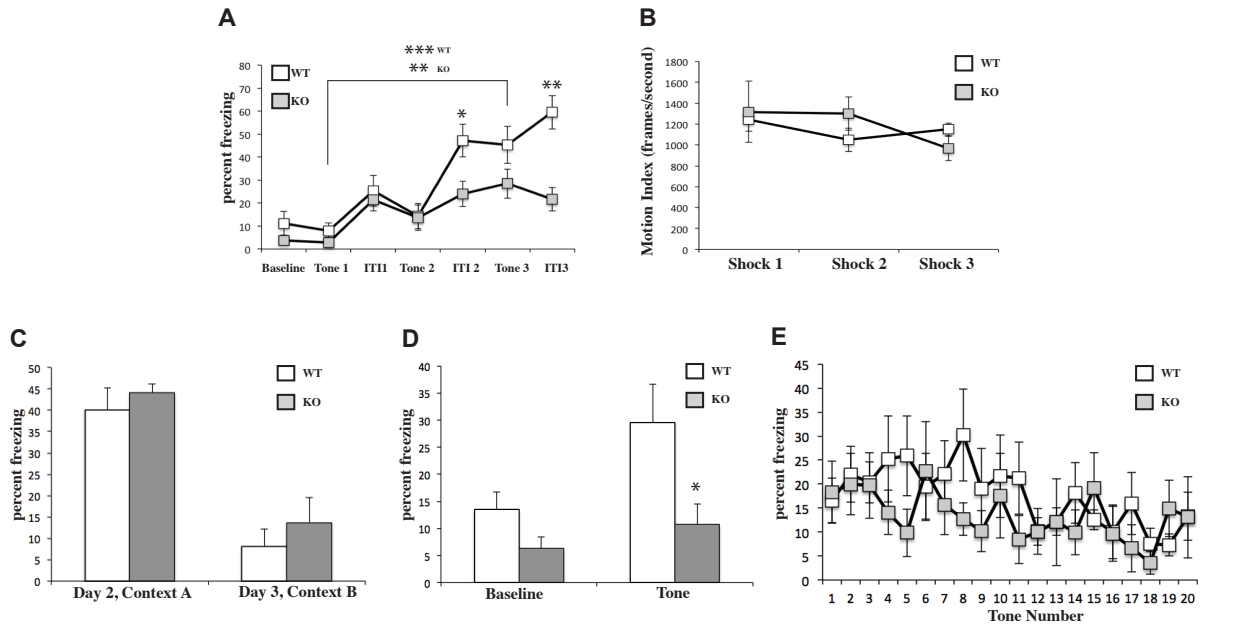

Figure 5-9. *Jakmip1* KO mice show deficits in fear conditioning.
Auditory Fear Conditioning.
(A) Acquisition of Fear Conditioning, Day 1, context A. Percent freezing to tone/foot shock pairing and intertone interval (ITI). (WT vs. KO: ITI2 ; P=0.027; IT3, P=0.001 : Tone 1 vs. Tone 3; WT learning, P=0.00054; KO learning, P=0.0051).
(B) Reaction to foot shock, Day 1, context A. *Jakmip1 KO* mice do not show impared shock response. A motion index was calculated after each shock to measure shock response.
(C) Contextual Fear and Generalized Fear assessment. Mice were placed in Context A one day after aquisition of fear conditioning or context B two days after conditioning. *Jakmip1* KO mice showed normal context-dependent fear conditioning.
(D) Noise cued fear response. *Jakmip1* KO mice display impaired noise cued fear conditioning. Mice were placed in a context B three days after acquisition of fear conditioning and percent freezing was measured after a tone was given. (P=0.049).
(E) Extinction of fear conditioning. *Jakmip1* KO mice show normal decrease of freezing after several trials of a tone given without a corresponding foot shock.
P values were calculated using a two sample, two tailed t-test (WT, N=9; KO, N=7).
Values are mean +/- SEM. * p <= 0.05, ** p<= 0.01, *** p <= 0.001.

5.5 Discussion

JAKMIP1 is dysregulated in ASD subjects with both FXS and maternally inherited dup (15q11-13). Moreover, JAKMIP1 has a developmental role in regulating translation. Abnormal translation leads to ASD related behaviors (Santini et al., 2013). Lastly, loss of *Jakmip1* reduces PSD95, which also results in ASD associated phenotypes (Feyder et al., 2010). Therefore, we reasoned that disruptions in *Jakmip1* would lead to ASD associated behaviors. We found that *in*

vivo ablation of *Jakmip1* results in behaviors that overlap several of the most consistent phenotypes reported in mouse models of Fragile X syndrome and ASD as well as mice lacking PSD95 and having disrupted translation.

First, we found that *Jakmip1* KO mice exhibit social impairments, one of the core deficits in ASD (Silverman et al., 2010), as they do not show a preference to interact with a novel mouse over an empty cup in the three chamber social test (Figure 5-7). Likewise, mouse models of Fragile X syndrome display social abnormalities (Spencer et al., 2005; Spencer et al., 2008). Moreover, several mouse models of ASD show impaired sociability (Cheh et al., 2006; Crawley et al., 2007; DeLorey et al., 2008; Ferguson et al., 2000; Jamain et al., 2008; Moy et al., 2009; Nakatani et al., 2009; Penagarikano et al., 2011; Scattoni et al., 2008; Scearce-Levie et al., 2008; Wersinger et al., 2002; Winslow et al., 2000). A recent mouse model of ASD, which exhibits disrupted translation through overexpression of the eukaryotic translation initiation factor 4E (eIF4E), a gene disrupted in ASD, also shows social interaction deficits. Specifically, this mouse, like the *Jakmip1* KO mouse, displays loss of preference for a stranger mouse over an object (Santini et al., 2013). Importantly, deletion of mouse PSD95, Dlg4, also leads to social abnormalities (Feyder et al., 2010).

Jakmip1 KO mice display a second core ASD deficit, restrictive and repetitive behavior (Silverman et al., 2010). *Jakmip1* KO mice exhibit both motor and neurological stereotypies. *Jakmip1* KO mice groom more than their WT counterparts (Figure 5-6, A) and show repetitive stereotyped jumping (Figure 5-6, B). *Jakmip1* KO mice also show neurological stereotypies, having less spontaneous alternations on the T maze test than WT mice (Figure 5-6, C). *Fmr1* KO mice also show repetitive behavior in the open field (Spencer et al., 2011). Several mouse models of ASD display restrictive and repetitive behaviors that mirror those of the *Jakmip1* KO

mouse. The *Cntnap2* KO mouse shows increased grooming and reduced T maze alternations (Penagarikano et al., 2011), and the *Shank2* KO mouse exhibits increased grooming, decreased digging and repetitive jumping (Won et al., 2012). Other notable mouse models of ASD that display restrictive and repetitive behaviors are the *En2* knockout mouse (Cheh et al., 2006; Moy et al., 2009), a mouse with a chromosome 7 duplication (15q11-13 duplication in human) (Nakatani et al., 2009), and a *Gabrb3* knockout mouse (DeLorey et al., 2008). *Dlg4* KO mice also show decreased spontaneous alterations and increased grooming (Feyder et al., 2010). Moreover, eIF4E overexpressing mice show increased grooming and neurological inflexibility in the Y-maze task (Santini et al., 2013). It is interesting that some mouse models of ASD exhibit grooming stereotypies, while others groom and jump repetitively. Study of *Jakmip1* KO mice may prove useful in clarifying the underlying circuitry dictating these behaviors.

We additionally found that *Jakmip1* loss leads to decreased anxiety (Figure 5-8). Disruptions in anxiety are one of the most consistent phenotypes in mouse models of Fragile X syndrome (Peier et al., 2000; Yan et al., 2004), and anxiety is a hallmark behavior of patients with Fragile X syndrome. Interestingly, mice with translational deficits due to a knock in of I304N, a missense mutation found in a single FXS patient, exhibit decreased anxiety as measured by the light/dark box test, just as we found with *Jakmip1* KO mice (Zang et al., 2009). *Jakmip1* and *Fmr1* KO mice also both show decreased acoustic startle response at high decibels (Nielsen et al., 2002) and impaired fear memory (Zhao et al., 2005) (Figure 5-5, A; Figure 5-9, D).

Taken together, our results show that loss of JAKMIP1 recapitulates the behavioral profiles of other mouse models of ASD and those of Fragile X syndrome. This mouse serves as an important tool in understanding JAKMIP1 function in the context of ASD and will be helpful in therapeutic development.

5.6 Methods

Mice

Jakmip1 KO, HET, and WT mice were generated from crossing heterozygous mice. Mice had ad-lib access to food and water and were housed in a 12 hour light/12 hour dark cycle. Experiments were carried out in accordance with UCLA's animal research committee.

Quantitative RTPCR

RNA was extracted using a miRNeasy kit (Qiagen, Germantown, MD) according to manufacturer's instructions. RT–PCR was performed as described (Spiteri et al., 2007) with the exception that random hexamers were used to synthesize cDNA. Expression fold changes from *Jakmip1* KO, WT, and HET mice were calculated using primer sets to *Jakmip1* exons 3-4 and 6-7, a location within the LacZ-neo cassette, and loading control primer sets to *Hprt* and *bactin*. The HET to WT transcript fold change was calculated by averaging four fold changes values generated from the two *Jakmip1* primer sets, each with two loading controls.

Western blotting

Immunoblotting was carried out according to section 2.6

β-galactosidase staining

Mouse brains were dissected and sectioned at 10uM onto Superfrost+ glass slides (Fisher Scientific, Waltham, MA) and were post-fixed in 4% paraformaldehyde. Sections were incubated in a LacZ staining solution containing 2mM MgCl2, 0.01% Deoxycholic acid, 0.02% IGEPAL CA-630, 0.1% X-Gal in dimethylformamide, 5mM Potassium Ferrocyanide, 5mM Potassium Ferricyanide in 1X PBS overnight at 37 C. Sections were fixed for 1 hour in 10% neutral buffered formalin and dehydrated in an ethanol gradient followed by incubation in

Xylene. Permount (Fisher Scientific, Waltham, MA) was used to mount slides onto coverslips.

Immunohistochemical Staining

To detect changes in gross morphology, we perfused p30 mouse brains (WT, N=3; HET, N=3; KO, N=3) and cryosectioned coronally at 40uM. We immunostained the brains using the chemical stains DAPI, to detect nuclear staining, and NeuroTrace to identify neurons (Brain Stain Imaging Kit, Invitrogen, Carlsbad, CA) and analyzed the stained sections by microscopy. To determine changes in neuronal number, we perfused p30 mouse brains, cryosectioned coronally at 20uM, and immunostained sections with an anti NeuN antibody (Catalogue number MAB377, Millipore, Billerica, MA) [WT; N=4, 29 sections, 38 images: KO; N=3, 23 sections, 45 images]. Microscopy images were taken and analyzed using Image J software (National Institutes of Heath, Bethesda, Maryland) to determine positively stained cells.

Behavioral Tests

Experiments were conducted using C57BL/6 *Jakmip1* WT, HET, and KO mice greater than p40.

Open field test

General activity of mice inside of a 27.5cm x 27.5cm clear plexiglass arena was recorded by the automated system, Top Scan (Clever Sys, Inc., Reston, VA) over a 20 minute period.

Hot plate startle

Mice were placed on a 55 C hot plate and time was recorded from time of placement to the first sign of pain, which included licking or kicking of the paws. The mouse was allowed to stay on the plate for a maximum of 15 seconds. The experiment was performed blinded to genotype.

Nesting behavior

On day 1, each mouse was placed into a new, individual cage and provided with one unit of tightly packed nesting material. Cages with mice were then mounted into the wall bracket and

left undisturbed overnight. On the second day, mice were first prodded away from nesting site and then extracted out from the cage and placed back into their respective home cages. Two images of the nesting were taken, one at a close distance and one at a further distance. Nests were scored blinded to genotype according to previously published criteria (Deacon, 2006).

Marble Burying Test

Approximately two inches of extra bedding was placed in two testing cages in a sterile hood. Bedding was then compacted using disinfected and gloved hand. 12 marbles were placed equidistantly in a 3x4 grid. Mice were then placed in the middle of the cage. Lids were placed on the cages shortly after to prevent escape of jumping mice. After a 30 minute trial, mice were extracted and placed back into home cage. The number of marbles that were buried more than two thirds into the bedding were counted and one photograph was taken for each cage to verify results. In between trials, bedding was re-compacted and marbles were cleaned with 1% VIRKON disinfectant spray, dried, and rearranged in a 3x4 grid. This test was run blinded to genotype.

Rotorod

Mice were acclimated to rotorod testing room for 15 minutes before testing. Each mouse was then subjected to two tests, each lasting up to 180 seconds. The first test was the "constant" test, and had an initial rotation rate of 5 rpm and accelerated to 20 rpm in 10 seconds. The second test was the "accelerating" test, and had an initial rotation rate of 5 rpm and accelerated to 60 rpm in 10 seconds. Latency to fall or to rotate for four times on the bar was recorded. Before each test, each mouse was acclimated to the rotorod's initial 5 rpm rotation rate for two minutes before beginning the acceleration. Mice were run in the same order through the ‘constant’ and ‘accelerating’ trials. This test was run blinded to genotype.

Wire Hang Test

Mice were acclimated to wire cage lid for 30 seconds. The lid was then shaken for 10 seconds for the mice to obtain a grip and then swiftly inverted. Latency to fall was measured over a 60 second maximum session. Mice that fell in less than 10 seconds were given up to two retries. This test was run blinded to genotype.

Gait test

Mice were handled two times before the trial to acclimate to handling. Mice were given two practice runs down a rectangular runway in which one side was brightly lit and the other contained a dark box with home cage bedding. The mouse's front paws were painted red and the back paws were painted green with nontoxic paint. Two test runs were conducted. Experiment was run blinded to genotype. The data from each test run was collapsed. Average mean stride length (number of strides divided by total distance traveled), average stride length difference (longest stride minus shortest stride), and average stride length variation were calculated for both the left and right sides of the mouse and analyzed across genotypes. Average gait width and average linearity were additionally analyzed. Linearity is a measurement of path directionality and was calculated using the angles between each stride and the parallel line representing the mouse's overall direction of path.

Acoustic Startle Response and prepulse inhibition

Tests were run blinded to genotype and performed as previously described (Penagarikano et al., 2011).

Home Cage Behavior

Mice were placed in juxtaposed cages containing fresh bedding. Opaque panels were placed in between cages to prevent mice from observing each other. Mice were allowed to acclimate to the new cage for 10 minutes. Behavior was recorded by the automated system, Top Scan (Clever Sys, Inc., Reston, VA) over a following 10 minute period. Videos were scored blinded to genotype for repetitive hindlimb jumping, digging, and grooming. Repetitive jumping was defined by a bout in which the mouse reared against the cage, and then jumped consecutively three times or more. The bout ended when the mouse unreared.

T maze spontaneous alternation test

The T maze spontaneous alternation test was performed as previously described (Penagarikano et al., 2011). A Chi-squared test was performed on the number of overall choices of left or right. No bias in arm choice was observed. For drug treaments, Risperidone (Sigma, St. Louis, Missouri) was administered intraperitoneally at 0.2 mg/kg between 30 minutes and one hour prior to testing. 100ul was given per 10 grams of mouse in a 20ug/ml concentrated solution.

Three-Chamber Social Interaction Test

This test was conducted as previously described (Silverman et al., 2010). Briefly, each mouse was placed in the center of an interconnected three-chambered box after habituation. The center chamber was empty, while left and right chambers contained an empty wire cup or a sex-matched, novel wild-type mouse in a similar wire cup. Behavior was recorded by the automated system, Top Scan (Clever Sys, Inc., Reston, VA) over a following 10 minute period. Time spent sniffing the mouse-containing cup or the empty cup and time in each chamber was scored manually, blinded to genotype.

Light Dark Exploration Test

This test was conducted as previously described (Penagarikano et al., 2011). The latency to enter the illuminated compartment, time in the dark and light chambers, and number of cross overs between light and dark chambers was recorded by the automated system, Top Scan (Clever Sys, Inc., Reston, VA) over a 10 minute period.

Morris Water Maze

The training phase of the MWM test was conducted as previously described (Vorhees and Williams, 2006).

Auditory Fear Conditioning

Mice were pre handled four days before the day 1 acquisition trial by being removed from the cage and placed in sterilized beaker for 30 seconds. On day 1, mice were taught the tone-shock pairing. Mice are placed in context A and subjected to the following protocol: two minute wait, 30-second tone with two second shock during the last two seconds of tone, one minute wait, 30-second tone with two second shock during the last two seconds of tone, 1 minute wait, 30-second tone with two second shock during the last two seconds of tone, two minute wait. Freezing was recorded. On the second day (day 2), mice were tested for contextual fear by being placed in context A. Freezing was recorded over an eight minute period with no shock or tone administered. On day 3, mice were tested for generalized contextual fear by being placed in a novel context B. Freezing was recorded over an eight minute period with no shock or tone administered. On day 4, long term memory acquisition of the tone-shock pairing was tested. Mice were placed in context B and subjected to the following protocol: two minute wait, 30-second tone, one minute wait, 30-second tone, one minute wait, 30-second tone, two minute

wait. Freezing was recorded. On day five, extinction of the learning of tone/shock pairing was conducted in context B by the following protocol: two minute wait, 20 times of 30 second tones separated by one minute wait, two minute wait. Freezing was recorded. The shock intensity used was 0.5 mA, and the shock duration was two seconds. The tone intensity was 80dB, tone length was 30 seconds, and tone frequency was 2000 hertz (Hz). Mice were allowed 30 minutes to habituate to the room before trials.

Chapter 6: Transcriptome profiling of the *Jakmip1* KO mouse brain

6.1 Introduction

We have defined a clear role for JAKMIP1 in FMRP-associated translation important for ASD and FXS behavioral profiles through proteomic-based molecular studies and mouse behavioral studies. We next investigated how JAKMIP1 loss *in vivo* affects the brain's transcriptome. I hypothesized that *Jakmip1* ablation would elicit changes in the transcriptome because JAKMIP1 binds RNA [Figure 3-7, (Couve et al., 2004)], and gene ontology analysis of JAKMIP1's top protein binders indicate its role in RNA post transcriptional modification (Figure 3-5, C). Thus, loss of JAKMIP1 could result in differential RNA expression by destabilization or stabilization of RNA (De Rubeis and Bagni, 2010) and/or aberrant transcript processing. JAKMIP1's role in the makeup of the translated transcriptome could, additionally, be analyzed using *in vivo* BacTRAP technology (Heiman et al., 2008), but was not addressed here as it was resource and time prohibitive. Using brain transcriptome profiling, I hypothesized that *Jakmip1* ablation would lead to transcriptional changes mirroring those found in *Fmr1* KO brains and would destabilize mRNA targets shared with FMRP (Figure 3-7).

To test this, we carried out differential expression analysis using microarray technology in the brains of *Jakmip1* KO and WT postnatal mice. We chose to conduct our studies in developing brain at a time when JAKMIP1 protein peaks in expression (Figure 2-1). We reasoned that the most dramatic transcriptional changes would occur concomitantly with highest JAKMIP1 expression in WT brain. Furthermore, this allows for a more exact comparison with our previous molecular studies, which were conducted using postnatal brain.

We chose to examine mouse necortex, hippocampus, cerebellum, and striatum as *Jakmip1* is highly expressed in all of these tissues and these regions have distinct transcriptome profiles and anatomical functions. Furthermore, it is important to examine multiple structures, as

FMRP studies have revealed region-specific translational changes with *Fmr1* loss (D'Hulst et al., 2006; Miyashiro et al., 2003). We chose to study neocortex, as our previous studies were carried out in this tissue, facilitating comparisons between our transcriptome and proteomics data. We interrogated striatum, as *Jakmip1* loss leads to perseverative motor stereotypies, such as repetitive hindlimb jumping, that are mediated by cortico-striatal dopaminergic pathways (Presti et al., 2004). We additionally tested cerebellum as JAKMIP1 is expressed highly in postnatal cerebellum (Figure 2-5) and in Purkinje cells (Figure 2-6, Figure 2-7), a shared location with FMRP (Tamanini et al., 1997). Their coexpression here may influence *Jakmip1* KO mouse behavioral profiles if JAKMIP1 is important for FMRP function in this region, as both *Fmr1* knockout mice and FXS patients exhibit behavioral and morphological impairments involving the cerebellum (Koekkoek et al., 2005). Lastly, we examined hippocampal transcriptional profiles as this structure is involved in metabotropic glutamate receptor mediated synaptic plasticity in *Fmr1* knockout mice (Huber et al., 2002).

Differential gene expression analysis can generate thousands of genes. To narrow our focus, we conducted gene ontology analysis of the most significantly changed genes for each brain structure. We, additionally, compared our top changed genes with transcripts that are known to change with *Fmr1* knockout and with FMRP/JAKMIP1 shared mRNA targets. We found that *Jakmip1* ablation leads to differential expression of mRNA targets disrupted with *Fmr1* loss: GABA-A receptor subunits, *Rgs4*, and *Nxf1*. Moreover, all six of FMRP/JAKMIP1 shared mRNA targets are reduced in *Jakmip1* KO brains, with four showing highly significant changes. Lastly, we found gene ontology categories involving the structural formation of neurons to be most predominant across brain regions. We tested JAKMIP1's involvement in this biological process functionally by quantifying structural changes in differentiated neurons from

Jakmip1 KO and WT littermate pairs. We found that loss of *Jakmip1* reduces the longest branch length of neurons. Integrating these data with our previous findings clarify our results and open up new avenues of exploration for future work.

6.2 Characteristics of transcriptome signatures from *Jakmip1* KO postnatal brain regions

Differential expression analysis was conducted using cortex, hippocampus striatum, and cerebellum from postnatal brains of the same mice used for protein and RNA analysis in Chapter 4 (Figures 4-4 and 4-5). These mice represented three sex-matched litters, containing four *Jakmip1* KO mice and WT littermates. To determine the parameter that predominantly drives the data clustering, we generated a multidimensional scaling plot. In this analysis, anatomical region was the primary driver of expression differences and, as such, samples were normalized within region (Figure 6-1).

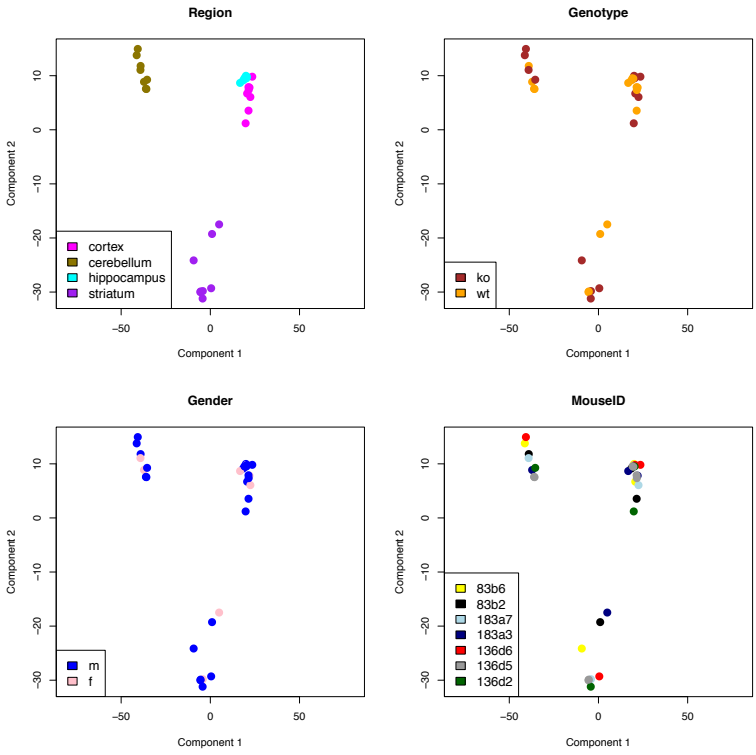

Figure 6-1. Multidimensional scaling plot shows gene expression clusters by brain region.

We conducted differential expression analysis, rather than Weighted Gene Co-Expression Network Analysis (WGCNA), as anatomical region drove expression differences and there were not enough samples within region to conduct WGCNA. To identify differentially expressed genes, we used a stringent p-value cut off of 0.005 (paired student's t-test; paired by littermate). Significantly changed genes showed a consistent expression pattern across independent *Jakmip1* KO samples for each region (Appendix Figure 2-1). We found the greatest number of genes changes in cerebellum (793) and striatum (573), with less genes changed in cortex (117) and hippocampus (216). The directionality of gene changes (up or down regulated) was roughly equal within and across brain regions (Figure 6-2).

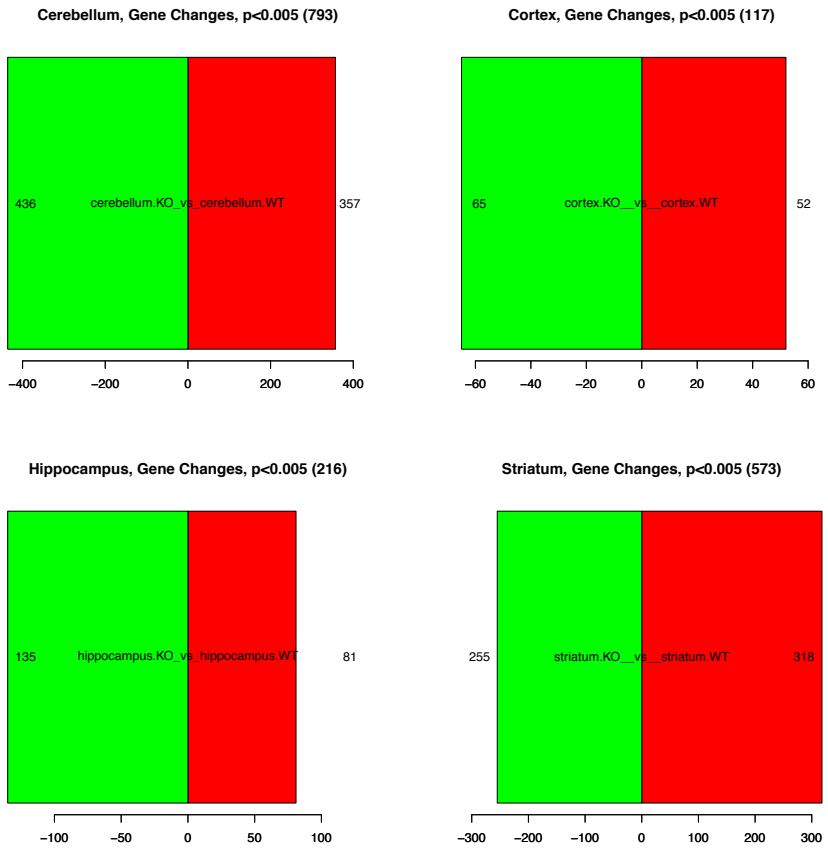

Figure 6-2. Gene expression profiles in *Jakmip1* KO versus WT brains stratified by region.
Red boxes denote upregulated genes, while green boxes denote downregulated genes.
The size of the boxes correspond to the number of genes changed.

We, additionally, identified the number of genes that were differentially expressed across tissues or showed regional differential expression. We found very few genes that were commonly dysregulated across anatomical regions (Figure 6-3). A few notable exceptions were *Map1b*, which was commonly down regulated in the cerebellum, hippocampus and striatum of *Jakmip1* KO mice versus sex matched wild-type littermates (Figure 6-3, C), Protocadherin-17 (PCDH17), which was also commonly dysregulated in these tissues although showed region-dependent directionality (Figure 6-3, C), and Huntingtin-associated protein 1 (*Hap1*) (Figure 6-3, B), which was decreased in cerebellum, cortex, and hippocampal tissue of *Jakmip1* KO mice.

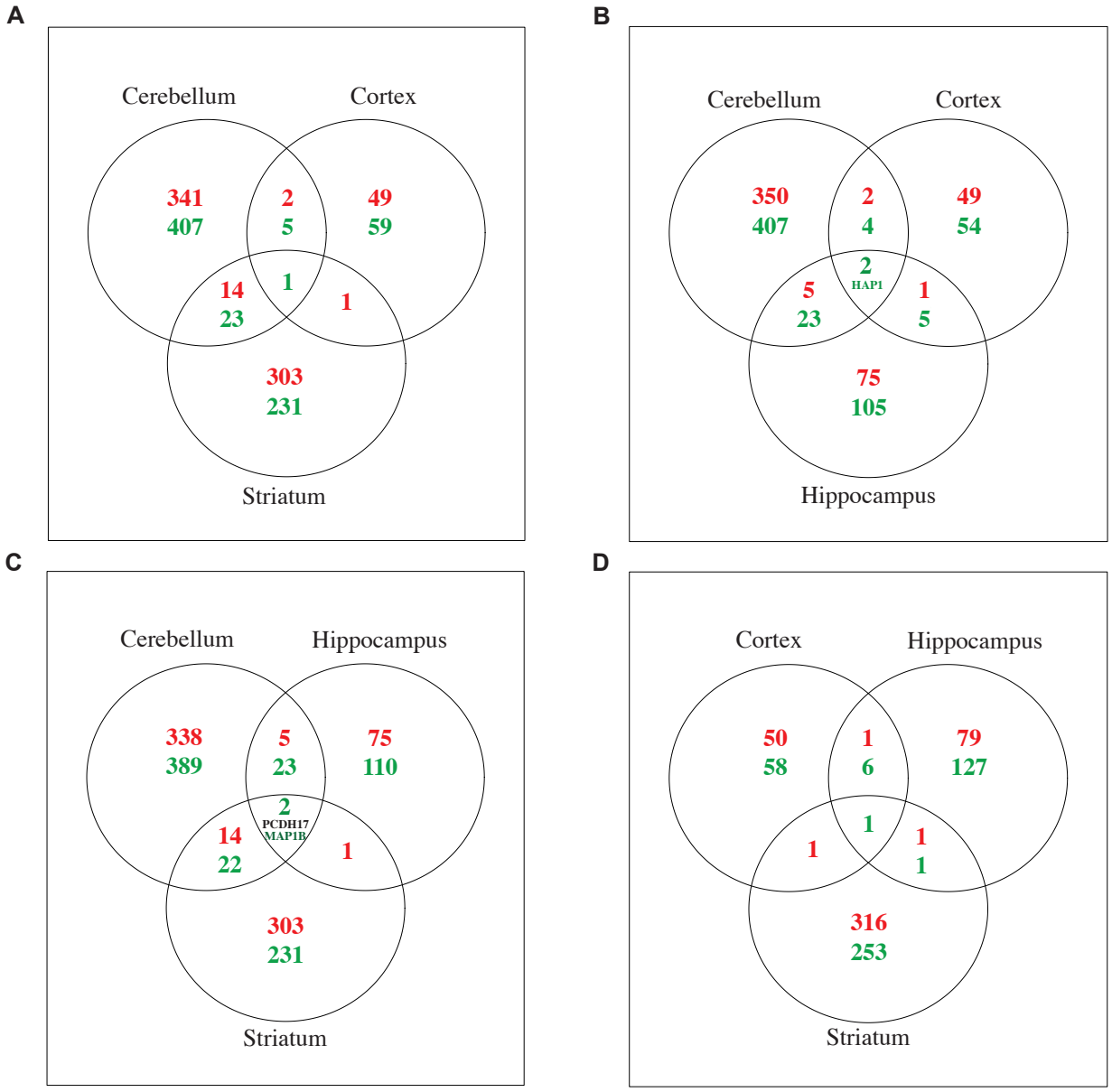

Figure 6-3. Gene expression changes show regional specificity. (A) Overlap of differentially expressed genes in the cerebellum, cortex and striatum. (B) Overlap of differentially expressed genes in the cerebellum, cortex and hippocampus. (C) Overlap of differentially expressed genes in the cerebellum, hippocampus and striatum. PCDH17 was upregulated in striatum, but downregulated in hippocampus and cerebellum. (D) Overlap of differentially expressed genes in the cortex, striatum, and hippocampus. Red numbers denote the number of genes that are overexpressed, while green numbers represent the number of genes that are underexpressed in *Jakmip1* KO compared to WT control brains. When less than three genes are dysregulated in all three anatomical regions, their names are listed, unless it is *Jakmip1*. Differentially expressed genes are defined as those with $P < 0.005$.

6.3 Gene ontology analysis of differentially expressed genes in *Jakmip1* KO postnatal brain

Our transcriptome analysis generated hundreds of differentially expressed genes. In order to organize these differentially expressed genes into functional categories, we conducted gene ontology analysis on the list of significantly changed genes ($P < 0.005$) for each brain region using The Database for Annotation, Visualization and Integrated Discovery (DAVID v6.7, http://david.abcc.ncifcrf.gov/). We examined gene ontology categories at $P<0.05$ falling under the umbrella terms 'Biological Processes' (Figure 6-4) and 'Molecular Functions' (Figure 6-5).

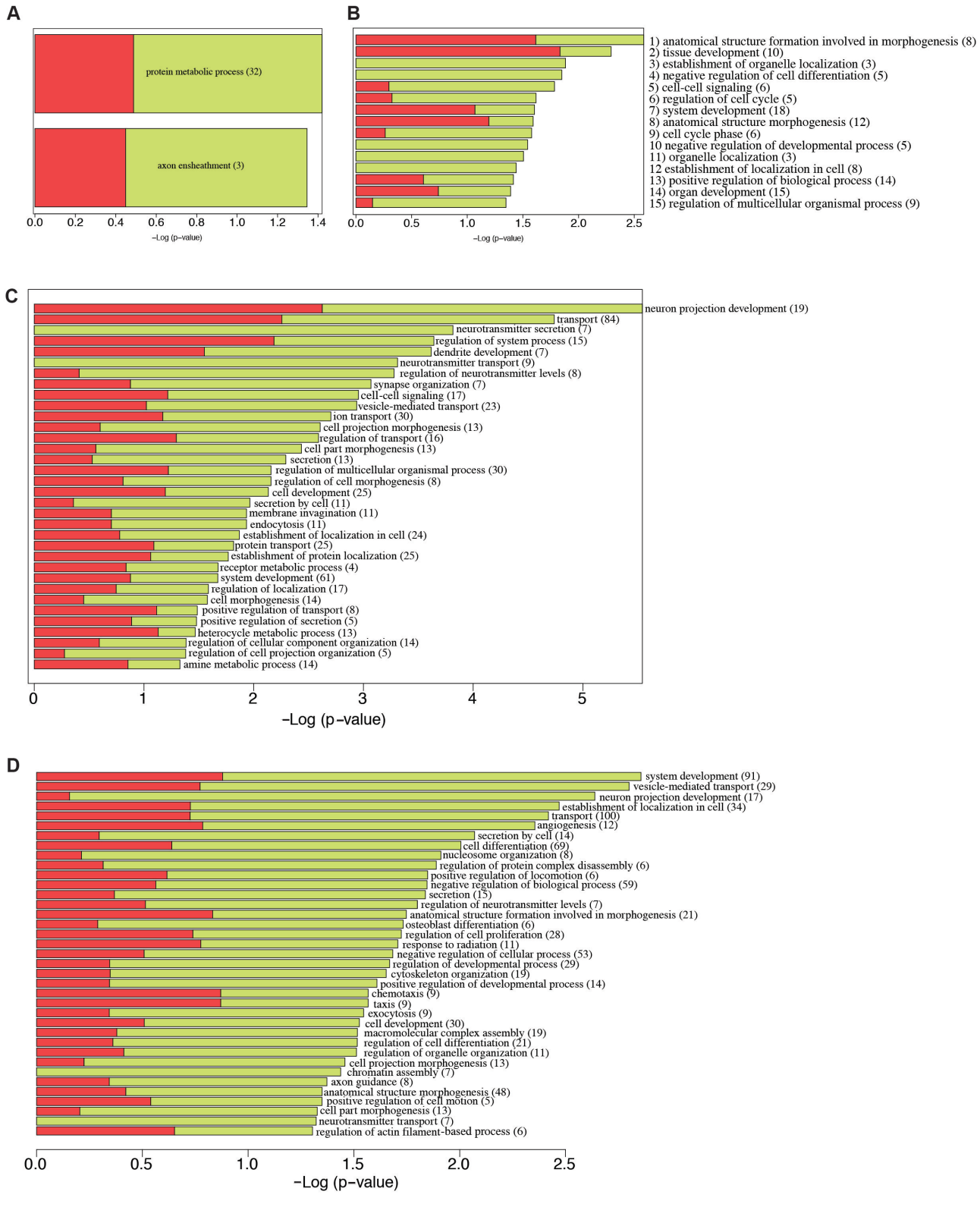
A
protein metabolic process (32)
axon ensheathment (3)
0.0 0.2 0.4 0.6 0.8 1.0 1.2 1.4
−Log (p−value)
B
1) anatomical structure formation involved in morphogenesis (8)
2) tissue development (10)
3) establishment of organelle localization (3)
4) negative regulation of cell differentiation (5)
5) cell-cell signaling (6)
6) regulation of cell cycle (5)
7) system development (18)
8) anatomical structure morphogenesis (12)
9) cell cycle phase (6)
10 negative regulation of developmental process (5)
11) organelle localization (3)
12 establishment of localization in cell (8)
13) positive regulation of biological process (14)
14) organ development (15)
15) regulation of multicellular organismal process (9)
0.0 0.5 1.0 1.5 2.0 2.5
−Log (p−value)
C
neuron projection development (19)
transport (84)
neurotransmitter secretion (7)
regulation of system process (15)
dendrite development (7)
neurotransmitter transport (9)
regulation of neurotransmitter levels (8)
synapse organization (7)
cell-cell signaling (17)
vesicle-mediated transport (23)
ion transport (30)
cell projection morphogenesis (13)
regulation of transport (16)
cell part morphogenesis (13)
secretion (13)
regulation of multicellular organismal process (30)
regulation of cell morphogenesis (8)
cell development (25)
secretion by cell (11)
membrane invagination (11)
endocytosis (11)
establishment of localization in cell (24)
protein transport (25)
establishment of protein localization (25)
receptor metabolic process (4)
system development (61)
regulation of localization (17)
cell morphogenesis (14)
positive regulation of transport (8)
positive regulation of secretion (5)
heterocycle metabolic process (13)
regulation of cellular component organization (14)
regulation of cell projection organization (5)
amine metabolic process (14)
0 1 2 3 4 5
−Log (p−value)
D
system development (91)
vesicle-mediated transport (29)
neuron projection development (17)
establishment of localization in cell (34)
transport (100)
angiogenesis (12)
secretion by cell (14)
cell differentiation (69)
nucleosome organization (8)
regulation of protein complex disassembly (6)
positive regulation of locomotion (6)
negative regulation of biological process (59)
secretion (15)
regulation of neurotransmitter levels (7)
anatomical structure formation involved in morphogenesis (21)
osteoblast differentiation (6)
regulation of cell proliferation (28)
response to radiation (11)
negative regulation of cellular process (53)
regulation of developmental process (29)
cytoskeleton organization (19)
positive regulation of developmental process (14)
chemotaxis (9)
taxis (9)
exocytosis (9)
cell development (30)
macromolecular complex assembly (19)
regulation of cell differentiation (21)
regulation of organelle organization (11)
cell projection morphogenesis (13)
chromatin assembly (7)
axon guidance (8)
anatomical structure morphogenesis (48)
positive regulation of cell motion (5)
cell part morphogenesis (13)
neurotransmitter transport (7)
regulation of actin filament-based process (6)
0.0 0.5 1.0 1.5 2.0 2.5
−Log (p−value)

Figure 6-4. Gene ontology of most significantly changed genes in *Jakmip1* KO brain regions: Biological Processes. Biological processes of significantly changed genes in the hippocampus (A), cortex (B), striatum (C), and cerebellum (D). X axis is the negative log of the p-value of the gene ontology category. Numbers in parentheses are the number of genes in each category. Red space denotes the proportion of upregulated genes, while green space represents the proportion of down regulated genes. Differentially expressed genes are defined as those with $P < 0.005$. Level 3 categories from DAVID are shown.

There were three common gene ontology category themes across tissues. The first was gene ontology categories involving neuronal structure formation. In the cortex, 'anatomical structure formation involved in morphogenesis' was the most significant gene ontology category, and 'anatomical structure morphogenesis' was an additional significant category in this brain region. In the striatum, 'neuron projection development' was the most significant category, and 'dendrite development' was the fifth most significant category. Likewise, in the cerebellum, 'neuron projection development' was the third most significant category. The second common theme was transport. 'Establishment of organelle localization', 'transport', and 'vesicle-mediated transport' were among the top three most significant categories in cortex, striatum and cerebellum, respectively. Lastly, differentiation was a recurring gene ontology category across brain regions. In cortex, 'Negative regulation of cell differentiation' was the fourth most significant gene ontology category. 'Cell differentiation' was among the top eight most significant categories in cerebellum (Figure 6-4).

Differentially expressed genes in striatum and cerebellum generated significant 'Molecular Function' gene ontology categories. Protein binding was the most consistent theme among molecular function gene ontology categories. 'Cytoskeletal protein binding', 'protein domain specific binding', and 'protein complex binding' were significant categories for both striatum and cerebellum (Figure 6-5). 'Ribonucleotide binding' was also significant for the striatum.

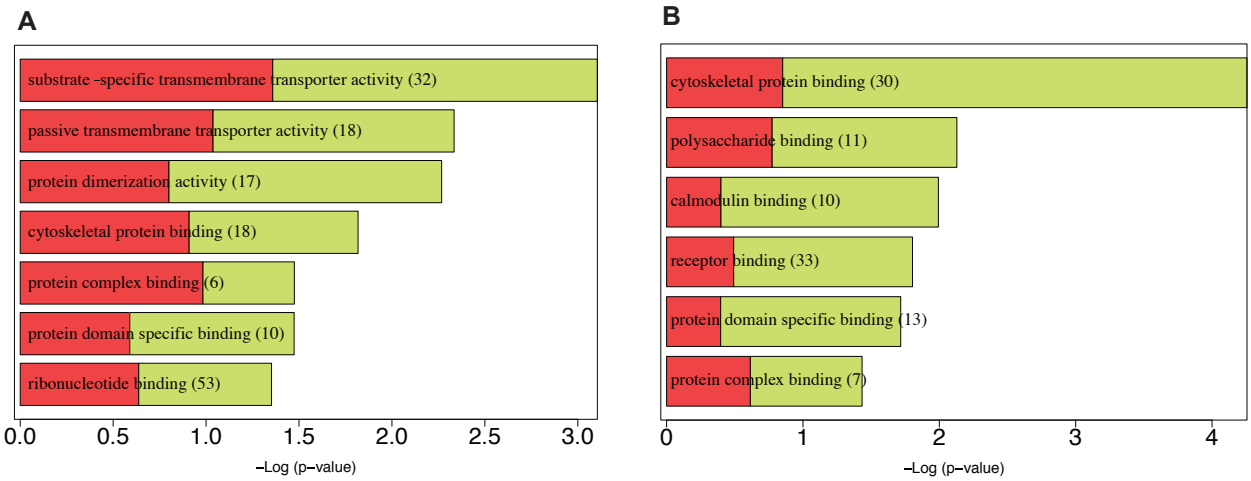

Figure 6-5. Gene ontology (Molecular Function) of most significantly changed genes in *Jakmip1* KO brain regions.
(A) Biological processes of significantly changed genes in the striatum.
(B) Biological processes of significantly changed genes in the cerebellum.
X axis is the negative log of the p-value of the gene ontology category. Numbers in parentheses are the number of genes in each category. Red space denotes the proportion of upregulated genes, while green space represents the proportion of downregulated genes. Differentially expressed genes are defined as those with $P < 0.005$.
Level 3 categories from DAVID are shown. There were no significant gene ontology categories in cortex or hippocampus.

6.4 Comparison of differentially expressed genes from *Jakmip1* KO postnatal brain with genes changed in *Fmr1* knockout mouse brains

JAKMIP1 is a component of the FMRP translational machinery. As such, I hypothesized that loss of JAKMIP1 would lead to transcriptional changes that would partially mimic those caused by *Fmr1* loss. A recent transcriptome-wide study of hippocampal tissue from *Fmr1* KO mice found only a handful of genes changed, one of which being a GABA-A receptor subunit (Gantois et al., 2006). A follow up study, using quantitative real time PCR, found significant reduction of GABA-A receptor subunits alpha 1, 3, 4, beta 1 and 2, gamma 1 and 2, and delta in *Fmr1* KO cortex, but not in cerebellum (D'Hulst et al., 2006). We compared the gene changes in GABA-A receptor subunits from our study with this previous study (Table 6-1). We found that

of these eight receptor subunits, five were also significantly changed with *Jakmip1* KO, three having corresponding p-values of 0.0005.

Rgs4 is reduced in the CA1 region of the hippocampus and the cortex of *Fmr1* KO mice (Tervonen et al., 2005). We also found this gene to be significantly changed in the hippocampus (P=0.002) and in the cerebellum (P=0.002), but not in the cortex or striatum of *Jakmip1* KO mice (Table 6-1). Lastly, *in vitro* studies suggest that FMRP destabilizes *Nxf1* mRNA and leads to an increase in this transcript with *Fmr1* loss (Zhang et al., 2007). In line with this, we found that loss of *Jakmip1* results in a significant increase in Nxf1 (P=0.002) in the cerebellum (Table 6-1).

Transcript	ILMN_Gene	Definition	CB KO vs. CB WT	CX KO vs. CX WT	HP KO vs. HP WT	ST KO vs. ST WT	CB KO vs. CB WT	CX KO vs. CX WT	HP KO vs. HP WT	ST KO vs. ST WT
ILMN_214944	GABRA1	GABA-A receptor, subunit alpha 1	0.08	0.03	0.02	0.04	0.160	0.622	0.649	0.460
ILMN_191356	GABRA2	GABA-A receptor, subunit alpha 2	0.03	-0.01	-0.06	-0.01	0.552	0.842	0.212	0.803
ILMN_209420	GABRA3	GABA-A receptor, subunit alpha 3	-0.21	-0.06	-0.03	-0.24	0.005	0.482	0.587	0.201
ILMN_212476	GABRA4	GABA-A receptor, subunit alpha 4	-0.04	0.02	0.00	-0.07	0.465	0.821	0.997	0.228
ILMN_211769	GABRA5	GABA-A receptor, subunit alpha 5	0.09	0.04	-0.01	-0.01	0.076	0.550	0.904	0.848
ILMN_221224	GABRA6	GABA-A receptor, subunit alpha 6	0.12	-0.09	0.01	-0.01	0.039	0.190	0.855	0.849
ILMN_221929	GABRB1	GABA-A receptor, subunit beta 1	-0.19	-0.27	-0.03	0.22	0.018	0.010	0.585	0.005
ILMN_218482	GABRB2	GABA-A receptor, subunit beta 2	-0.01	-0.01	0.02	0.05	0.868	0.948	0.722	0.565
ILMN_191191	GABRB3	GABA-A receptor, subunit beta 3	-0.14	0.10	0.01	0.14	0.037	0.142	0.886	0.122
ILMN_240761	GABRB3	GABA-A receptor, subunit beta 3	0.00	0.06	0.04	0.15	0.965	0.293	0.379	0.033
ILMN_240761	GABRB3	GABA-A receptor, subunit beta 3	0.03	-0.01	0.01	0.03	0.479	0.911	0.882	0.611
ILMN_218631	GABRD	GABA-A receptor, subunit delta	0.15	0.26	0.20	0.01	0.024	0.289	0.005	0.952
ILMN_218631	GABRD	GABA-A receptor, subunit delta	0.13	0.18	-0.02	-0.02	0.055	0.544	0.740	0.853
ILMN_220325	GABRE	GABA-A receptor, subunit epsilon	0.03	0.00	-0.02	0.02	0.544	0.987	0.754	0.749
ILMN_212516	GABRG1	GABA-A receptor, subunit gamma 1	-0.13	-0.03	-0.07	0.19	0.019	0.698	0.231	0.045
ILMN_213712	GABRG2	GABA-A receptor, subunit gamma 2	0.02	0.04	0.04	-0.09	0.796	0.645	0.603	0.614
ILMN_213712	GABRG2	GABA-A receptor, subunit gamma 2	-0.16	-0.02	0.03	-0.04	0.046	0.837	0.560	0.874
ILMN_222801	GABRG2	GABA-A receptor, subunit gamma 2	-0.14	-0.02	0.04	-0.14	0.029	0.862	0.399	0.536
ILMN_222801	GABRG2	GABA-A receptor, subunit gamma 2	-0.06	0.02	-0.08	-0.04	0.274	0.868	0.145	0.826
ILMN_209842	GABRG3	GABA-A receptor, subunit gamma 3	-0.07	-0.08	0.02	0.22	0.144	0.245	0.683	0.005
ILMN_212083	GABRP	GABA-A receptor, subunit Pi	0.06	-0.02	0.01	-0.08	0.253	0.676	0.869	0.235
ILMN_212083	GABRP	GABA-A receptor, subunit Pi	-0.03	-0.02	-0.03	-0.01	0.490	0.730	0.516	0.812
ILMN_208641	GABRQ	GABA-A receptor, subunit theta	-0.02	-0.01	0.05	-0.01	0.747	0.874	0.332	0.926
ILMN_219032	GABRR1	GABA-A receptor, subunit rho1	0.04	-0.02	-0.02	0.00	0.482	0.784	0.704	0.976
ILMN_219032	GABRR1	GABA-A receptor, subunit rho1	-0.07	0.04	0.02	-0.03	0.250	0.484	0.715	0.564
ILMN_212519	GABRR2	GABA-A receptor, subunit rho2	-0.06	0.09	-0.07	-0.01	0.215	0.179	0.224	0.859
ILMN_209130	RGS4	Regulator of G-protein signaling 4	-0.77	0.25	0.21	0.14	0.002	0.136	0.002	0.226
ILMN_219270	NXF1	Nuclear RNA export factor 1 homolog	0.21	-0.10	-0.03	0.01	0.002	0.143	0.658	0.846

Table 6-1. Genes changed in the *Jakmip1* KO mouse brain overlap with those changed in models of Fragile X syndrome. Gene expression changes from *Jakmip1* KO brains versus WT controls are shown for cerebellum (CB), cortex (CX), hippocampus (HP), and striatum (ST). Log Ratios of expression changes are listed in columns with green headings, while the corresponding p values of these changes are listed in columns with blue headings. P values less than or equal to 0.005 are highlighted yellow, while those less than or equal to 0.05 are colored light orange. The corresponding expression changes are colored green for decreased expression or red for increased expression. Genes are colored green in the Gene column when decreased or red when increased in Fragile X knockout systems (D'Hulst et al., 2006; Tervonen et al., 2005; Zhang et al., 2007). Genes that are commonly changed in *Jakmip1* KO and FXS models are boxed. Thin boxes represent p values less than or equal to 0.05 in the *Jakmip1* KO brain, while thick boxes represent p values less than or equal to 0.005 in *Jakmip1* KO brains. Genes with repeated names represent independent microarray probes.

We have previously shown that JAKMIP1 binds to the FMRP mRNA targets, *Sapap4*, *App*, *Dag1*, *PSD95*, *Camk2a*, and *Map1b* (Figure 3-6 and Figure 3-7). As such, I hypothesized that *Jakmip1* loss would cause a destabilization and subsequent reduction of these targets. Congruous with our hypothesis, we found significant reductions of *Sapap4* in striatum, *App* in cerebellum, *Dag1* in cerebellum, *PSD95* in cerebellum, *Camk2a* in cerebellum and striatum, and *Map1b* in cerebellum, hippocampus, and striatum (Table 6-2). Interestingly, we found slight increases in expression of *Sapap4* and *PSD95* in the cortex and of *Map1b* in the hippocampus, although the corresponding p values were marginally significant.

In order to determine if genes changed with *Jakmip1* loss show a statistically significant overlap with FMRP RNA binding partners, I compared the list of differentially expressed genes in *Jakmip1* KO brain ($p < 0.005$, N=1446) with high confidence FMRP RNA binding partners isolated by cross-linking immunoprecipitation (false discovery rate < 0.01, N=842) (Darnell et al., 2011), defining the population as all brain expressed genes (N=15,132) (Kang et al., 2011). 106 FMRP RNA binding partners were significantly changed in the *Jakmip1* KO mouse brain. The hypergeometic probability of the overlap was statistically significant (P=0.0018, calculated as described in section 3.8).

Transcript	ILMN_Gene	Alias	CB KO vs. CB WT	CX KO vs. CX WT	HP KO vs. HP WT	ST KO vs. ST WT	CB KO vs. CB WT	CX KO vs. CX WT	HP KO vs. HP WT	ST KO vs. ST WT
ILMN_185099	DLGAP4	SAPAP4	0.05	0.15	0.07	-0.35	0.356	0.036	0.205	0.001
ILMN_245521	DLGAP4	SAPAP4	-0.03	0.04	0.04	-0.35	0.708	0.503	0.440	0.002
ILMN_185099	DLGAP4	SAPAP4	-0.06	0.12	-0.01	-0.10	0.184	0.099	0.895	0.171
ILMN_245521	DLGAP4	SAPAP4	-0.02	0.07	-0.03	-0.08	0.738	0.318	0.582	0.241
ILMN_209617	APP		-0.11	-0.06	0.09	0.10	0.043	0.339	0.108	0.165
ILMN_220537	DAG1		-0.20	-0.08	-0.09	0.12	0.036	0.177	0.089	0.063
ILMN_220537	DAG1		-0.01	0.09	0.03	-0.07	0.781	0.306	0.698	0.322
ILMN_193460	DLGH4	PSD95	-0.29	0.14	0.11	0.04	0.001	0.043	0.250	0.757
ILMN_209509	CAMK2A		-0.33	0.05	0.10	-0.35	0.004	0.532	0.222	0.022
ILMN_209509	CAMK2A		-0.31	0.01	0.04	-0.09	0.002	0.897	0.569	0.545
ILMN_211686	CAMK2A		-0.03	-0.07	-0.02	0.02	0.494	0.357	0.705	0.815
ILMN_220448	MTAP1B	MAP1B	-0.53	0.10	-0.20	-0.35	0.000	0.221	0.003	0.001
ILMN_220448	MTAP1B	MAP1B	-0.15	-0.16	0.06	0.04	0.020	0.070	0.257	0.464
ILMN_220448	MTAP1B	MAP1B	-0.05	0.02	0.04	-0.03	0.321	0.821	0.515	0.549
ILMN_220448	MTAP1B	MAP1B	-0.36	-0.15	0.16	-0.01	0.001	0.099	0.046	0.929

Table 6-2. Shared JAKMIP1/FMRP mRNA targets show differential gene expression in *Jakmip1* KO brains compared to WT controls. Gene expression changes from *Jakmip1* KO brains versus WT controls are shown for cerebellum (CB), cortex (CX), hippocampus (HP), and striatum (ST). Log Ratios of expression changes are listed in columns with green headings, while the corresponding p values of these changes are listed in columns with blue headings. P values less than or equal to 0.005 are highlighted yellow, while those less than 0.05 are colored light orange. The corresponding expression changes are colored green for decreased expression or red for increased expression. Genes that are significantly changed in *Jakmip1* KO brains are boxed. Thin boxes represent p values less than 0.05, while thick boxes represent p values less than or equal to 0.005. Genes with repeated names represent independent microarray probes.

6.5 Morphological characteristics of neurons with *Jakmip1* loss

Based on the transcriptome signature in the *Jakmip1* KO brain, I hypothesized that loss of *Jakmip1* would lead to morphological changes in neurons. Significant gene ontology categories across brain structures converge on formation of neuronal structure (Figure 6-4). Moreover, two of the three genes that were commonly dysregulated across antamomical brain regions both bind to cytoskeletal elements. *Map1b*, which was commonly downregulated in the cerebellum, hippocampus and striatum of *Jakmip1* KO mice (Figure 6-3, C, Table 6-2) associates with microtubules. *Hap1*, which was decreased in cerebellum, cortex, and hippocampal tissue of *Jakmip1* KO mice (Figure 6-3, B) interacts with the cytoskeletal proteins, pericentriolar autoantigen protein 1 and dynactin.

To determine the effects of JAKMIP1 loss on neuronal morphology, we conducted Sholl analysis on two week differentiated WT and *Jakmip1* KO neurons using Neuromath software. We quantified cell size, total neurite length, number of branches and longest branch length in TUJ1-stained neurons in a preliminary study. We repeated this analysis on MAP2 positive, two

week differentiated neurons from three independent WT/KO littermate pairs. Consistent with our hypothesis, in both studies, we found a significant decrease in the longest branch length of neurons (Figure 6-6), however modest, most likely a factor of sample size.

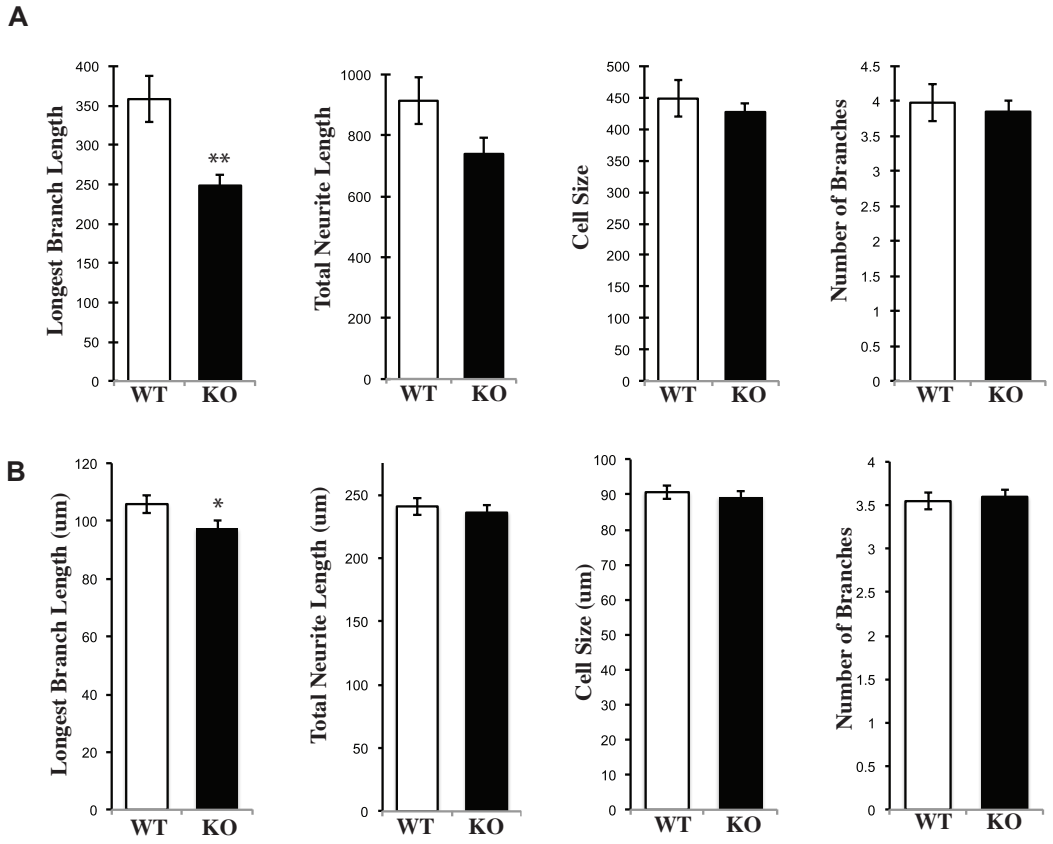

Figure 6-6. Loss of JAKMIP1 results in decreased longest branch length in neurons.
(A) *Jakmip1* loss leads to a significant decrease in the longest branch length of TUJ1 positive neurons (Preliminary experiment). Y axis is arbitrary units. (WT, N=43 neurons; KO, N=120 neurons; one littermate pair: P=0.0011).
(B) *Jakmip1* loss leads to a significant decrease in the longest branch length of MAP2 positive neurons (WT, N=238 neurons ; KO, N=295 neurons; three littermate pairs: P=0.038).
Y axis lists neuronal characteristics analyzed.
P values calculated using a two sample, two tailed unpaired t-test.
Values are mean +/- SEM. * p <= 0.05, ** p<= 0.01, *** p <= 0.001.

6.6 Discussion

We found JAKMIP1 to be a novel member of an FMRP containing translational complex. As such, I hypothesized that loss of JAKMIP1 would result in transcriptional brain changes mirroring those seen in *Fmr1* KO brains and that JAKMIP1 ablation would destabilize, and thus decrease, the expression of JAKMIP1 mRNA binding partners. To test these hypotheses, we used microarray transcriptome profiling, an inherently hypothesis neutral approach, which additionally allowed for identification of JAKMIP1-associated biological processes.

GABA-A receptor subunits are among the few genes whose expression changes with *Fmr1* loss (D'Hulst et al., 2006; Gantois et al., 2006). We found that GABA receptor alpha 3, beta 1, and delta also showed significant changes (P=0.005) in *Jakmip1* KO mouse brains. In *Fmr1* KO mice, decreases in these transcripts are found in cortex, but not in cerebellum (D'Hulst et al., 2006). Interestingly, we observed gene expression changes in other brain regions (alpha 3 in cerebellum, beta 1 in striatum, and delta in hippocampus), and in some cases with opposite direction of change (beta 1 and delta showed increased expression). Like *Fmr1* loss, *Jakmip1* loss also resulted in differential expression of gamma 1 and 2, although with less significance. *Jakmip1* ablation also led to the differential expression of the GABA-A receptors subunit gamma 3 in striatum, which may have been missed by previous studies of *Fmr1* loss that did not examine striatal tissue (D'Hulst et al., 2006; Gantois et al., 2006).

These results suggest that neuroanatomical context is important for direction and/or presence of differential expression. For instance, if JAKMIP1 and FMRP have redundant functions in the cortex, than loss of JAKMIP1 would not result in FMRP-related gene changes there. However, if JAKMIP1 is necessary for proper FMRP functioning in other brain regions,

than its loss may result in FMRP-related gene expression changes. Importantly, loss of *Jakmip1* led to differential expression of both *Rgs4* and *Nxf1*, two additional genes known to change with *Fmr1* loss (Tervonen et al., 2005; Zhang et al., 2007). Based on these results, further exploration of JAKMIP1's role in GABAergic synaptic transmission would be a promising avenue of study.

We previously found that JAKMIP1 binds to a subset FMRP mRNA targets (Figure 3-7). I, thus, hypothesized that absence of JAKMIP1 would destabilize these targets, resulting in their decreased expression (De Rubeis and Bagni, 2010). Consistent with our hypothesis, we found significant reductions of *Sapap4* in striatum, *PSD95* in cerebellum, *Camk2a* in cerebellum, and *Map1b* in cerebellum, hippocampus, and striatum (Table 6-2). All p-values less than 0.005 corresponded to reduced mRNA levels, in line with our hypothesis that JAKMIP1 is involved in stabilizing its RNA binding partners. Notably, PSD95's decrease in the cerebellum, but not cortex, is a pattern seen in both *Jakmip1* and *Fmr1* KO mouse brains (Zalfa et al., 2007). I additionally found a statistically significant overlap of genes differentially expressed in the *Jakmip1* KO brain with a list of high-confidence FMRP RNA interactors identified using stringent methodology (Darnell et al., 2011).

Functional organization of our data into statistically significant gene ontology categories revealed neuronal anatomical structure formation as a convergent theme, implicating JAKMIP1 in this process (Figure 6-4). Moreover, both cytoskeleton-associated proteins, *Map1b* and *Hap1*, were among the few genes commonly dysregulated across multiple tissue types (Figure 6-3). To functionally test JAKMIP1's role in neuronal structure, we quantified four aspects of morphology, longest branch length, total neurite length, cell size, and number of branches, in differentiated neurons from *Jakmip1* KO versus WT littermate pairs. We found a significant decrease in the longest branch length of neurons with loss of *Jakmip1*, both in a preliminary

study of TUJ1 immunostained neurons and in a study of MAP2 stained neurons. This is consistent with a recent study that found a decreased number of projections in primary embryonic mouse cortical neurons with shRNA-mediated reduction of JAKMIP1 (Vidal et al., 2012). Moreover, JAKMIP1's involvement in cell structure is congruent with its role as a microtubule binder (Steindler et al., 2004; Vidal et al., 2007). To note, the second most predominant gene ontology category, 'transport', is consistent with JAKMIP1's role in bidirectional transport along the dendrites of microtubules (Vidal et al., 2007). Additionally, the recurring gene ontology theme 'differentiation' complements our initial findings that JAKMIP1 is expressed in differentiated neurons (Figure 2-8, Figure 2-9, Figure 2-10).

Taken together, differential expression profiling in the *Jakmip1* knockout brain implicates JAKMIP1 in FMRP related GABAergic pathways, stability of FMRP shared mRNA binding partners, and in proper formation of neuronal structure. These studies further support a major role for JAKMIP1 in the development of the central nervous system.

6.7 Methods

Microarray transcriptome profiling

Differential gene expression profiling was conducted using Illumina Mouse Chip Mouse ref 8 chips at the UCLA Neuroscience Genomic Core. To control for batch effects between chips, one sex-matched littermate pair (WT, KO) was run per chip, with all four structures represented for each mouse. The fourth chip contained a technical replicate of the third litter's WT mouse, as this litter contained two KO mice. RNA quality was determined using an Agilent Bioanalyzer (Santa Clara, California) prior to microarray analysis, and a detection score analysis was conducted after analysis to ensure the quality of each sample. Sample outliers were identified in the following way. We first plotted the Z score distributions of all samples, and removed any

sample that was two or more standard deviations from the mean. By this analysis, one striatal sample was excluded from further analysis along with its corresponding littermate sample. Secondly, gene expression array clustering analysis was conducted. By this analysis, one cortical sample was a clear outlier, and was excluded from further analysis along with its matched littermate sample. No cerebellar or hippocampal samples were removed from the analysis.

Morphological analysis of *Jakmip1* KO neurons

Cell culture, differentiation, and immunocytochemistry was conducted as described in sections 2.6 and 4.6. Microscopy images were taken at 40X magnification. Neuronal signal was retraced in Adobe Photoshop to eliminate background noise. Sholl analysis was then conducted on the retraced image using Neuromath software (Weizmann Institute of Science).

Chapter 7: Conclusions

7.1 Significance of these Discoveries and Future Directions

In this dissertation, I took a comprehensive approach to understand the developmental role of *JAKMIP1*, a newly identified autism candidate gene dysregulated in idiopathic ASD and in ASD subjects with Fragile X syndrome and 15 q duplication patients (Nishimura et al., 2007). After defining the time and place of JAKMIP1 expression during CNS development, I identified JAKMIP1 as a novel interactor of the FMRP translational complex, regulating both FMRP-related translation and global neuronal translation. To determine the behavioral ramifications of *Jakmip1* loss during neural development, I generated and characterized a novel *Jakmip1* KO mouse. I found that loss of *Jakmip1* results in impairments in the core phenotypes of ASD as well as those associated with Fragile X syndrome. I, finally, annotated the transcriptome signatures of various brain regions from *Jakmip1* KO mice. Transcriptome profiling from postnatal *Jakmip1* KO mice supported the intersection of JAKMIP1 and FMRP biology. Gene expression profiles from *Jakmip1* KO mouse brain both recapitulate that of models of Fragile X syndrome and are consonant with JAKMIP1's binding to FMRP mRNA translational targets.

We made four main discoveries pertaining to the molecular function of JAKMIP1 during development. First, using an unbiased proteomics approach, we discovered that JAKMIP1 is a novel component of an FMRP-containing RNP granule during brain development. Second, we found that JAKMIP1 binds FMRP mRNA targets including PSD95 mRNA, and affects their expression at the synapse. Third, we showed that JAKMIP1 regulates PSD95 protein levels at synaptosomal membranes, likely through translation, as PSD95 mRNA is unloaded off of the translational machinery in postnatal brains of *Jakmip1* KO mice. Lastly, we found that JAKMIP1 associates with polyribosomes and regulates neuronal translation.

Consistent with our hypothesis that JAKMIP1 is involved in ASD and FXS, we found that loss of *Jakmip1 in vivo* leads to behavioral impairments observed in both disorders. *Jakmip1* KO mice display repetitive and restrictive behaviors, including motor stereotypies such as increased grooming and myoclonic hindlimb jumping, as well as perseverative neurological stereotypies. *Jakmip1* KO mice also display impairments in social behavior and show decreased anxiety. Interestingly, loss of *Jakmip1* results in postnatal loss of prepulse inhibition and learning impairments, behaviors seen in the *Fmr1* KO mouse. *Jakmip1* KO mice additionally show abnormalities in motor coordination, which is gaining appreciation as a phenotype comorbid with ASD (Fournier et al., 2010). Intriguingly, several of the behaviors exhibited by *Jakmip1* KO mice mirror those of mice with PSD95 loss and those having disrupted translation. This work provides another piece of evidence linking translational control to major disturbances in behavior.

Gene expression profiling of the *Jakmip1* KO brain further supports JAKMIP1 binding to FMRP RNP complexes and regulating mRNA targets shared with FMRP. Both *Jakmip1* KO and *Fmr1* KO cause changes in the expression of GABA-A receptor subunits. Moreover, both *Rgs4* and *Nxf1*, two genes from a short list changed with *Fmr1* loss, are differentially expressed in *Jakmip1* KO brains. Additionally, mRNA that binds to both JAKMIP1 and FMRP protein, *PSD95*, *Map1b*, *Camk2a*, *Sapap4, App, and Dag 1,* were all significantly decreased in *Jakmip1* KO brains, in line with JAKMIP1 binding to and stabilizing these RNAs. Lastly, significantly changed genes in *Jakmip1* KO mouse brain show statistically significant overlap with a high confidence list of FMRP RNA interactors. Organization of the differential gene expression profiles by gene ontology analysis additionally revealed JAKMIP1's contribution to neuronal

structure, which we confirmed functionally by demonstrating a morphological change in neurons from *Jakmip1* KO mice compared to WT controls.

Although progress has been made in understanding FMRP biology since its discovery 20 years ago, there is a paucity of known FMRP interactors that influence its function (Bear et al., 2004; Darnell et al.; Darnell et al., 2011; De Rubeis and Bagni, 2011; Huber et al., 2002; Napoli et al., 2008; Santoro et al., 2012). Therefore, identification of an ASD candidate gene that is not only a molecular regulator of FMRP, but is also involved in behaviors and gene expression profiles related to Fragile X syndrome is a significant contribution to the field.

Understanding the dynamic relationship between JAKMIP1 and FMRP and how this influences synapse function and morphology is an important area of future work. One aspect of this research will be to determine if JAKMIP1 and FMRP regulate translation in series or in parallel. We found that loss of JAKMIP1 leads to a reduction in global translation, a decrease in PSD95 translation, and a disruption in the components of the translational machinery. Although FMRP reduction is known to increase basal translation (Gross and Bassell, 2011; Osterweil et al., 2010; Qin et al., 2005), its loss reduces activity dependent increases in general translation and of specific targets (De Rubeis and Bagni, 2011; Greenough et al., 2001; Muddashetty et al., 2007; Todd et al., 2003). Given the fact that JAKMIP1 and FMRP belong to the same translational complex, their loss reduces translation, and JAKMIP1 is likely downstream of FMRP, JAKMIP1 and FMRP likely regulate translation in series. Testing this specifically using double KO systems will be of great value, as the relation between JAKMIP1 and FMRP has potential clinical implications. For instance, it is tempting to speculate that our identification of the functional intersection of FMRP and JAKMIP1 provides a potential mechanism for the variable penetrance of ASD (De Rubeis and Bagni, 2011), as JAKMIP1 is decreased in ASD

patient brains with increased levels of CYFIP1 and changed in the lymphoblastoid cell lines of FXS patients. For example, JAKMIP1 may serve as a modifier, which could exacerbate or attenuate the functional impact of FMRP loss. JAKMIP1 may also provide a balancing translational function related to FMRP, given the similar biology shared by the two proteins - both bind to kinesin 1 and are bidirectionally mobile along dendritic microtubules (Dictenberg et al., 2008; Vidal et al., 2007).

Elucidation of the precise molecular interactions within the JAKMIP1 and FMRP-associated complex, its relationship to neuronal activity, as well as the interaction of JAKMIP1 with the transport and translational machinery are exciting new directions that now can be explored. This work opens up a field of research centered on the detailed mechanisms by which loss of JAKMIP1 leads to behaviors associated with ASD and Fragile X syndrome, research that will be important for generating novel therapeutics for these disorders.

Appendix I: Characteristics of the *Jakmip1* heterozygous mouse

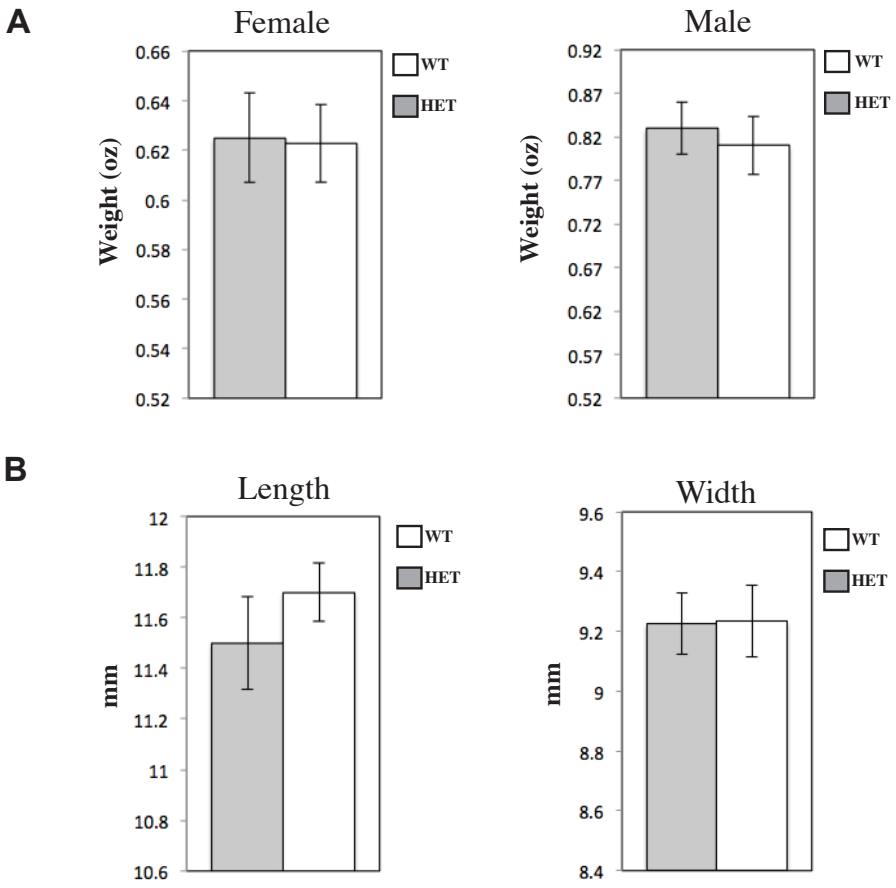

Appendix Figure 1-1, related to Figure 5-2. Somatic characteristics of the *Jakmip1* HET mouse. (A) *Jakmip1* HET mice do not differ in weight from WT mice. Mice were weighed between p44 and p47. Female mice: WT, N=11; HET, N=12. Male mice: WT, N=10; HET, N=10. (B) *Jakmip1* HET mice do not differ in brain length or width from WT mice. Length: WT, N=3; HET, N=4. Width: WT, N=3; HET, N=4. Values are mean +/- SEM.

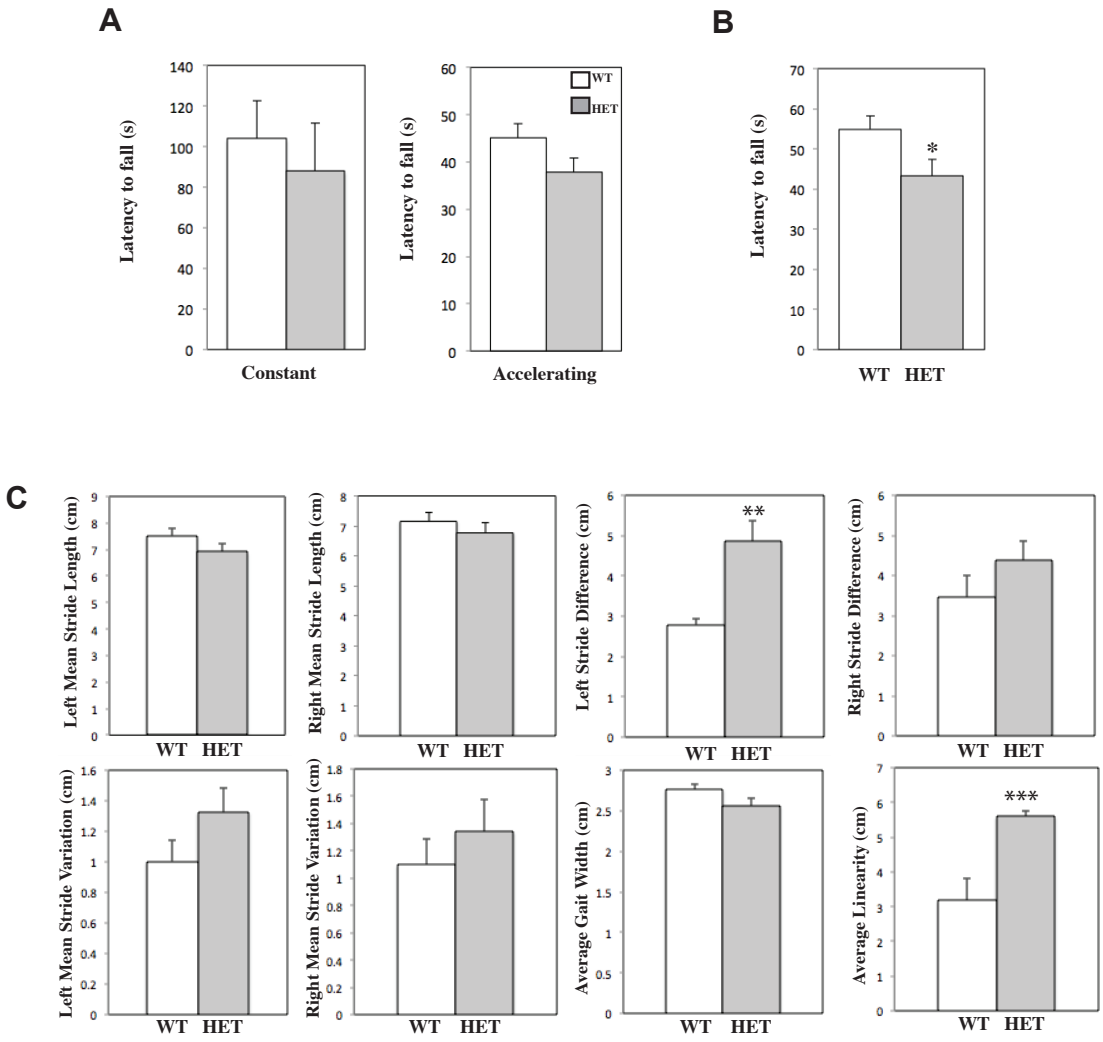

Appendix Figure 1-2, related to Figure 5-4. *Jakmip1* HET mice show slightly impaired motor coordination.

(A) Rotorod. Constant and accelerating speed tests shown. Y axis is latency to fall from the rotorod. Maxium time of trial is 180 s. (WT, N=15; HET, N=11).

(B) Wire Hang Test. Y axis is latency to fall from an inverted wire cage top. Maximum time of trial is 60 seconds. P value calculated using the non-parametric Mann-Whitney test (WT, N=9; HET, N=11: P=0.033).

(C) Gait test. Average stride length, stride difference, stride variation, gait width and linearity are shown. P value calculated using a two sample, two tailed t-test (WT, N=9; HET, N=11, mean stride difference (left), P=0.0088; average linearty, P=0.00079).

Values are mean +/- SEM. * p <= 0.05, ** p<= 0.01, *** p <= 0.001.

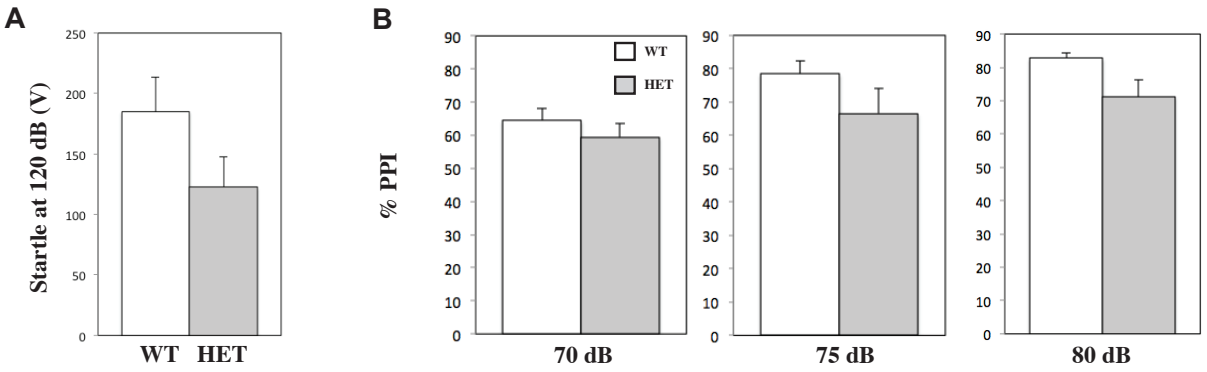

Appendix Figure 1-3, related to Figure 5-5. *Jakmip1* HET mice show normal acoustic startle response and prepulse inhibition.
(A) Starle response. Amplitude of startle following a 120 dB sound. (WT, N=9; HET, N=11).
(B) Prepulse inhibition. Percentage of inhibition when a 70 dB, 75 dB and 80 dB sound is given prior to a 120 dB tone. (WT, N=9; HET, N=11).

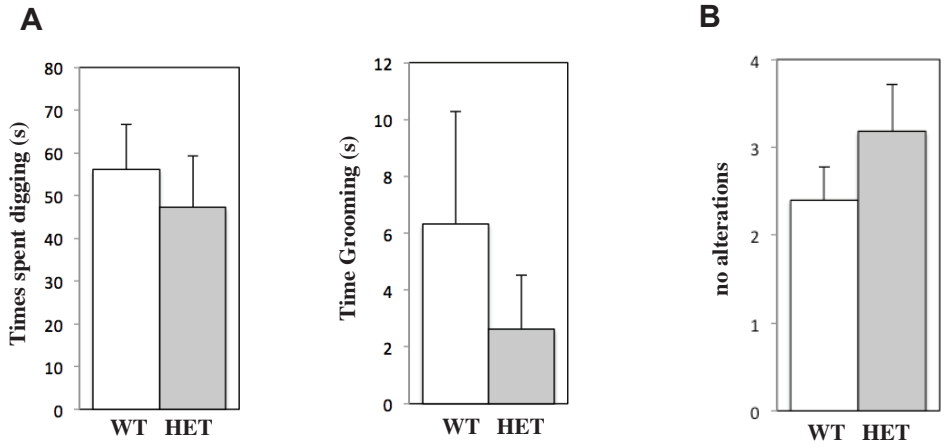

Appendix Figure 1-4, related to Figure 5-6. *Jakmip1* HET mice do not show repetitive and perseverative behavior.
(A) Home cage Behavior. Time spent digging (left) or grooming (right) within a 10 minute period (WT, N=15; HET, N=11).
(B) T maze spontaneous alternation test. Number of alterations shown (WT, N=15; HET, N=11).

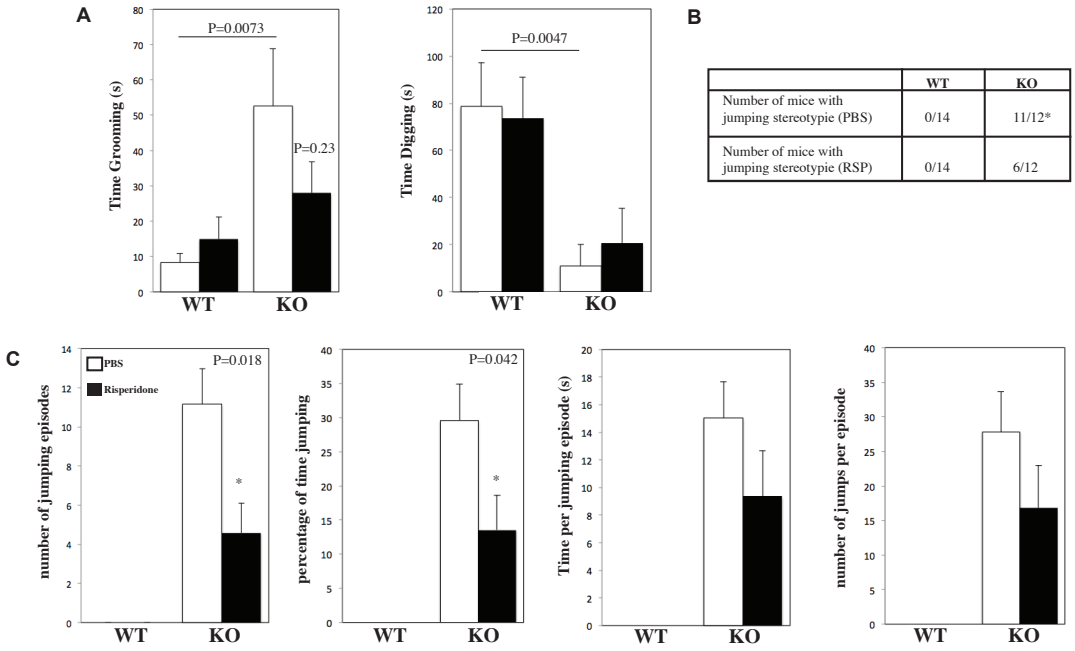

	WT	KO
Number of mice with jumping stereotypie (PBS)	0/14	11/12*
Number of mice with jumping stereotypie (RSP)	0/14	6/12

Appendix Figure 1-5. Risperidone rescues repetitive behavior in *Jakmip1* KO mice.

(A) Risperidone shows a trend toward rescuing perseverative grooming behavior (left), but not digging behavior (right) in *Jakmip1* KO mice. P values calculated using a two sample, two tailed unpaired (WT vs. KO) or paired (KO drug vs KO PBS) t-test.

(B) Risperidone decreases the number of *Jakmip1* KO mice that display jumping stereotypies. *Mouse that did not jump showed repetitive jumping in the open field test.

(C) Risperidone rescues jumping architecture in the *Jakmip1* KO mouse. P values calculated using a two sample, two tailed paired t-test.

Home cage behavior was assessed in over 10 minutes. WT, N=14; KO, N=12 for both PBS and Risperdione in a cross over design. Two age groups of mice were combined [3 months (N=11); 16-18.5 months (N=15)].

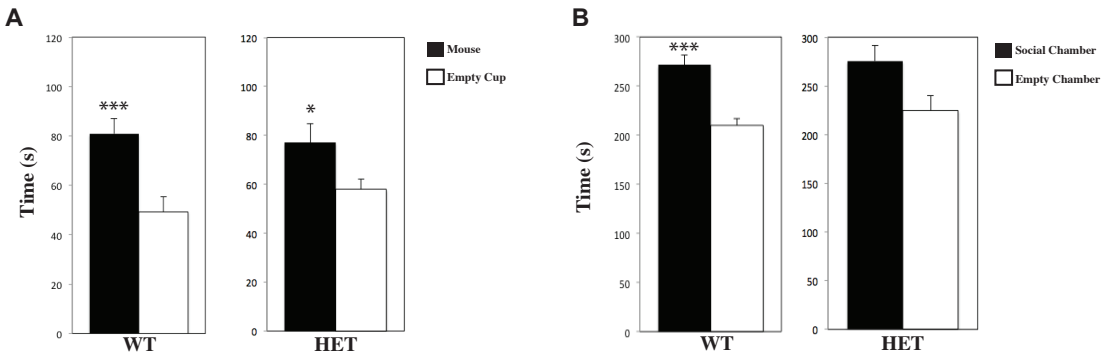

Appendix Figure 1-6, related to Figure 5-7. *Jakmip1* HET mice show slightly impaired social behavior.
Three-chamber social interaction test.
(A) Time spent sniffing a sex-matched novel mouse or an empty cup over a 10 minute period.
P value calculated using a two sample, two tailed, paired t-test [WT, N=15; HET, N=11 : WT, P=0.00051 ; HET, P= 0.052]
(B) Time spent in the social chamber containing a novel mouse or in the chamber containing an empty cup.
P value calculated using a two sample, two tailed, paired t-test [WT, N=15; HET, N=11 : WT, P=0.00064 ; HET, P= 0.12]
Values are mean +/- SEM. * p <= 0.05, ** p<= 0.01, *** p <= 0.001.

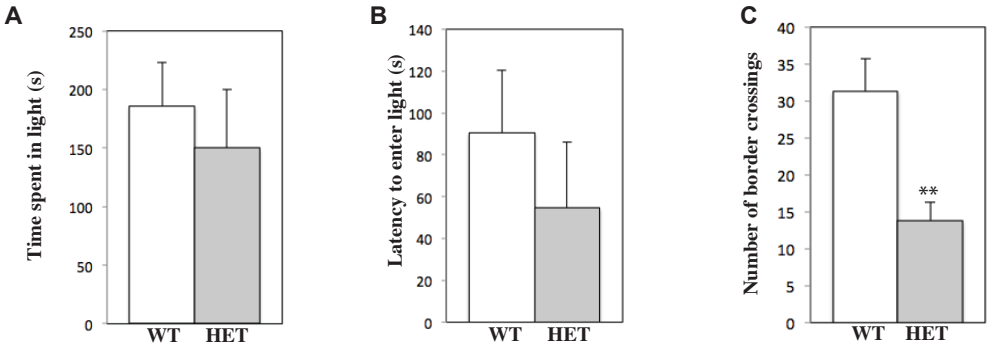

Appendix Figure 1-7, related to Figure 5-8. *Jakmip1* HET mice make less border crossings than WT mice.
Light-dark box test.
(A) Time spent in the bright compartment over a 10 min period (WT, N=15; HET, N=11).
(B) Time before the mouse first enters the bright compartment (WT, N=15; HET, N=11).
(C) Number of times the mouse crosses from the light to the dark compartment over a 10 minute period (WT, N=15; HET, N=11 : P=0.0038).
P values calculated using a two sample, two tailed unpaired t-test.
Values are mean +/- SEM. * p <= 0.05, ** p<= 0.01, *** p <= 0.001.

Appendix II: Differential expression profiling in *Jakmip1* KO mouse brains

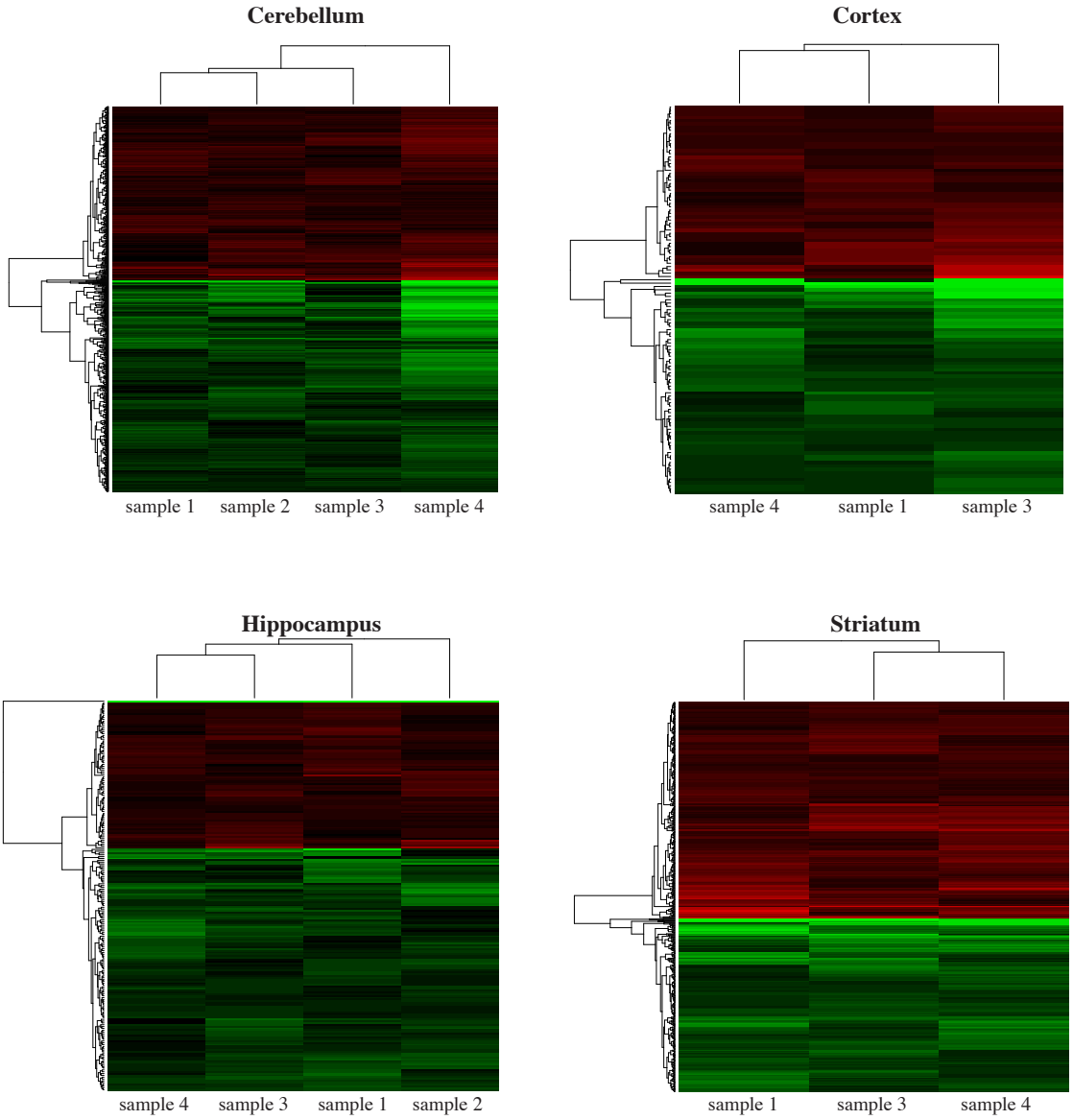

Appendix 2-1. Significantly changed genes demonstrate consistent expression patterns across *Jakmip1* KO samples.
Red color denotes upregulate genes, while green color denotes downregulated genes.
X axis are samples, while Y axis are genes. Gene clustering is shown to the far left on the Y -axis.
Significantly changed genes are defined at P <0.005 .

The following are the top 50 differentially expressed genes by p value in the cortex (CX), cerebellum (CB), striatum (ST), and hippocampus (HP) of *Jakmip1* KO brains versus WT controls. Log Ratios of expression changes (green, decreased; red, increased) are listed in columns with green headings, while p values of these changes are listed in columns with blue headings.

Transcript	ILMN_Gene	CX KO vs. CX WT	CX KO vs. CX WT
ILMN_218013	GABABRBP	-1.904	0.00001
ILMN_209408	LIG1	0.427	0.00024
ILMN_218680	5330410G16RIK	0.368	0.00037
ILMN_186007	LSAMP	-0.39	0.00039
ILMN_218085	LSP1	0.47	0.00041
ILMN_219791	SLC23A3	-0.408	0.00041
ILMN_213620	HSPD1	-0.348	0.00049
ILMN_223756	ACOT1	-0.321	0.00058
ILMN_186128	FHL2	0.329	0.00062
ILMN_216862	HAP1	-0.431	0.00079
ILMN_223370	RESP18	-0.505	0.0008
ILMN_221348	RTN1	-0.476	0.00086
ILMN_219998	KCTD6	-0.305	0.0009
ILMN_216432	CCL27	0.454	0.0009
ILMN_215167	MAS1	-0.334	0.00092
ILMN_219936	SLC8A2	0.369	0.00095
ILMN_223923	DIO3	-0.568	0.00095
ILMN_191066	AI851790	-0.357	0.00097
ILMN_190343	GALT	0.323	0.00098
ILMN_216122	IFIT2	0.312	0.00111
ILMN_220251	CART	0.552	0.00113
ILMN_214278	TCFCP2L2	-0.359	0.00114
ILMN_212208	RERG	-0.329	0.00116
ILMN_244720	GPR17	-0.301	0.00119
ILMN_216466	SLC29A4	-0.478	0.00127
ILMN_207470	KIF1B	-0.349	0.00127
ILMN_212382	RHOBTB2	0.311	0.00129
ILMN_223572	1810057C19RIK	-0.351	0.00133
ILMN_216522	RTN4	0.313	0.00135
ILMN_216236	LRRTM1	0.329	0.00138
ILMN_223702	PDYN	0.367	0.00138
ILMN_209796	CABP7	-0.292	0.00142
ILMN_213142	AP1S1	-0.312	0.00143
ILMN_215264	SLC17A8	0.483	0.00143
ILMN_255747	COBL	0.298	0.00149
ILMN_254951	BRSK1	0.29	0.00161
ILMN_222091	NPY2R	-0.4	0.00167
ILMN_210028	CCND1	-0.474	0.00168
ILMN_223471	ALDH3A1	-0.265	0.00178
ILMN_210171	SMPDL3B	-0.47	0.00179
ILMN_217576	HNRPH1	-0.289	0.00183
ILMN_210028	CCND1	-0.27	0.00188
ILMN_209293	PEX5	-0.317	0.00192
ILMN_243060	RNU6	-0.264	0.00193
ILMN_184733	TPP2	0.263	0.00207
ILMN_189581	SYN2	-0.305	0.00209
ILMN_213307	HAP1	-1.073	0.0021
ILMN_219763	RBM21	0.257	0.00214
ILMN_215395	IRF6	0.317	0.0022
ILMN_220489	ATP1A2	-0.275	0.00223

Transcript	ILMN_Gene	CB KO vs. CB WT	CB KO vs. CB WT
ILMN_212337	GRB14	-0.419	0.00001
ILMN_220861	KCNA2	-0.442	0.00001
ILMN_215366	DNM	-0.37	0.00002
ILMN_223331	ENPP6	-0.5	0.00002
ILMN_220448	MTAP1B	-0.53	0.00002
ILMN_209116	SORCS1	-0.346	0.00003
ILMN_236878	PCDH17	-0.488	0.00003
ILMN_192134	TRF	-0.637	0.00003
ILMN_209546	MAPK13	0.377	0.00006
ILMN_214652	MAMDC1	-0.508	0.00006
ILMN_261337	ANKRD6	-0.325	0.00007
ILMN_198297	LOC232680	0.354	0.00007
ILMN_208863	2610528E23RIK	0.331	0.00007
ILMN_209126	C530050O22RIK	-0.396	0.00007
ILMN_221976	GM1012	-0.328	0.00007
ILMN_216217	CADM2	-0.424	0.00007
ILMN_218013	GABABRBP	-1.21	0.00009
ILMN_219885	CORO1A	0.342	0.0001
ILMN_214746	MUS81	0.343	0.00011
ILMN_219316	SEPM	0.315	0.00011
ILMN_195053	SORL1	-0.38	0.00011
ILMN_209605	SPNB2	-0.335	0.00012
ILMN_219987	HSP105	-0.282	0.00012
ILMN_216052	E430034L04RIK	-0.404	0.00013
ILMN_211515	PPP1R1A	0.288	0.00013
ILMN_230689	TYMS-PS	0.329	0.00013
ILMN_217024	9130210N20RIK	0.309	0.00013
ILMN_218677	SLC35F3	-0.282	0.00013
ILMN_209126	C530050O22RIK	-0.296	0.00013
ILMN_223315	ENPP4	-0.373	0.00013
ILMN_212062	ANK3	-0.367	0.00014
ILMN_233534	BANF1	0.267	0.00015
ILMN_213894	EGR4	-0.352	0.00015
ILMN_219259	MBNL1	-0.293	0.00015
ILMN_209000	BC049806	-0.32	0.00016
ILMN_194814	ODZ4	-0.443	0.00016
ILMN_218459	2900041A09RIK	-0.441	0.00016
ILMN_214117	ADAMTS4	-0.486	0.00016
ILMN_208626	NOSIP	0.326	0.00017
ILMN_227724	SMAD3	0.362	0.00017
ILMN_186566	GLG1	-0.361	0.00017
ILMN_194550	WFS1	-0.279	0.00019
ILMN_216580	RAB6	-0.325	0.00019
ILMN_222572	PBK	0.481	0.00019
ILMN_193337	TXNL4B	0.268	0.00019
ILMN_260117	MIA1	0.406	0.0002
ILMN_212743	PCSK4	0.297	0.0002
ILMN_188343	PEG3	-0.279	0.00022
ILMN_217274	CNTNAP2	-0.322	0.00022
ILMN_188259	TOLLIP	-0.334	0.00022

Transcript	ILMN_Gene	ST KO vs. ST WT	ST KO vs. ST WT
ILMN_218013	GABABRBP	-1.988	0
ILMN_219824	LOC328644	-0.552	0.00003
ILMN_253543	GALNT9	-1.448	0.00003
ILMN_219653	1300010A20RIK	-0.577	0.00003
ILMN_251569	CDH8	0.549	0.00003
ILMN_209647	ARC	-1.057	0.00004
ILMN_216280	DAPK2	-0.613	0.00005
ILMN_222329	CRYM	0.855	0.00005
ILMN_218696	NRN1	-1.911	0.00005
ILMN_215330	GPR123	-0.734	0.00005
ILMN_243519	PPM1E	-0.67	0.00005
ILMN_215684	SUMO3	0.507	0.00006
ILMN_217284	DOK3	-0.482	0.00007
ILMN_223365	GLUD1	0.599	0.00007
ILMN_193235	TMEM25	-0.871	0.00009
ILMN_214764	PPP1R1B	0.589	0.00009
ILMN_223365	GLUD1	0.58	0.0001
ILMN_212740	BTG1	0.453	0.0001
ILMN_215853	CLK1	-0.46	0.00011
ILMN_215684	SUMO3	0.515	0.00011
ILMN_188426	TRIM9	-0.473	0.00011
ILMN_210734	E130309F12RIK	0.442	0.00011
ILMN_193234	TNFRSF25	-0.527	0.00014
ILMN_217740	A830036E02RIK	-0.717	0.00015
ILMN_214933	CD63	0.462	0.00015
ILMN_210734	E130309F12RIK	0.455	0.00016
ILMN_218070	CACNA1G	-0.931	0.00016
ILMN_231589	BEX4	0.459	0.00016
ILMN_211000	IFT172	-0.411	0.00017
ILMN_184996	RBMX	0.428	0.00018
ILMN_215622	SSBP2	0.416	0.00018
ILMN_215586	PPM1A	0.406	0.0002
ILMN_218832	GPR162	-0.476	0.00022
ILMN_219410	ELMO2	-0.425	0.00022
ILMN_192520	EPB4.1L2	0.495	0.00023
ILMN_208673	TITF1	0.412	0.00023
ILMN_237878	RASGRF1	0.459	0.00023
ILMN_212926	BC003885	0.462	0.00023
ILMN_212812	NME7	0.411	0.00023
ILMN_194839	ADHFE1	0.398	0.00024
ILMN_218559	HR	-0.531	0.00025
ILMN_218767	1110019L22RIK	-0.481	0.00026
ILMN_218559	HR	-0.519	0.00032
ILMN_212121	DUSP1	-0.603	0.00032
ILMN_222514	F630022B06RIK	-0.427	0.00033
ILMN_220142	ADAM15	-0.399	0.00033
ILMN_212725	COX6A2	-0.504	0.00036
ILMN_196067	GFAP	0.579	0.00036
ILMN_220109	PFC	-0.699	0.00036
ILMN_210734	E130309F12RIK	0.483	0.00036

Transcript	ILMN_Gene	HP KO vs. HP WT	HP KO vs. HP WT
ILMN_218013	GABABRBP	-2.025	0
ILMN_244182	MOBP	-0.436	0.00001
ILMN_220427	SRPR	-0.33	0.00003
ILMN_211935	MAL	-0.4	0.00005
ILMN_216145	PRKCQ	-0.294	0.00006
ILMN_210908	MYT1L	0.312	0.00007
ILMN_191708	MOBP	-0.287	0.00008
ILMN_194359	UGT8	-0.402	0.00009
ILMN_255417	CITED4	0.299	0.00011
ILMN_222241	FA2H	-0.335	0.00012
ILMN_217710	MKKS	-0.301	0.00013
ILMN_216865	HIST1H2BE	-0.274	0.00013
ILMN_211357	MOG	-0.415	0.00015
ILMN_223263	CIRBP	0.262	0.00016
ILMN_209625	GJA12	-0.292	0.00017
ILMN_190343	GALT	0.263	0.00018
ILMN_220415	GJA9	-0.302	0.00019
ILMN_193482	UQCRB	-0.273	0.0002
ILMN_187678	VPS29	-0.339	0.0002
ILMN_191561	UBE2Q	-0.272	0.00021
ILMN_244182	MOBP	-0.378	0.00021
ILMN_211617	PDLIM2	-0.291	0.00022
ILMN_193699	TMEM10	-0.326	0.00023
ILMN_212337	GRB14	-0.376	0.00025
ILMN_212011	GAD1	-0.268	0.00026
ILMN_220756	KCNH3	0.246	0.00026
ILMN_217624	TES3	-0.261	0.00027
ILMN_212610	NEFH	-0.242	0.00028
ILMN_219015	6330530A05RIK	-0.274	0.00028
ILMN_216940	HIST1H2BC	-0.31	0.0003
ILMN_222844	PTMA	-0.286	0.0003
ILMN_229041	POGZ	0.261	0.00034
ILMN_213412	LASS2	-0.261	0.00037
ILMN_194436	ZFP537	0.46	0.00038
ILMN_210655	0710001E13RIK	0.357	0.00039
ILMN_185695	TPD52L1	-0.289	0.0004
ILMN_220923	9630019K15RIK	-0.241	0.00043
ILMN_252169	ELOVL1	-0.257	0.00046
ILMN_218789	CCNG2	-0.243	0.0005
ILMN_215725	SLN	-0.564	0.0005
ILMN_222768	LDB2	0.303	0.00056
ILMN_187925	CCND2	-0.279	0.0006
ILMN_218089	CCKBR	0.264	0.00062
ILMN_213620	HSPD1	-0.228	0.00064
ILMN_218088	NDUFA5	-0.238	0.00066
ILMN_213619	CAV2	0.224	0.00067
ILMN_196288	PPM1B	0.229	0.00067
ILMN_216306	PHR1	0.211	0.00069
ILMN_197005	LOC381297	-0.284	0.00073
ILMN_245994	RPS25	0.23	0.00074

Bibliography

Abrahams, B.S., and Geschwind, D.H. (2008). Advances in autism genetics: on the threshold of a new neurobiology. Nat Rev Genet *9*, 341-355.

Abrahams, B.S., and Geschwind, D.H. (2010). Connecting genes to brain in the autism spectrum disorders. Arch Neurol *67*, 395-399.

Aihara, Y., Mashima, H., Onda, H., Hisano, S., Kasuya, H., Hori, T., Yamada, S., Tomura, H., Yamada, Y., Inoue, I., *et al*. (2000). Molecular cloning of a novel brain-type Na(+)-dependent inorganic phosphate cotransporter. J Neurochem *74*, 2622-2625.

Akhmanova, A., and Hoogenraad, C.C. (2005). Microtubule plus-end-tracking proteins: mechanisms and functions. Curr Opin Cell Biol *17*, 47-54.

Alarcon, M., Abrahams, B.S., Stone, J.L., Duvall, J.A., Perederiy, J.V., Bomar, J.M., Sebat, J., Wigler, M., Martin, C.L., Ledbetter, D.H., *et al*. (2008). Linkage, association, and gene-expression analyses identify CNTNAP2 as an autism-susceptibility gene. Am J Hum Genet *82*, 150-159.

Alexander, A.L., Lee, J.E., Lazar, M., Boudos, R., DuBray, M.B., Oakes, T.R., Miller, J.N., Lu, J., Jeong, E.K., McMahon, W.M., *et al*. (2007). Diffusion tensor imaging of the corpus callosum in Autism. Neuroimage *34*, 61-73.

Anderson, P., and Kedersha, N. (2006). RNA granules. J Cell Biol *172*, 803-808.

Angenstein, F., Evans, A.M., Settlage, R.E., Moran, S.T., Ling, S.C., Klintsova, A.Y., Shabanowitz, J., Hunt, D.F., and Greenough, W.T. (2002). A receptor for activated C kinase is part of messenger ribonucleoprotein complexes associated with polyA-mRNAs in neurons. J Neurosci *22*, 8827-8837.

Anney, R., Klei, L., Pinto, D., Regan, R., Conroy, J., Magalhaes, T.R., Correia, C., Abrahams, B.S., Sykes, N., Pagnamenta, A.T., *et al*. (2010). A genome-wide scan for common alleles affecting risk for autism. Hum Mol Genet *19*, 4072-4082.

Arguello, P.A., and Gogos, J.A. (2012). Genetic and cognitive windows into circuit mechanisms of psychiatric disease. Trends Neurosci *35*, 3-13.

Arking, D.E., Cutler, D.J., Brune, C.W., Teslovich, T.M., West, K., Ikeda, M., Rea, A., Guy, M., Lin, S., Cook, E.H., *et al*. (2008). A common genetic variant in the neurexin superfamily member CNTNAP2 increases familial risk of autism. Am J Hum Genet *82*, 160-164.

Bagni, C., and Greenough, W.T. (2005). From mRNP trafficking to spine dysmorphogenesis: the roots of fragile X syndrome. Nature reviews Neuroscience *6*, 376-387.

Bakkaloglu, B., O'Roak, B.J., Louvi, A., Gupta, A.R., Abelson, J.F., Morgan, T.M., Chawarska, K., Klin, A., Ercan-Sencicek, A.G., Stillman, A.A., *et al*. (2008). Molecular cytogenetic analysis and resequencing of contactin associated protein-like 2 in autism spectrum disorders. Am J Hum Genet *82*, 165-173.

Barlow, C., Hirotsune, S., Paylor, R., Liyanage, M., Eckhaus, M., Collins, F., Shiloh, Y., Crawley, J.N., Ried, T., Tagle, D., *et al*. (1996). Atm-deficient mice: a paradigm of ataxia telangiectasia. Cell *86*, 159-171.

Barnby, G., Abbott, A., Sykes, N., Morris, A., Weeks, D.E., Mott, R., Lamb, J., Bailey, A.J., and Monaco, A.P. (2005). Candidate-gene screening and association analysis at the autism-susceptibility locus on chromosome 16p: evidence of association at GRIN2A and ABAT. Am J Hum Genet *76*, 950-966.

Barnea-Goraly, N., Kwon, H., Menon, V., Eliez, S., Lotspeich, L., and Reiss, A.L. (2004). White matter structure in autism: preliminary evidence from diffusion tensor imaging. Biol Psychiatry *55*, 323-326.

Bassell, G.J., and Warren, S.T. (2008). Fragile X syndrome: loss of local mRNA regulation alters synaptic development and function. Neuron *60*, 201-214.

Bear, M.F., Huber, K.M., and Warren, S.T. (2004). The mGluR theory of fragile X mental retardation. Trends Neurosci *27*, 370-377.

Beique, J.C., and Andrade, R. (2003). PSD-95 regulates synaptic transmission and plasticity in rat cerebral cortex. J Physiol *546*, 859-867.

Ben-David, E., and Shifman, S. (2012). Networks of neuronal genes affected by common and rare variants in autism spectrum disorders. PLoS Genet *8*, e1002556.

Berg, J.M., and Geschwind, D.H. (2012). Autism genetics: searching for specificity and convergence. Genome Biol *13*, 247.

Berger, A.H., Knudson, A.G., and Pandolfi, P.P. (2011). A continuum model for tumour suppression. Nature *476*, 163-169.

Berkel, S., Marshall, C.R., Weiss, B., Howe, J., Roeth, R., Moog, U., Endris, V., Roberts, W., Szatmari, P., Pinto, D., *et al*. (2010). Mutations in the SHANK2 synaptic scaffolding gene in autism spectrum disorder and mental retardation. Nat Genet *42*, 489-491.

Bill, B.R., and Geschwind, D.H. (2009). Genetic advances in autism: heterogeneity and convergence on shared pathways. Curr Opin Genet Dev *19*, 271-278.

Bodmer, W., and Bonilla, C. (2008). Common and rare variants in multifactorial susceptibility to common diseases. Nat Genet *40*, 695-701.

Bourgeron, T. (2007). The possible interplay of synaptic and clock genes in autism spectrum disorders. Cold Spring Harb Symp Quant Biol *72*, 645-654.

Brown, V., Jin, P., Ceman, S., Darnell, J.C., O'Donnell, W.T., Tenenbaum, S.A., Jin, X., Feng, Y., Wilkinson, K.D., Keene, J.D., *et al*. (2001). Microarray identification of FMRP-associated brain mRNAs and altered mRNA translational profiles in fragile X syndrome. Cell *107*, 477-487.

Bucan, M., Abrahams, B.S., Wang, K., Glessner, J.T., Herman, E.I., Sonnenblick, L.I., Alvarez Retuerto, A.I., Imielinski, M., Hadley, D., Bradfield, J.P., *et al*. (2009). Genome-wide analyses of exonic copy number variants in a family-based study point to novel autism susceptibility genes. PLoS Genet *5*, e1000536.

Butler, M.G., Dasouki, M.J., Zhou, X.P., Talebizadeh, Z., Brown, M., Takahashi, T.N., Miles, J.H., Wang, C.H., Stratton, R., Pilarski, R., *et al*. (2005). Subset of individuals with autism spectrum disorders and extreme macrocephaly associated with germline PTEN tumour suppressor gene mutations. J Med Genet *42*, 318-321.

Cahoy, J.D., Emery, B., Kaushal, A., Foo, L.C., Zamanian, J.L., Christopherson, K.S., Xing, Y., Lubischer, J.L., Krieg, P.A., Krupenko, S.A., *et al*. (2008). A transcriptome database for astrocytes, neurons, and oligodendrocytes: a new resource for understanding brain development and function. J Neurosci *28*, 264-278.

Campbell, D.B., Sutcliffe, J.S., Ebert, P.J., Militerni, R., Bravaccio, C., Trillo, S., Elia, M., Schneider, C., Melmed, R., Sacco, R., *et al*. (2006). A genetic variant that disrupts MET transcription is associated with autism. Proc Natl Acad Sci U S A *103*, 16834-16839.

Cantor, R.M., Yoon, J.L., Furr, J., and Lajonchere, C.M. (2007). Paternal age and autism are associated in a family-based sample. Mol Psychiatry *12*, 419-421.

Carvalho, P.C., Fischer, J.S., Chen, E.I., Yates, J.R., 3rd, and Barbosa, V.C. (2008). PatternLab for proteomics: a tool for differential shotgun proteomics. BMC Bioinformatics *9*, 316.

Casanova, M.F. (2006). Neuropathological and genetic findings in autism: the significance of a putative minicolumnopathy. Neuroscientist *12*, 435-441.

Centonze, D., Rossi, S., Mercaldo, V., Napoli, I., Ciotti, M.T., De Chiara, V., Musella, A., Prosperetti, C., Calabresi, P., Bernardi, G., *et al*. (2008). Abnormal striatal GABA transmission in the mouse model for the fragile X syndrome. Biol Psychiatry *63*, 963-973.

Chahrour, M.H., Yu, T.W., Lim, E.T., Ataman, B., Coulter, M.E., Hill, R.S., Stevens, C.R., Schubert, C.R., Greenberg, M.E., Gabriel, S.B., *et al*. (2012). Whole-exome sequencing and homozygosity analysis implicate depolarization-regulated neuronal genes in autism. PLoS Genet *8*, e1002635.

Chakrabarti, S., and Fombonne, E. (2005). Pervasive developmental disorders in preschool children: confirmation of high prevalence. Am J Psychiatry *162*, 1133-1141.

Cheh, M.A., Millonig, J.H., Roselli, L.M., Ming, X., Jacobsen, E., Kamdar, S., and Wagner, G.C. (2006). En2 knockout mice display neurobehavioral and neurochemical alterations relevant to autism spectrum disorder. Brain Res *1116*, 166-176.

Constantino, J.N., Todorov, A., Hilton, C., Law, P., Zhang, Y., Molloy, E., Fitzgerald, R., and Geschwind, D. (2012). Autism recurrence in half siblings: strong support for genetic mechanisms of transmission in ASD. Mol Psychiatry *[Epub ahead of print]*.

Cook, E.H., Jr., Lindgren, V., Leventhal, B.L., Courchesne, R., Lincoln, A., Shulman, C., Lord, C., and Courchesne, E. (1997). Autism or atypical autism in maternally but not paternally derived proximal 15q duplication. Am J Hum Genet *60*, 928-934.

Costa, V., Conte, I., Ziviello, C., Casamassimi, A., Alfano, G., Banfi, S., and Ciccodicola, A. (2007). Identification and expression analysis of novel Jakmip1 transcripts. Gene *402*, 1-8.

Cottrell, C.E., Bir, N., Varga, E., Alvarez, C.E., Bouyain, S., Zernzach, R., Thrush, D.L., Evans, J., Trimarchi, M., Butter, E.M., *et al*. (2011). Contactin 4 as an autism susceptibility locus. Autism Res *4*, 189-199.

Courchesne, E., Carper, R., and Akshoomoff, N. (2003). Evidence of brain overgrowth in the first year of life in autism. JAMA *290*, 337-344.

Courchesne, E., and Pierce, K. (2005). Why the frontal cortex in autism might be talking only to itself: local over-connectivity but long-distance disconnection. Curr Opin Neurobiol *15*, 225-230.

Couve, A., Restituito, S., Brandon, J.M., Charles, K.J., Bawagan, H., Freeman, K.B., Pangalos, M.N., Calver, A.R., and Moss, S.J. (2004). Marlin-1, a novel RNA-binding protein associates with GABA receptors. J Biol Chem *279*, 13934-13943.

Crawley, J.N., Chen, T., Puri, A., Washburn, R., Sullivan, T.L., Hill, J.M., Young, N.B., Nadler, J.J., Moy, S.S., Young, L.J., *et al*. (2007). Social approach behaviors in oxytocin knockout mice: comparison of two independent lines tested in different laboratory environments. Neuropeptides *41*, 145-163.

Crawley, J.N., and Paylor, R. (1997). A proposed test battery and constellations of specific behavioral paradigms to investigate the behavioral phenotypes of transgenic and knockout mice. Hormones and behavior *31*, 197-211.

Cruz-Martin, A., Crespo, M., and Portera-Cailliau, C. (2010). Delayed stabilization of dendritic spines in fragile X mice. J Neurosci *30*, 7793-7803.

D'Hulst, C., De Geest, N., Reeve, S.P., Van Dam, D., De Deyn, P.P., Hassan, B.A., and Kooy, R.F. (2006). Decreased expression of the GABAA receptor in fragile X syndrome. Brain Res *1121*, 238-245.

Darnell, J.C., Mostovetsky, O., and Darnell, R.B. (2005). FMRP RNA targets: identification and validation. Genes Brain Behav *4*, 341-349.

Darnell, J.C., Van Driesche, S.J., Zhang, C., Hung, K.Y., Mele, A., Fraser, C.E., Stone, E.F., Chen, C., Fak, J.J., Chi, S.W., *et al*. (2011). FMRP stalls ribosomal translocation on mRNAs linked to synaptic function and autism. Cell *146*, 247-261.

De Rubeis, S., and Bagni, C. (2010). Fragile X mental retardation protein control of neuronal mRNA metabolism: Insights into mRNA stability. Mol Cell Neurosci *43*, 43-50.

De Rubeis, S., and Bagni, C. (2011). Regulation of molecular pathways in the Fragile X Syndrome: insights into Autism Spectrum Disorders. J Neurodev Disord *3*, 257-269.

Deacon, R.M. (2006). Assessing nest building in mice. Nat Protoc *1*, 1117-1119.

del Prete, M.J., Vernal, R., Dolznig, H., Mullner, E.W., and Garcia-Sanz, J.A. (2007). Isolation of polysome-bound mRNA from solid tissues amenable for RT-PCR and profiling experiments. RNA *13*, 414-421.

DeLorey, T.M., Sahbaie, P., Hashemi, E., Homanics, G.E., and Clark, J.D. (2008). Gabrb3 gene deficient mice exhibit impaired social and exploratory behaviors, deficits in non-selective attention and hypoplasia of cerebellar vermal lobules: a potential model of autism spectrum disorder. Behavioural brain research *187*, 207-220.

Dictenberg, J.B., Swanger, S.A., Antar, L.N., Singer, R.H., and Bassell, G.J. (2008). A direct role for FMRP in activity-dependent dendritic mRNA transport links filopodial-spine morphogenesis to fragile X syndrome. Dev Cell *14*, 926-939.

Dieterich, D.C., Hodas, J.J., Gouzer, G., Shadrin, I.Y., Ngo, J.T., Triller, A., Tirrell, D.A., and Schuman, E.M. (2010). In situ visualization and dynamics of newly synthesized proteins in rat hippocampal neurons. Nat Neurosci *13*, 897-905.

Durand, C.M., Betancur, C., Boeckers, T.M., Bockmann, J., Chaste, P., Fauchereau, F., Nygren, G., Rastam, M., Gillberg, I.C., Anckarsater, H., *et al*. (2007). Mutations in the gene encoding the synaptic scaffolding protein SHANK3 are associated with autism spectrum disorders. Nat Genet *39*, 25-27.

Elia, J., Gai, X., Xie, H.M., Perin, J.C., Geiger, E., Glessner, J.T., D'Arcy, M., deBerardinis, R., Frackelton, E., Kim, C., *et al*. (2010). Rare structural variants found in attention-deficit hyperactivity disorder are preferentially associated with neurodevelopmental genes. Mol Psychiatry *15*, 637-646.

Etherton, M.R., Blaiss, C.A., Powell, C.M., and Sudhof, T.C. (2009). Mouse neurexin-1alpha deletion causes correlated electrophysiological and behavioral changes consistent with cognitive impairments. Proc Natl Acad Sci U S A *106*, 17998-18003.

Ferguson, J.N., Young, L.J., Hearn, E.F., Matzuk, M.M., Insel, T.R., and Winslow, J.T. (2000). Social amnesia in mice lacking the oxytocin gene. Nat Genet *25*, 284-288.

Fernandez, T., Morgan, T., Davis, N., Klin, A., Morris, A., Farhi, A., Lifton, R.P., and State, M.W. (2008). Disruption of Contactin 4 (CNTN4) results in developmental delay and other features of 3p deletion syndrome. Am J Hum Genet *82*, 1385.

Feyder, M., Karlsson, R.M., Mathur, P., Lyman, M., Bock, R., Momenan, R., Munasinghe, J., Scattoni, M.L., Ihne, J., Camp, M., *et al*. (2010). Association of mouse Dlg4 (PSD-95) gene deletion and human DLG4 gene variation with phenotypes relevant to autism spectrum disorders and Williams' syndrome. Am J Psychiatry *167*, 1508-1517.

Flavell, S.W., Kim, T.K., Gray, J.M., Harmin, D.A., Hemberg, M., Hong, E.J., Markenscoff-Papadimitriou, E., Bear, D.M., and Greenberg, M.E. (2008). Genome-wide analysis of MEF2 transcriptional program reveals synaptic target genes and neuronal activity-dependent polyadenylation site selection. Neuron *60*, 1022-1038.

Florens, L., Carozza, M.J., Swanson, S.K., Fournier, M., Coleman, M.K., Workman, J.L., and Washburn, M.P. (2006). Analyzing chromatin remodeling complexes using shotgun proteomics and normalized spectral abundance factors. Methods *40*, 303-311.

Fournier, K.A., Hass, C.J., Naik, S.K., Lodha, N., and Cauraugh, J.H. (2010). Motor coordination in autism spectrum disorders: a synthesis and meta-analysis. Journal of autism and developmental disorders *40*, 1227-1240.

Freimer, N., and Sabatti, C. (2004). The use of pedigree, sib-pair and association studies of common diseases for genetic mapping and epidemiology. Nat Genet *36*, 1045-1051.

Friedman, J.I., Vrijenhoek, T., Markx, S., Janssen, I.M., van der Vliet, W.A., Faas, B.H., Knoers, N.V., Cahn, W., Kahn, R.S., Edelmann, L., *et al*. (2008). CNTNAP2 gene dosage variation is associated with schizophrenia and epilepsy. Mol Psychiatry *13*, 261-266.

Gabis, L., Raz, R., and Kesner-Baruch, Y. (2010). Paternal age in autism spectrum disorders and ADHD. Pediatr Neurol *43*, 300-302.

Galvez, R., and Greenough, W.T. (2005). Sequence of abnormal dendritic spine development in primary somatosensory cortex of a mouse model of the fragile X mental retardation syndrome. Am J Med Genet A *135*, 155-160.

Gantois, I., Vandesompele, J., Speleman, F., Reyniers, E., D'Hooge, R., Severijnen, L.A., Willemsen, R., Tassone, F., and Kooy, R.F. (2006). Expression profiling suggests underexpression of the GABA(A) receptor subunit delta in the fragile X knockout mouse model. Neurobiology of disease *21*, 346-357.

Gebauer, F., and Hentze, M.W. (2004). Molecular mechanisms of translational control. Nat Rev Mol Cell Biol *5*, 827-835.

Geschwind, D.H. (2008). Autism: many genes, common pathways? Cell *135*, 391-395.

Geschwind, D.H. (2011). Genetics of autism spectrum disorders. Trends Cogn Sci *15*, 409-416.

Geschwind, D.H., and Levitt, P. (2007). Autism spectrum disorders: developmental disconnection syndromes. Curr Opin Neurobiol *17*, 103-111.

Gibson, J.R., Bartley, A.F., Hays, S.A., and Huber, K.M. (2008). Imbalance of neocortical excitation and inhibition and altered UP states reflect network hyperexcitability in the mouse model of fragile X syndrome. J Neurophysiol *100*, 2615-2626.

Gilman, S.R., Iossifov, I., Levy, D., Ronemus, M., Wigler, M., and Vitkup, D. (2011). Rare de novo variants associated with autism implicate a large functional network of genes involved in formation and function of synapses. Neuron *70*, 898-907.

Girirajan, S., Brkanac, Z., Coe, B.P., Baker, C., Vives, L., Vu, T.H., Shafer, N., Bernier, R., Ferrero, G.B., Silengo, M., *et al*. (2011). Relative burden of large CNVs on a range of neurodevelopmental phenotypes. PLoS Genet *7*, e1002334.

Glessner, J.T., Wang, K., Cai, G., Korvatska, O., Kim, C.E., Wood, S., Zhang, H., Estes, A., Brune, C.W., Bradfield, J.P., *et al*. (2009). Autism genome-wide copy number variation reveals ubiquitin and neuronal genes. Nature *459*, 569-573.

Golzio, C., Willer, J., Talkowski, M.E., Oh, E.C., Taniguchi, Y., Jacquemont, S., Reymond, A., Sun, M., Sawa, A., Gusella, J.F., *et al*. (2012). KCTD13 is a major driver of mirrored neuroanatomical phenotypes of the 16p11.2 copy number variant. Nature *485*, 363-367.

Gottesman, II, and Gould, T.D. (2003). The endophenotype concept in psychiatry: etymology and strategic intentions. Am J Psychiatry *160*, 636-645.

Greenough, W.T., Klintsova, A.Y., Irwin, S.A., Galvez, R., Bates, K.E., and Weiler, I.J. (2001). Synaptic regulation of protein synthesis and the fragile X protein. Proc Natl Acad Sci U S A *98*, 7101-7106.

Gross, C., and Bassell, G.J. (2011). Excess protein synthesis in FXS patient lymphoblastoid cells can be rescued with a p110beta-selective inhibitor. Mol Med.

Guilmatre, A., Dubourg, C., Mosca, A.L., Legallic, S., Goldenberg, A., Drouin-Garraud, V., Layet, V., Rosier, A., Briault, S., Bonnet-Brilhault, F., *et al*. (2009). Recurrent rearrangements in synaptic and neurodevelopmental genes and shared biologic pathways in schizophrenia, autism, and mental retardation. Arch Gen Psychiatry *66*, 947-956.

Hallett, P.J., Collins, T.L., Standaert, D.G., and Dunah, A.W. (2008). Biochemical fractionation of brain tissue for studies of receptor distribution and trafficking. Curr Protoc Neurosci *Chapter 1*, Unit 1 16.

Hallmayer, J., Cleveland, S., Torres, A., Phillips, J., Cohen, B., Torigoe, T., Miller, J., Fedele, A., Collins, J., Smith, K., *et al*. (2011). Genetic heritability and shared environmental factors among twin pairs with autism. Arch Gen Psychiatry *68*, 1095-1102.

Harold, D., Abraham, R., Hollingworth, P., Sims, R., Gerrish, A., Hamshere, M.L., Pahwa, J.S., Moskvina, V., Dowzell, K., Williams, A., *et al*. (2009). Genome-wide association study identifies variants at CLU and PICALM associated with Alzheimer's disease. Nat Genet *41*, 1088-1093.

Harris, S.W., Hessl, D., Goodlin-Jones, B., Ferranti, J., Bacalman, S., Barbato, I., Tassone, F., Hagerman, P.J., Herman, H., and Hagerman, R.J. (2008). Autism profiles of males with fragile X syndrome. Am J Ment Retard *113*, 427-438.

Hatton, D.D., Sideris, J., Skinner, M., Mankowski, J., Bailey, D.B., Jr., Roberts, J., and Mirrett, P. (2006). Autistic behavior in children with fragile X syndrome: prevalence, stability, and the impact of FMRP. Am J Med Genet A *140A*, 1804-1813.

Hedges, D.J., Hamilton-Nelson, K.L., Sacharow, S.J., Nations, L., Beecham, G.W., Kozhekbaeva, Z.M., Butler, B.L., Cukier, H.N., Whitehead, P.L., Ma, D., *et al*. (2012). Evidence of novel fine-scale structural variation at autism spectrum disorder candidate loci. Molecular autism *3*, 2.

Heiman, M., Schaefer, A., Gong, S., Peterson, J.D., Day, M., Ramsey, K.E., Suarez-Farinas, M., Schwarz, C., Stephan, D.A., Surmeier, D.J., *et al*. (2008). A translational profiling approach for the molecular characterization of CNS cell types. Cell *135*, 738-748.

Hertz-Picciotto, I., and Delwiche, L. (2009). The rise in autism and the role of age at diagnosis. Epidemiology *20*, 84-90.

Hines, R.M., Wu, L., Hines, D.J., Steenland, H., Mansour, S., Dahlhaus, R., Singaraja, R.R., Cao, X., Sammler, E., Hormuzdi, S.G., *et al*. (2008). Synaptic imbalance, stereotypies, and

impaired social interactions in mice with altered neuroligin 2 expression. J Neurosci *28*, 6055-6067.

Hisaoka, T., Nakamura, Y., Senba, E., and Morikawa, Y. (2010). The forkhead transcription factors, Foxp1 and Foxp2, identify different subpopulations of projection neurons in the mouse cerebral cortex. Neuroscience *166*, 551-563.

Hou, L., Antion, M.D., Hu, D., Spencer, C.M., Paylor, R., and Klann, E. (2006). Dynamic translational and proteasomal regulation of fragile X mental retardation protein controls mGluR-dependent long-term depression. Neuron *51*, 441-454.

Hou, L., and Klann, E. (2004). Activation of the phosphoinositide 3-kinase-Akt-mammalian target of rapamycin signaling pathway is required for metabotropic glutamate receptor-dependent long-term depression. J Neurosci *24*, 6352-6361.

Huber, K.M., Gallagher, S.M., Warren, S.T., and Bear, M.F. (2002). Altered synaptic plasticity in a mouse model of fragile X mental retardation. Proc Natl Acad Sci U S A *99*, 7746-7750.

Hunt, A., and Shepherd, C. (1993). A prevalence study of autism in tuberous sclerosis. J Autism Dev Disord *23*, 323-339.

Iossifov, I., Ronemus, M., Levy, D., Wang, Z., Hakker, I., Rosenbaum, J., Yamrom, B., Lee, Y.H., Narzisi, G., Leotta, A., *et al*. (2012). De novo gene disruptions in children on the autistic spectrum. Neuron *74*, 285-299.

Irwin, S. (1968). Comprehensive observational assessment: Ia. A systematic, quantitative procedure for assessing the behavioral and physiologic state of the mouse. Psychopharmacologia *13*, 222-257.

Irwin, S.A., Patel, B., Idupulapati, M., Harris, J.B., Crisostomo, R.A., Larsen, B.P., Kooy, F., Willems, P.J., Cras, P., Kozlowski, P.B., *et al*. (2001). Abnormal dendritic spine characteristics in the temporal and visual cortices of patients with fragile-X syndrome: a quantitative examination. Am J Med Genet *98*, 161-167.

Ishizuka, A., Siomi, M.C., and Siomi, H. (2002). A Drosophila fragile X protein interacts with components of RNAi and ribosomal proteins. Genes Dev *16*, 2497-2508.

Itsara, A., Wu, H., Smith, J.D., Nickerson, D.A., Romieu, I., London, S.J., and Eichler, E.E. (2010). De novo rates and selection of large copy number variation. Genome Res *20*, 1469-1481.

Jacquemont, M.L., Sanlaville, D., Redon, R., Raoul, O., Cormier-Daire, V., Lyonnet, S., Amiel, J., Le Merrer, M., Heron, D., de Blois, M.C., *et al*. (2006). Array-based comparative genomic hybridisation identifies high frequency of cryptic chromosomal rearrangements in patients with syndromic autism spectrum disorders. J Med Genet *43*, 843-849.

Jacquemont, S., Hagerman, R.J., Hagerman, P.J., and Leehey, M.A. (2007). Fragile-X syndrome and fragile X-associated tremor/ataxia syndrome: two faces of FMR1. Lancet Neurol *6*, 45-55.

Jamain, S., Betancur, C., Quach, H., Philippe, A., Fellous, M., Giros, B., Gillberg, C., Leboyer, M., and Bourgeron, T. (2002). Linkage and association of the glutamate receptor 6 gene with autism. Mol Psychiatry *7*, 302-310.

Jamain, S., Quach, H., Betancur, C., Rastam, M., Colineaux, C., Gillberg, I.C., Soderstrom, H., Giros, B., Leboyer, M., Gillberg, C., *et al*. (2003). Mutations of the X-linked genes encoding neuroligins NLGN3 and NLGN4 are associated with autism. Nat Genet *34*, 27-29.

Jamain, S., Radyushkin, K., Hammerschmidt, K., Granon, S., Boretius, S., Varoqueaux, F., Ramanantsoa, N., Gallego, J., Ronnenberg, A., Winter, D., *et al*. (2008). Reduced social interaction and ultrasonic communication in a mouse model of monogenic heritable autism. Proc Natl Acad Sci U S A *105*, 1710-1715.

Jin, J., Smith, F.D., Stark, C., Wells, C.D., Fawcett, J.P., Kulkarni, S., Metalnikov, P., O'Donnell, P., Taylor, P., Taylor, L., *et al*. (2004). Proteomic, functional, and domain-based analysis of in vivo 14-3-3 binding proteins involved in cytoskeletal regulation and cellular organization. Curr Biol *14*, 1436-1450.

Judson, M.C., Bergman, M.Y., Campbell, D.B., Eagleson, K.L., and Levitt, P. (2009). Dynamic gene and protein expression patterns of the autism-associated met receptor tyrosine kinase in the developing mouse forebrain. J Comp Neurol *513*, 511-531.

Kaiser, M.D., Hudac, C.M., Shultz, S., Lee, S.M., Cheung, C., Berken, A.M., Deen, B., Pitskel, N.B., Sugrue, D.R., Voos, A.C., *et al*. (2010). Neural signatures of autism. Proc Natl Acad Sci U S A *107*, 21223-21228.

Kanai, Y., Dohmae, N., and Hirokawa, N. (2004). Kinesin transports RNA: isolation and characterization of an RNA-transporting granule. Neuron *43*, 513-525.

Kang, H.J., Kawasawa, Y.I., Cheng, F., Zhu, Y., Xu, X., Li, M., Sousa, A.M., Pletikos, M., Meyer, K.A., Sedmak, G., *et al*. (2011). Spatio-temporal transcriptome of the human brain. Nature *478*, 483-489.

Kanner, L. (1943). Autistic disturbances of affective contact. . Nerv Child 2, 217-250.

Kelleher, R.J., 3rd, and Bear, M.F. (2008). The autistic neuron: troubled translation? Cell *135*, 401-406.

Kertesz, A. (2011). The overlapping syndromes of the pick complex. Curr Alzheimer Res *8*, 224-228.

Khwaja, O.S., and Sahin, M. (2011). Translational research: Rett syndrome and tuberous sclerosis complex. Curr Opin Pediatr *23*, 633-639.

Kiebler, M.A., and DesGroseillers, L. (2000). Molecular insights into mRNA transport and local translation in the mammalian nervous system. Neuron *25*, 19-28.

Kim, H.G., Kishikawa, S., Higgins, A.W., Seong, I.S., Donovan, D.J., Shen, Y., Lally, E., Weiss, L.A., Najm, J., Kutsche, K., *et al*. (2008). Disruption of neurexin 1 associated with autism spectrum disorder. Am J Hum Genet *82*, 199-207.

King, M., and Bearman, P. (2009). Diagnostic change and the increased prevalence of autism. International journal of epidemiology *38*, 1224-1234.

Koekkoek, S.K., Yamaguchi, K., Milojkovic, B.A., Dortland, B.R., Ruigrok, T.J., Maex, R., De Graaf, W., Smit, A.E., VanderWerf, F., Bakker, C.E., *et al*. (2005). Deletion of FMR1 in Purkinje cells enhances parallel fiber LTD, enlarges spines, and attenuates cerebellar eyelid conditioning in Fragile X syndrome. Neuron *47*, 339-352.

Konopka, G., Wexler, E., Rosen, E., Mukamel, Z., Osborn, G.E., Chen, L., Lu, D., Gao, F., Gao, K., Lowe, J.K., *et al*. (2012). Modeling the functional genomics of autism using human neurons. Mol Psychiatry *17*, 202-214.

Krupka, N., Strappe, P., Gotz, J., and Ittner, L.M. (2010). Gateway-compatible lentiviral transfer vectors for ubiquitin promoter driven expression of fluorescent fusion proteins. Plasmid *63*, 155-160.

Kumar, R.A., KaraMohamed, S., Sudi, J., Conrad, D.F., Brune, C., Badner, J.A., Gilliam, T.C., Nowak, N.J., Cook, E.H., Jr., Dobyns, W.B., *et al*. (2008). Recurrent 16p11.2 microdeletions in autism. Hum Mol Genet *17*, 628-638.

Laumonnier, F., Bonnet-Brilhault, F., Gomot, M., Blanc, R., David, A., Moizard, M.P., Raynaud, M., Ronce, N., Lemonnier, E., Calvas, P., *et al*. (2004). X-linked mental retardation and autism are associated with a mutation in the NLGN4 gene, a member of the neuroligin family. Am J Hum Genet *74*, 552-557.

Lauritsen, M.B., Pedersen, C.B., and Mortensen, P.B. (2005). Effects of familial risk factors and place of birth on the risk of autism: a nationwide register-based study. J Child Psychol Psychiatry *46*, 963-971.

Leblond, C.S., Heinrich, J., Delorme, R., Proepper, C., Betancur, C., Huguet, G., Konyukh, M., Chaste, P., Ey, E., Rastam, M., *et al*. (2012). Genetic and functional analyses of SHANK2 mutations suggest a multiple hit model of autism spectrum disorders. PLoS Genet *8*, e1002521.

Lee, E.K., Kim, H.H., Kuwano, Y., Abdelmohsen, K., Srikantan, S., Subaran, S.S., Gleichmann, M., Mughal, M.R., Martindale, J.L., Yang, X., *et al*. (2010). hnRNP C promotes APP translation by competing with FMRP for APP mRNA recruitment to P bodies. Nat Struct Mol Biol *17*, 732-739.

Levy, D., Ronemus, M., Yamrom, B., Lee, Y.H., Leotta, A., Kendall, J., Marks, S., Lakshmi, B., Pai, D., Ye, K., *et al*. (2011). Rare de novo and transmitted copy-number variation in autistic spectrum disorders. Neuron *70*, 886-897.

Llinas RR, W.K., Lang EJ (2004). Cerebellum. In The Synaptic Organization of the Brain, S. GM, ed. (New York: Oxford University Press).

Lundstrom, S., Haworth, C.M., Carlstrom, E., Gillberg, C., Mill, J., Rastam, M., Hultman, C.M., Ronald, A., Anckarsater, H., Plomin, R., *et al*. (2010). Trajectories leading to autism spectrum disorders are affected by paternal age: findings from two nationally representative twin studies. J Child Psychol Psychiatry *51*, 850-856.

Luo, R., Sanders, S.J., Tian, Y., Voineagu, I., Huang, N., Chu, S.H., Klei, L., Cai, C., Ou, J., Lowe, J.K., *et al*. (2012). Genome-wide Transcriptome Profiling Reveals the Functional Impact of Rare De Novo and Recurrent CNVs in Autism Spectrum Disorders. Am J Hum Genet *[Epub ahead of print]*.

Malhotra, D., and Sebat, J. (2012). CNVs: Harbingers of a Rare Variant Revolution in Psychiatric Genetics. Cell *148*, 1223-1241.

Marshall, C.R., Noor, A., Vincent, J.B., Lionel, A.C., Feuk, L., Skaug, J., Shago, M., Moessner, R., Pinto, D., Ren, Y., *et al*. (2008). Structural variation of chromosomes in autism spectrum disorder. Am J Hum Genet *82*, 477-488.

McDougle, C.J., Scahill, L., McCracken, J.T., Aman, M.G., Tierney, E., Arnold, L.E., Freeman, B.J., Martin, A., McGough, J.J., Cronin, P., *et al*. (2000). Research Units on Pediatric Psychopharmacology (RUPP) Autism Network. Background and rationale for an initial controlled study of risperidone. Child and adolescent psychiatric clinics of North America *9*, 201-224.

McDougle, C.J., Stigler, K.A., Erickson, C.A., and Posey, D.J. (2008). Atypical antipsychotics in children and adolescents with autistic and other pervasive developmental disorders. The Journal of clinical psychiatry *69 Suppl 4*, 15-20.

McKinney, B.C., Grossman, A.W., Elisseou, N.M., and Greenough, W.T. (2005). Dendritic spine abnormalities in the occipital cortex of C57BL/6 Fmr1 knockout mice. Am J Med Genet B Neuropsychiatr Genet *136B*, 98-102.

Mill, J., Tang, T., Kaminsky, Z., Khare, T., Yazdanpanah, S., Bouchard, L., Jia, P., Assadzadeh, A., Flanagan, J., Schumacher, A., *et al*. (2008). Epigenomic profiling reveals DNA-methylation changes associated with major psychosis. Am J Hum Genet *82*, 696-711.

Miyashiro, K.Y., Beckel-Mitchener, A., Purk, T.P., Becker, K.G., Barret, T., Liu, L., Carbonetto, S., Weiler, I.J., Greenough, W.T., and Eberwine, J. (2003). RNA cargoes associating with FMRP reveal deficits in cellular functioning in Fmr1 null mice. Neuron *37*, 417-431.

Molyneaux, B.J., Arlotta, P., Menezes, J.R., and Macklis, J.D. (2007). Neuronal subtype specification in the cerebral cortex. Nature reviews Neuroscience *8*, 427-437.

Monuki, E.S., and Walsh, C.A. (2001). Mechanisms of cerebral cortical patterning in mice and humans. Nat Neurosci *4 Suppl*, 1199-1206.

Morrow, E.M., Yoo, S.Y., Flavell, S.W., Kim, T.K., Lin, Y., Hill, R.S., Mukaddes, N.M., Balkhy, S., Gascon, G., Hashmi, A., *et al*. (2008). Identifying autism loci and genes by tracing recent shared ancestry. Science *321*, 218-223.

Moss, J., and Howlin, P. (2009). Autism spectrum disorders in genetic syndromes: implications for diagnosis, intervention and understanding the wider autism spectrum disorder population. Journal of intellectual disability research : JIDR *53*, 852-873.

Moy, S.S., Nadler, J.J., Young, N.B., Nonneman, R.J., Grossman, A.W., Murphy, D.L., D'Ercole, A.J., Crawley, J.N., Magnuson, T.R., and Lauder, J.M. (2009). Social approach in genetically engineered mouse lines relevant to autism. Genes Brain Behav *8*, 129-142.

Muddashetty, R.S., Kelic, S., Gross, C., Xu, M., and Bassell, G.J. (2007). Dysregulated metabotropic glutamate receptor-dependent translation of AMPA receptor and postsynaptic density-95 mRNAs at synapses in a mouse model of fragile X syndrome. J Neurosci *27*, 5338-5348.

Musumeci, S.A., Bosco, P., Calabrese, G., Bakker, C., De Sarro, G.B., Elia, M., Ferri, R., and Oostra, B.A. (2000). Audiogenic seizures susceptibility in transgenic mice with fragile X syndrome. Epilepsia *41*, 19-23.

Nakatani, J., Tamada, K., Hatanaka, F., Ise, S., Ohta, H., Inoue, K., Tomonaga, S., Watanabe, Y., Chung, Y.J., Banerjee, R.*, et al*. (2009). Abnormal behavior in a chromosome-engineered mouse model for human 15q11-13 duplication seen in autism. Cell *137*, 1235-1246.

Napoli, I., Mercaldo, V., Boyl, P.P., Eleuteri, B., Zalfa, F., De Rubeis, S., Di Marino, D., Mohr, E., Massimi, M., Falconi, M.*, et al*. (2008). The fragile X syndrome protein represses activity-dependent translation through CYFIP1, a new 4E-BP. Cell *134*, 1042-1054.

Neale, B.M., Kou, Y., Liu, L., Ma'ayan, A., Samocha, K.E., Sabo, A., Lin, C.F., Stevens, C., Wang, L.S., Makarov, V.*, et al*. (2012). Patterns and rates of exonic de novo mutations in autism spectrum disorders. Nature *485*, 242-245.

Nielsen, D.M., Derber, W.J., McClellan, D.A., and Crnic, L.S. (2002). Alterations in the auditory startle response in Fmr1 targeted mutant mouse models of fragile X syndrome. Brain Res *927*, 8-17.

Niklasson, L., Rasmussen, P., Oskarsdottir, S., and Gillberg, C. (2009). Autism, ADHD, mental retardation and behavior problems in 100 individuals with 22q11 deletion syndrome. Res Dev Disabil *30*, 763-773.

Nishimura, Y., Martin, C.L., Vazquez-Lopez, A., Spence, S.J., Alvarez-Retuerto, A.I., Sigman, M., Steindler, C., Pellegrini, S., Schanen, N.C., Warren, S.T.*, et al*. (2007). Genome-wide expression profiling of lymphoblastoid cell lines distinguishes different forms of autism and reveals shared pathways. Hum Mol Genet *16*, 1682-1698.

Noctor, S.C., Martinez-Cerdeno, V., and Kriegstein, A.R. (2007). Contribution of intermediate progenitor cells to cortical histogenesis. Arch Neurol *64*, 639-642.

O'Roak, B.J., Deriziotis, P., Lee, C., Vives, L., Schwartz, J.J., Girirajan, S., Karakoc, E., Mackenzie, A.P., Ng, S.B., Baker, C., *et al*. (2011). Exome sequencing in sporadic autism spectrum disorders identifies severe de novo mutations. Nat Genet *43*, 585-589.

O'Roak, B.J., Deriziotis, P., Lee, C., Vives, L., Schwartz, J.J., Girirajan, S., Karakoc, E., Mackenzie, A.P., Ng, S.B., Baker, C., *et al*. (2012). Exome sequencing in sporadic autism spectrum disorders identifies severe de novo mutations. Nat Genet *44*, 471.

Ohashi, S., Koike, K., Omori, A., Ichinose, S., Ohara, S., Kobayashi, S., Sato, T.A., and Anzai, K. (2002). Identification of mRNA/protein (mRNP) complexes containing Puralpha, mStaufen, fragile X protein, and myosin Va and their association with rough endoplasmic reticulum equipped with a kinesin motor. J Biol Chem *277*, 37804-37810.

Oldham, M.C., Konopka, G., Iwamoto, K., Langfelder, P., Kato, T., Horvath, S., and Geschwind, D.H. (2008). Functional organization of the transcriptome in human brain. Nat Neurosci *11*, 1271-1282.

Olmos-Serrano, J.L., Paluszkiewicz, S.M., Martin, B.S., Kaufmann, W.E., Corbin, J.G., and Huntsman, M.M. (2010). Defective GABAergic neurotransmission and pharmacological rescue of neuronal hyperexcitability in the amygdala in a mouse model of fragile X syndrome. J Neurosci *30*, 9929-9938.

Osterweil, E.K., Krueger, D.D., Reinhold, K., and Bear, M.F. (2010). Hypersensitivity to mGluR5 and ERK1/2 leads to excessive protein synthesis in the hippocampus of a mouse model of fragile X syndrome. J Neurosci *30*, 15616-15627.

Ozonoff, S., Young, G.S., Carter, A., Messinger, D., Yirmiya, N., Zwaigenbaum, L., Bryson, S., Carver, L.J., Constantino, J.N., Dobkins, K., *et al*. (2011). Recurrence risk for autism spectrum disorders: a Baby Siblings Research Consortium study. Pediatrics *128*, e488-495.

Papoulas, O., Monzo, K.F., Cantin, G.T., Ruse, C., Yates, J.R., 3rd, Ryu, Y.H., and Sisson, J.C. (2010). dFMRP and Caprin, translational regulators of synaptic plasticity, control the cell cycle at the Drosophila mid-blastula transition. Development *137*, 4201-4209.

Paylor, R., and Crawley, J.N. (1997). Inbred strain differences in prepulse inhibition of the mouse startle response. Psychopharmacology *132*, 169-180.

Peca, J., Feliciano, C., Ting, J.T., Wang, W., Wells, M.F., Venkatraman, T.N., Lascola, C.D., Fu, Z., and Feng, G. (2011). Shank3 mutant mice display autistic-like behaviours and striatal dysfunction. Nature *472*, 437-442.

Peier, A.M., McIlwain, K.L., Kenneson, A., Warren, S.T., Paylor, R., and Nelson, D.L. (2000). (Over)correction of FMR1 deficiency with YAC transgenics: behavioral and physical features. Hum Mol Genet *9*, 1145-1159.

Penagarikano, O., Abrahams, B.S., Herman, E.I., Winden, K.D., Gdalyahu, A., Dong, H., Sonnenblick, L.I., Gruver, R., Almajano, J., Bragin, A., *et al*. (2011). Absence of CNTNAP2 leads to epilepsy, neuronal migration abnormalities, and core autism-related deficits. Cell *147*, 235-246.

Pierce, K. (2011). Early functional brain development in autism and the promise of sleep fMRI. Brain Res *1380*, 162-174.

Pinto, D., Pagnamenta, A.T., Klei, L., Anney, R., Merico, D., Regan, R., Conroy, J., Magalhaes, T.R., Correia, C., Abrahams, B.S., *et al*. (2010). Functional impact of global rare copy number variation in autism spectrum disorders. Nature *466*, 368-372.

Poliak, S., Gollan, L., Martinez, R., Custer, A., Einheber, S., Salzer, J.L., Trimmer, J.S., Shrager, P., and Peles, E. (1999). Caspr2, a new member of the neurexin superfamily, is localized at the juxtaparanodes of myelinated axons and associates with K+ channels. Neuron *24*, 1037-1047.

Prasad, T.S., Kandasamy, K., and Pandey, A. (2009). Human Protein Reference Database and Human Proteinpedia as discovery tools for systems biology. Methods Mol Biol *577*, 67-79.

Presti, M.F., Watson, C.J., Kennedy, R.T., Yang, M., and Lewis, M.H. (2004). Behavior-related alterations of striatal neurochemistry in a mouse model of stereotyped movement disorder. Pharmacology, biochemistry, and behavior *77*, 501-507.

Qin, M., Kang, J., Burlin, T.V., Jiang, C., and Smith, C.B. (2005). Postadolescent changes in regional cerebral protein synthesis: an in vivo study in the FMR1 null mouse. J Neurosci *25*, 5087-5095.

Redcay, E., and Courchesne, E. (2005). When is the brain enlarged in autism? A meta-analysis of all brain size reports. Biol Psychiatry *58*, 1-9.

Reichenberg, A., Gross, R., Weiser, M., Bresnahan, M., Silverman, J., Harlap, S., Rabinowitz, J., Shulman, C., Malaspina, D., Lubin, G., *et al*. (2006). Advancing paternal age and autism. Arch Gen Psychiatry *63*, 1026-1032.

Ripke, S., Sanders, A.R., Kendler, K.S., Levinson, D.F., Sklar, P., Holmans, P.A., Lin, D.Y., Duan, J., Ophoff, R.A., Andreassen, O.A., *et al*. (2011). Genome-wide association study identifies five new schizophrenia loci. Nat Genet *43*, 969-976.

Risch, N., and Merikangas, K. (1996). The future of genetic studies of complex human diseases. Science *273*, 1516-1517.

Rogers, S.J., Wehner, D.E., and Hagerman, R. (2001). The behavioral phenotype in fragile X: symptoms of autism in very young children with fragile X syndrome, idiopathic autism, and other developmental disorders. J Dev Behav Pediatr *22*, 409-417.

Roohi, J., Montagna, C., Tegay, D.H., Palmer, L.E., DeVincent, C., Pomeroy, J.C., Christian, S.L., Nowak, N., and Hatchwell, E. (2009). Disruption of contactin 4 in three subjects with autism spectrum disorder. J Med Genet *46*, 176-182.

Rosenberg, R.E., Law, J.K., Yenokyan, G., McGready, J., Kaufmann, W.E., and Law, P.A. (2009). Characteristics and concordance of autism spectrum disorders among 277 twin pairs. Arch Pediatr Adolesc Med *163*, 907-914.

Rousseau, F., Labelle, Y., Bussieres, J., and Lindsay, C. (2011). The fragile x mental retardation syndrome 20 years after the FMR1 gene discovery: an expanding universe of knowledge. Clin Biochem Rev *32*, 135-162.

Sacco, R., Militerni, R., Frolli, A., Bravaccio, C., Gritti, A., Elia, M., Curatolo, P., Manzi, B., Trillo, S., Lenti, C., *et al*. (2007). Clinical, morphological, and biochemical correlates of head circumference in autism. Biol Psychiatry *62*, 1038-1047.

Sakai, Y., Shaw, C.A., Dawson, B.C., Dugas, D.V., Al-Mohtaseb, Z., Hill, D.E., and Zoghbi, H.Y. (2011). Protein interactome reveals converging molecular pathways among autism disorders. Sci Transl Med *3*, 86ra49.

Sanders, S.J., Ercan-Sencicek, A.G., Hus, V., Luo, R., Murtha, M.T., Moreno-De-Luca, D., Chu, S.H., Moreau, M.P., Gupta, A.R., Thomson, S.A., *et al*. (2011). Multiple recurrent de novo CNVs, including duplications of the 7q11.23 Williams syndrome region, are strongly associated with autism. Neuron *70*, 863-885.

Sanders, S.J., Murtha, M.T., Gupta, A.R., Murdoch, J.D., Raubeson, M.J., Willsey, A.J., Ercan-Sencicek, A.G., DiLullo, N.M., Parikshak, N.N., Stein, J.L., *et al*. (2012). De novo mutations revealed by whole-exome sequencing are strongly associated with autism. Nature *485*, 237-241.

Sanderson, K. (2012). Universities clash by the Nile. Nature *485*, 21.

Santini, E., Huynh, T.N., MacAskill, A.F., Carter, A.G., Pierre, P., Ruggero, D., Kaphzan, H., and Klann, E. (2013). Exaggerated translation causes synaptic and behavioural aberrations associated with autism. Nature *493*, 411-415.

Santoro, M.R., Bray, S.M., and Warren, S.T. (2012). Molecular mechanisms of fragile X syndrome: a twenty-year perspective. Annu Rev Pathol *7*, 219-245.

Sarbassov, D.D., Ali, S.M., and Sabatini, D.M. (2005). Growing roles for the mTOR pathway. Curr Opin Cell Biol *17*, 596-603.

Scattoni, M.L., McFarlane, H.G., Zhodzishsky, V., Caldwell, H.K., Young, W.S., Ricceri, L., and Crawley, J.N. (2008). Reduced ultrasonic vocalizations in vasopressin 1b knockout mice. Behavioural brain research *187*, 371-378.

Scearce-Levie, K., Roberson, E.D., Gerstein, H., Cholfin, J.A., Mandiyan, V.S., Shah, N.M., Rubenstein, J.L., and Mucke, L. (2008). Abnormal social behaviors in mice lacking Fgf17. Genes Brain Behav *7*, 344-354.

Schaaf, C.P., Sabo, A., Sakai, Y., Crosby, J., Muzny, D., Hawes, A., Lewis, L., Akbar, H., Varghese, R., Boerwinkle, E.*, et al*. (2011). Oligogenic heterozygosity in individuals with high-functioning autism spectrum disorders. Hum Mol Genet *20*, 3366-3375.

Scheiffele, P., and Beg, A.A. (2010). Neuroscience: Angelman syndrome connections. Nature *468*, 907-908.

Schroer, R.J., Phelan, M.C., Michaelis, R.C., Crawford, E.C., Skinner, S.A., Cuccaro, M., Simensen, R.J., Bishop, J., Skinner, C., Fender, D.*, et al*. (1998). Autism and maternally derived aberrations of chromosome 15q. Am J Med Genet *76*, 327-336.

Scott-Van Zeeland, A.A., Abrahams, B.S., Alvarez-Retuerto, A.I., Sonnenblick, L.I., Rudie, J.D., Ghahremani, D., Mumford, J.A., Poldrack, R.A., Dapretto, M., Geschwind, D.H.*, et al*. (2010). Altered functional connectivity in frontal lobe circuits is associated with variation in the autism risk gene CNTNAP2. Sci Transl Med *2*, 56ra80.

Sebat, J., Lakshmi, B., Malhotra, D., Troge, J., Lese-Martin, C., Walsh, T., Yamrom, B., Yoon, S., Krasnitz, A., Kendall, J.*, et al*. (2007). Strong association of de novo copy number mutations with autism. Science *316*, 445-449.

Silverman, J.L., Yang, M., Lord, C., and Crawley, J.N. (2010). Behavioural phenotyping assays for mouse models of autism. Nature reviews Neuroscience *11*, 490-502.

Siomi, M.C., Zhang, Y., Siomi, H., and Dreyfuss, G. (1996). Specific sequences in the fragile X syndrome protein FMR1 and the FXR proteins mediate their binding to 60S ribosomal subunits and the interactions among them. Mol Cell Biol *16*, 3825-3832.

Spencer, C.M., Alekseyenko, O., Hamilton, S.M., Thomas, A.M., Serysheva, E., Yuva-Paylor, L.A., and Paylor, R. (2011). Modifying behavioral phenotypes in Fmr1KO mice: genetic background differences reveal autistic-like responses. Autism Res *4*, 40-56.

Spencer, C.M., Alekseyenko, O., Serysheva, E., Yuva-Paylor, L.A., and Paylor, R. (2005). Altered anxiety-related and social behaviors in the Fmr1 knockout mouse model of fragile X syndrome. Genes Brain Behav *4*, 420-430.

Spencer, C.M., Graham, D.F., Yuva-Paylor, L.A., Nelson, D.L., and Paylor, R. (2008). Social behavior in Fmr1 knockout mice carrying a human FMR1 transgene. Behavioral neuroscience *122*, 710-715.

Spencer, C.M., Serysheva, E., Yuva-Paylor, L.A., Oostra, B.A., Nelson, D.L., and Paylor, R. (2006). Exaggerated behavioral phenotypes in Fmr1/Fxr2 double knockout mice reveal a functional genetic interaction between Fragile X-related proteins. Hum Mol Genet *15*, 1984-1994.

Spiteri, E., Konopka, G., Coppola, G., Bomar, J., Oldham, M., Ou, J., Vernes, S.C., Fisher, S.E., Ren, B., and Geschwind, D.H. (2007). Identification of the transcriptional targets of FOXP2, a gene linked to speech and language, in developing human brain. Am J Hum Genet *81*, 1144-1157.

Splawski, I., Timothy, K.W., Sharpe, L.M., Decher, N., Kumar, P., Bloise, R., Napolitano, C., Schwartz, P.J., Joseph, R.M., Condouris, K., *et al*. (2004). Ca(V)1.2 calcium channel dysfunction causes a multisystem disorder including arrhythmia and autism. Cell *119*, 19-31.

Splawski, I., Yoo, D.S., Stotz, S.C., Cherry, A., Clapham, D.E., and Keating, M.T. (2006). CACNA1H mutations in autism spectrum disorders. J Biol Chem *281*, 22085-22091.

State, M.W., and Levitt, P. (2011). The conundrums of understanding genetic risks for autism spectrum disorders. Nat Neurosci *14*, 1499-1506.

Stefani, G., Fraser, C.E., Darnell, J.C., and Darnell, R.B. (2004). Fragile X mental retardation protein is associated with translating polyribosomes in neuronal cells. J Neurosci *24*, 7272-7276.

Steindler, C., Li, Z., Algarte, M., Alcover, A., Libri, V., Ragimbeau, J., and Pellegrini, S. (2004). Jamip1 (marlin-1) defines a family of proteins interacting with janus kinases and microtubules. J Biol Chem *279*, 43168-43177.

Steiner, P., Higley, M.J., Xu, W., Czervionke, B.L., Malenka, R.C., and Sabatini, B.L. (2008). Destabilization of the postsynaptic density by PSD-95 serine 73 phosphorylation inhibits spine growth and synaptic plasticity. Neuron *60*, 788-802.

Strauss, K.A., Puffenberger, E.G., Huentelman, M.J., Gottlieb, S., Dobrin, S.E., Parod, J.M., Stephan, D.A., and Morton, D.H. (2006). Recessive symptomatic focal epilepsy and mutant contactin-associated protein-like 2. N Engl J Med *354*, 1370-1377.

Szatmari, P., Paterson, A.D., Zwaigenbaum, L., Roberts, W., Brian, J., Liu, X.Q., Vincent, J.B., Skaug, J.L., Thompson, A.P., Senman, L., *et al*. (2007). Mapping autism risk loci using genetic linkage and chromosomal rearrangements. Nat Genet *39*, 319-328.

Szczypka, M.S., Kwok, K., Brot, M.D., Marck, B.T., Matsumoto, A.M., Donahue, B.A., and Palmiter, R.D. (2001). Dopamine production in the caudate putamen restores feeding in dopamine-deficient mice. Neuron *30*, 819-828.

Tabuchi, K., Blundell, J., Etherton, M.R., Hammer, R.E., Liu, X., Powell, C.M., and Sudhof, T.C. (2007). A neuroligin-3 mutation implicated in autism increases inhibitory synaptic transmission in mice. Science *318*, 71-76.

Tamanini, F., Willemsen, R., van Unen, L., Bontekoe, C., Galjaard, H., Oostra, B.A., and Hoogeveen, A.T. (1997). Differential expression of FMR1, FXR1 and FXR2 proteins in human brain and testis. Hum Mol Genet *6*, 1315-1322.

Tervonen, T., Akerman, K., Oostra, B.A., and Castren, M. (2005). Rgs4 mRNA expression is decreased in the brain of Fmr1 knockout mouse. Brain research Molecular brain research *133*, 162-165.

Thomas, A., Burant, A., Bui, N., Graham, D., Yuva-Paylor, L.A., and Paylor, R. (2009). Marble burying reflects a repetitive and perseverative behavior more than novelty-induced anxiety. Psychopharmacology *204*, 361-373.

Tierney, E., Nwokoro, N.A., Porter, F.D., Freund, L.S., Ghuman, J.K., and Kelley, R.I. (2001). Behavior phenotype in the RSH/Smith-Lemli-Opitz syndrome. Am J Med Genet *98*, 191-200.

Todd, P.K., Mack, K.J., and Malter, J.S. (2003). The fragile X mental retardation protein is required for type-I metabotropic glutamate receptor-dependent translation of PSD-95. Proc Natl Acad Sci U S A *100*, 14374-14378.

Tsai, P.T., Hull, C., Chu, Y., Greene-Colozzi, E., Sadowski, A.R., Leech, J.M., Steinberg, J., Crawley, J.N., Regehr, W.G., and Sahin, M. (2012). Autistic-like behaviour and cerebellar dysfunction in Purkinje cell Tsc1 mutant mice. Nature *488*, 647-651.

Tuchman, R., and Rapin, I. (2002). Epilepsy in autism. Lancet Neurol *1*, 352-358.

van der Gucht, E., Vandesande, F., and Arckens, L. (2001). Neurofilament protein: a selective marker for the architectonic parcellation of the visual cortex in adult cat brain. J Comp Neurol *441*, 345-368.

Vidal, R.L., Fuentes, P., Valenzuela, J.I., Alvarado-Diaz, C.P., Ramirez, O.A., Kukuljan, M., and Couve, A. (2012). RNA interference of Marlin-1/Jakmip1 results in abnormal morphogenesis and migration of cortical pyramidal neurons. Mol Cell Neurosci *51*, 1-11.

Vidal, R.L., Ramirez, A., Castro, M., Concha, II, and Couve, A. (2008). Marlin-1 is expressed in testis and associates to the cytoskeleton and GABAB receptors. J Cell Biochem *103*, 886-895.

Vidal, R.L., Ramirez, O.A., Sandoval, L., Koenig-Robert, R., Hartel, S., and Couve, A. (2007). Marlin-1 and conventional kinesin link GABAB receptors to the cytoskeleton and regulate receptor transport. Mol Cell Neurosci *35*, 501-512.

Vidal, R.L., Valenzuela, J.I., Lujan, R., and Couve, A. (2009). Cellular and subcellular localization of Marlin-1 in the brain. BMC Neurosci *10*, 37.

Villace, P., Marion, R.M., and Ortin, J. (2004). The composition of Staufen-containing RNA granules from human cells indicates their role in the regulated transport and translation of messenger RNAs. Nucleic Acids Res *32*, 2411-2420.

Voineagu, I. (2012). Gene expression studies in autism: moving from the genome to the transcriptome and beyond. Neurobiology of disease *45*, 69-75.

Voineagu, I., Wang, X., Johnston, P., Lowe, J.K., Tian, Y., Horvath, S., Mill, J., Cantor, R.M., Blencowe, B.J., and Geschwind, D.H. (2011). Transcriptomic analysis of autistic brain reveals convergent molecular pathology. Nature *474*, 380-384.

Volk, H.E., Hertz-Picciotto, I., Delwiche, L., Lurmann, F., and McConnell, R. (2011). Residential proximity to freeways and autism in the CHARGE study. Environmental health perspectives *119*, 873-877.

Vorhees, C.V., and Williams, M.T. (2006). Morris water maze: procedures for assessing spatial and related forms of learning and memory. Nature protocols *1*, 848-858.

Vorstman, J.A., Staal, W.G., van Daalen, E., van Engeland, H., Hochstenbach, P.F., and Franke, L. (2006). Identification of novel autism candidate regions through analysis of reported cytogenetic abnormalities associated with autism. Mol Psychiatry *11*, 1, 18-28.

Wang, D.O., Kim, S.M., Zhao, Y., Hwang, H., Miura, S.K., Sossin, W.S., and Martin, K.C. (2009). Synapse- and stimulus-specific local translation during long-term neuronal plasticity. Science *324*, 1536-1540.

Waung, M.W., and Huber, K.M. (2009). Protein translation in synaptic plasticity: mGluR-LTD, Fragile X. Curr Opin Neurobiol *19*, 319-326.

Weiss, L.A., Arking, D.E., Daly, M.J., and Chakravarti, A. (2009). A genome-wide linkage and association scan reveals novel loci for autism. Nature *461*, 802-808.

Wersinger, S.R., Ginns, E.I., O'Carroll, A.M., Lolait, S.J., and Young, W.S., 3rd (2002). Vasopressin V1b receptor knockout reduces aggressive behavior in male mice. Mol Psychiatry *7*, 975-984.

Wexler, E.M., Rosen, E., Lu, D., Osborn, G.E., Martin, E., Raybould, H., and Geschwind, D.H. (2011). Genome-wide analysis of a Wnt1-regulated transcriptional network implicates neurodegenerative pathways. Sci Signal *4*, ra65.

Whitney, E.R., Kemper, T.L., Rosene, D.L., Bauman, M.L., and Blatt, G.J. (2008). Calbindin-D28k is a more reliable marker of human Purkinje cells than standard Nissl stains: a stereological experiment. Journal of neuroscience methods *168*, 42-47.

Williams, P.G., and Hersh, J.H. (1998). Brief report: the association of neurofibromatosis type 1 and autism. J Autism Dev Disord *28*, 567-571.

Winslow, J.T., Hearn, E.F., Ferguson, J., Young, L.J., Matzuk, M.M., and Insel, T.R. (2000). Infant vocalization, adult aggression, and fear behavior of an oxytocin null mutant mouse. Hormones and behavior *37*, 145-155.

Wohlschlegel, J.A. (2009). Identification of SUMO-conjugated proteins and their SUMO attachment sites using proteomic mass spectrometry. Methods Mol Biol *497*, 33-49.

Won, H., Lee, H.R., Gee, H.Y., Mah, W., Kim, J.I., Lee, J., Ha, S., Chung, C., Jung, E.S., Cho, Y.S., *et al*. (2012). Autistic-like social behaviour in Shank2-mutant mice improved by restoring NMDA receptor function. Nature *486*, 261-265.

Wonders, C.P., and Anderson, S.A. (2006). The origin and specification of cortical interneurons. Nature reviews Neuroscience *7*, 687-696.

Yan, Q.J., Asafo-Adjei, P.K., Arnold, H.M., Brown, R.E., and Bauchwitz, R.P. (2004). A phenotypic and molecular characterization of the fmr1-tm1Cgr fragile X mouse. Genes Brain Behav *3*, 337-359.

Yao, W.D., Gainetdinov, R.R., Arbuckle, M.I., Sotnikova, T.D., Cyr, M., Beaulieu, J.M., Torres, G.E., Grant, S.G., and Caron, M.G. (2004). Identification of PSD-95 as a regulator of dopamine-mediated synaptic and behavioral plasticity. Neuron *41*, 625-638.

Zahir, F.R., Baross, A., Delaney, A.D., Eydoux, P., Fernandes, N.D., Pugh, T., Marra, M.A., and Friedman, J.M. (2008). A patient with vertebral, cognitive and behavioural abnormalities and a de novo deletion of NRXN1alpha. J Med Genet *45*, 239-243.

Zaichenko, M.I., Vanetsian, G.L., and Merzhanova, G. (2011). [Differences in behavior of impulsive and self-controlled rats in the open-field and light-dark tests]. Zhurnal vysshei nervnoi deiatelnosti imeni I P Pavlova *61*, 340-350.

Zalfa, F., Achsel, T., and Bagni, C. (2006). mRNPs, polysomes or granules: FMRP in neuronal protein synthesis. Curr Opin Neurobiol *16*, 265-269.

Zalfa, F., Eleuteri, B., Dickson, K.S., Mercaldo, V., De Rubeis, S., di Penta, A., Tabolacci, E., Chiurazzi, P., Neri, G., Grant, S.G., *et al*. (2007). A new function for the fragile X mental retardation protein in regulation of PSD-95 mRNA stability. Nat Neurosci *10*, 578-587.

Zalfa, F., Giorgi, M., Primerano, B., Moro, A., Di Penta, A., Reis, S., Oostra, B., and Bagni, C. (2003). The fragile X syndrome protein FMRP associates with BC1 RNA and regulates the translation of specific mRNAs at synapses. Cell *112*, 317-327.

Zang, J.B., Nosyreva, E.D., Spencer, C.M., Volk, L.J., Musunuru, K., Zhong, R., Stone, E.F., Yuva-Paylor, L.A., Huber, K.M., Paylor, R., *et al*. (2009). A mouse model of the human Fragile X syndrome I304N mutation. PLoS Genet *5*, e1000758.

Zhang, M., Wang, Q., and Huang, Y. (2007). Fragile X mental retardation protein FMRP and the RNA export factor NXF2 associate with and destabilize Nxf1 mRNA in neuronal cells. Proc Natl Acad Sci U S A *104*, 10057-10062.

Zhang, Y.Q., Bailey, A.M., Matthies, H.J., Renden, R.B., Smith, M.A., Speese, S.D., Rubin, G.M., and Broadie, K. (2001). Drosophila fragile X-related gene regulates the MAP1B homolog Futsch to control synaptic structure and function. Cell *107*, 591-603.

Zhao, M.G., Toyoda, H., Ko, S.W., Ding, H.K., Wu, L.J., and Zhuo, M. (2005). Deficits in trace fear memory and long-term potentiation in a mouse model for fragile X syndrome. J Neurosci *25*, 7385-7392.

Zhao, X., Leotta, A., Kustanovich, V., Lajonchere, C., Geschwind, D.H., Law, K., Law, P., Qiu, S., Lord, C., Sebat, J., *et al*. (2007). A unified genetic theory for sporadic and inherited autism. Proc Natl Acad Sci U S A *104*, 12831-12836.

Zoghbi, H.Y., and Bear, M.F. (2012). Synaptic Dysfunction in Neurodevelopmental Disorders Associated with Autism and Intellectual Disabilities. Cold Spring Harb Perspect Biol.

Zweier, C., de Jong, E.K., Zweier, M., Orrico, A., Ousager, L.B., Collins, A.L., Bijlsma, E.K., Oortveld, M.A., Ekici, A.B., Reis, A., *et al*. (2009). CNTNAP2 and NRXN1 are mutated in autosomal-recessive Pitt-Hopkins-like mental retardation and determine the level of a common synaptic protein in Drosophila. Am J Hum Genet *85*, 655-666.